NASA TECHNICAL MEMORANDUM

NASA TM X- 74032

NASA TM X- 74032

RESULTS FROM THE NATIONAL AERONAUTICS AND SPACE ADMINISTRATION REMOTE SENSING EXPERIMENTS IN THE NEW YORK BIGHT - APRIL 7-17, 1975

COMPILED BY

JOHN B. HALL, JR.

and

ALBIN O. PEARSON

(NASA-TM-X-74032) RESULTS FROM THE NATIONAL AERONAUTICS AND SPACE ADMINISTRATION REMOTE SENSING EXPERIMENTS IN THE NEW YORK BIGHT, 7-17 APRIL 1975 (NASA) 190 p HC A09/MF A01 CSCL 05B G3/43

N77-23573

Unclas 26119

April 1977

National Aeronautics and Space Administration

Langley Research Center
Hampton, Virginia 23665

1. Report No.	2. Government Accession No.	3. Recipient's Catalog No.
NASA TM X-74032		

4. Title and Subtitle	5. Report Date
Results From The National Aeronautics and Space administration Remote Sensing Experiments In The New York Bight - April 1975	April 1977
	6. Performing Organization Code: 6210
7. Author(s): John B. Hall, Jr. and Albin O. Pearson	8. Performing Organization Report No.: NASA TM X-74032
	10. Work Unit No.: 176-30-31
9. Performing Organization Name and Address: National Aeronautics and Space Administration, Langley Research Center, Hampton, Virginia 23665	11. Contract or Grant No.
	13. Type of Report and Period Covered: Technical Memorandum
12. Sponsoring Agency Name and Address: National Aeronautics and Space Administration, Washington, DC 20546	14. Sponsoring Agency Code

15. Supplementary Notes

16. Abstract

A cooperative operation between the National Aeronautics and Space Administration (NASA) and the National Oceanic and Atmospheric Administration (NOAA) was conducted in the New York Bight during April 7-17, 1975, to evaluate the role of NASA remote sensing technology to monitor ocean dumping. Six NASA remote sensing experiments were flown on the C-54, U-2, and C-130 NASA aircraft, while NOAA obtained concurrent sea truth information using helicopters and surface platforms. The experiments included 1) a Radiometer/Scatterometer (RADSCAT), 2) an Ocean Color Scanner (OCS), 3) a Multichannel Ocean Color Sensor (MOCS), 4) four Hasselblad cameras, 5) an Ebert spectrometer, and 6) a Reconafax IV infrared scanner and a Precision Radiation Thermometer (PRT-5).

The purpose of this report is to present the results of these experiments relative to the use of remote sensors to detect, quantify, and determine the dispersion of pollutants dumped into the New York Bight. Descriptions of the experiments, experimental methods, data analyses techniques, and significant results for each experiment are given in separate sections of the report.

17. Key Words (Suggested by Author(s))	18. Distribution Statement
Earth Resources (43) Remote Sensing, MESA/NY Bight Project, Ocean dumping monitoring, Water Quality	Unclassified-Unlimited

19. Security Classif. (of this report)	20. Security Classif. (of this page)	21. No. of Pages	22. Price*
Unclassified	Unclassified	186	$7.50

* For sale by the National Technical Information Service, Springfield, Virginia 22161

NASA - LANGLEY RESEARCH CENTER

RESULTS FROM THE NATIONAL AERONAUTICS AND SPACE ADMINISTRATION REMOTE SENSING EXPERIMENTS IN THE NEW YORK BIGHT - APRIL 1975

John B. Hall, Jr. and Albin O. Pearson

ABSTRACT

A cooperative operation between the National Aeronautics and Space Administration (NASA) and the National Oceanic and Atmospheric Administration (NOAA) was conducted in the New York Bight during April 7-17, 1975, to evaluate the role of NASA remote sensing technology to monitor ocean dumping. Six NASA remote sensing experiments were flown on the C-54, U-2, and C-130 NASA aircraft, while NOAA obtained concurrent sea truth information using helicopters and surface platforms. The experiments included 1) a Radiometer/Scatterometer (RADSCAT), 2) an Ocean Color Scanner (OCS), 3) a Multichannel Ocean Color Sensor (MOCS), 4) four Hasselblad cameras, 5) an Ebert spectrometer, and 6) a Reconafax IV infrared scanner and a Precision Radiation Thermometer (PRT-5).

The purpose of this report is to present the results of these experiments relative to the use of remote sensors to detect, quantify, and determine the dispersion of pollutants dumped into the New York Bight. Descriptions of the experiments, experimental methods, data analyses techniques, and significant results for each experiment are given in separate sections of the report.

RESULTS FROM THE NATIONAL AERONAUTICS AND SPACE ADMINISTRATION REMOTE SENSING EXPERIMENTS IN THE NEW YORK BIGHT - APRIL 7-17, 1975

COMPILED BY

JOHN B. HALL, JR.

and

ALBIN O. PEARSON

FEBRUARY 24, 1977

TABLE OF CONTENTS

RESULTS FROM THE NATIONAL AERONAUTICS AND SPACE ADMINISTRATION REMOTE SENSING EXPERIMENTS IN THE NEW YORK BIGHT - APRIL 7-17, 1975

COMPILED BY

John B. Hall Jr. and Albin O. Pearson

SUMMARY

Six remote sensing experiments were conducted by the National Aeronautics and Space Administration (NASA) in conjunction with the National Oceanic and Atmospheric Administration (NOAA) in the New York Bight between April 7-17, 1975, to evaluate the role of NASA remote sensing technology to monitoring ocean dumping. Sixteen remote sensors were flown on the C-54, U-2, and C-130 NASA aircraft, while NOAA obtained concurrent in situ sea truth data using helicopters and surface platforms. The six primary sensor experiments included (1) a Radiometer Scatterometer (RADSCAT), (2) an Ocean Color Scanner (OCS), (3) a Multichannel Ocean Color Sensor (MOCS), (4) four Hasselblad cameras, (5) an Ebert spectrometer, (6) a Reconofax IV infrared scanner and a Precision Radiation Thermometer (PRT-5).

The purpose of this report is to present the results of these experiments. Descriptions of the primary sensors, experimental methods, and data analysis techniques along with significant results for each experiment, are given in separate sections of this report.

INTRODUCTION

The National Oceanic and Atmospheric Administration (NOAA)* in 1974 initiated a 7-year Marine Ecosystem Analysis (MESA) Program to obtain environmental information in selected marine locations. The New York Bight is the first site selected for intensive study under the MESA program. The program is focused to provide information to better understand, utilize, and minimize man's impact on the New York Bight. A more efficient utilization of the Bight resources requires techniques for a rapid and accurate assessment of the effects of man's activities on the Bight ecology. This requirement, coupled with the dynamic nature of the marine environment, accents the need for the synoptic spatial and temporal advantages of remote sensing systems. Accordingly, as a cooperative effort in the MESA program, NOAA requested that NASA evaluate the use of remote sensing technology to define circulation features in the New York Bight and to apply this technology for monitoring and managing ocean dumping. The first step of this cooperative effort was accomplished in the New York Bight during April 7-17, 1975. The area selected by NOAA for this joint NOAA/NASA evaluation was primarily the apex of the New York Bight as shown in figure 1. The New York Bight extends from Cape May, New Jersey, to Montauk Point, New York, and seaward to the edge of the continental shelf (200 meter depth). The apex is bounded on the north by Long Island, on the south by latitude $40^{\circ}10'N$, and on the east by longitude meridian $73^{\circ}30'W$. Presently, within the apex, sewage sludge is dumped at a

*The authors are grateful to John W. Sherman and James B. Zaitzeff of NOAA for their guidance and coordination of NOAA activities in implementing this effort.

location about 18 km (9.7 nautical miles (n. mi.)) south of Long Island. Acid wastes are dumped at a location about 10 km (5.4 n. mi.) southeast of the sewage sludge dump site. Six remote sensing experiments were conducted by NASA using 16 remote sensors flown onboard aircraft platforms to obtain sea surface information relative to these dump sites. Concurrently NOAA obtained in situ "sea truth" information with a combination of helicopters and surface platforms. NASA operations associated with these experiments are given in reference 1.

The purpose of this report is to present the results of the NASA remote sensing experiments. The following sections of this report contain descriptions of the remote sensors, experimental methods, data analysis techniques, and pertinent experiment results.

Reference

1. Usry, J. W. and Hall, J. B., Jr.: National Aeronautics and Space Administration Operations - Remote Sensing Experiments in the New York Bight, April 7-17, 1975. NASA TMX-72802, November 1975.

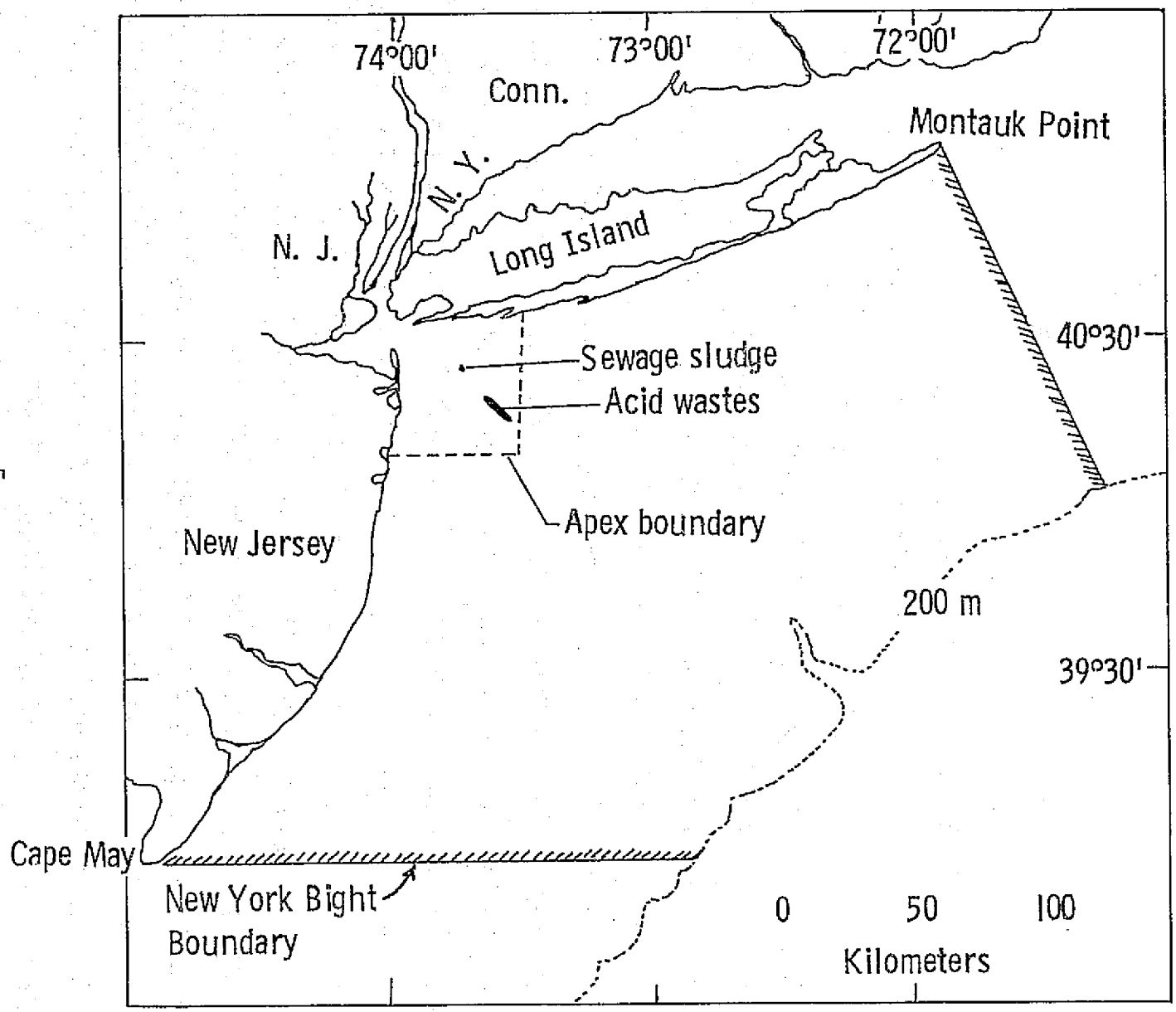

Figure 1. - MESA Defined New York Bight and Apex.

OCEAN COLOR SCANNER (OCS)

BY

WARREN A. HOVIS

OCEAN COLOR SCANNER (OCS)

by

Warren A. Hovis

SUMMARY

The NASA U-2 aircraft participated in the MESA experiments in the New York Bight during April 7-17, 1975. The OCS and four Mitchell-Vinten 70-mm cameras were flown onboard the NASA U-2 aircraft on April 9, 13, and 14, 1975. The purpose of this report is to present the results of this investigation.

EXPERIMENT DESCRIPTION

The Ocean Color Scanner (fig. 1) was flown on the U-2 aircraft at an altitude of 19.8 km (65,000 ft) and was supported by four 70-mm Mitchell-Vinten cameras. The OCS is a 10-channel multispectral scanner ranging from 433 to 772 nanometer (nm) center wavelength with a 90° total scan angle and spatial resolution of 3.5 milliradians. Spectral bands and saturation radiance values used in these investigations are shown in table 1. The radiance for saturation shown in table 1 is for a gain of one for each channel. Gain may be increased separately for each channel in steps of 1.5, 2, and 3 to allow for changing Sun angle due to seasonal changes or time of flight. All channels, except 9, are optimized for water scenes, including atmospheric backscatter as seen from an altitude of 19.8 km. Channel 9 has the same level of gain as the Landsat band 6 that covers 700 to 800 nm.

Four 70-mm Mitchell-Vinten cameras were flown with the OCS to provide high resolution photography to aid in locating the U-2 position. Three of these cameras contained black and white film, and one contained color film. A photograph of this system is shown in figure 2. Specific camera details pertinent to this experiment are shown in table 2.

DATA ACQUISITION

Flight lines for the U-2 are given in reference 1. These lines were established to allow the aircraft to fly directly toward, or away from the Sun, to avoid Sun glint in the scanner imagery. The morning flights were in a general southeast to northwest direction while afternoon flights were generally southwest to northeast. A slight "fan" effect is seen due to allowance for Sun motion during the time of each flight sequence. The actual flight lines flown, flight altitudes, flight line locations, and sensor operation times are given in reference 1.

DATA ANALYSIS AND RESULTS

The flight on April 9 was successful for U-2 operations. Surface truth, however, was not available due to lack of communication between the ship and helicopter operations in the Bight, and the U-2 base at NASA Wallops Flight Center. The U-2 decision to fly was based upon the weather forecast available at Wallops.

The photographic and scanner data were both of excellent quality for this flight. The scanner data were processed to a pictorial product using two different enhancement techniques and, despite the lack of surface truth, still show some interesting information as shown in figure 3. Figure 3 is a

"conventionally" enhanced image. It was made from an enhancement where a direct current offset is applied to each of the channels used in making the image to allow for atmospheric backscatter. The amount of offset is wavelength dependent. The image in figure 3 was made from the enhanced data from channels 465, 582, and 662 nm. The image shows the New Jersey shore from Barnegat Inlet to just south of Sandy Hook Point and a portion of the south shore of Long Island. A new acid dump is seen as a sharp "U", while the older dumps are shown drifting to the west. The westward drift is characteristic of all imagery obtained of this area. In addition, the older dumps are shown as being diffused in a southerly direction. Also shown in figure 3 is a square-shaped dump to the north of the acid waste dumps. This feature is a sewage sludge dump that was observed in its early stages during the morning overpass at approximately 1450 g.m.t. The brightest part of this feature, the north edge in the northwest corner, is the initial dumping area. This indicates that the dump is not uniform with time and that the concentration is higher in the initial dump area or that the sludge is not uniformly mixed. It appears that the material dumped first is brighter in the spectral regions sensed than that dumped later. The bright area along the New Jersey shore is the Hudson River plume. This is the normal flow pattern of the plume as seen in a number of images of this area. The high relative reflectivity of the plume indicates a high particulate loading which was confirmed by sea truth measurements on April 13. The plume appears rather featureless in figure 3. Further enhancement was performed by squaring all of the radiance values in the first enhanced tape. The image that results from this enhancement is shown in figure 4. In this image, gradations in the plume are more easily observed. An apparent layering on the

east edge in the plume is observed as the plume bends after leaving the Hudson River. The April 13 flight was performed in the morning. Cloud cover precluded an afternoon flight. The position of the helicopter sampling grid was located on the scanner image, and radiance levels at most of the helicopter stations were determined. The radiance, in all channels, showed a general increase with increased sediment concentration.* Figure 5 shows the measured upwelling radiance as measured by the scanner versus the log of the measured sediment concentration. There is no immediate explanation for the four points at the high sediment levels that appear offset from the others. In an attempt to extract qualitative information from the radiometric data, the method of characteristic vector signatures was tried with the addition of variation from mean radiance as an attempt to compensate for atmospheric effects. Briefly, a mean overall radiance level is determined for the water in the scene, and the departure from the mean determined for each spectral band. As shown in the formula in figure 6, the total radiance consists of the mean radiance, the atmospheric radiance, and a contribution due to sediment and chlorophyll. The vector signature can be either positive or negative which denotes either scattering brighter than the mean or absorption darker than the mean. The sediment signature shown at the top of figure 6 is positive at all wavelengths which indicates no specific absorber; i.e., a near grey color. The chlorophyll signature shows that some chlorophyll absorption can be detected in the plume even though chlorophyll is a minor constituent. There is a reasonable degree of correlation between the total

*The author is grateful to Dennis S. Clark and Terry A. Nelson of NOAA for the use of their unpublished sea truth information.

sediment and the chlorophyll concentration (fig. 7). This is to be expected since the plume is virtually all of organic origin. The chlorophyll content is measured in μg/ℓ while the sediment content is measured in mg/ℓ. An attempt was made to relate measured radiance to chlorophyll content in the plume with only modest success as shown in figure 8. This result is expected when sea truth information shows that only a small portion of the plume is composed of chlorophyll. Chlorophyll has its specific absorption, while the major components of the plume have spectral character. Correlation of the calculated and measured sediment concentrations is given in figure 9. Here the agreement is good and would give considerable confidence that a contour map of total sediment could be made by applying the sediment vector signature to the entire area of the plume. It is apparent from the plume analysis that it will be difficult to determine concentrations of minor constituents of a plume from radiometric data only. It may be possible, however, to infer the minor constituent concentration if its quantitative relation to the total sediment load is known.

The magnetic tape recorder failed during the April 14 flight. Failure was due to damage sustained in a previous shipment from Wallops Flight Center to the Ames Research Center. The photographic quality was good, but could not be used for quantitative analysis.

Reference

1. Usry, J. W. and Hall, J. B., Jr.: National Aeronautics and Space Administration Operations - Remote Sensing Experiments in the New York Bight, April 7-17, 1975. NASA TMX-72802, November 1975.

TABLE 1.- OCEAN COLOR SCANNER

Channel	Center Wavelength (nm)	Bandwidth (nm)	Radiance for Saturation (Gain X 1) mv/cm^2
1	433	22.5	40.10
2	471	21.5	26.00
3	509	27.0	23.60
4	547	24.5	14.70
5	583	25.0	11.80
6	620	26.0	10.00
7	662	22.0	7.55
8	698	20.5	5.00
9	733	22.5	11.90
10	772	23.0	3.47

TABLE 2.- MITCHELL-VINTEN CAMERAS

Camera Number	Lens Focal Length, cm(in.)	Film Format, cm(in)	Film Number	Shutter Speed, sec	Filter Number	Spectral Range Nanometer	F Stop	Spatial Resolution m (ft)
1	4.43 (1.75)	5.72 X 5.56 ($2\frac{1}{4}$ X $2\frac{3}{16}$)	Panatomic X, 3400	1/250	Wratten 12	510-700	9.6	9.1 to 15.2 (30 to 50)
2	4.43 (1.75)	5.72 X 5.56 ($2\frac{1}{4}$ X $2\frac{3}{16}$)	Panatomic X, 3400	1/250	Schott GG 475 + Schott BG 18	475-575	5.6	9.1 to 15.2 (30 to 50)
3	4.43 (1.75)	5.72 X 5.56 ($2\frac{1}{4}$ X $2\frac{3}{16}$)	Panatomic X, 3400	1/250	Schott OG 570 + Schott BG 38	580-680	5.6	9.1 to 15.2 (30 to 50)
4	4.43 (1.75)	5.72 X 5.58 ($2\frac{1}{4}$ X $2\frac{3}{16}$)	Aerial Color SO-242	1/250	None	400-700	3.5	9.1 to 15.2 (30 to 50)

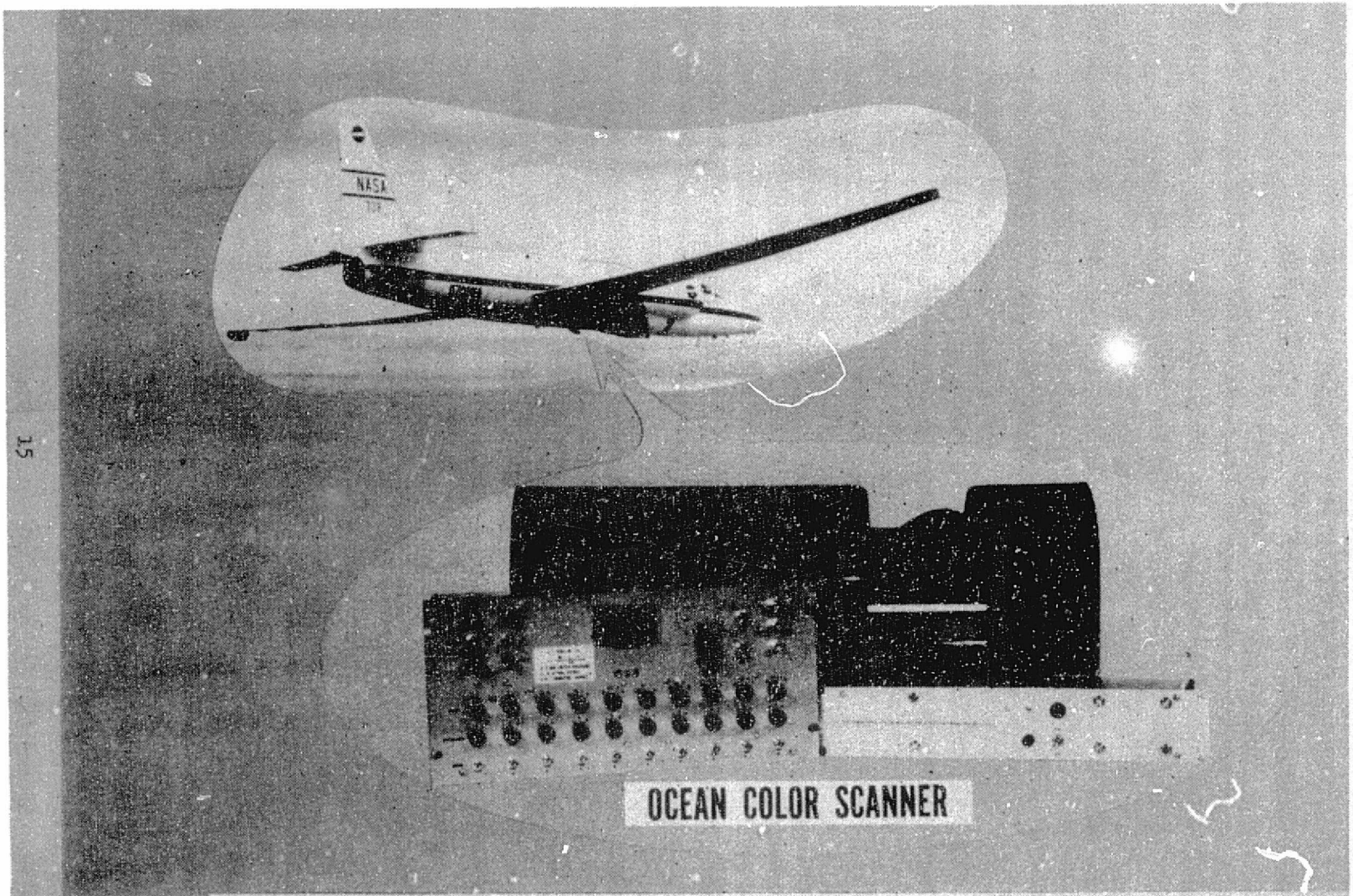

FIGURE 1 - OCEAN COLOR SCANNER INSTALLATION IN THE U-2

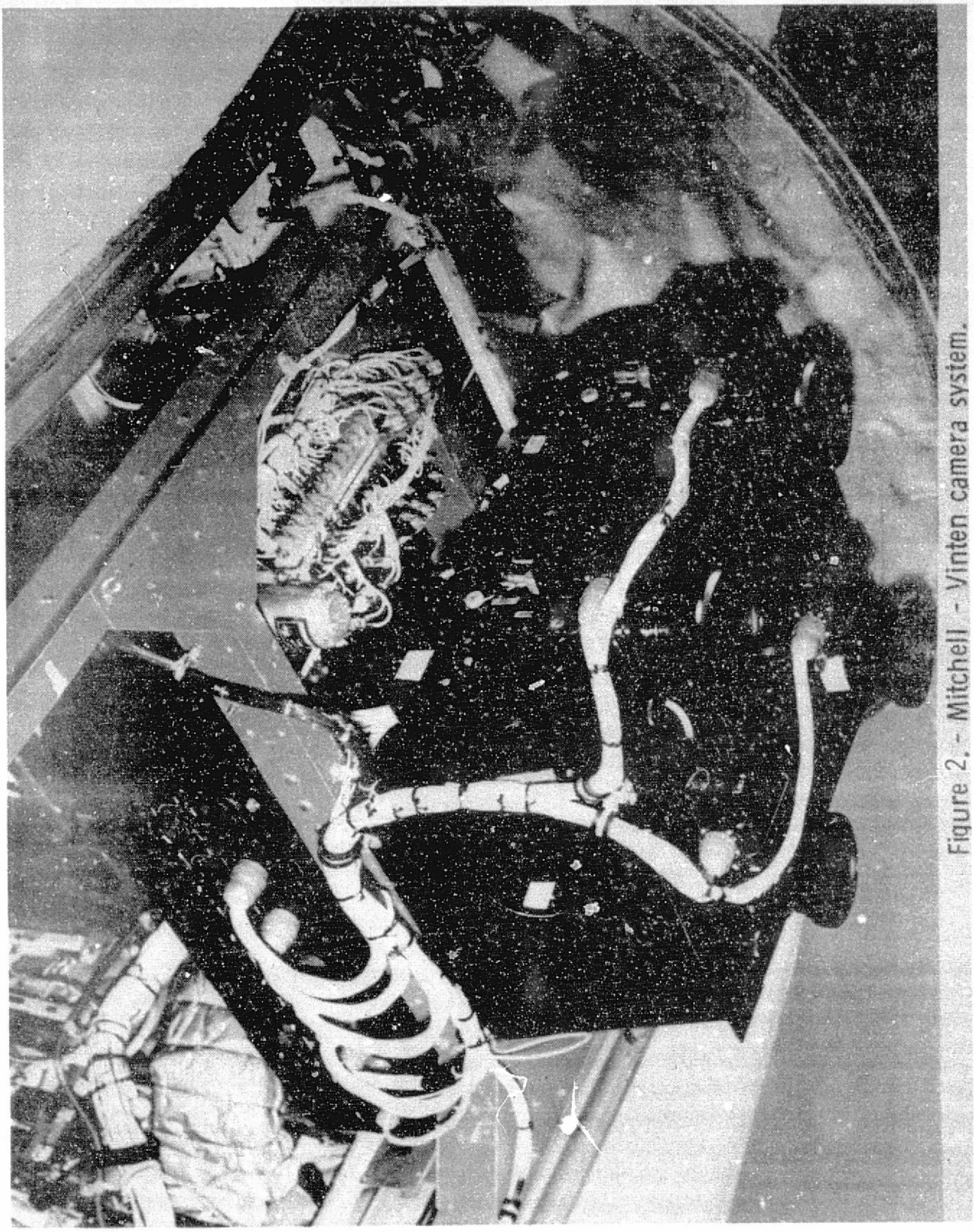

Figure 2. - Mitchell - Vinten camera system.

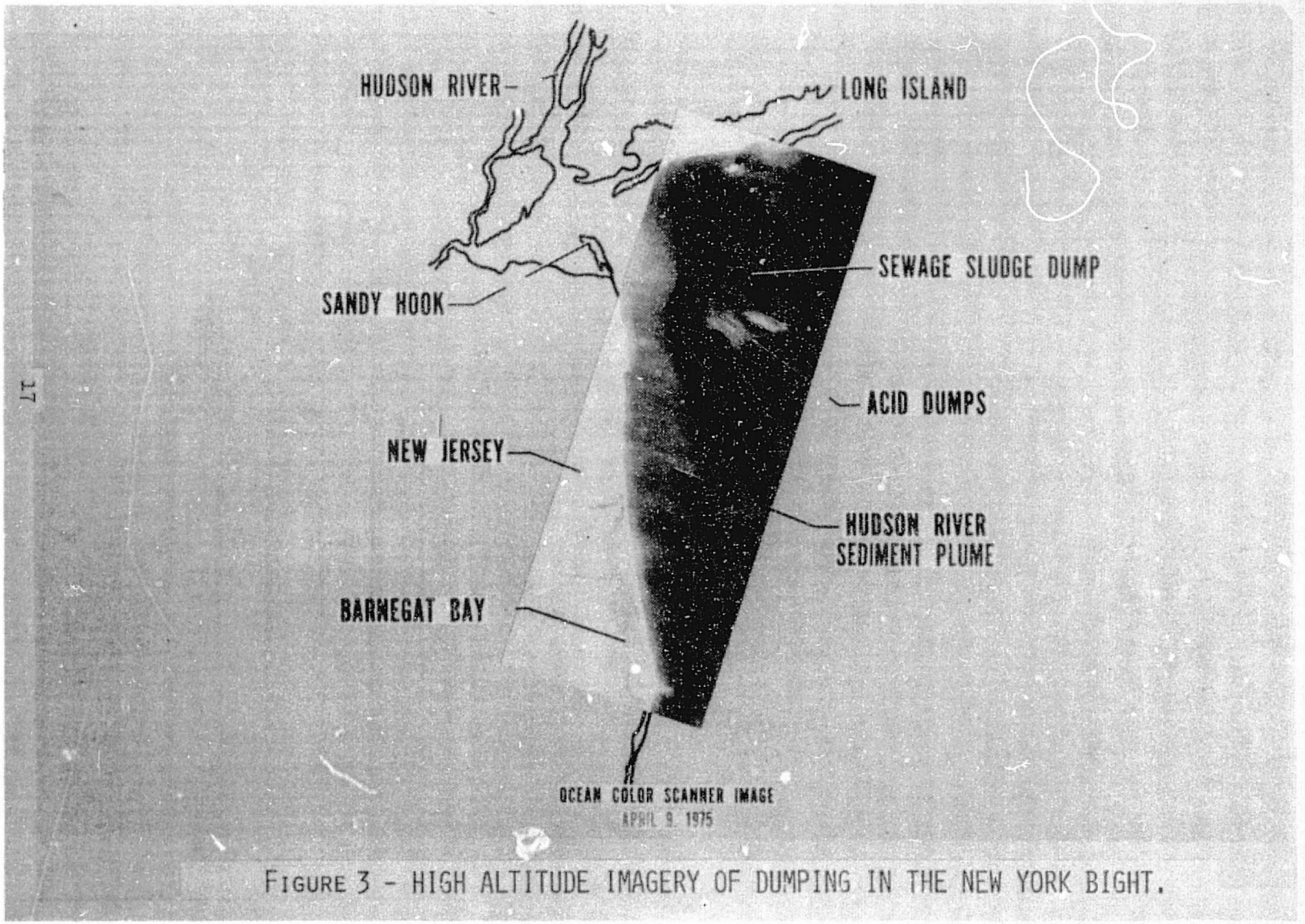

FIGURE 3 - HIGH ALTITUDE IMAGERY OF DUMPING IN THE NEW YORK BIGHT.

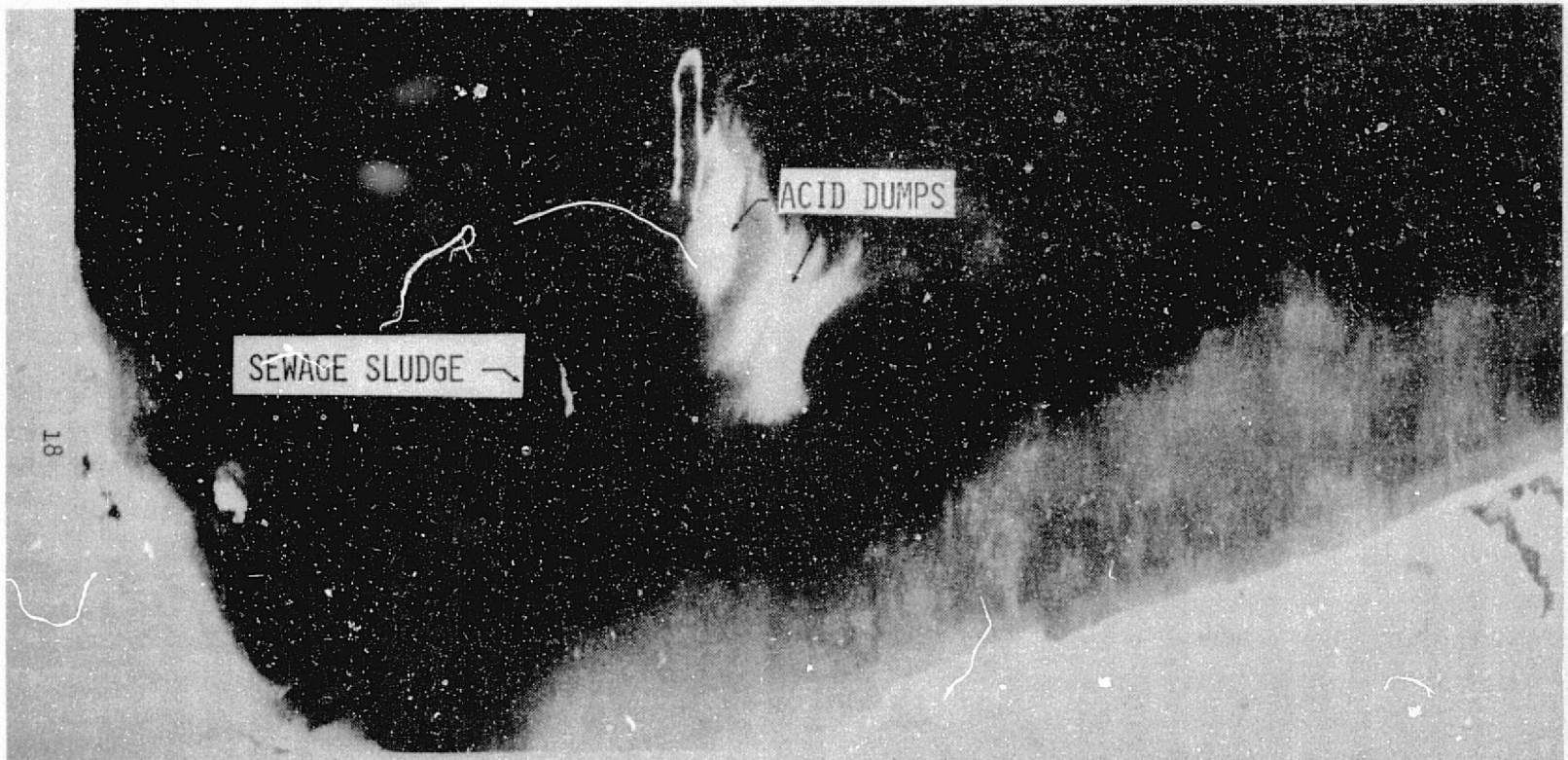

FIGURE 4 - OCEAN COLOR SCANNER ENHANCED DATA - NEW YORK BIGHT
APRIL 9, 1975.

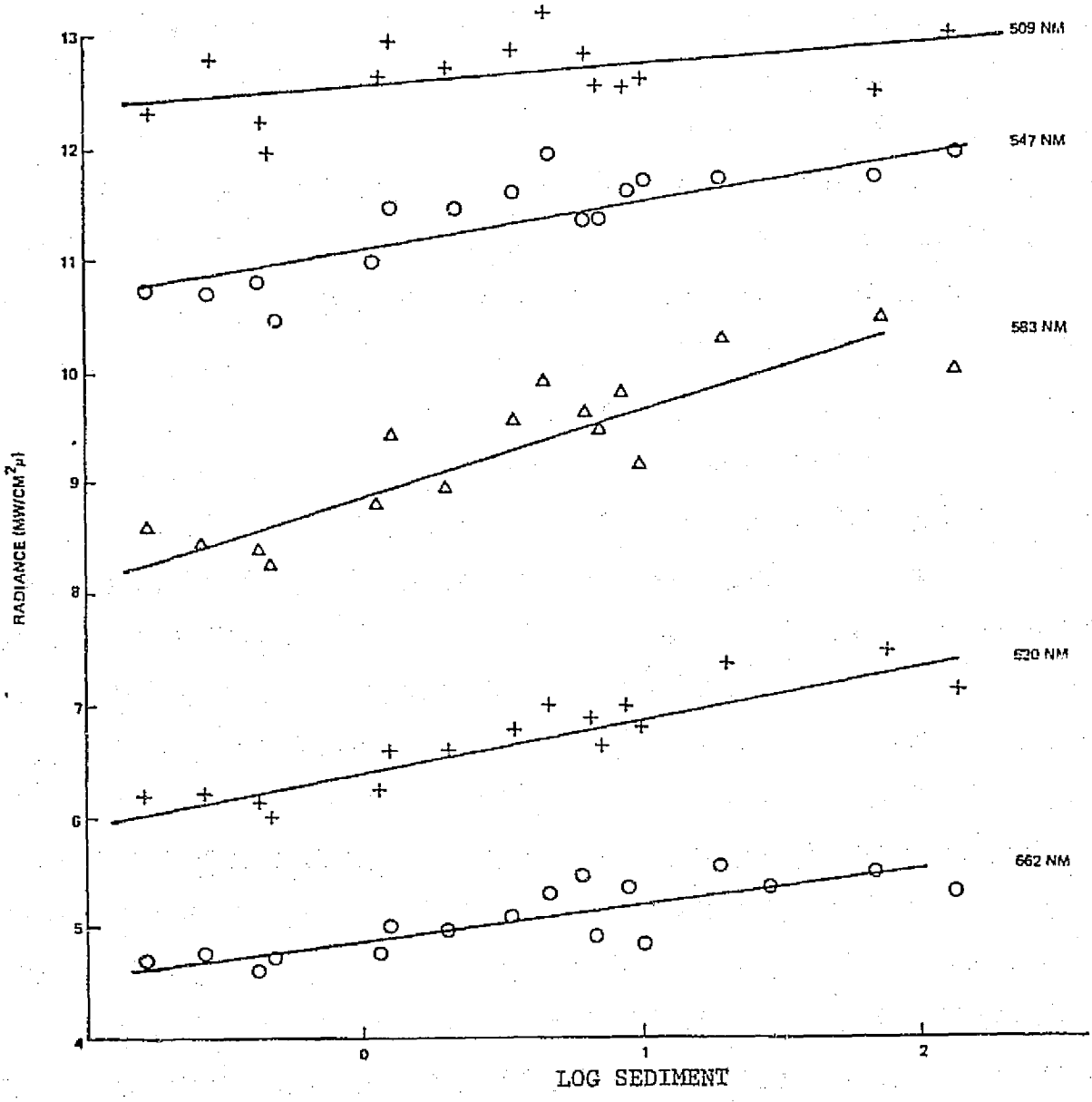

FIGURE 5 - OCEAN COLOR SCANNER RADIANCE VS SEDIMENT DATA FOR APRIL 13, 1975.

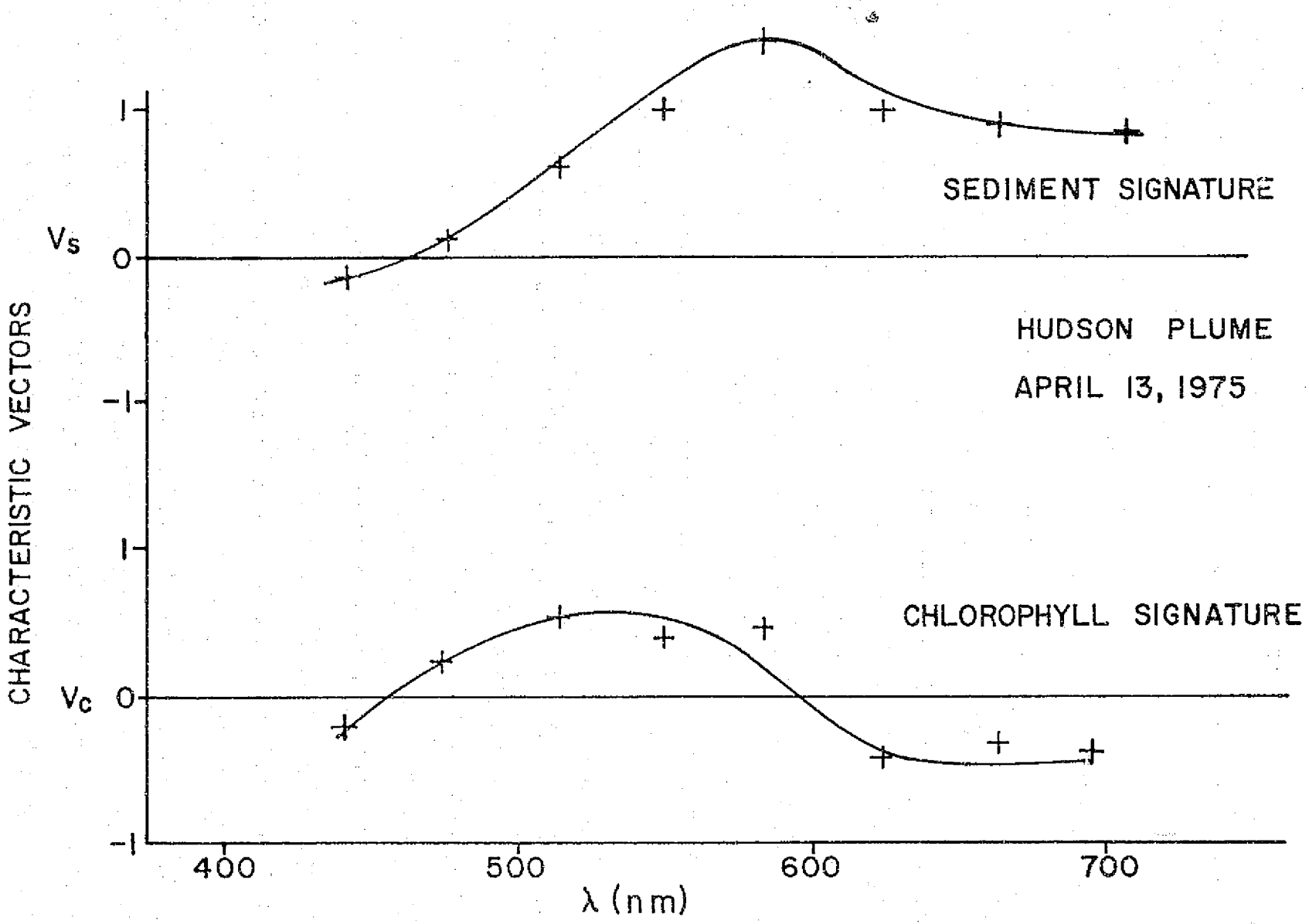

$$S = S_o + \log \langle S \rangle \, V_s + \log \langle C \rangle \, V_c$$

S=MEASURED RADIANCE $\langle S \rangle$ =SEDIMENT CONCENTRATION

S_o = MEAN RADIANCE $\langle C \rangle$ = CHLOROPHYLL CONCENTRATION

FIGURE 6 - CHARACTERISTIC VECTORS FOR SEDIMENT AND CHLOROPHYLL.

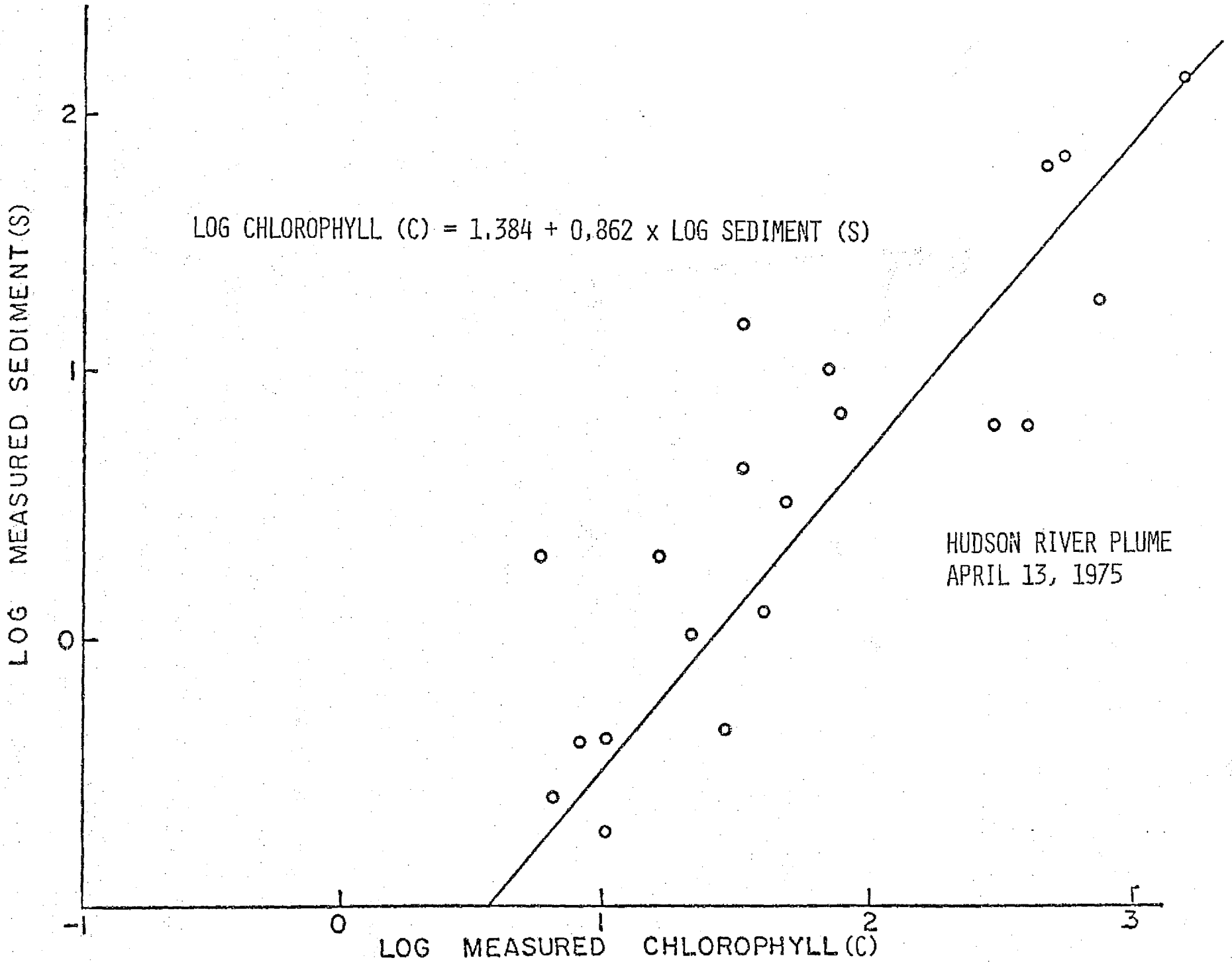

FIGURE 7 - LOG MEASURED CHLOROPHYLL VS LOG MEASURED SEDIMENT.

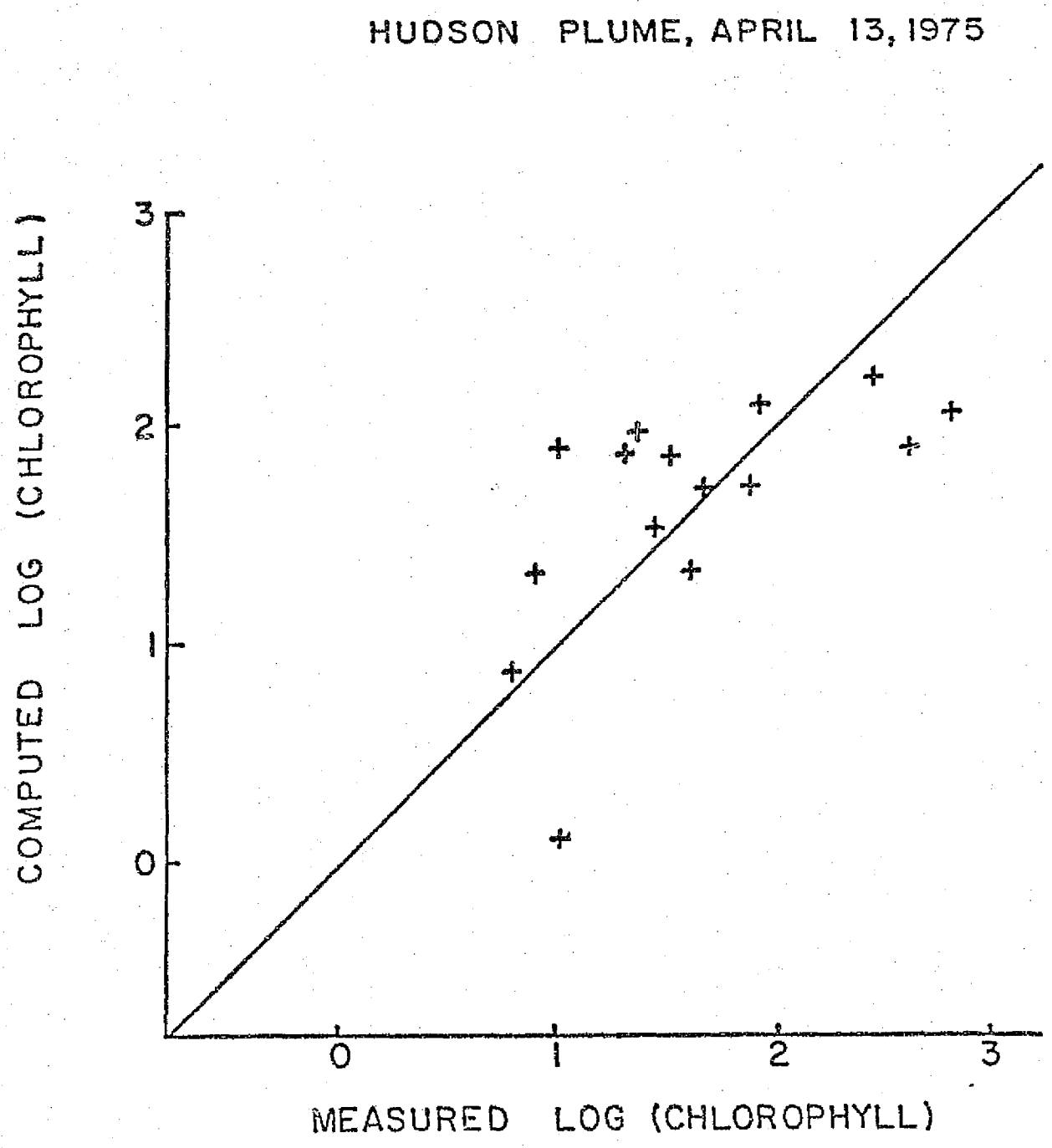

FIGURE 8 - LOG MEASURED CHLOROPHYLL VS LOG COMPUTED CHLOROPHYLL.

HUDSON PLUME, APRIL 13, 1975

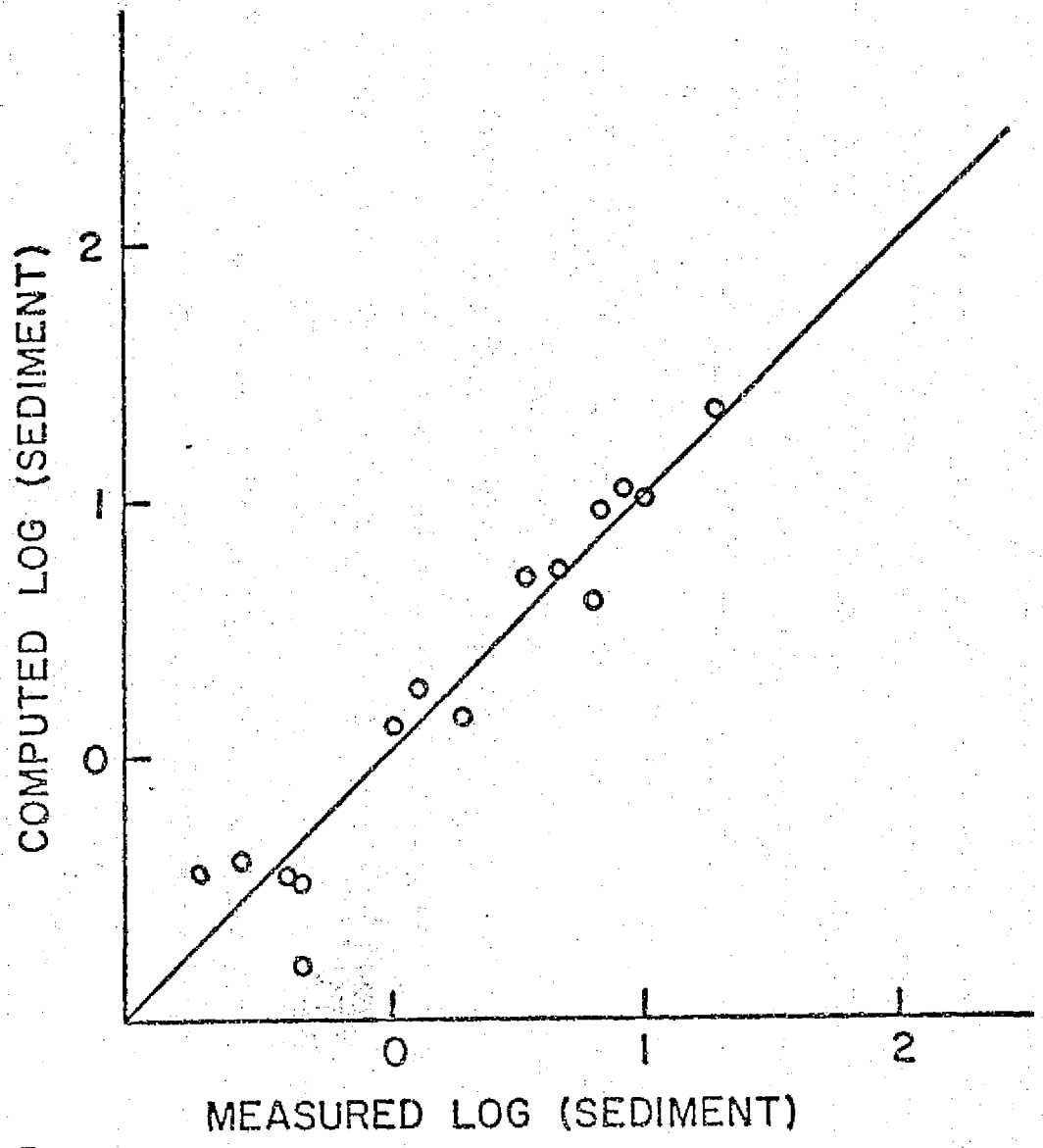

FIGURE 9 - LOG MEASURED SEDIMENT VS LOG COMPUTED SEDIMENT.

Preliminary Analysis of Ocean Color Spectra Measured With an Ebert Spectrometer During the NASA/NOAA Spring 1975 Experiment in the New York Bight

By

James L. Mueller

PRELIMINARY ANALYSIS OF OCEAN COLOR SPECTRA MEASURED WITH AN EBERT SPECTROMETER DURING THE NASA/NOAA APRIL 1975 MESA EXPERIMENT IN THE NEW YORK BIGHT

by

James L. Mueller

INTRODUCTION

During the April 1975 NASA/NOAA MESA experiment in the New York Bight, ocean color spectra were measured from a low flying aircraft. The short duration of available sampling flights precluded statistically correlating these ocean color spectra with simultaneous ground truth observations. Nevertheless, the ocean color spectra are suitable for comparison, using characteristic vector analysis, with earlier results[1,2] and for studying the spectral signature of the acid waste pollutant routinely dumped in the New York Bight Apex.

In radiometry, a "spectrum" is the distribution of radiant energy, or of some optical property of the medium, as a function of wavelength. The ocean color spectrum is defined as

$$U_j = \frac{N_j}{\bar{N}}; \; j = 1, 2, \ldots, 55, \tag{1}$$

where N_j is the upwelled radiance from the sea in the j^{th} 5 nanometer (nm) wide wavelength band between 420 and 695 nm, and the normalization factor $\bar{N}$ is the average radiance, i.e.

$$\bar{N} = 1/55 \sum_{j=1}^{55} N_j.$$

The spectrum U_j must be numerically parameterized before it can be efficiently correlated with other measurable properties of sea water. Mueller[1,2] reviewed previously proposed parameterizations of ocean color spectra[3-6] and applied the method of characteristic vectors to the problem. It was shown for a sample of ocean color spectra measured off Oregon, that the first four characteristic vectors of the sample covariance matrix yielded a highly accurate parameterization. To compare Mueller's earlier work with the MESA ocean color data, certain of those results must be recast in terms of the spectrum U_j rather than in terms of reflectance

$$R_j = \frac{N_j \bar{E}}{\bar{N} E_j}$$

where E_j and $\bar{E}$ are the incident irradiance spectrum and its wavelength average. This change must be made because there is no consistent means of estimating E_j for the independent ocean color samples that will be examined.

In the present report the characteristic vectors of U_j spectra from the MESA experiment will be compared with similar results from two other independent samples of ocean color spectra measured elsewhere. The purpose of this comparison is to test the working hypothesis that ocean color spectra may be parameterized, globally, with a few standard, characteristic basis vectors.

In addition, the spectral signature of the acid waste material routinely dumped in the New York Bight will be examined. It will be demonstrated that this material has a spectral signature that is uniquely different from any other ocean color spectrum yet observed.

CHARACTERISTIC VECTOR ANALYSIS OF COLOR SPECTRA

The use of characteristic vectors[7] to parametrize ocean color spectra was recently discussed by Mueller[1,2]. Morrison[8] gives a comprehensive discussion of the method within the general context of multivariate statistical analysis.

A spectrum U_{jn}, the n^{th} of a sample of N ocean color spectra, is parametrized by its first K principal components

$$Y_{kn} = \sum_{j=1}^{55} e_{kj}(U_{jn} - M_j); \; k = 1, 2, \ldots, K \; \& \; n = 1, 2, \ldots, N, \qquad (2)$$

where e_{kj} is the k^{th} characteristic vector of the sample covariance matrix, M_j is the sample mean spectrum, and the index j denotes one of 55 discrete wavelength bands. The inverse approximation relating the spectrum U_{jn} to its first K principal components Y_{kn} is

$$U_{jn} = M_j + \sum_{k=1}^{K} Y_{kn} e_{kj}; \; j = 1, 2, \ldots, J \; \& \; n = 1, 2, \ldots, N. \qquad (3)$$

The characteristic vectors e_{kj} are extracted from the sample covariance matrix such that e_{1j} is alined in the direction of maximum sample dispersion (i.e., it accounts for the largest possible proportion of sample variance). Then, e_{2j} is extracted in alinement with the largest remaining proportion of dispersion (sample variance) orthogonal to e_{1j}. And each succeeding unique characteristic vector accounts for a smaller percentage of sample variance than any of its predecessors. The accuracy with which a spectrum U_{jn} ($j = 1, 2, \ldots, 55$) is parametrized by its first K principal components Y_{kn} ($k = 1, \ldots, K$), therefore, is measured by the cumulative

percentage of sample variance accounted for by the first K characteristic vectors e_{kj}.

The "γ percent significant degrees of freedom" in ocean color spectra of a given sample will be defined as the independent scalar parameters which retain a specified cumulative percent (γ) of total sample variance. For each of the three samples considered here, there are five 99 percent significant degrees of freedom contained in $\bar{N}$ (overall brightness) and the first four principal components (Y_1, Y_2, Y_3, Y_4) (spectral shape parameters).

Thus far characteristic vectors applied only within the context of a single sample of ocean color spectra have been discussed. Now some elementary relationships between characteristic vectors of two independent samples of ocean color spectra must be considered. For convenience, consideration will be given only to samples with five 99 percent significant desgrees of freedom.

The characteristic vectors determined from a sample α of ocean color spectra are related to those determined from sample β by the equation:

$$e^{\alpha}_{ij} = \sum_{k=1}^{4} C^{\alpha}_{ki\beta} \cdot e^{\beta}_{kj} + \epsilon^{\alpha}_{ij\beta} \qquad (4)$$

where $\epsilon^{\alpha}_{ij\beta}$ is an error vector describing an orthogonal discrepancy between the two vector systems, and

$$C^{\alpha}_{ki\beta} = \sum_{j=1}^{55} e^{\alpha}_{ij} \cdot e^{\beta}_{kj} \quad (i, k = 1, 2, 3, 4) . \qquad (5)$$

The mean ocean color spectra of the two samples are related by the equations

$$M^{\alpha}_{j} = M^{\beta}_{j} + \sum_{k=1}^{4} B^{\alpha}_{k\beta} e^{\beta}_{kj} + \rho^{\alpha}_{j\beta} \qquad (6)$$

where $\rho^{\alpha}_{j\beta}$ is an error vector similar to $\epsilon^{\alpha}_{ij\beta}$ and

$$B^{\alpha}_{k\beta} = \sum_{j=1}^{55} e^{\beta}_{kj} \, (M^{\alpha}_{j} - M^{\beta}_{j}) \quad k = 1, 2, 3, 4. \tag{7}$$

It follows directly from equations (2) and (4) through (7) that the principal components of an ocean color spectrum are related, in the two characteristic vector systems, by the equation

$$Y^{\alpha}_{i} = \sum_{k=1}^{4} C^{\alpha}_{ki\beta} \, Y^{\beta}_{k} + \sum_{k=1}^{4} C^{\alpha}_{ki\beta} \, B^{\alpha}_{k\beta} + \delta^{\alpha}_{i\beta} \tag{8}$$

where $\delta^{\alpha}_{i\beta}$ are residual errors due to any unresolved orthogonality between the characteristic vectors of the two samples.

When the spectra U_j of sample α are parametrized with the sample β characteristic vectors, the cumulative proportion of total sample variance retained by the cross-sample parametrization is given by

$$V^{\alpha}_{\beta} = \sum_{i=1}^{4} v^{\alpha}_{i} \left[\sum_{k=1}^{4} \left(C^{\alpha}_{ki\beta} \right)^{2} \right] \tag{9}$$

where v^{α}_{i} is the proportion of sample variance associated with the i^{th} principal component Y_i, i.e., as determined with its own α-sample characteristic vectors.

The method of characteristic vectors may also be extended to study the spectral signatures of specific pollutants as contained in a spectrum of U^{ϵ}_{j}. This is possible, however, only if color spectra of water containing that pollutant were not included in the sample used to derive the characteristic

vectors. Given this circumstance, the α-sample principal components $Y_i^{\alpha\varepsilon}$ of U_j^{ζ} are computed as:

$$Y_i^{\alpha\zeta} = \sum_{j=1}^{55} e_{ij}^{\alpha} \, (U_j^{\zeta} - M_j^{\alpha}); \; i = 1, 2, 3, 4. \tag{10}$$

Then, the residual spectral signature of the specific pollutant is computed as:

$$S_j^{\alpha\zeta} = U_j^{\zeta} - [M_j^{\alpha} + \sum_{i=1}^{4} Y_i^{\zeta} \, e_{ij}^{\alpha}]. \tag{11}$$

If $|S|^{\alpha\zeta} = [\sum_{j=1}^{55} (S_j^{\alpha\zeta})^2]^{1/2}$ is significant relative to unity, then the pollutant may be detected in sea water solely on the basis of its unique residual spectral signature. On the other hand, should $|S|^{\alpha\zeta}$ be negligibly small, then except possibly in a relative sense, a pollutant-dominated spectrum U_j^{ζ} is not uniquely distinguishable from "ordinary" ocean color spectra in sample α.

EXPERIMENTAL RESULTS

Upwelled radiance spectra N_j were measured with an Ebert spectrometer aimed at nadir through the bottom of an NASA C-54 aircraft. The aircraft flew over the ocean at an altitude of 523 meters (1,700 ft), covering tracklines that included relatively clear offshore water, highly turbid Hudson River effluent, and pollutant dumps in the New York Bight Apex. The spectrometer's field of view was approximately 30°, thus including a circle approximately 270 meters in diameter. During the 1.5 seconds required to observe a single spectrum, aircraft motion displaced the field of view approximately 115 meters along the trackline.

A grating in an Ebert spectrometer reflects the diffracted spectrum through a slit. In this experiment, the slit was set to pass an approximately 2.5 nanometer (nm) wide band of wavelengths onto a photomultiplier tube. The grating is rotated to scan the spectrum across the slit, so that a time record of the photomultiplier's output voltage may be calibrated to yield radiance as a function of wavelength. For the MESA experiment, the GSFC Ebert spectrometer was calibrated using the diffuse integrating sphere at Goddard Space Flight Center.

A selected subsample of the observed spectra was digitized into 55 channels, each 5 nm wide over the wavelength interval 420 to 695 nm. This particular representation was selected to facilitate comparison with earlier results[1,2]. The individual radiance spectra were then calibrated and normalized to obtain ocean color spectra U_j as defined by equation (1). Five U_j spectra measured in the vicinity of the acid waste dump site were set aside for separate analysis. The remaining sample of 32 spectra U_{jn} ($j = 1, 2, \ldots, 55$; $n = 1, 2, \ldots, 32$) was then subjected to characteristic vector analysis.

The first four characteristic vectors e_{ij} ($i = 1, 2, 3, 4$; $j = 1, 2, \ldots, 55$) of the MESA sample covariance matrix are shown, together with the sample mean spectrum M_j ($j = 1, 2, \ldots, 55$), as dashed curves in figure 1. Also shown in figure 1 are similar results for Mueller's[1,2] Oregon data (OSU sample) and Hovis's[9] ocean color spectrum measurements made on his 1972 NASA Convair 990 flights (CV 990 sample). Inspection of table 1 shows that the first four characteristic vectors account for 99 percent of total sample variance in each of the three samples. Internally, therefore, each of the three

samples has exactly five 99 percent significant degrees of freedom associated with $\bar{N}$ and the first four principal components (Y_1, Y_2, Y_3, Y_4).

That the samples merely have the same number of 99 percent significant degrees of freedom is not, however, sufficient evidence to support the hypothesis that standard characteristic vectors are applicable to all three samples. Obviously the parameter $\bar{N}$ is common to all three samples. The key question, then, concerns the degree to which the characteristic vectors e_{ij} are mutually interchangeable between samples. Intersample agreement can be measured by the orthogonal discrepancy terms $\epsilon^{\alpha}_{ij\beta}$, $\rho^{\alpha}_{j\beta}$, and $\delta^{\alpha}_{i\beta}$ in equations (4) through (8), and by the percent of variance retention V^{α}_{β} in cross-sample representations (eq. (9)). Pending results of a larger sample analysis now in progress, part of which will correct for intersample spectrometer calibration discrepancies, $\rho_{i\beta}$ will be neglected and it will be assumed that

$$\delta^{\alpha}_{i\beta} \sim |\epsilon^{\alpha}_{i\beta}| = 1 - \{\sum_{k=1}^{4} (C_{ik\beta})^2\}^{1/2} \qquad (12)$$

Characteristic vector coupling coefficients $C^{\alpha}_{ik\beta}$ (eq. (5)) are given in table 2A for α = MESA and β = OSU samples, and in table 2B for α = MESA and β = CV 990 samples. The magnitude of orthogonal discrepancies $|\epsilon^{\alpha}_{i\beta}|$ as defined by equation (11), are given in table 3, together with cross-sample variance retention V^{α}_{β}.

As indicated by the large values of the diagonal elements $C^{\alpha}_{ik\beta}$ (table 2), the MESA characteristic vectors are reasonably well alined with their counterparts for the OSU and CV 990 samples. The percentage variance distributions are also similar, although the proportion (about 90 percent) of

sample variance associated with e_{1j} is larger than the corresponding proportion (approximately 80 percent) for the other two samples. This may be due, in part, to the relatively restricted subsample on which the present MESA results are based.

Of more importance than either of the variance direction similarities shown by tables 1 and 2, however, are the very small values of $|\varepsilon^{\alpha}_{i\beta}|$ in table 3. These values show that only a few hundredths of the total lengths of e_{1j} and e_{2j} are not completely transferable between any of the samples. And only about a tenth of e_{3j} and e_{4j} is not similarly transferable. Because of this overall cross-sample equivalence in the first four characteristic vectors, 96 percent to 97 percent of total sample variance is retained if MESA spectra are parametrized with OSU or CV 990 vectors, and vice versa. This result strongly implies that four standard characteristic vectors could well provide a common five percent significant degrees of freedom parametrization basis for the three samples of ocean color spectra.

Turning finally to the acid waste signature, two U^{ζ}_{j} spectra from within a recent acid waste dump and on U^{ζ}_{j} spectrum from 200 meters beyond the visible edge of the dump were selected for analysis. The two acid U^{ζ}_{j} spectra are shown as solid lines in figures 2A and 2B. The third U^{ζ}_{j} spectrum is in figure 2C. These spectra, together with the MESA mean and characteristic vectors, (fig. 1), were substituted into equations (10) and (11) to obtain residual spectral signatures $S^{\alpha\zeta}_{j}$, which are shown as dashed curves in figure 2. Obviously, the two acid U_j spectra have a significant residual spectral signature $S^{\alpha\zeta}_{j}$, whereas the third spectrum does not.

Visual comparison of the overall and residual acid spectra (figs. 2A and 2B) with the reflectrance spectrum of iron hydroxide powder (not shown) suggests

that a precipitate of that substance, rather than of iron oxide, may be responsible for the observed spectral signature of the acid dump.

CONCLUSIONS

The results of an ocean color spectrum analysis have been presented which use the method of characteristic vector. The following conclusions are made from the analysis:

1. There is strong evidence to support the working hypothesis that a standard set of a four characteristic basis vectors plus a standard "mean" vector may be used globally to parametrize "ordinary" ocean color spectra. An individual spectrum would be parametrized by its mean radiance $\bar{N}$ and four standard principal components (Y_1, Y_2, Y_3, Y_4) representing the five 97 percent significant degrees of freedom found in "ordinary" ocean color data. It is emphasized, however, that much additional data is required before such a system could be accepted for standard use. By specifying "ordinary" ocean color it is meant to exclude waters containing industrial and acid waste materials.
2. The acid waste material routinely dumped into the New York Bight appears to have a spectral signature with a unique component orthogonal to the characteristic vectors of ocean color spectra observed elsewhere. This unusual spectral signature may be caused by a FeOOH precipitate that forms after the pollutant enters the water. If constant from dump-to-dump and stable with time in the water, the residual spectral signature may be used to accurately discriminate the acid waste from, e.g., sediments or chlorophyll, and to map its dispersal patterns in remote ocean color imagery.

In closing, it is emphasized that the numerical results given here are preliminary and subject to modification in the future. The MESA and CV 990 spectra were measured with the same spectrometer, but in different configurations and based on separate calibrations. The OSU spectra were measured with a different spectrometer which was independently calibrated by a different method entirely. Errors in any or all of the radiance calibrations of the spectrometers used will contribute to the error terms $\varepsilon^{\alpha}_{ij\beta}$, $\rho^{\alpha}_{j\beta}$ and $\delta_{i\beta}$. Recognizing these errors, a method of estimating the spectral intercalibration discrepancies between samples has been derived. Preliminary calculations suggest that using this method to adjust all spectra to a common calibration base virtually eliminates mean spectral orthogonal discrepancies $\rho^{\alpha}_{j\beta}$. Corresponding improvements in $\varepsilon^{\alpha}_{ij\beta}$ and $\delta^{\alpha}_{i\beta}$ are expected.

REFERENCES AND FOOTNOTES

1. J. L. Mueller. The Influence of Phytoplankton on Ocean Color Spectra. (PhD Thesis, Oregon State Univ., Corvallis, 1973).

2. J. L. Mueller, Applied Optics. 15, 394 (1976).

3. G. L. Clarke, G. C. Ewing, and C. J. Lorenzen. Science 167, 1119 (1970).

4. P. G. White, in Second Annual Earth Resources Program Status Review, 16-18 Sept. 1969. (NASA Manned Spacecraft Center, Houston, Texas. 1969).

5. J. C. Arveson, E. C. Weaver, and J. P. Millard, Rapid Assessment of Water Pollution by Airborne Measurement of Chlorophyll Content. (American Inst. of Aeronautics and Astronautics Paper 71-1097, 1971).

6. I. V. Semenchenko, Oceanology 6(6), 861 (1967).

7. In references 1 and 8 the term eigenvector is precisely synonynous with our usage of characteristic vector, which follows the usage of Ref. 2.

8. D. F. Morrison, Multivariate Statistical Methods. (McGraw-Hill, New York, 1967).

9. W. A. Hovis, M. L. Forman, and L. R. Blaine, Detection of Ocean Color Changes from High Altitudes (NASA Rep. X-652-73-371, 1973).

Table 1. Percentage of total sample variance associated with the first four characteristic vector of sample convariance matrix for three independent samples of ocean color spectra.

	OSU Sample	CV 990 Sample	MESA Sample
e_{1j}	78.6%	82.9%	90.8%
e_{2j}	17.1%	15.1%	5.9%
e_{3j}	2.4%	1.2%	1.3%
e_{4j}	0.9%	0.3%	0.7%

Table 2. Characteristic vector coupling coefficients $C^{\alpha}_{ki\beta}$ and $C^{\beta}_{ik\alpha}$, defining the projections of characteristic vectors e^{α}_{ij} of sample α on those e^{β}_{kj} of sample β and vice versa for MESA ocean color data in comparison with OSU and CV 990 samples. (See text for explanation of terms).

A. MESA (sample α) vs OSU (sample β).

		OSU (Sample β)			
	i \ k	1	2	3	4
MESA (Sample α)	1	0.850	-0.413	0.040	0.306
	2	0.417	0.861	0.125	0.033
	3	-0.170	-0.147	0.858	0.198
	4	-0.227	0.168	-0.132	0.812

B. MESA (Sample α) vs CV 990 (Sample β).

		CV 990 (Sample β)			
	i \ k	1	2	3	4
MESA (Sample α)	1	0.933	-0.255	0.043	0.241
	2	0.288	0.915	0.044	-0.111
	3	-0.027	-0.141	0.836	-0.197
	4	-0.169	0.199	0.320	0.746

Table 3. Cross-sample unresolved orthogonality errors $|\varepsilon^{\alpha}_{i\beta}|$ and percent of cross sample variance retention V^{α}_{β} for MESA ocean color spectra compared to OSU and CV 990 samples. (See text for explanation of terms.)

Sample α	OSU	MESA	CV 990	MESA
Sample β	MESA	OSU	MESA	CV 990
$\lvert\varepsilon^{\alpha}_{1\beta}\rvert$	0.006	0.012	0.002	0.009
$\lvert\varepsilon^{\alpha}_{2\beta}\rvert$	0.035	0.020	0.033	0.019
$\lvert\varepsilon^{\alpha}_{3\beta}\rvert$	0.091	0.122	0.129	0.102
$\lvert\varepsilon^{\alpha}_{4\beta}\rvert$	0.130	0.109	0.147	0.184
V^{α}_{β}	96.8%	95.7%	97.4%	97.1%

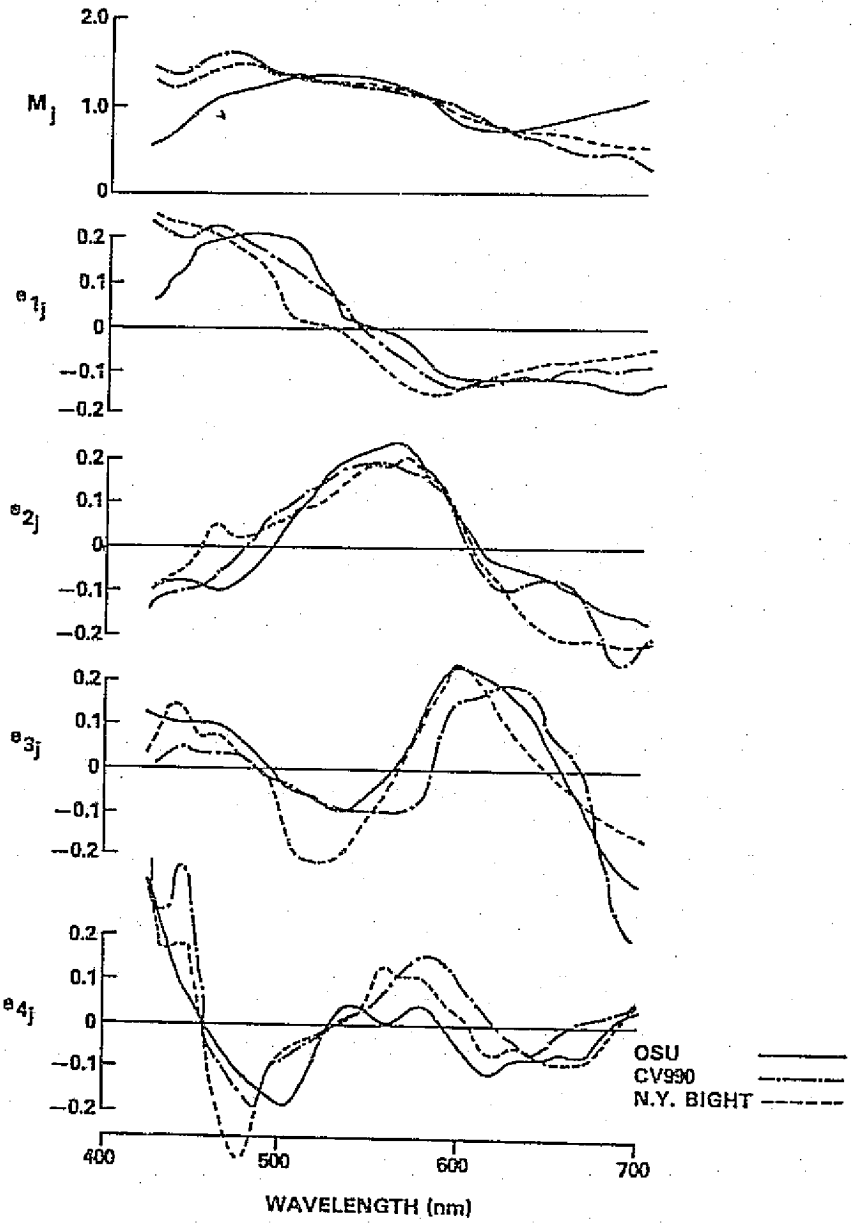

Figure 1. - The mean vectors (M_j) and first four characteristic vectors (e_{ij}) of the sample covariance matrices for three samples of ocean color spectra measured in different geographical regions. Vectors M_j are in units of relative radiance. Vectors e_{ij} are dimensionless and of unit length.

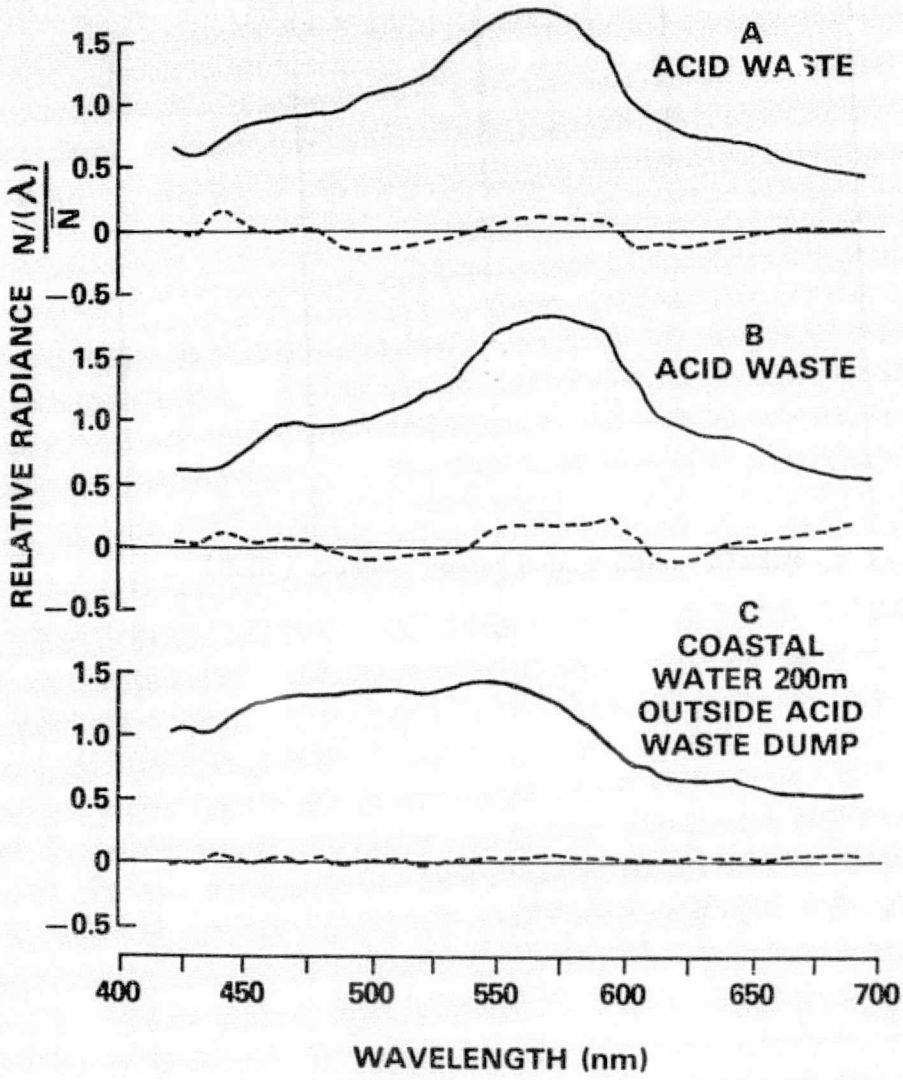

Figure 2.- Ocean color spectra (solid curves) and residual signatures (dashed curves) obtained as described in the main text in the vicinity of the acid waste dump in the New York Bight.

MULTICHANNEL OCEAN COLOR SENSOR (MOCS)

By

Gary W. Grew

MULTICHANNEL OCEAN COLOR SENSOR (MOCS)

by

Gary W. Grew

SUMMARY

An algorithm for the remote detection and quantification of chlorophyll-A in coastal zone waters has been established for concentrations above 15 µg/l. For concentrations above and below this limit chlorophyll-A has been detected and identified by a signature extraction technique developed for analysis of data collected with (Multichannel Ocean Color Sensor), (MOCS) a multispectral scanner. This paper presents MOCS data collected in the New York Bight in April 1975 as part of an NASA-NOAA Remote Sensing Program. Spectral signatures of algae, acid waste, and sediment are presented.

INTRODUCTION

It has long been recognized that the color of the ocean can be altered by the presence of algae. It is natural, therefore, to expect that man would investigate the possibility of remotely identifying and quantifying algae from aircraft and spacecraft. The desirability of generating contour plots of algae in the ocean is clear. Regions abundant with algae are of

Acknowledgment: The author is grateful to National Oceanic and Atmospheric Administration personnel, in particular Dennis S. Clark of the National Environmental Satellite Service, and Terry Nelson of the Atlantic Oceanographic and Meteorological Laboratory, for use of their unpublished ground truth information.

particular interest to various user organizations for a number of reasons. For example, in order to support large populations of algae, regional waters must be rich in nutrients. The sources and circulation of these nutrients are important directly or indirectly to the following groups: (1) to oceanographers in studying ocean and coastal currents (upwelling currents in particular), (2) to commercial fishermen in locating feeding grounds for fish, (3) to ecologists in locating sources of pollution, and (4) to marine biologists in studying red tides. In the latter case, monitoring of red tides, dense populations of certain dinoflagellate algae, are important because they can be toxic to sea life and man and have been detrimental to the seafood industry, especially in the states of Florida, Massachusetts, and California. Thus, interest in large area mapping of algae in the sea by remote-sensing techniques has been brewing since the onset of the U.S. space program.

The feasibility of remotely detecting algae has been demonstrated by a number of researchers.[1-3] However, it appears that, as yet, no generally accepted algorithms for the identification and quantification of algae remotely has been established. The major difficulty is that the total upwelling light is dependent on so many variables, as illustrated in figure 1 The variables shown in the figure are dependent upon such factors as solar elevation, atmospheric conditions, sea surface roughness, and composition and vertical distributions of the suspensoids in the sea, water depth, and ocean floor composition. Thus, an algorithm for algae that appears to work for one set of data may not work for a different set. An algorithm must be found that negates or minimizes the influence of all other variables.

Fortunately, algae possess characteristic absorption spectra which can be used to some, as yet unknown, degree. The ability of plant cells to absorb light depends upon their pigments. Figure 2 shows examples of absorption spectra measured by Yentsch.[4] These curves show a strong absorption peak at about 675 nm in the red region of the spectrum due primarily to chlorophyll-A and a second broader peak at 450 nm in the blue region resulting from the combined absorption of chlorophyll and carotenoid pigments. The use of these two major absorption characteristics of plants is currently under investigation by the author for remotely quantifying algae in the sea. As will be discussed in later paragraphs, the chlorophyll-a peak in the red is useful at high concentrations (>15 μg/l of chlorophyll-a), but not at lower concentrations where the strong absorption characteristics of water (fig. 3) overshadow that of algae.[5] At lower concentrations the absorption maxima in the blue is still usable, but it becomes increasingly more difficult to separate algae from sediment, the other major suspended matter in the ocean. It is the purpose of this paper to report the progress to date made in resolving these problems.

The data presented in this paper were collected using Multichannel Ocean Color Sensor (MOCS), a multispectral scanner. This instrument was developed under NASA contract by TRW, Inc., as part of the Advanced Applications Flight Experiments Program (AAFE). MOCS is being flown on an NASA Wallops C-54 aircraft with the prime objective of collecting ocean color data that can be used in a computer program developed at Langley for extracting spectral signatures and algorithms that uniquely identify algae, sediment, and pollutants in our coastal waters. Results presented in this report were provided by MOCS data collected on an NASA-NOAA flight in the New York Bight

on April 13, 1975. A good data set of chlorophyll spectra was collected on that mission. This data set is supported by some ground truth information provided by NOAA.

MOCS INSTRUMENT DESCRIPTION

MOCS is a visible imaging spectroradiometer which performs multispectral scanning electronically. It has no moving parts. MOCS was specifically designed for measurements of small differences in ocean color from space. It measures the intensity in 20 spectral bands at each of 150 spatial sites of the ocean across the field of view. MOCS is unique in that it uses only one detector and, as a result, it is compact and very light, weighing only 23 pounds.

Figure 4 is a schematic of the optical arrangement of MOCS and a listing of its specifications. The results of recent measurements of the center frequency of each band are given in table 1. In operation, light from the water is focused by the objective lens on the entrance slit. The instrument is designed to form a high-quality optical image of the ocean surface on the slit, so that light from one edge of the field of view is imaged at one end of the slit, light from the center of the field is imaged at the center of the slit, and so forth. The light is then collimated, dispersed by a blazed transmission diffraction grating, and reimaged on the face of the image dissector. The resulting image consists of a large number of adjacent spectra, each one composed of radiation coming from a different site across the instantaneous field of view. The spectra are scanned in sequence in a raster pattern on the photosensitive surface of the tube. The resulting video signal is a measure of the spectral intensities of the light coming from each

of 150 spatial sites. The scan rate is such that the whole raster (one frame) is read out in the time (286 msec) it takes the spacecraft or aircraft to move forward over the ocean one resolution element. The scan is then repeated at a rate of about 3.5 frames/sec to give contiguous coverage of the ocean. MOCS has a 17.1 degree field of view and a spatial resolution of 2 by 4 milliradians.

The present MOCS system has an alternate mode of operation made possible by changing the image dissector. In this mode the spectral resolution (5 nm) is increased by a factor of 3 at the expense of a factor of 3 reduction in spatial resolution.

The output of MOCS is fed to an A/D converter and stored on magnetic tape. The bit rate from the converter is 137 kbits/seconds. A detailed description of MOCS and its associated electronics can be found in reference 6. Figure 5 is a photograph of MOCS.

NEW YORK BIGHT MISSION

Remote-sensing experiments were conducted in the New York Bight between April 7-17, 1975, as part of cooperative program between NASA and the National Oceanic and Atmospheric Administration (NOAA). The objective of this mission was to evaluate multispectral, infrared, microwave, and photographic remote-sensing techniques for determining surface circulation features and for detecting sediment, chlorophyll, and other water quality parameters in the New York Bight.[7] This mission was one of several Marine Ecosystems Analysis (MESA) programs that are being planned by NOAA. The MESA program is focused on providing information to better understand and minimize man's impact on the coastal zone.

Aircraft flights of the MOCS Experiment were conducted on April 10th and April 13th. The aircraft flight lines, environmental conditions, and water masses were generally the same on both days. The surface winds and, therefore, the waves were higher on April 13th. Good MOCS data were collected on both days and analysis of the data revealed similar results. Since more extensive ground truth data were collected by NOAA on April 13th, that mission is presented here. MOCS and other experiments were flown on a Wallops C-54 aircraft at 5.33 km altitude. The flight lines consisted of five parallel tracks about 3.35 km apart and 55 km long in northwest-southeast direction as shown in figure 6. These flight lines are superimposed on an NOAA generated map showing (1) the locations of water samples collected by helicopter, (2) the chlorophyll-a concentrations measured from these samples, and (3) possible contour lines of the apparent algae bloom on April 13th.

Three sampling stations near Sandy Hook indicated high concentrations of chlorophyll-a (fig. 6). Based on discussions with NOAA of their preliminary analysis of the ground truth data, it appears highly probable that the primary constituent in this plume was algae. Figure 7 is a plot of averaged MOCS data for spectral band 5 (460 nm) along line D beginning just offshore of Staten Island. A plot of the ratio of band 14 (601 nm) and band 5 for the same data is shown in figure 8 along with the approximate location of ground truth points collected by means of helicopter and the NOAA ship Kelez. The chlorophyll-a levels and the times between each water sample pickup and the C-54 overflight are indicated.

The ratio plotted in figure 8 is used by the author as an "indicator" of turbidity. Selection of these bands was based on the examination of a large number of MOCS spectra which revealed that the maxima and minima of the

spectral variations of light from the sea were at or were near bands 14 and 5, respectively. Note that the inflection point of the attenuation length curve in figure 3 occurs at band 14. Under ideal conditions (clear, windless day and solar elevation 20° - 50°) this turbidity indicator (TI) ratio using uncorrected MOCS data is about 0.28 for clear water and 0.60 for very turbid water.

Figure 8 indicates turbid water in the lower bay between Staten Island and Sandy Hook. The plume boundary beyond Sandy Hook is quite evident. Beyond the plume there is a relatively clear water region followed by a sulfuric acid waste dump. By inspection the correlation between the TI ratio and the chlorophyll-a levels is reasonably good. Figures 9 and 10 are plots of the TI ratio for all five flight lines on April 13th and April 10th. The turbid plumes and acid waste dumps are evident in both figures.

In the following paragraphs a signature extraction technique is outlined and at the same time spectral signatures of the plume water and acid waste in the Bight are presented.

SPECTRAL SIGNATURE EXTRACTION

As previously stated, many environmental parameters influence the spectra of upwelling light from the sea. The contribution of the backscattered light from a particular suspensoid is often a small percentage of the total signal. Thus, spectral data collected over similar water masses but under different environmental conditions yield different spectra. It is, therefore, extremely difficult to extract any information from a single spectrum. An investigator must examine the variations in the spectral data that result from variations in the concentrations of a suspensoid.

The MOCS data used here to demonstrate the MOCS signature extraction technique is a set of spectra collected on April 13th along line D. This data set was collected in about 20 seconds over a 1-mile path in a region where the chlorophyll-a concentration is assumed to have varied between 6 and 14 μg/l (see fig. 8). This assumption is based on the ground truth and MOCS data consistency. Figure 11 shows rather uninspiring sample reflectance spectra from this "chlorophyll" data set. One needs to examine the spectral differences between these spectra. Figure 12 shows plots of the fractional differences between spectra selected at random from the data set. Although interesting features appear, they are partially lost in the "noise." A technique is needed to extract an average fractional difference spectrum. This can be derived in the following manner.

In figure 12 there appear to be fair correlations between spectral bands. For bands 12 (568 nm) and 14 (601 nm), for example, a linear regression equation can be determined for the chlorophyll data set of the form

$$I_{12} = A\, I_{14} + B \tag{1}$$

where $I_{12}(I_{14})$ is the signal of band 12 (band 14) for a given spectrum. A and B are constants. For the data set, the correlation coefficient for equation (1) was found to be 0.94. Likewise, an equation and correlation coefficient can be determined for each of the other 18 MOCS spectral bands with respect to band 14. These equations can be written

$$I_i = A_{i,14}\, I_{14} + B_{i,14} \qquad \begin{matrix} i = 1, 2 \ldots 20 \\ i \neq 14 \end{matrix} \tag{2}$$

Now the relative fractional change, $g(i,14)$, for band i for the curves in figure 12 can be written

$$g(i,14) = \frac{1}{\hat{I}_i} \frac{dI_i}{dI_{14}} \tag{3}$$

or from equation (2)

$$g(i,14) = \frac{A_{i,14}}{\hat{I}_i} \qquad \begin{matrix} i = 1, 2 \ldots 20 \\ i \neq 14 \end{matrix} \tag{4}$$

where $\hat{I}_i$ is the average signal of band i. Plots of $g(i,14)$ (normalized by the peak value of $g(i,14)$) and their corresponding correlation coefficients for the chlorophyll data set are shown in figures 13 and 14, respectively. Compare figures 12 and 13. Figure 13 can be considered to be a variant spectral signature of the chlorophyll data set. Figure 15 shows plots of variant spectral signatures determined from 50 different subsets of 75 spectra each from the chlorophyll data set. The plot in figure 13 is actually an average $g(i,14)$ of the data in figure 15.

Selection of band 14 in Eq. (4) was somewhat arbitrary. For a selected band j equation (4) can be rewritten in general as

$$g(i,j) = \frac{A_{i,j}}{\hat{I}_i} \qquad \begin{matrix} i = 1, 2, \ldots 20 \\ i \neq j \end{matrix} \tag{5}$$

A normalized variant spectral signature using $j = 12$ is plotted in figure 16. Figures 13 and 16 are essentially the same. Note that the undefined

quantity g(12,12) has been artifically added to figure 16 by interpolation using the values of bands 11, 12, and 13 in figure 13. The variable $\hat{I}_i$ in equation (5) re-introduces the atmospheric scattering component of the upwelling light into the spectral signatures. This component, however, does not seriously influence the spectral features; it merely decreases the magnitudes of g(i,j), particularly in the blue bands. The term is used for two basic reasons. First, the algorithms selected for each suspensoid will probably consist of ratios of two or more spectral bands. Variations in these ratios depend on the fractional changes, $\Delta I_i/I_i$, of the <u>total</u> signal for each band. Second, g(i,j) is independent of the sensor used, that is, for all ocean color systems at the same altitude, the spectral signature of a particular water mass obtained by means of equation (5) would be identical. No sensor calibration is required.

Further examples of variant spectral signatures extracted for the April 13th mission are shown in figure 17. The data set for this case was collected over a sulfuric acid waste dump in the New York Bight. Differences between the chlorphyll and acid waste signatures can be seen in figure 18.

ALGAE

Additional algae signatures shown in figure 19 were extracted from the New York Bight data. One was extracted from a data set in which the chlorophyll-a concentration varied between 14 and 24 µg/l along line D on April 13th (see fig. 8). The second signature was obtained from the plume on April 10th. Other similar spectra have been extracted from data collected with MOCS in the Chesapeake Bay region.

A prominent feature of these signatures is the chlorophyll-a absorption peak at band 19 (678 nm) in the red region of the spectrum. Note that the absorption peak is negative going in the reflectance spectra (fig. 19) and positive going in the absorption spectra in figure 2. A possible secondary absorption peak due to chloroph. l-a or some other pigment is evident at band 16 (631 nm). Absorption in the blue region of the spectrum due to chlorophyll-a and carotenoid pigments is indicated by the sharp slopes of the spectra beginning at band 14 (601 nm) and leveling off near band 9 (521 nm).

Since the relative signal of each band in figure 19 is positive, some of the variable component of the upwelling light is being backscattered rather than absorbed by the algae pigments. Whether this backscattering is due primarily to algae itself or some other process in the sea is unclear. Further distortion of the absorption spectra due to increased backscattering is evident in figure 20. This signature was extracted from a data set which included spectra all along line D from Staten Island to the plume boundary, excluding shallow water regions. A more extensive knowledge of the composition of the suspended matter in the water is needed before these spectral signatures can be understood.

Even so, the chlorophyll-a absorption in the red region of the spectrum should be useful to some extent for quantifying algae. As the concentration of algae increases this chlorophyll-a feature becomes more pronounced. This principle is illustrated in figure 21 in which the ratio I_{19}/I_{17} versus the ratio of I_{20}/I_{19} is plotted for data points along line D. As the chlorophyll-a feature becomes more prominent with increasing concentration I_{19}/I_{17} decreases and I_{20}/I_{19} increases as verified by the ground truth data.

With the exception of the "tail" in the lower right of the plot, a good linear relationship exists between these ratios, and should, therefore, be useful in quantifying chlorophyll-a in the sea. Analysis of the data points in the "tail" indicates that this deviation is due to bottom reflection in very shallow water (<3 meters). Once the effect of shallow water is clear, an optimum algorithm for chlorophyll in very shallow water can be selected using spectral bands 17, 19, and 20. Perhaps a combination of the two ratios, I_{19}/I_{17} and I_{20}/I_{19}, should be used. For example $I_{20} \cdot I_{17}/(I_{19})$ is plotted in figure 22 versus I_{20}/I_{19} for comparison. Notice the effect of the shallow water data for each ratio.

Since only a very few data points occur over very shallow water, the ratio I_{20}/I_{19} was used in figure 23 to generate the false color map of chlorophyll-a concentration along line D. The algorithm used for this map was

$$N = C \cdot \frac{I_{20}}{I_{19}} + D \ , \qquad (6)$$

where N is the chlorophyll-a concentration and C and D are constants. Notice the ground truth measurement of 32.2 µg/l in figure 6 at a station off Sandy Hook, but outside the field of view of MOCS for line D. It is in agreement with the color coded level, $\geq$29 µg/l, indicated near Sandy Hook in figure 23, which was determined from equation (6). Figure 24 shows plots of I_{20}/I_{19} for the five flight lines on April 13th. The algae plume appears to be quite strong in New York's Lower Bay and along the New Jersey shore in agreement with the ground truth data in figure 6. Line A shows high concentrations of algae in Rockaway Inlet and much lower concentrations offshore of

Rockaway Beach as verified also in figure 25. A similar plume existed on April 10th as shown in figure 26 except that it extended farther seaward and its boundary was more sharply defined.

As demonstrated by the data in figures 21 and 25, the chlorophyll-a peak at band 19 does not appear to be useful for quantifying algae much below 15 μg/l. As the algae population thins out, absorption of light by the ocean increases. A point is reached in which absorption of light by water is much greater than by the chlorophyll-a pigment at band 19 and the feature becomes lost in the noise. Thus, for low concentrations, another algorithm must be found - one using spectral bands in the blue and green regions where absorption by water is not as strong. Several promising algorithms are currently under investigation.

SEDIMENT

Two authors demonstrate elsewhere in this document that there is a high correlation between the sea truth measurements in the Bight of suspended solids and chlorophyll-a. This result practically precludes the use of this sea truth data to separate out these two suspended materials. Moreover, this high correlation suggests that the primary constituent in the plume was algae, as previously indicated.

A variant spectral signature of sediment, compared in figure 27 with an algae signature, has been extracted from MOCS data on another mission (ref. 8). This sediment signature exhibits no unique features, suggesting that clear separation of sediment from other constituents in the ocean may be limited. However, two separation techniques are currently under investigation by the author. Their preliminary results are beyond the scope of this report.

CONCLUDING REMARKS

Variant spectral signatures of algae, sediment, and acid waste have been obtained by a signature extraction technique developed specifically for analysis of MOCS data. The signatures were normalized such that they are independent of the ocean color sensor used; no instrument calibration is required. As demonstrated in this paper, a distinct advantage of the variant spectral signatures is that they can be used directly to establish algorithms.

The chlorophyll-a absorption peak in the red region of the spectrum is clearly evident in the spectral signatures of algae. This feature appears to be useful for quantifying chlorophyll-a above about 15 μg/l by use of bands 17 (647 nm), 19 (678 nm), and 20 (694 nm). A comparison between the ratios I_{19}/I_{17} and I_{20}/I_{19} clearly separates out chlorophyll-a for the algae in the New York Bight on April 10th and 13th. The latter ratio can be used in deep water. For very shallow water (<3 meters) perhaps the ratio $I_{20} \cdot I_{17}/(I_{19})^2$ should be used. Whether or not these algorithms can be used for most saltwater and freshwater species is, of course, uncertain.

References

[1]Clarke, G. L., Ewing, G. C., and Lorenzen, C. J., "Spectra of Backscattered Light From the Sea Obtained From Aircraft as a Measure of Chlorophyll Concentration," Science, 161, 1970, pp. 1119-1121.

[2]Duntley, Serbert Q., "Detection of Ocean Chlorophyll From Earth Orbit," Fourth Annual Earth Resources Program Review, Vol. IV, Presented at the Manned Spacecraft Center, Houston, Texas, January 17-21, 1972.

[3]Grew, Gary W., "Remote Detection of Water Pollution With MOCS: An Imaging Multispectral Scanner," Presented at the Second Conference on Environmental Quality Sensors, Las Vegas, Nevada, October 10-12, 1973.

[4]Yentsch, C. S., "The Influence of Phytoplankton Pigments on the Color of Sea Water," Deep-Sea Research, 7, 1960, pp. 1-9.

[5]Duntley, Serbert Q., "Light in the Sea," Journal of Optical Society of America, 53, 1963, pp. 214-233.

[6]White, P. G., Jenkin, K. R., Ramsey, R. C., and Sorkin, M., "Development and Flight Test of the Multichannel Ocean Color Sensor (MOCS)," NASA CR-2311, 1973.

[7]Usry, J. W., and Hall, J. B., Jr., "National Aeronautics and Space Administration Operations - Remote Sensing Experiments in the New York Bight, April 7-17, 1975," NASA TM X-72802, 1975.

[8]Grew, Gary W.; Remote Detection of Chlorophyll-A in Coastal Waters. Presented at the Fifth Annual Remote Sensing of Earth Resources Conference, Tullahoma, Tennessee, March 29-31, 1976.

Table 1 MOCS Spectral Bands

Band	Center wavelength (nanometers)	Band	Center wavelength (nanometers)
1	400	11	552
2	415	12	568
3	430	13	584
4	445	14	601
5	460	15	616
6	475	16	631
7	490	17	647
8	506	18	663
9	521	19	678
10	537	20	694

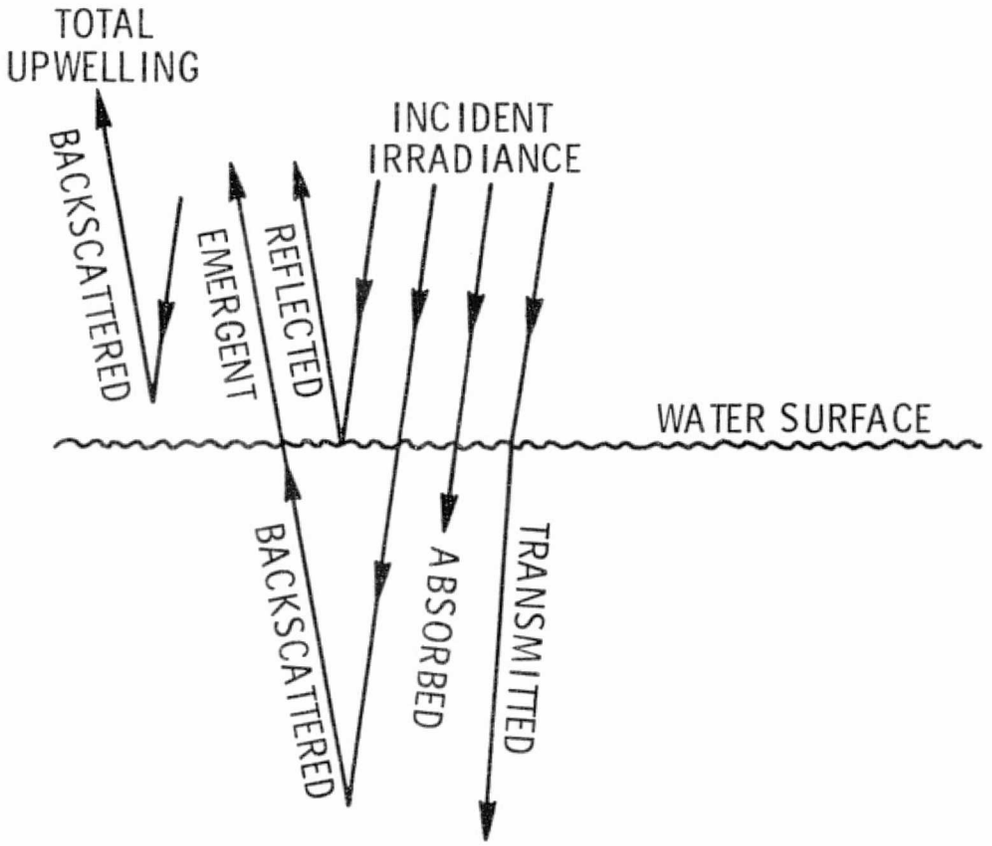

Figure 1.- Interactions of light with the atmosphere and the ocean.

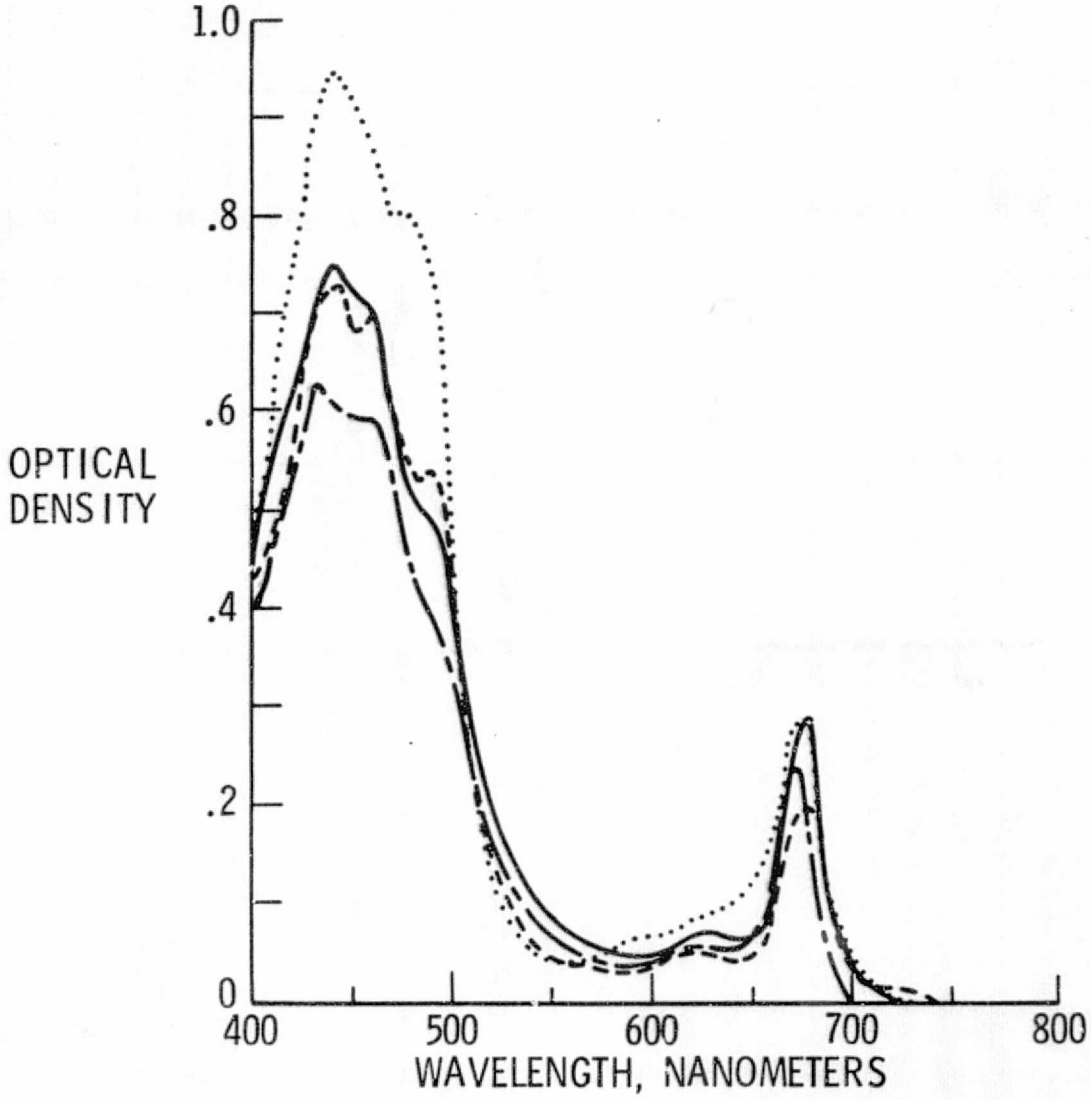

Figure 2.- Absorption spectra of extracts of plankton algae (from Yentsch[4]).

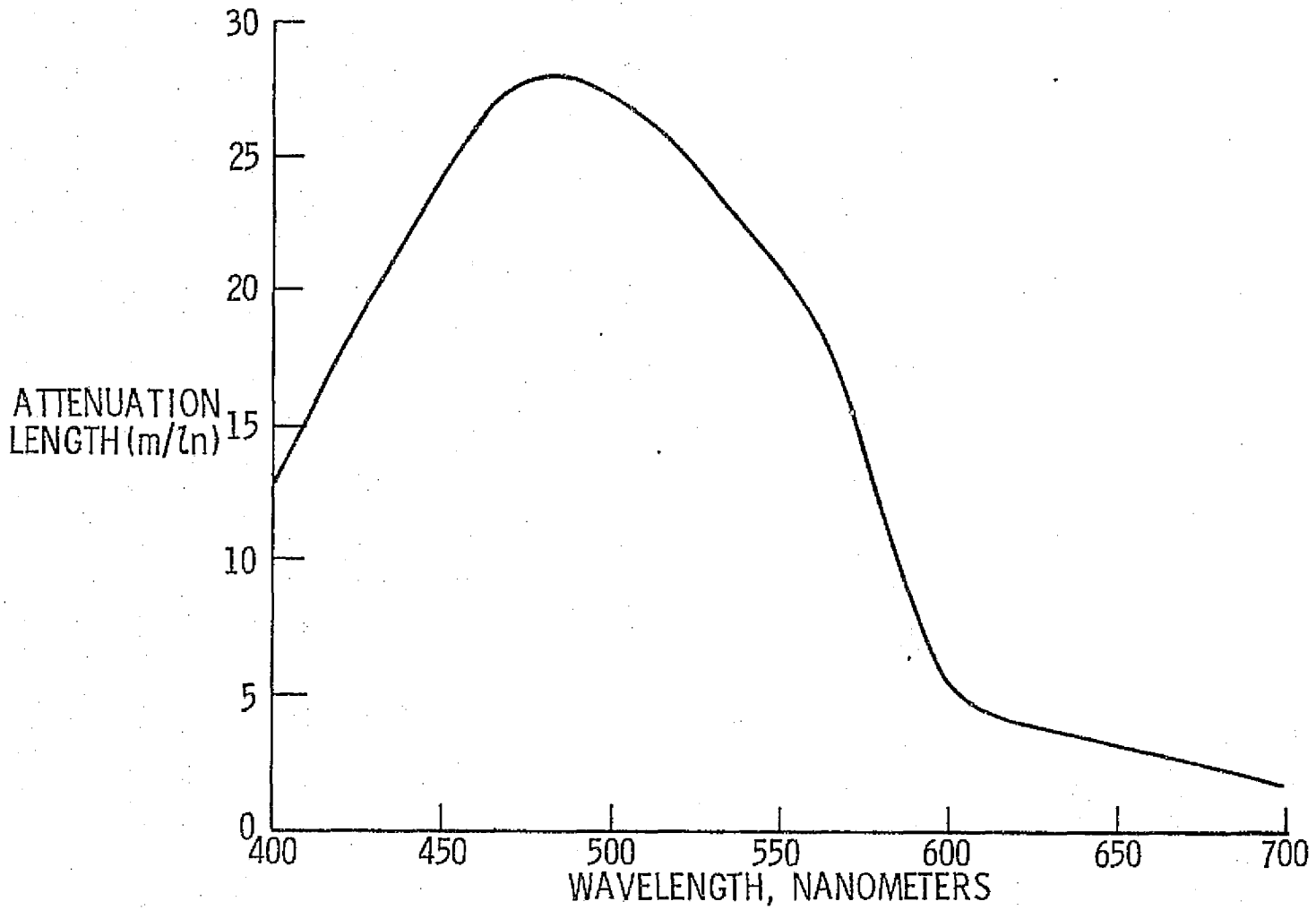

Figure 3.- Attenuation length or the reciprocal of the volume attenuation coefficient of distilled water.[5]

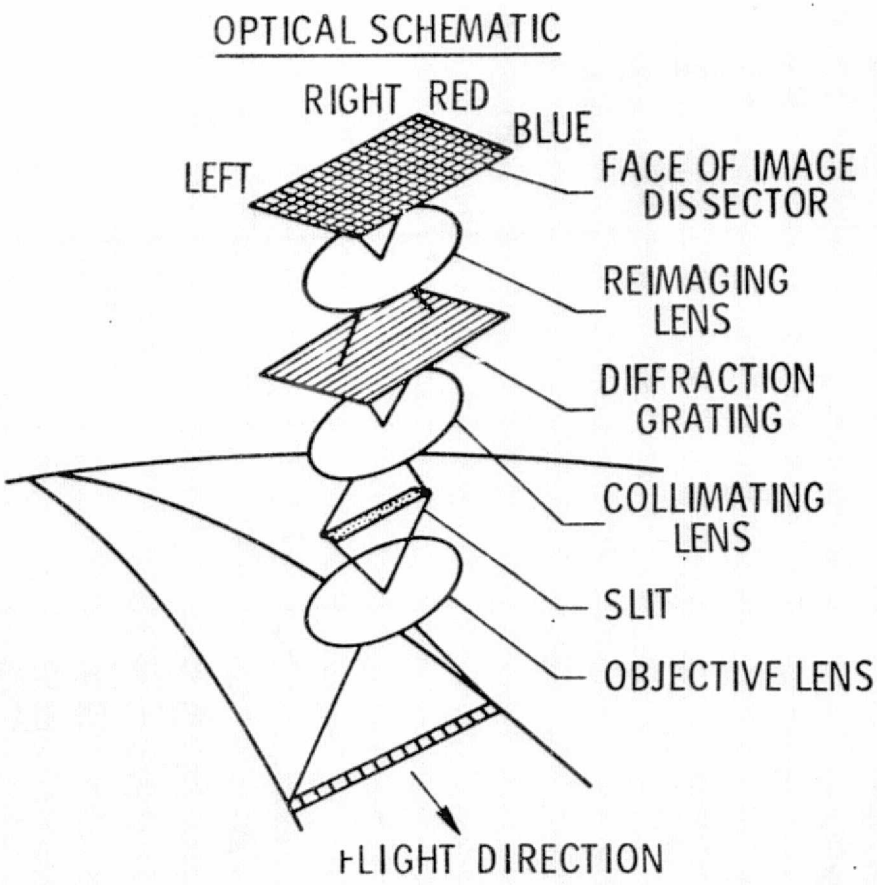

SPECIFICATIONS

400-700 nm SPECTRAL RANGE

15 nm SPECTRAL RESOLUTION

20 SPECTRAL BANDS

150 SPECTRA/ SWATH WIDTH

17.1^{0} FIELD OF VIEW

22.5 pounds

7.5 watts

.35 cubic feet

Figure 4.- Optical schematic and specifications of MOCS.

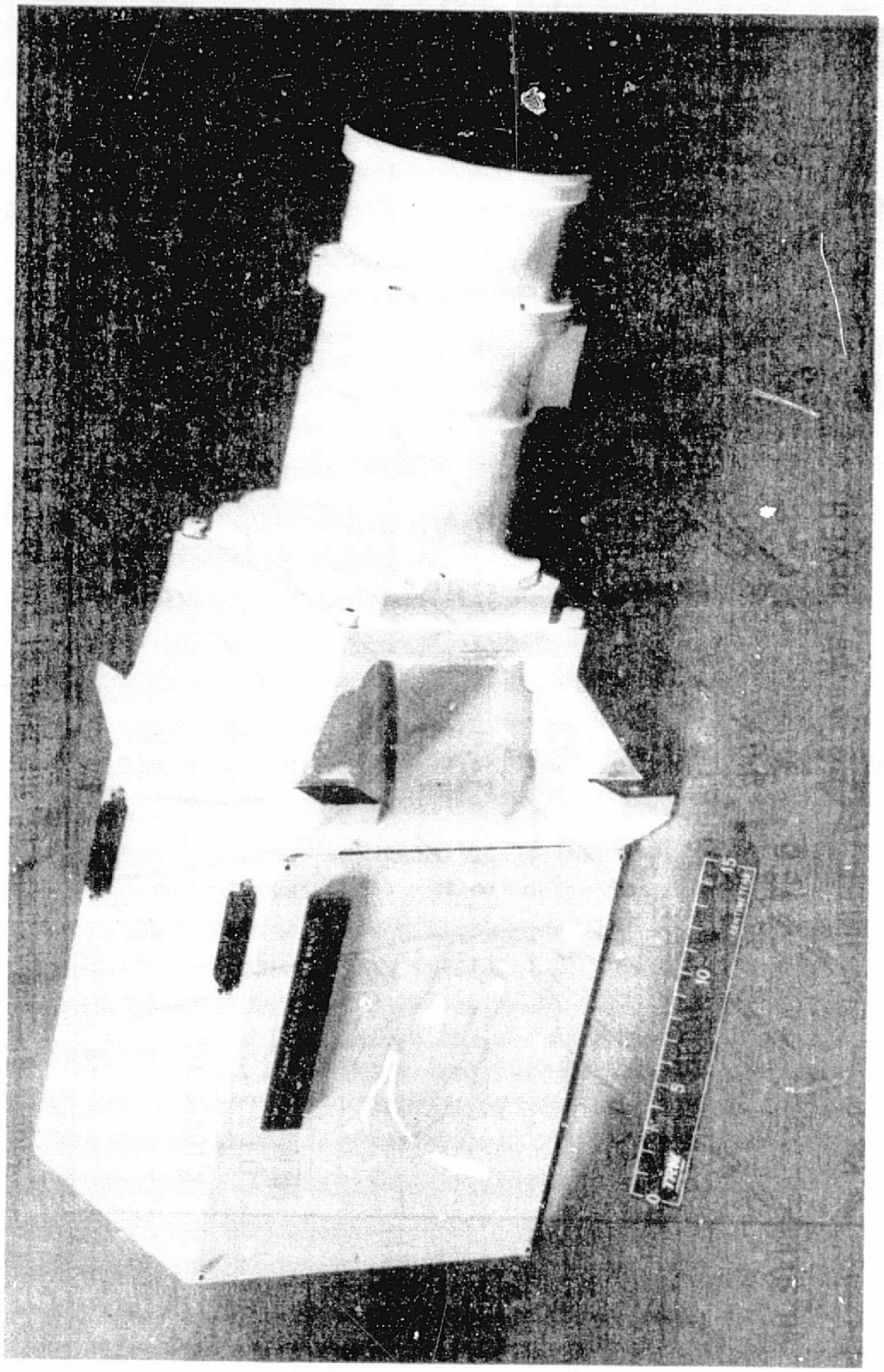

Figure 5.- Photograph of MOCS.

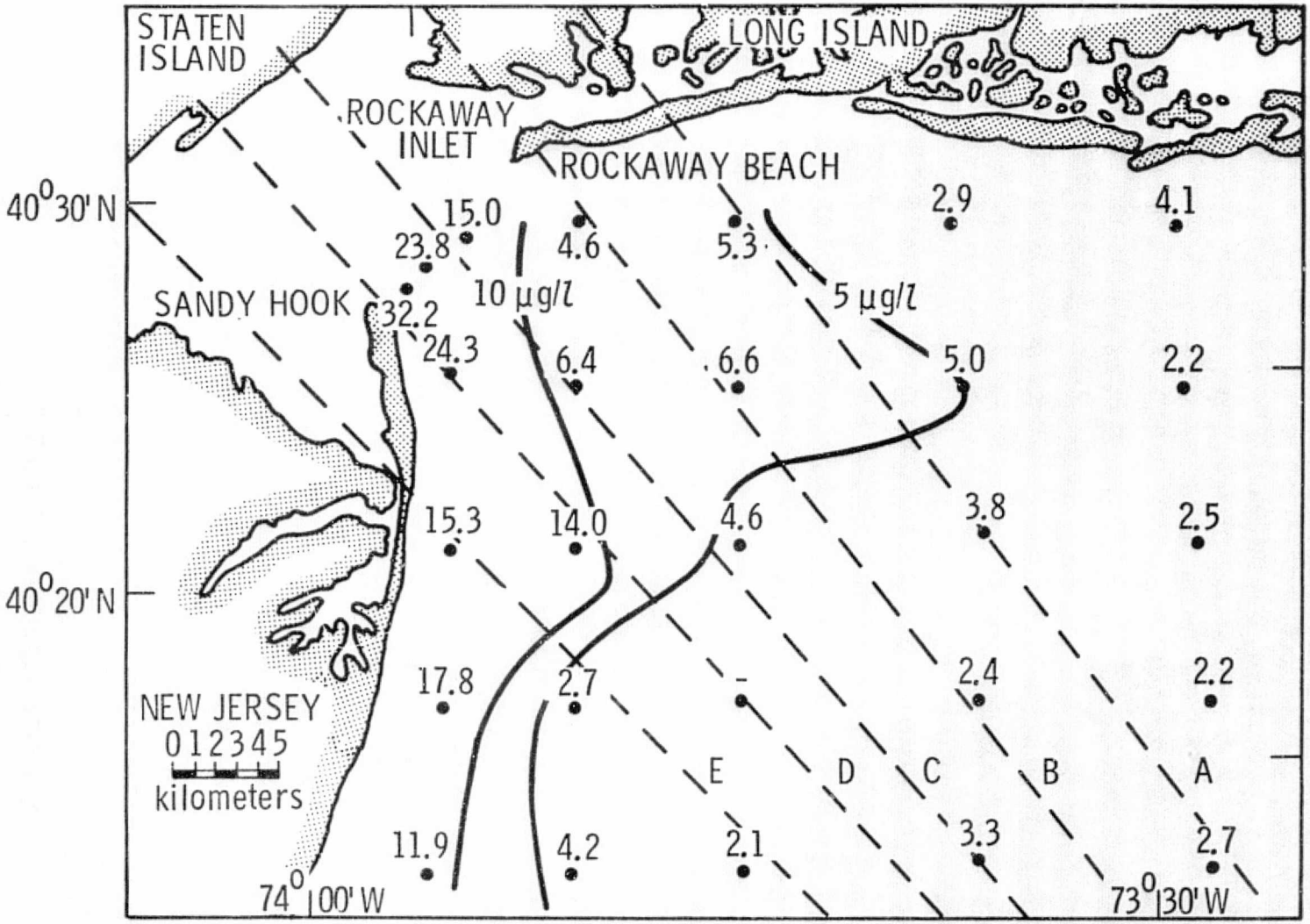

Figure 6.- Approximate flight lines of the NASA Wallops C-54 on April 13, 1975, superimposed on a NOAA generated map showing locations of stations where chlorophyll-A (µg/l) measurements were determined from water samples collected by helicopter.

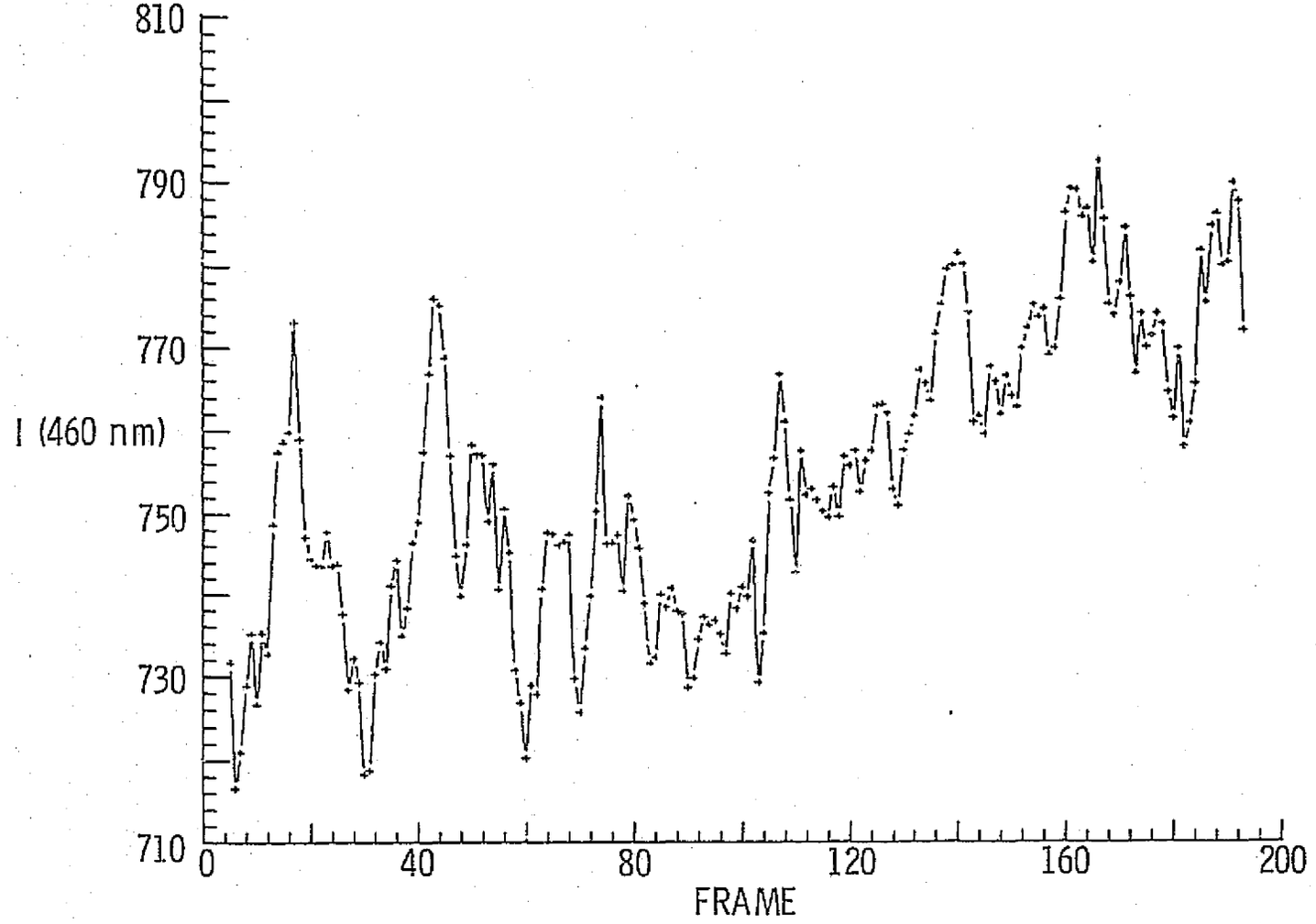

Figure 7.- Averaged data points along line D (fig. 6) for MOCS spectral band 5 (460 nm).

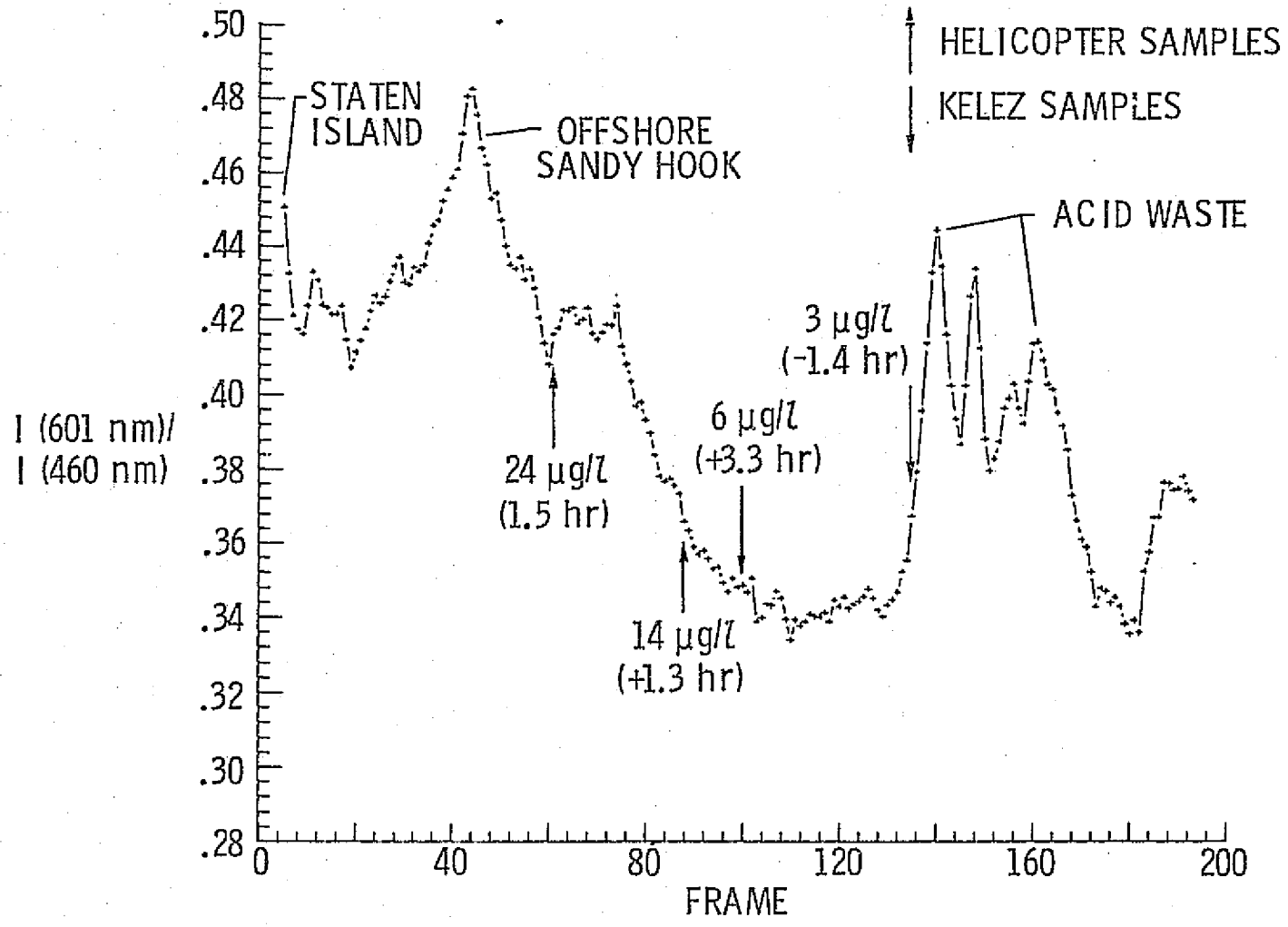

Figure 8.- Averaged data points along line D for ratio of band 14 (601 nm) and band 5 (460 nm). Chlorophyll-a levels (µg/l) collected by helicopter and the NOAA ship Kelez are indicated along with times (hours) in parentheses between water sample pickups and C-54 overflight.

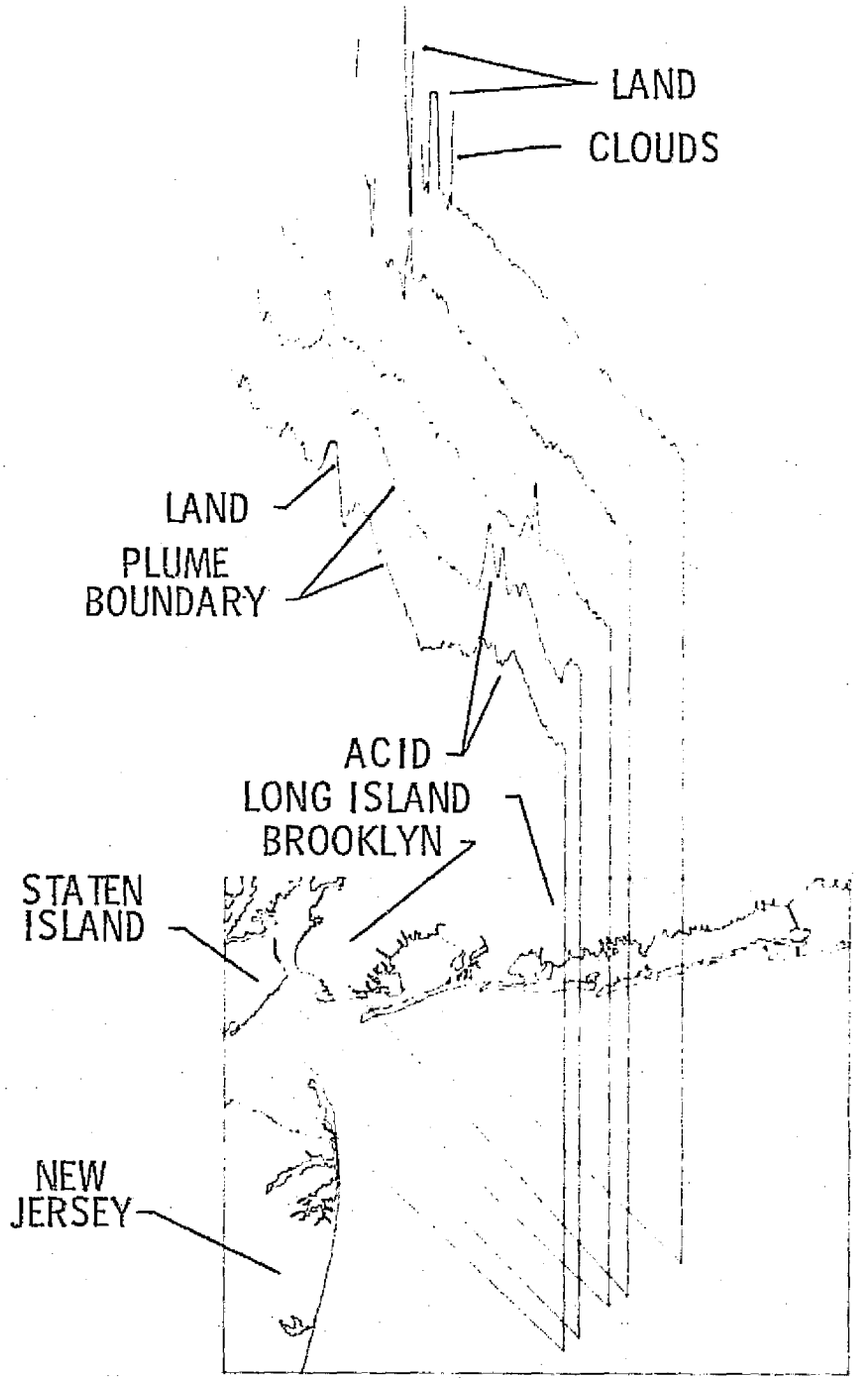

Figure 9.- TI ratio for all five flight lines in the New York Bight on April 13, 1975.

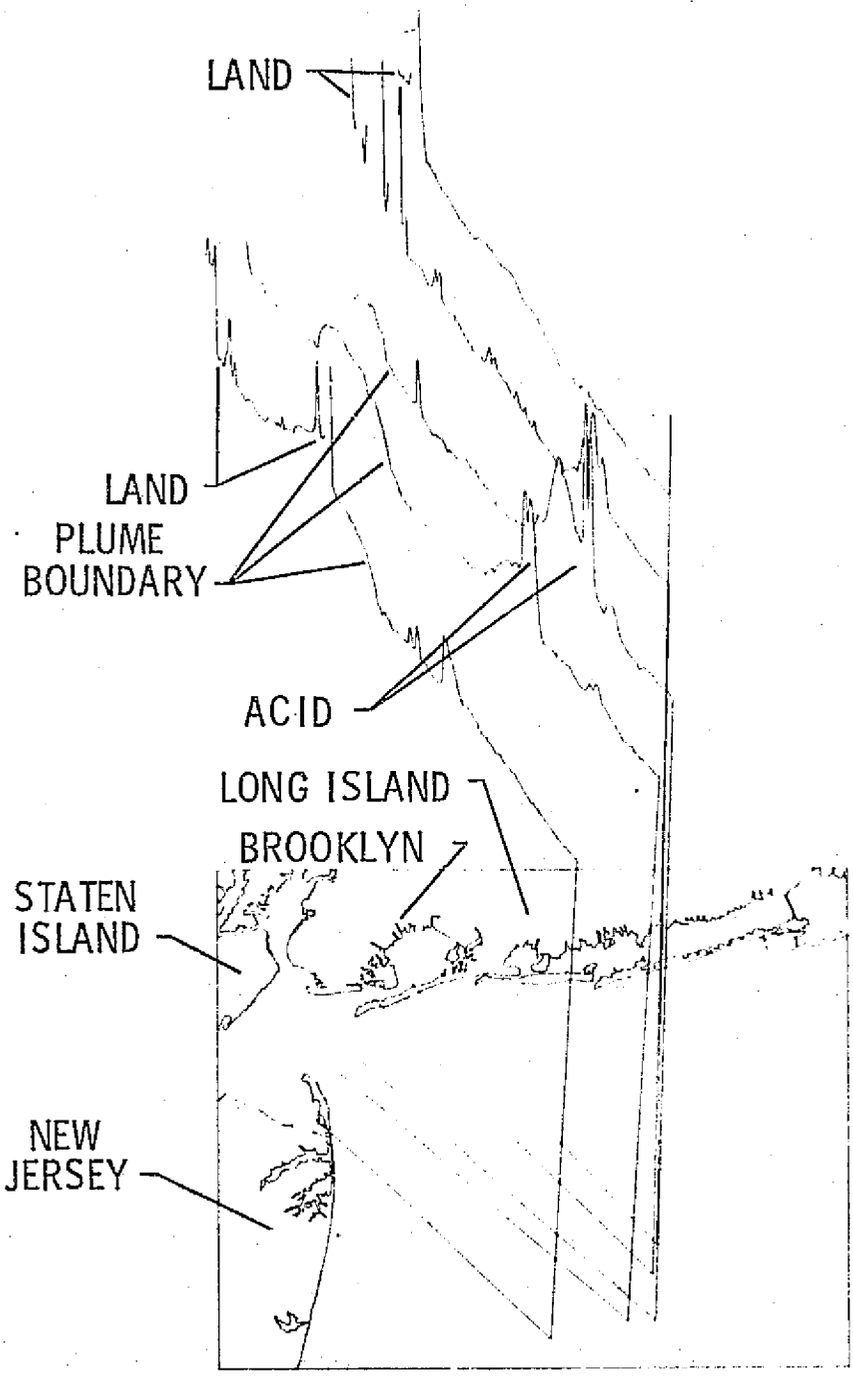

Figure 10.- TI ratio for all five flight lines in the New York Bight on April 10, 1975.

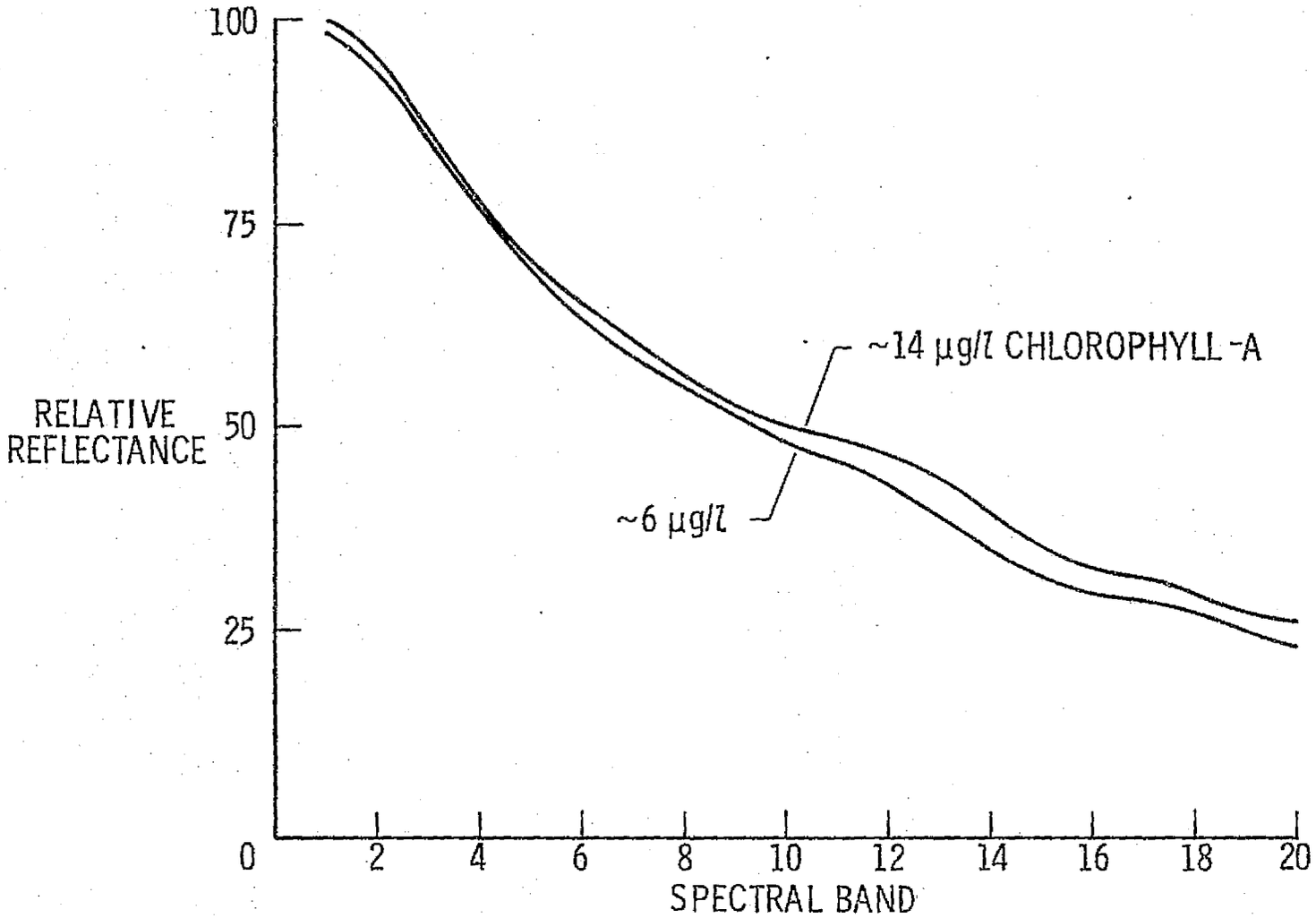

Figure 11.- Sample reflectance spectra from MOCS data collected at 5.33 km altitude along line D.

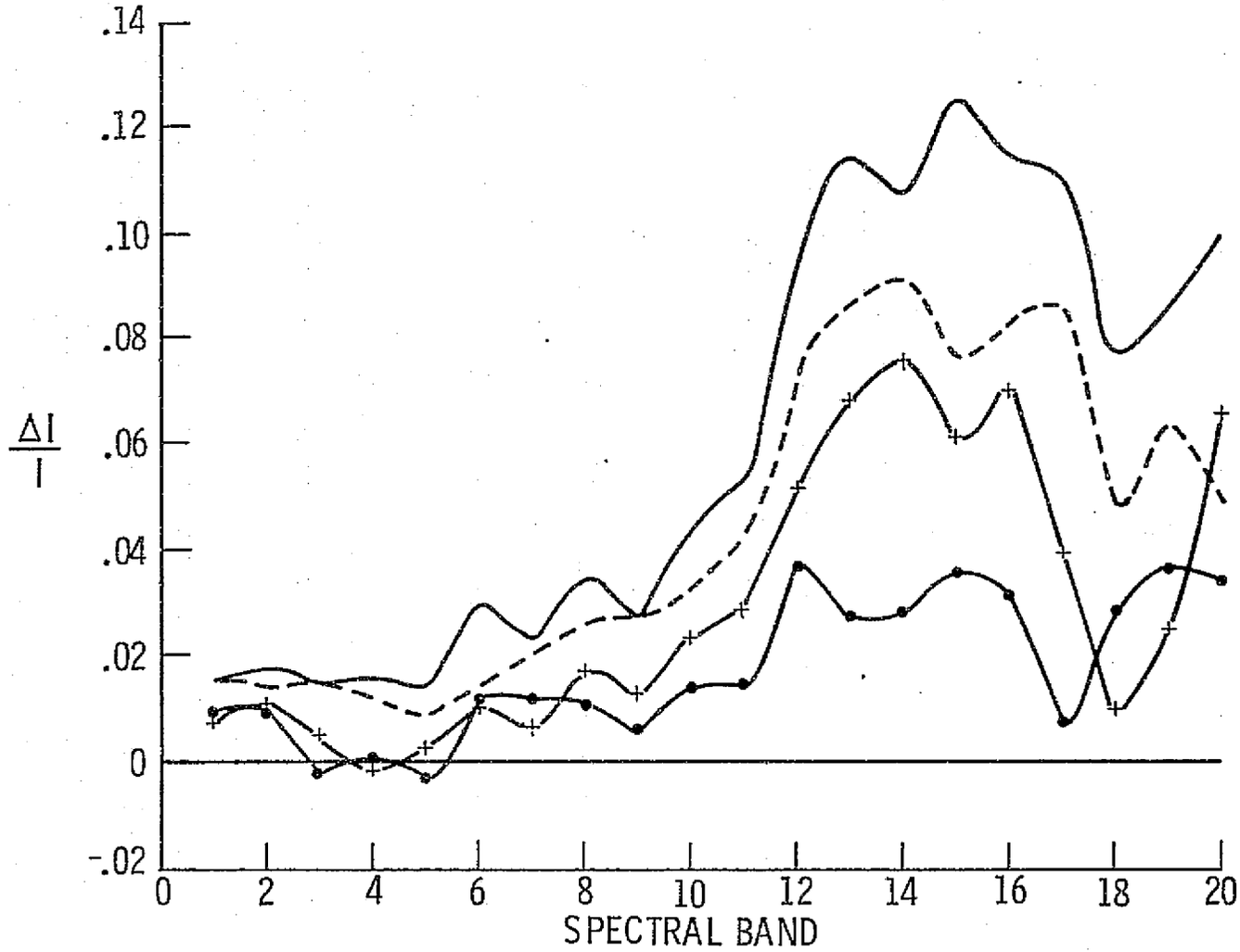

Figure 12.- Sample fractional difference spectra from MOCS data.

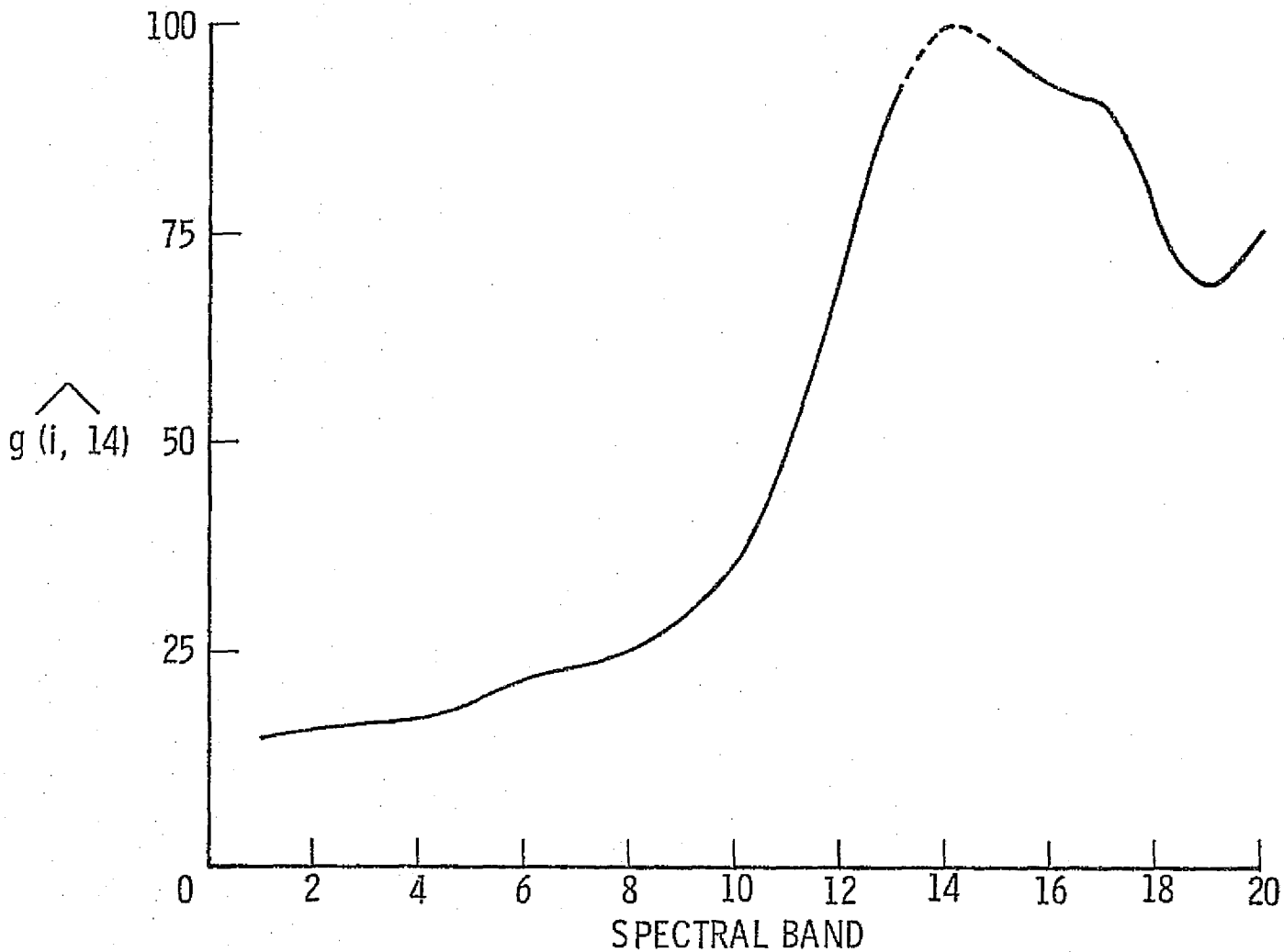

Figure 13.- Variant spectral signature of chlorophyll-a data set using j = 14.

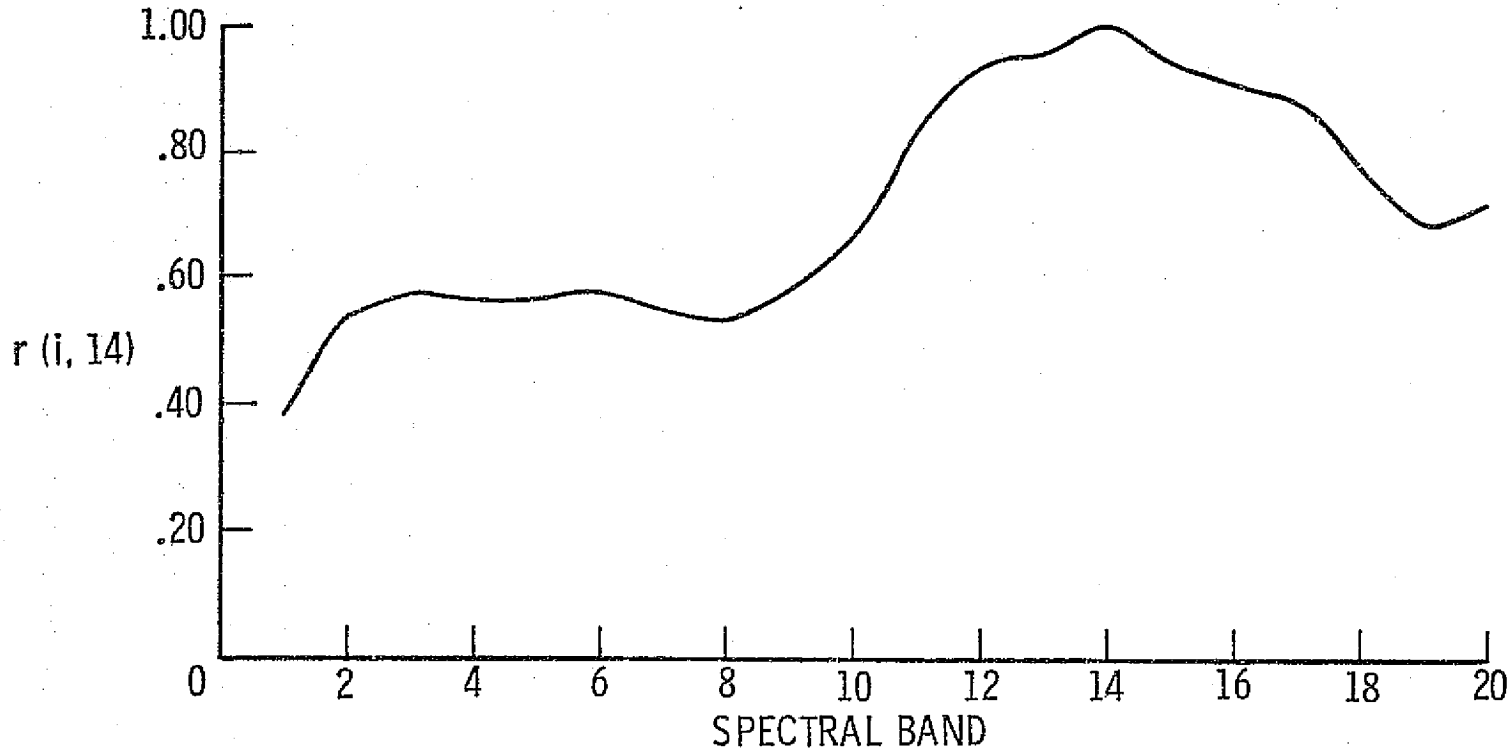

Figure 14.- Correlation coefficient of spectral band i and band 14 for the data in figure 13.

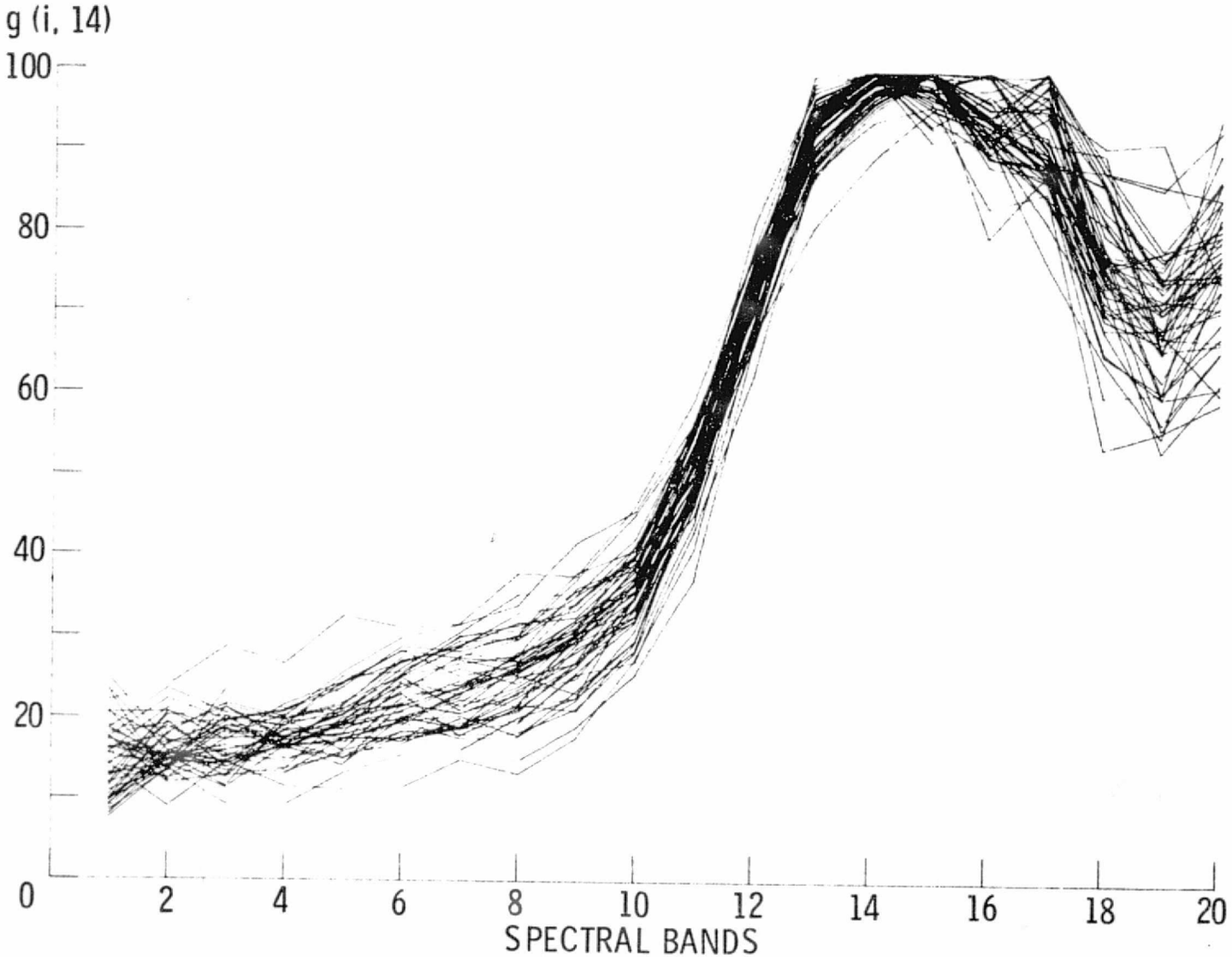

Figure 15.- Variant spectral signatures of 50 subsets of the chlorophyll-a data set, j = 14.

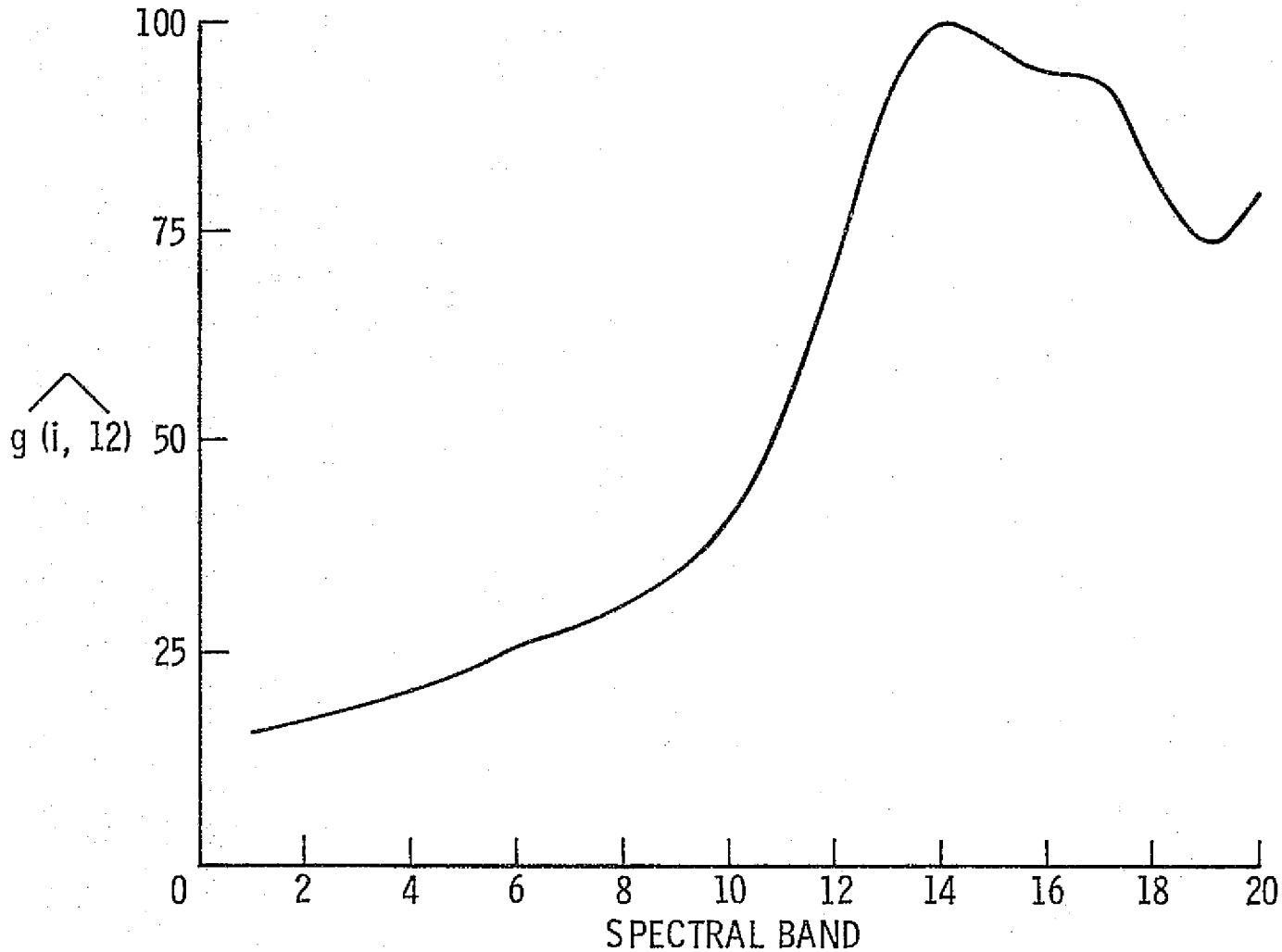

Figure 16.- Variant spectral signature of chlorophyll-a data set, j = 12.

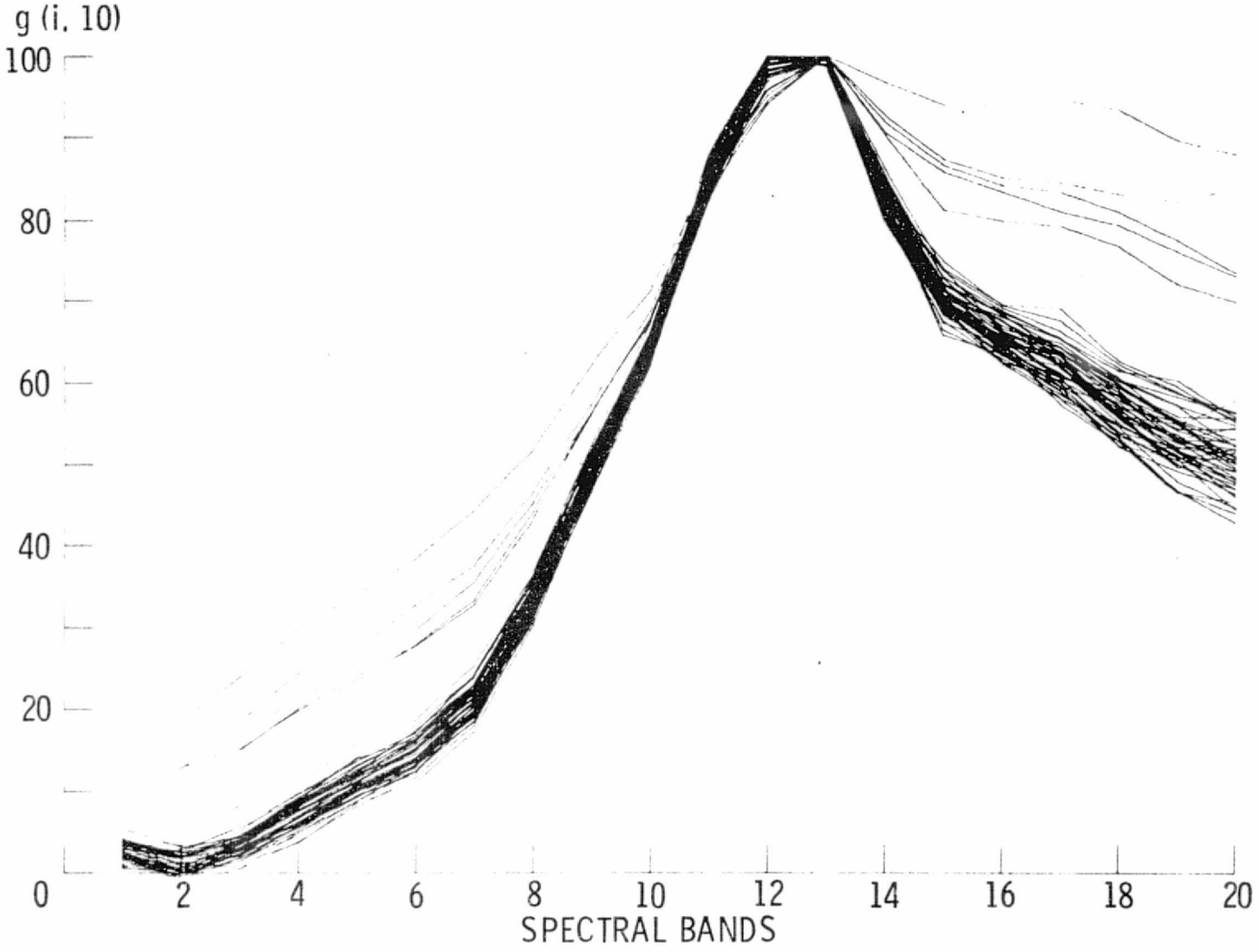

Figure 17.- Variant spectral signatures of 50 subsets of acid waste dump j = 10.

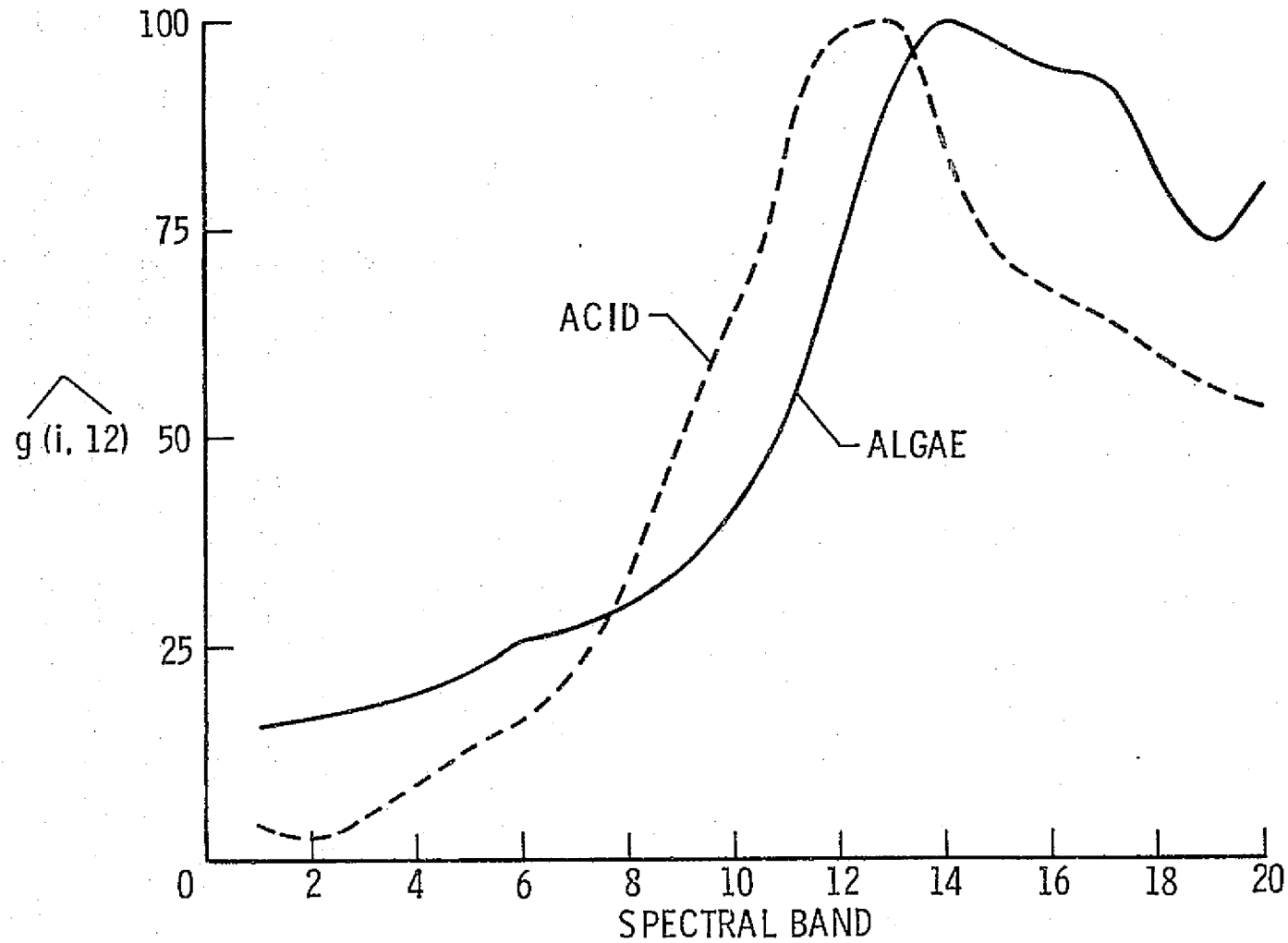

Figure 18.- Comparison between variant spectral signatures of algae and acid.

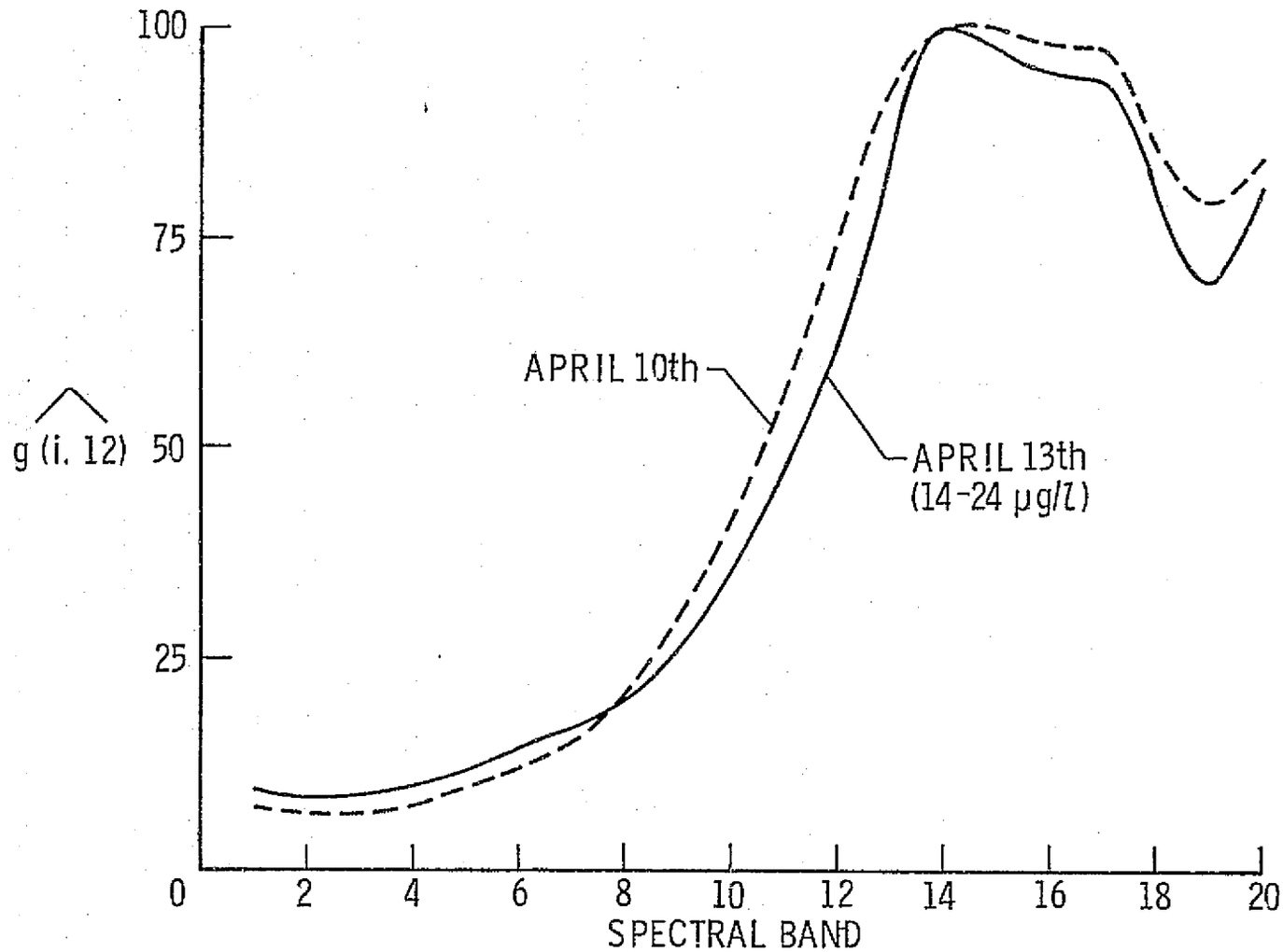

Figure 19.- Variant spectral signatures of algae from New York Bight data sets.

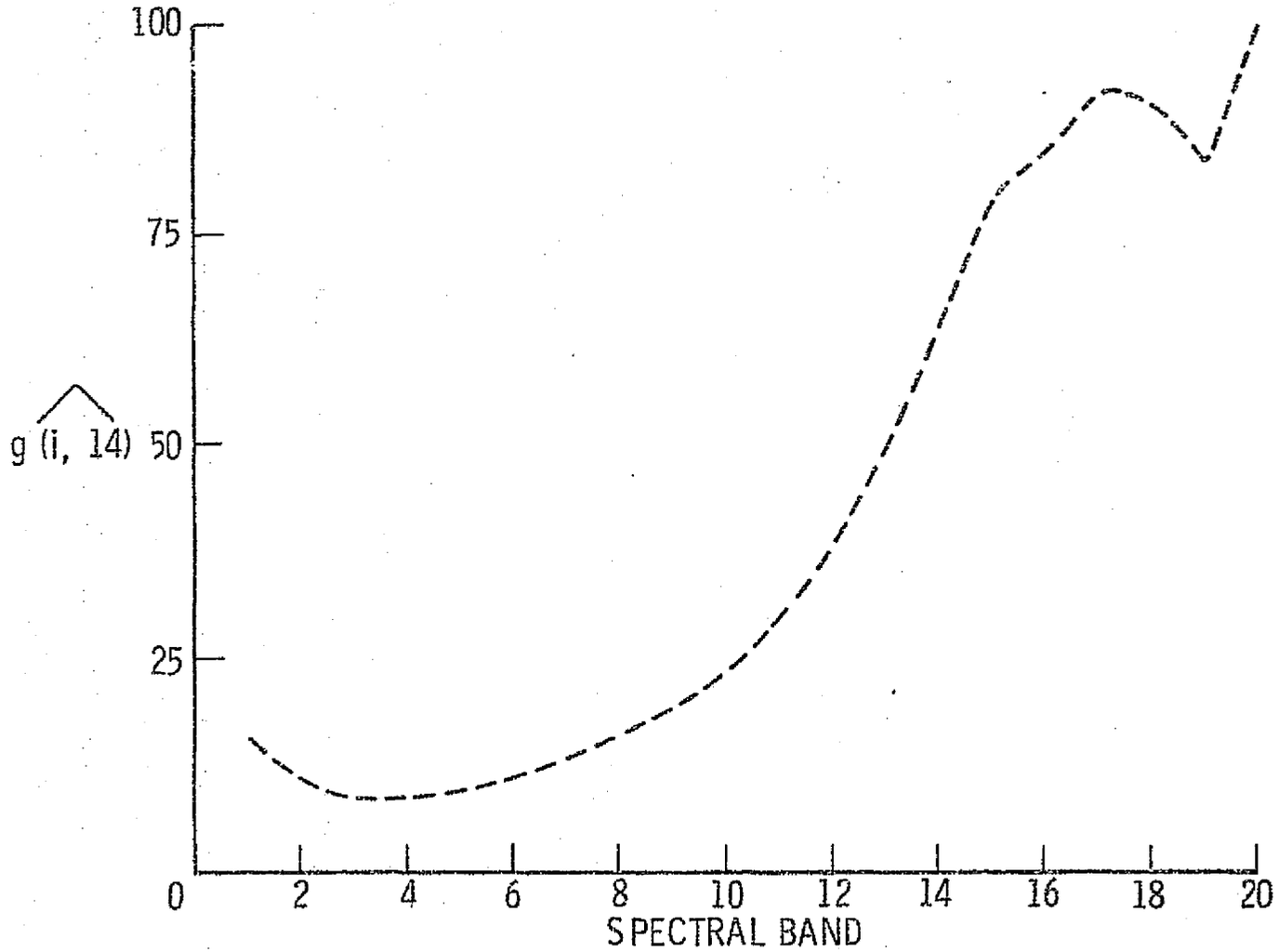

Figure 20.- Variant spectral signature of a data set consisting of spectra all along the plume water from its outer boundary to Staten Island.

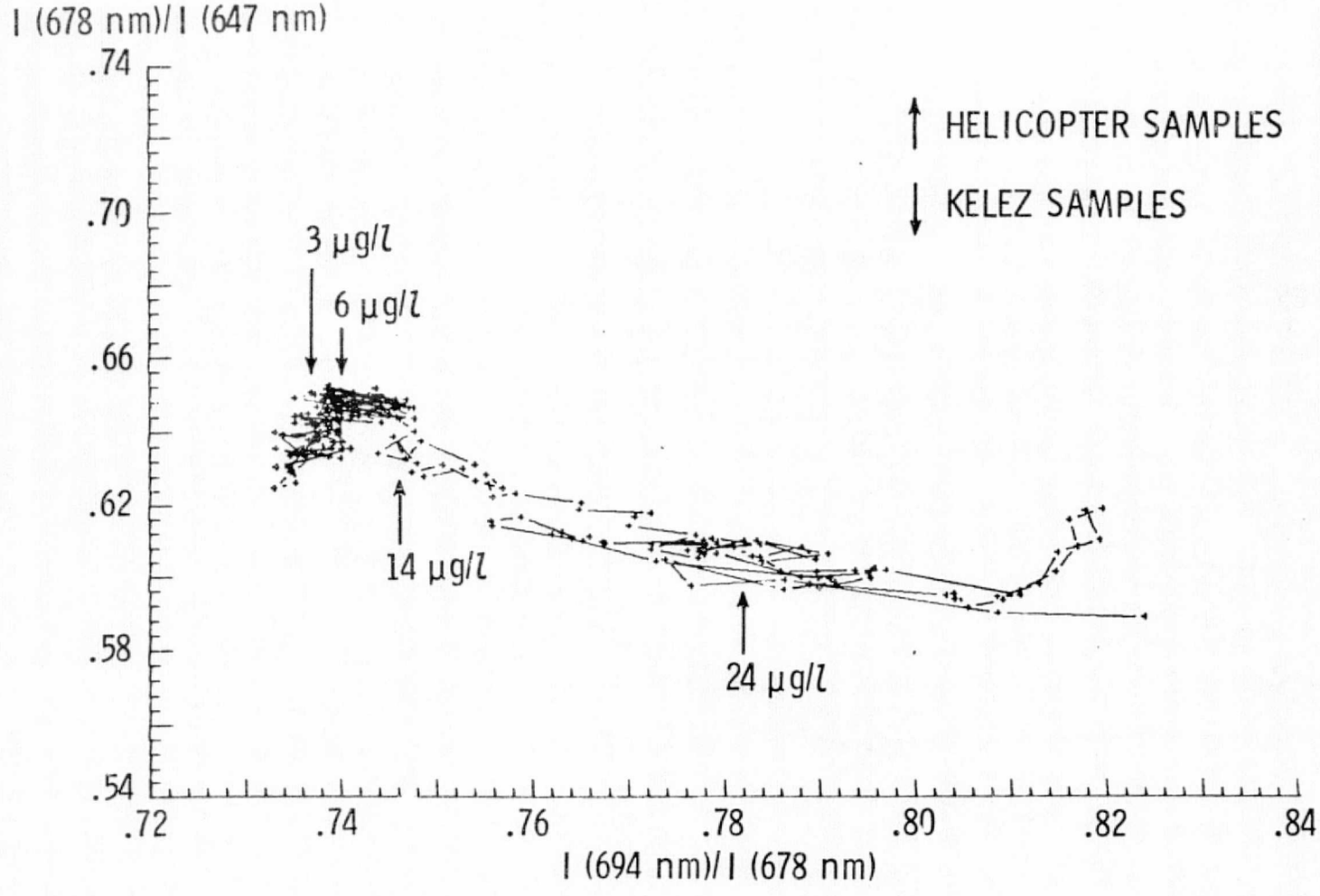

Figure 21.- I_{19}/I_{17} versus I_{20}/I_{19} for data points along line D. Lines join adjacent points along the track. Chlorophyll-a levels are indicated in µg/l.

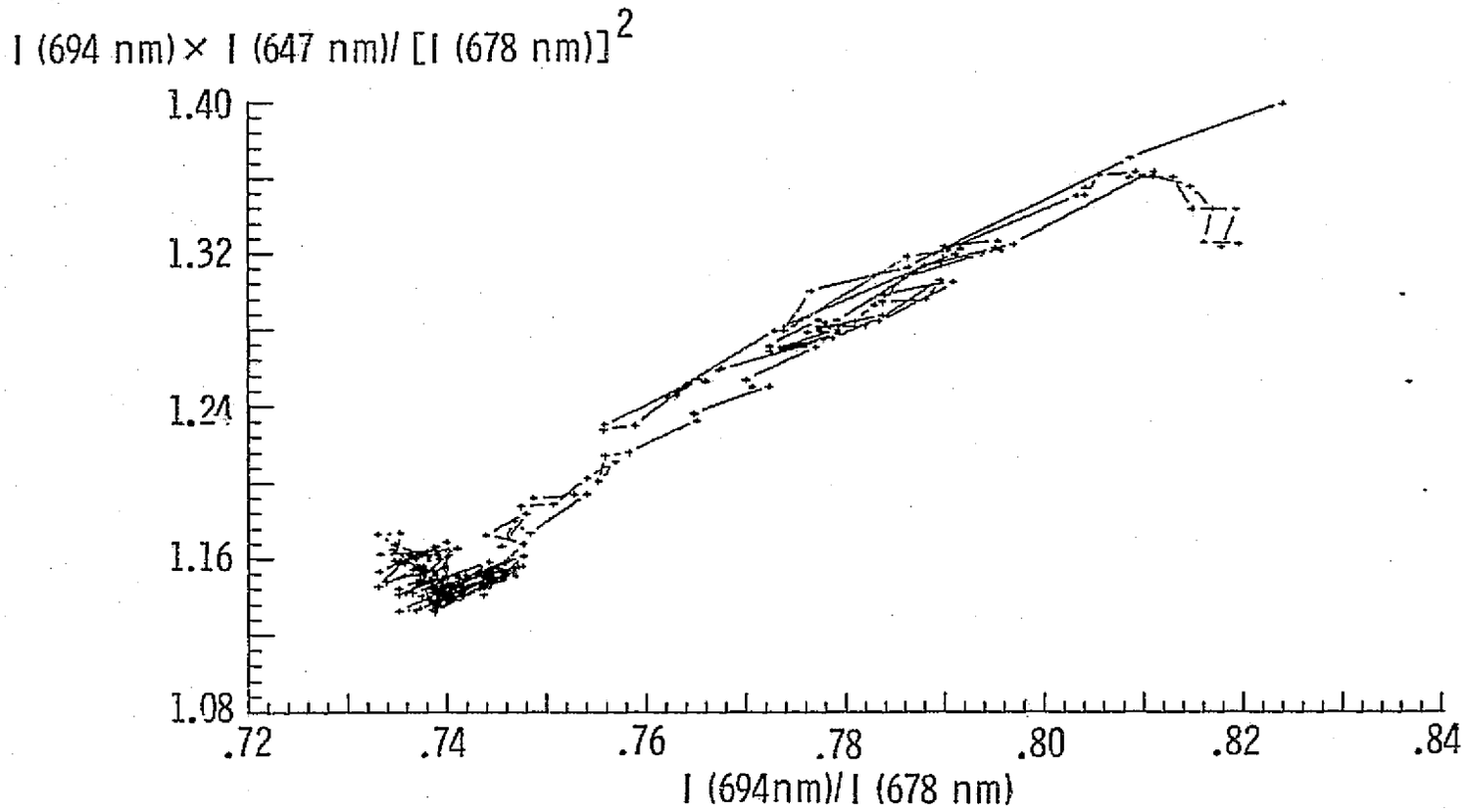

Figure 22.- $I_{20} \cdot I_{17}/(I_{19})^2$ versus I_{20}/I_{19} for data points along line D.

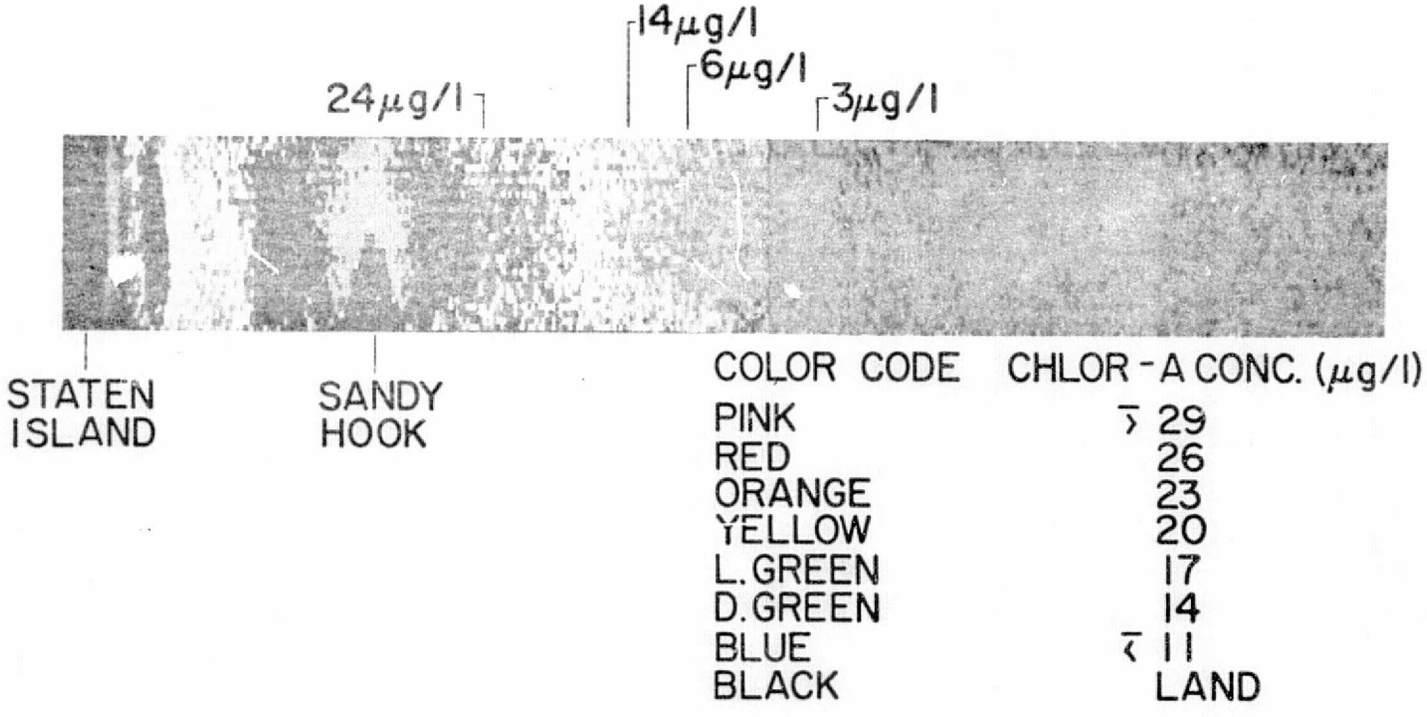

Figure 23.- False color map of chlorophyll-a concentration along line D in the New York Bight. Arrows point to approximate locations of ground truth stations.

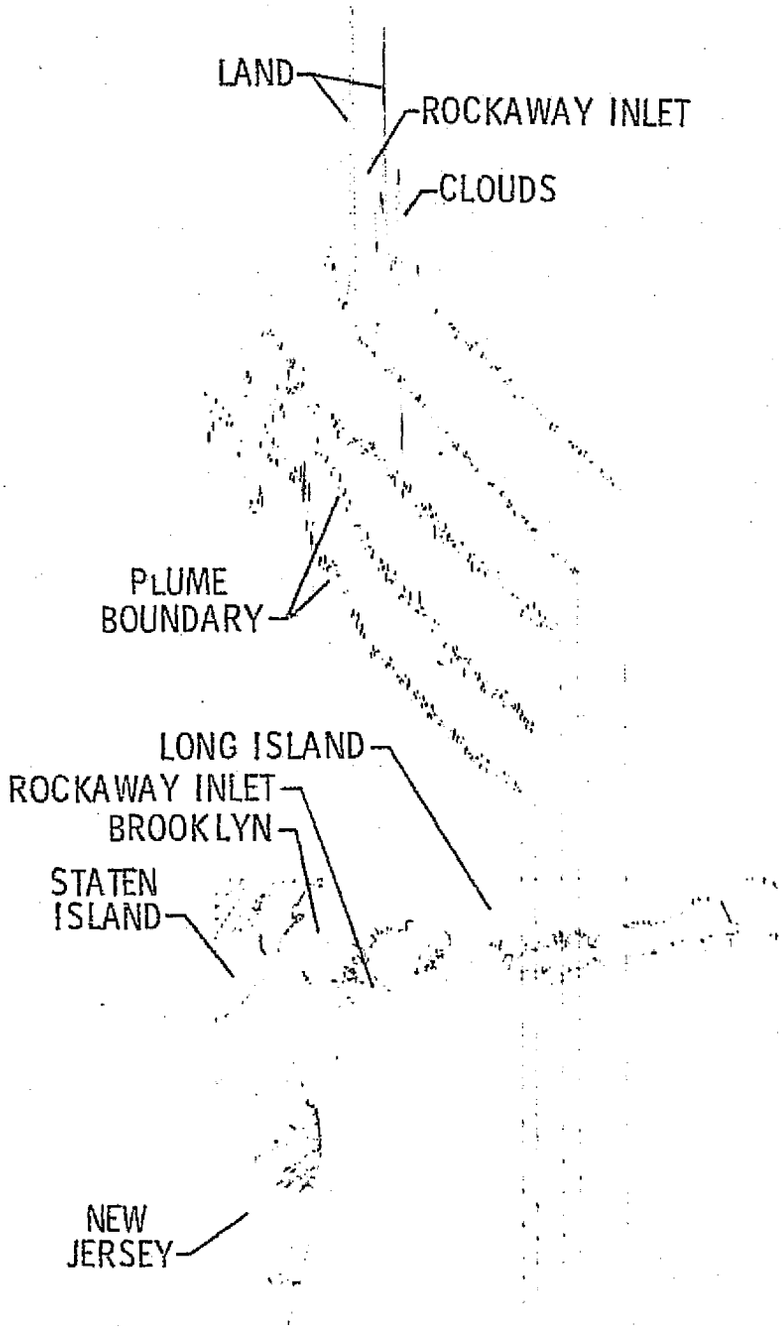

Figure 24.- I_{20}/I_{19} for all five flight lines in the New York Bight on April 13, 1975.

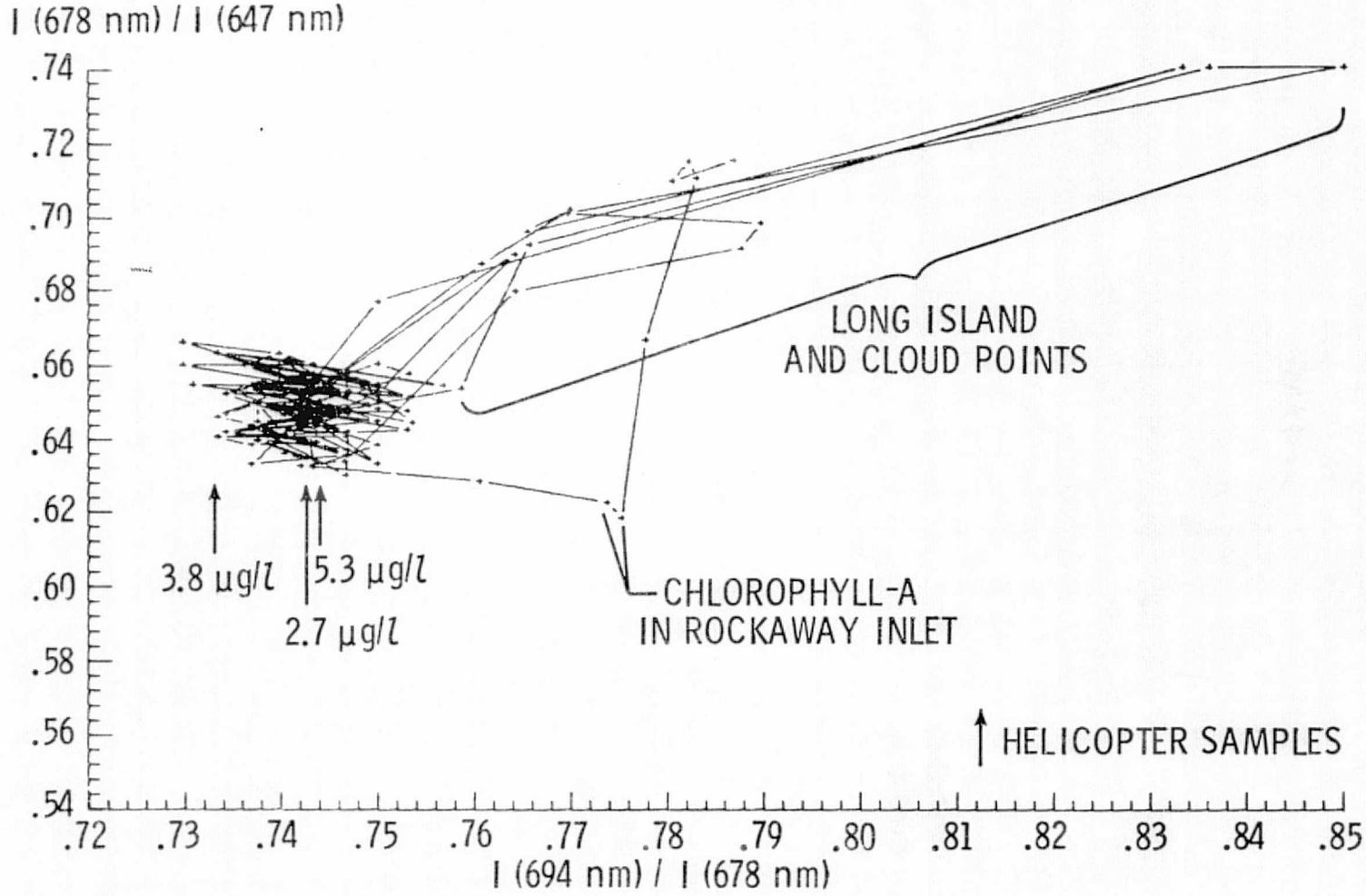

Figure 25.- I_{19}/I_{17} versus I_{20}/I_{19} for data points along line A. (Compare with fig. 21.) chlorophyll-a levels (µg/l) collected by helicopter are indicated.

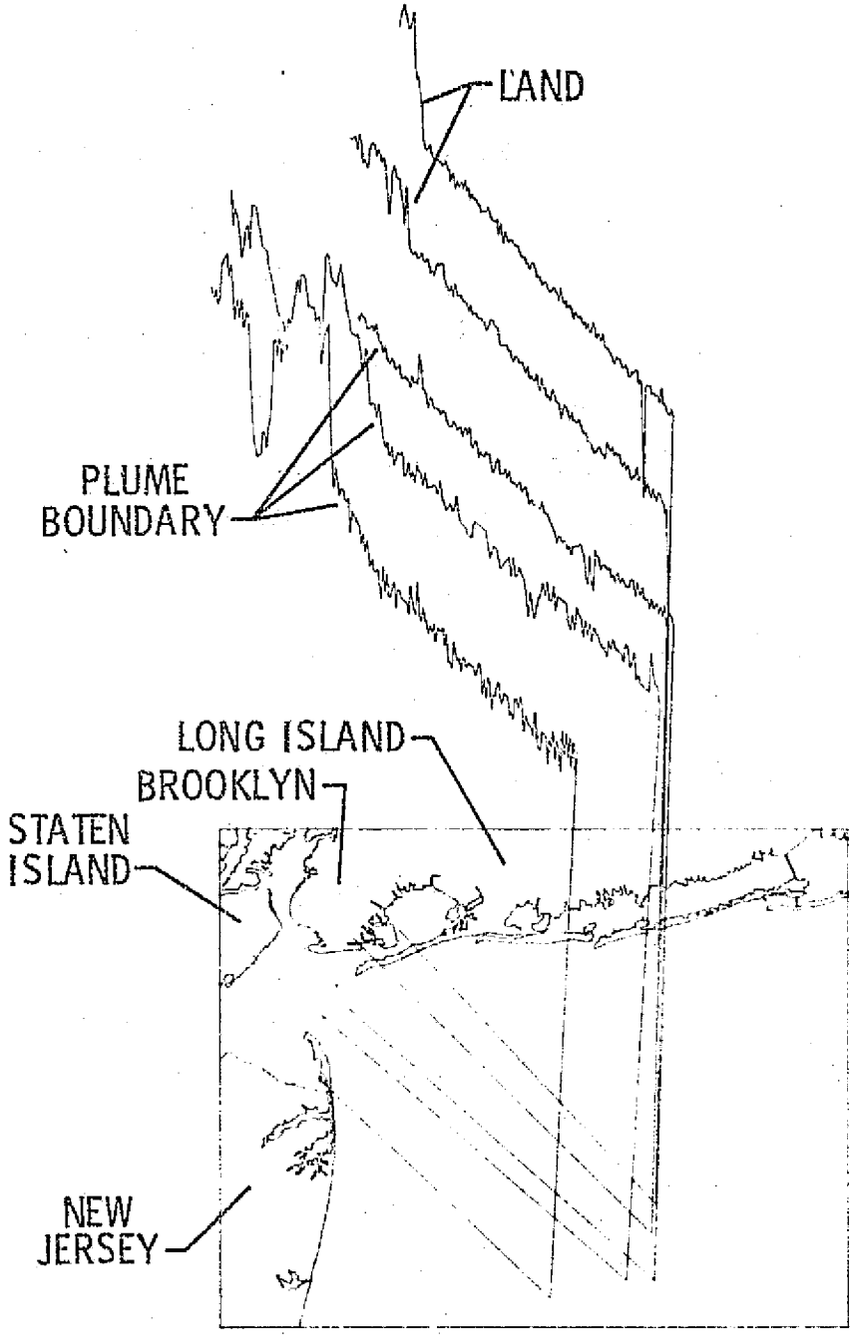

Figure 26.- I_{20}/I_{19} for all five flight lines in the New York Bight on April 10, 1975.

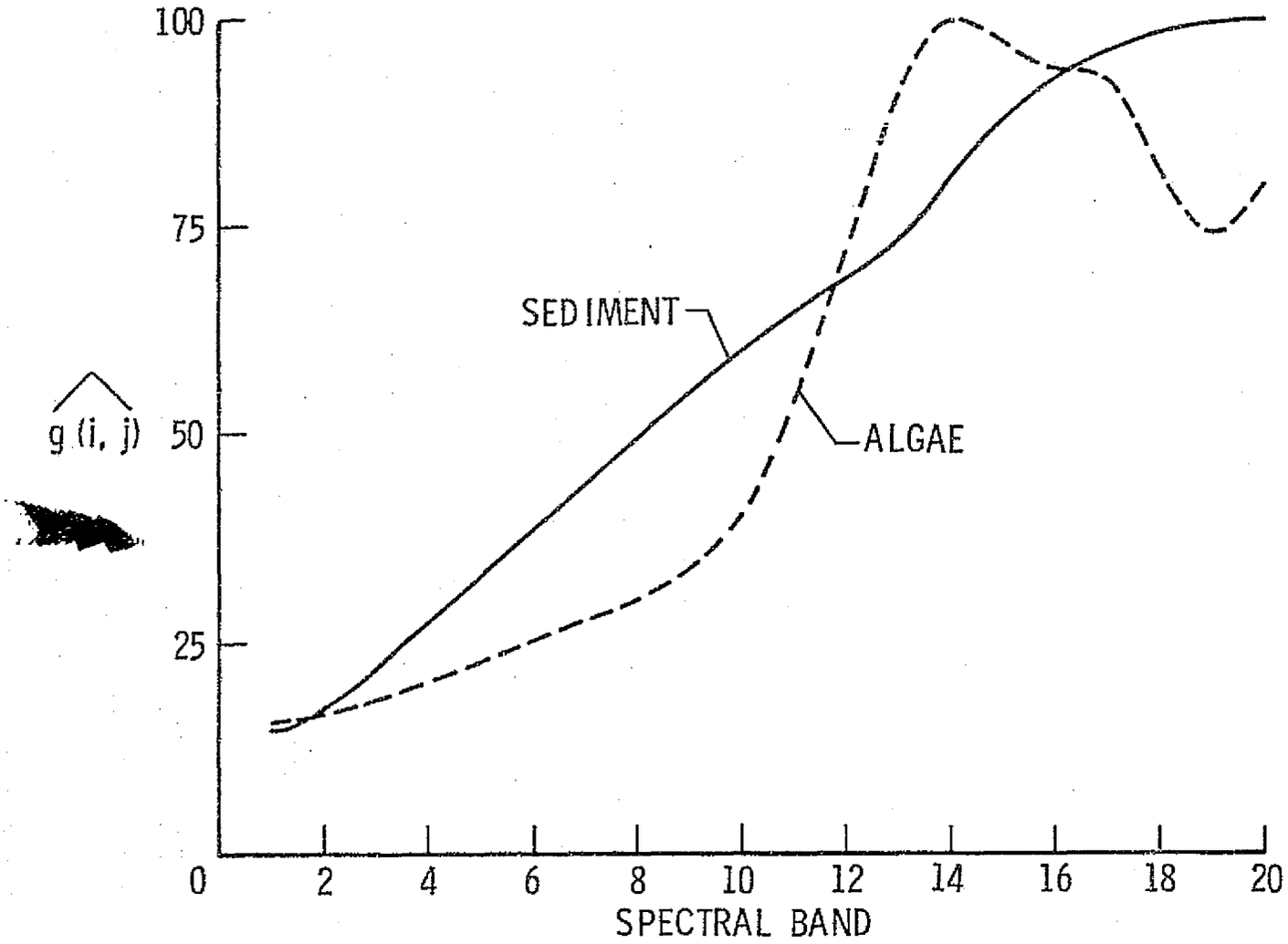

Figure 27.- Variant spectral signatures of algae and sediment.
(From ref. 8.)

Remote Infrared Measurements of Water

Thermal Anomalies During the

New York Bight Experiment

By

Charles A. Hardesty

REMOTE INFRARED MEASUREMENTS OF WATER THERMAL ANOMALIES DURING THE NEW YORK BIGHT EXPERIMENT

by

Charles A. Hardesty

SUMMARY

This paper presents thermal data collected in the New York Bight in April 1975 from the C-54 aircraft platform as part of a NASA-NOAA cooperative program. These thermal data were collected for correlation with MOCS data and are not to be confused with thermal data collected onboard other flight platforms during this effort. Thermal data are presented here and compared with MOCS spectral signatures for algae.

ACKNOWLEDGMENT

The author is grateful to National Oceanic and Atmospheric Administration personnel, in particular Dennis S. Clark and Dr. Alan E. Strong of the National Environmental Satellite Service, for use of their unpublished ground truth information.

INTRODUCTION

Remote measurement of sea surface temperatures using infrared radiometers has been widely studied and the technique used on many occasions. Absolute accuracies of better than $0.5^{\circ}C$ are obtainable from aircraft platforms provided the infrared radiation measurements have been processed to remove the atmospheric effects and by using ground truth calibration. The infrared experiments flown on April 10th and April 13th were a part of the mission to

evaluate multispectral, infrared, microwave, and photographic remote sensing techniques for determining surface circulation and water quality features in the New York Bight.

The purpose of including the infrared thermal scanning experiments on this mission (C-54 aircraft) was to correlate the observable thermal anomalies in the water with the remote measurements collected by the Multichannel Ocean Color Sensor (MOCS). Water is essentially opaque to the infrared radiation in the 8 to 14 micron range. Therefore, the upper 0.1 mm of sea surface determines the radiance variation from point to point and the temperature of the marine background. The thermal data collected have not been processed to remove the effects of atmospheric constituents. These data are presented in this report as temperature changes along the flight lines. The poor quality of the thermal scanner film records and the magnetic data tapes prevented digitizing the data and providing image enhancement and false color maps as was originally planned.

DESCRIPTION OF INFRARED INSTRUMENTATION

A Precision Radiation Thermometer (PRT-5), table 1, and a Reconofax IV, table 2, were flown on the New York Bight mission. The PRT-5 consists of an optical unit and an electronic unit. The optical unit compares the amount of radiant energy emitted by the target with that emitted by an internally controlled, optically chopped temperature cavity, thus providing absolute values of infrared radiation levels. The unit uses a hyperimmersed thermistor detector with the area of the active element only 50 micron square. An objective lens and special interference filter are used to limit the pass band to the atmospheric 8 to 14 micron window. With the 2 degree (2°) field of view, the

instrument covers a ground swath of 15.9 meters and 186 meters for altitudes of 0.45 and 5.33 km (1400 and 17,500 ft), respectively.

The Reconofax instrument shown in figure 1 is a single channel infrared mapper. Incoming radiation from ground targets is reflected from the 45 degree surface of the rotating (11,000 rpm) scanner mirror into a parabolic mirror. The parabolic mirror focuses this energy via a small right angle folding mirror onto the sensitive surface of the detector. The varying intensity of the received energy produces an electrical signal. The resulting video signal is used to modulate a crater lamp and record the scanned image on 70 mm film. A mercury doped germanium sensor cooled to approximately 30°K was used on this mission with an 8 to 14 micron atmospheric filter. Since this Reconofax did not have an onboard calibration system, only relative infrared radiation levels were obtained with the scanner.

The remote infrared and MOCS experiments were mounted on the Wallops Flight Center's C-54 aircraft platform and flown on April 10th and April 13th. Flight data were collected at the 0.45 and 5.33 km (1400 and 17,500 ft) altitudes. The flight lines consisted of five parallel tracks (A thru E) about 3.55 km (1.92 nautical miles, n. mi.) apart and 55 km (29.9 n. mi.) long in the northeast-southeast direction as shown in figure 2. Flight lines 1, 2, 3, 4, and the extended C-1 line, were flown on April 10th at an altitude of 0.45 km (1400 ft.).

NOAA provided the ground truth data for both days, but the most extensive set of temperature data were collected on April 13th. In most cases there was a considerable time spread between the NOAA ground truth data points and the NASA remote sensing data obtained from the C-54 aircraft.

DISCUSSION

Figure 3 provides an excellent sample of the quality of the Reconofax IV thermal scanner film records obtained during the spring mission. This figure shows flight lines A-1 and D-1 flown on April 10th at an altitude of 5.33 km (17,500 ft.). Some of the fine detail has been lost in reproduction, but close observation of the film records shows several small ships (small dots) along with their cooler wake trails. This observed temperature difference is a result of cooler water being brought to the surface by the mixing motion of the moving ships. The thermal boundary off shore of Long Island is quite pronounced in this picture which indicates a temperature difference on the surface due to the mixing motion (flow) of the water. The sewage sludge dump is also quite apparent in the middle of the photograph and the presence of the wake from the dumping ship indicates that this was a fresh sewage dump. The sewage dump was first noted in flight line B-1 and it can still be seen in run B-2, approximately 100 minutes later. The reason for this strong sewage sludge signature and its persistence has yet to be determined. Additional information is needed on the sludge temperature and composition at the time of discharge to clarify this point. It is possible that the sludge enrichment of the overlying waters may have resulted in formation of extensive surface films. The old acid dump is not visible in the photographs. This is reasonable, because the Reconofax IV can only see a temperature change of $\pm$ 0.3^{o}K or larger in the top 0.1 mm surface of water, or a change in the emissivity of the surface. Other features to be noted on the Reconofax records are the small hairline scratches running parallel with the pictures along with two heavier dark lines. These marks were caused

by the film magazine in the scanner and makes it very difficult to digitize and analyze the data using a densitometer.

Figure 4 is an example of the Reconofax records for the 0.45 km (1400 ft.) low altitude radial lines 1 and 2 (reduced by 2/3 to permit printing on a single page) flown on April 10th. Line 1 starts just South of Sandy Hook and ends at the bridge on Rockaway Beach. Shown are thermal gradients located approximately midway (arrows) between the land points, and just off the shore of Rockaway Beach. The PRT-5 low level record in figure 5 is an example of the last 15 minutes of data for the 85 km (46 n. mi.) "C" line on April 13th showing two thermal boundaries in the surface of the water. These boundaries correlate with the scanner film record and are verified by ground truth data points 23, 24, and 54. The Kelez data points are approximately 1.4°C warmer than the airborne measurements which is reasonable, since the data have not been corrected for atmospheric effects as mentioned and the time spread between the data sets varied from 0.5 to 2.5 hours. The magnitude of the thermal anomalies at the boundaries varied between 0.3 and 0.6°C.

One interesting phenomenon was observed on the A-2 line flown at 5.33 km (17,500 ft) altitude on April 10th, and it appears on both the Reconofax (fig. 6b) and PRT-5 (fig. 7b) records. This feature appears as many small thermal anomalies on the Reconofax film record with a faint leading (boundary) edge to the anomaly area. Because the footprint (swath width) of the PRT-5 is 186 meters (614 ft.) for the high altitude pass, it tends to smooth or average the small gradients seen on the Reconofax record (16-meter IFOV) for a total change of approximately 1°C over the area. The thermal feature mentioned was not apparent on the A-1 (fig. 6a and 7a)

line flown approximately 30 minutes earlier, but the gradient is still faintly visible in the B-2 line flown 30 minutes after the A-2 line. These high altitude flight lines were flown in the sequence of C-1, E-1, D-1, A-1, C-2, A-2, D-2, and B-2. The phenomenon first appeared on the A-2 line, but the area was obscured by cloud coverage on the C-2 and D-2 flight lines, which prevented pin-pointing the time of the occurrence. This anomaly occurred at the approximate time of maximum current movement for this area of the New York Bight, thus indicating a possible convergence and mixing of the water mass. In some respects, the anomaly seen on the Reconofax record (fig. 6b) resembles the edge of the plume area indicated in figure 8, a sketch made from previous 1973 flight data over the Bight area. The MOCS record for the A-2 line also shows an increased amount of turbidity for this time frame, thus indicating in this case some correlation between the observed surface thermal anomalies and the MOCS data.

Figures 9 and 10 are plots of the PRT-5 thermal data for the first five high altitude flight lines flown on April 10, and April 13, 1975, over the New York Bight. These data can be compared to the MOCS data for ratio I_{20}/I_{19} in figures 24 and 26 in reference 1. A comparison of these data sets suggests there may be some correlation between the surface thermal anomalies and MOCS data.

CONCLUDING REMARKS

Thermal records for the PRT-5 and Reconofax IV were obtained for all flight lines flown on the C-54 aircraft for April 10, and April 13, 1975. The Reconofax records for April 13th show less thermal activity than on April 10th. The quality of the Reconofax film records and magnetic tapes

prevented digitizing the data as originally planned. A comparison of the thermal IR and MOCS data sets indicated correlation in some cases, but not in others. More consistent correlation between data sets may be obtained by using different ratios of MOCS data other than the I_{20}/I_{19} ratio. The thermal patterns seen on the Reconofax records for this mission are indicative of water flow conditions and are similar in appearance (ref. 2) to the results obtained by the Environmental Research Institute of Michigan in their work over the New York Bight in 1973.

REFERENCES

1. Grew, Gary W.; Remote Detection of Chlorophyll-A in Coastal Waters. Presented at the Fifth Annual Remote Sensing of Earth Resources Conference, Tullahoma, Tennessee, March 29-31, 1976.

2. Wezernak, C. T.; Lyzenga, D. R.; Polcyn, F. C.; Remote Sensing Studies in The New York Bight. NOAA Grant No. 04-4-158-33, July 1975.

TABLE 1. - PRECISION RADIATION THERMOMETER (PRT-5)

DESCRIPTION: A LIGHTWEIGHT, PORTABLE, BATTERY-POWERED THERMAL INFRARED RADIOMETER

SPECTRAL CHARACTERISTICS: SINGLE BANDPASS = 8 TO 14 μM WAVELENGTH

SPATIAL CHARACTERISTICS: 2° FIELD OF VIEW OR 186 METERS @ 5,335 METERS

16 METERS @ 457 M. ALTITUDE

PHYSICAL PARAMETER MEASURED: THERMAL INFRARED RADIATION IN THE 8 TO 14 MICRON WAVELENGTH BAND TO ±0.5° C

EARTH RESOURCES PROGRAM APPLICATIONS: PROVIDES A TARGET TEMPERATURE REFERENCE

MANUFACTURER: BARNES RADIATION

PHYSICAL SPECIFICATIONS: TWO MAJOR COMPONENTS - OPTICAL UNIT

ELECTRONICS

REQUIRES ON-BOARD RECORDER

TABLE 2. - RECONOFAX IV - IR SCANNER

DESCRIPTION:	SINGLE CHANNEL INFRARED LINE-SCANNING IMAGING SYSTEM THAT RECORDS RADIANT ENERGY IN THE 8 TO 14 μM RANGE
SPECTRAL CHARACTERISTICS:	SINGLE CHANNEL - 8 TO 14 μM WAVELENGTH
SPATIAL CHARACTERISTICS:	120° SCAN (±60° FROM NADIR) 3 MRAD INSTANTANEOUS FOV
RESOLUTION:	FOV @ 5,335 M ALT.: 16 METERS
	FOV @ 457 M ALT.: 1.4 M
	GROUND SWATH @ 5,335 M; 18,300 METERS
	GROUND SWATH @ 457 M; 1,500 METERS
PHYSICAL PARAMETERS MEASURED:	INFRARED RADIANT ENERGY IN THE 8 TO 14 μM WAVELENGTH BAND TO ±0.3 ° K
DATA RECORD:	IMAGE RECORDED ON 70 MM FILM

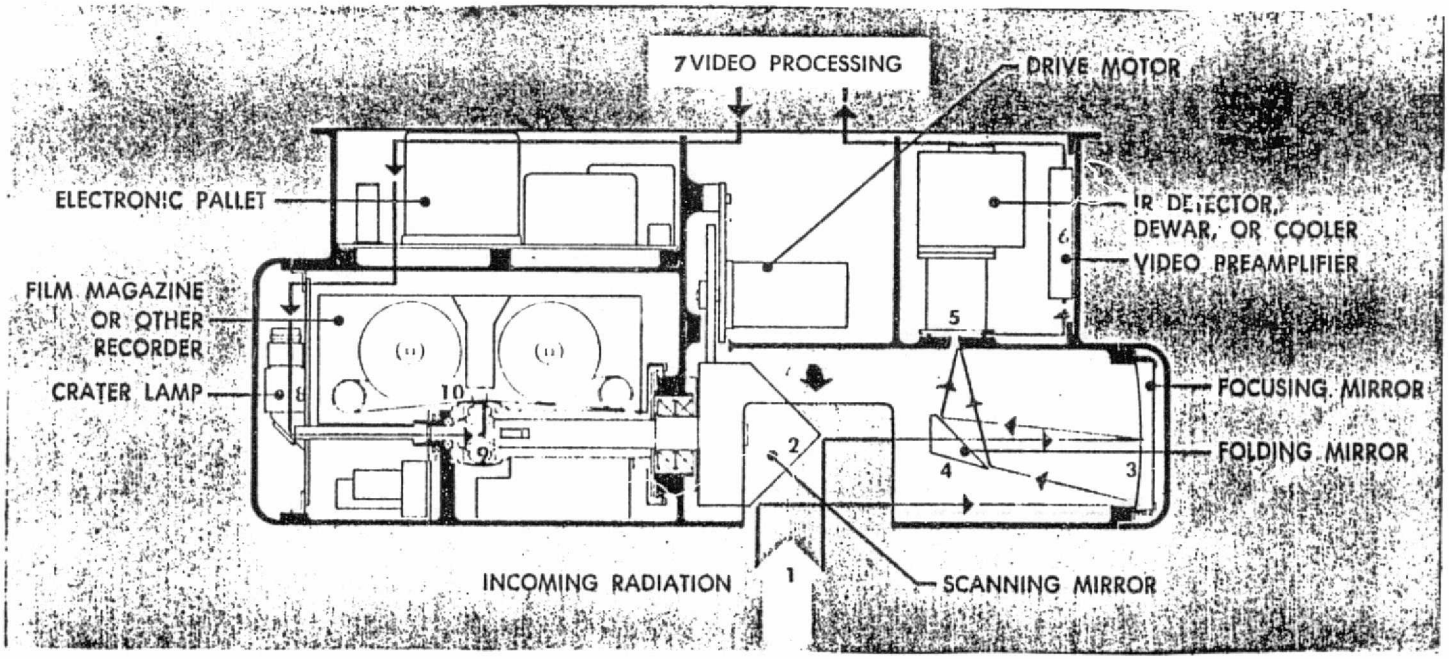

FIGURE 1. - RECONFAX IV IR MAPPER

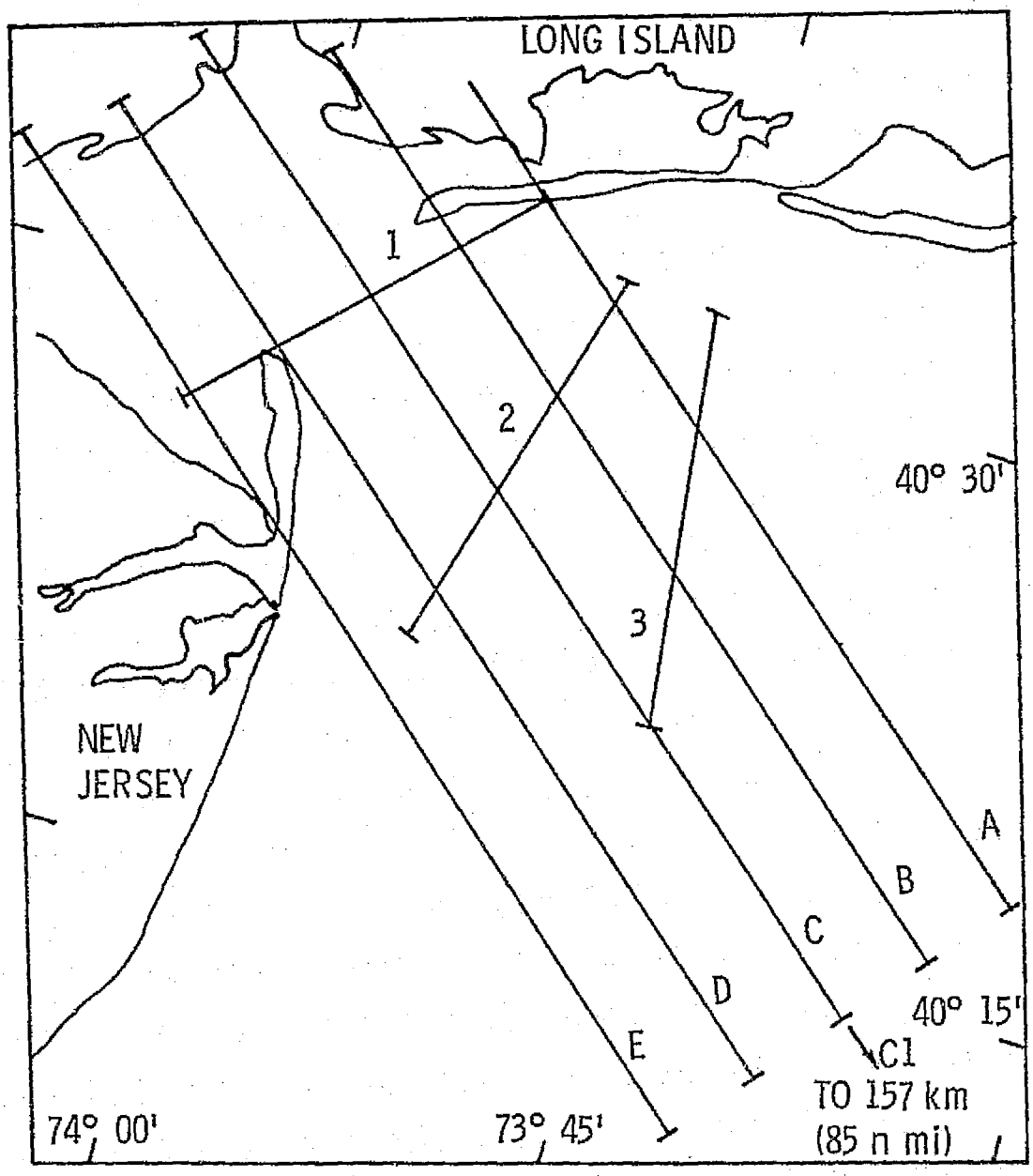

FLIGHT LINES APRIL 10, 1975

FIGURE 2 - C-54 flight lines, flight parameter and data identification parameters

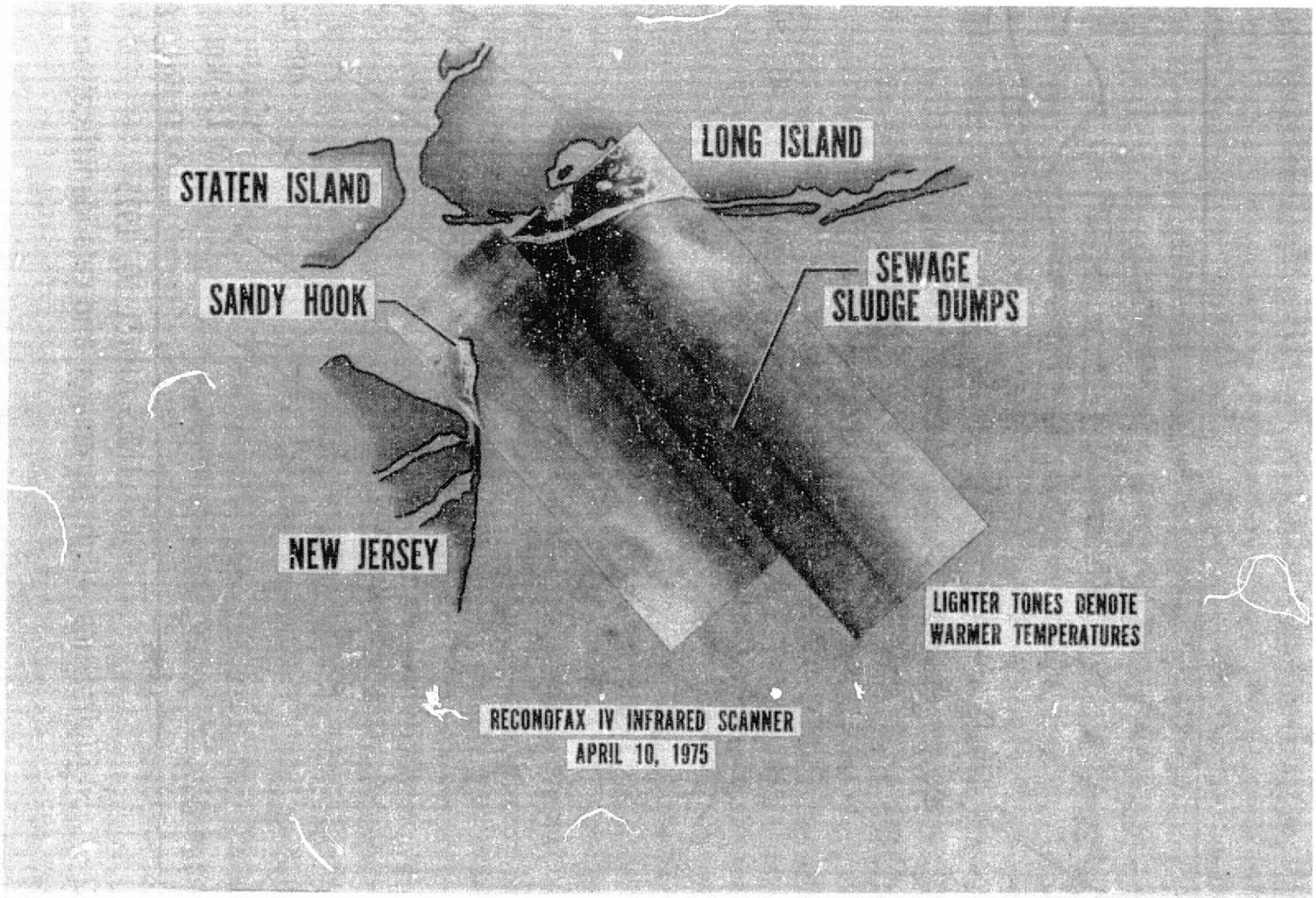

FIGURE 3 - Thermal imagery of dumping in the New York Bight

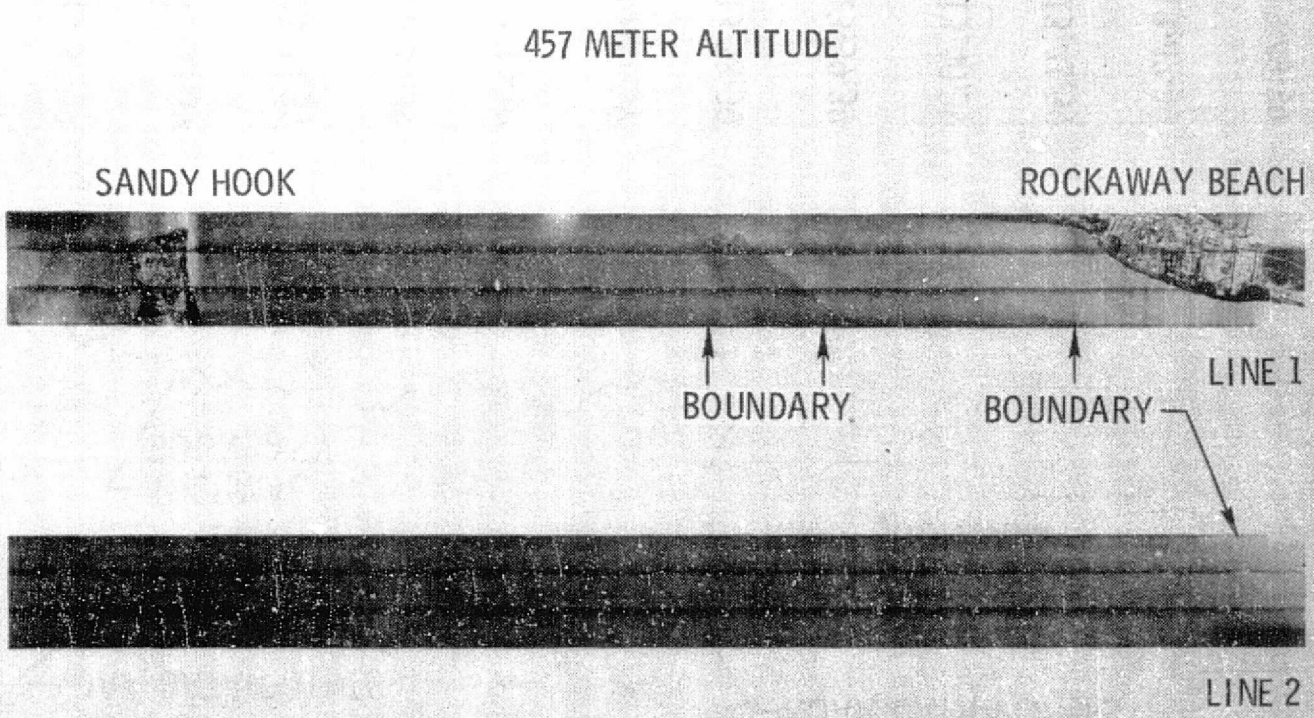

FIGURE 4 - Reconofax thermal record of the New York Bight area - April 10, 1975

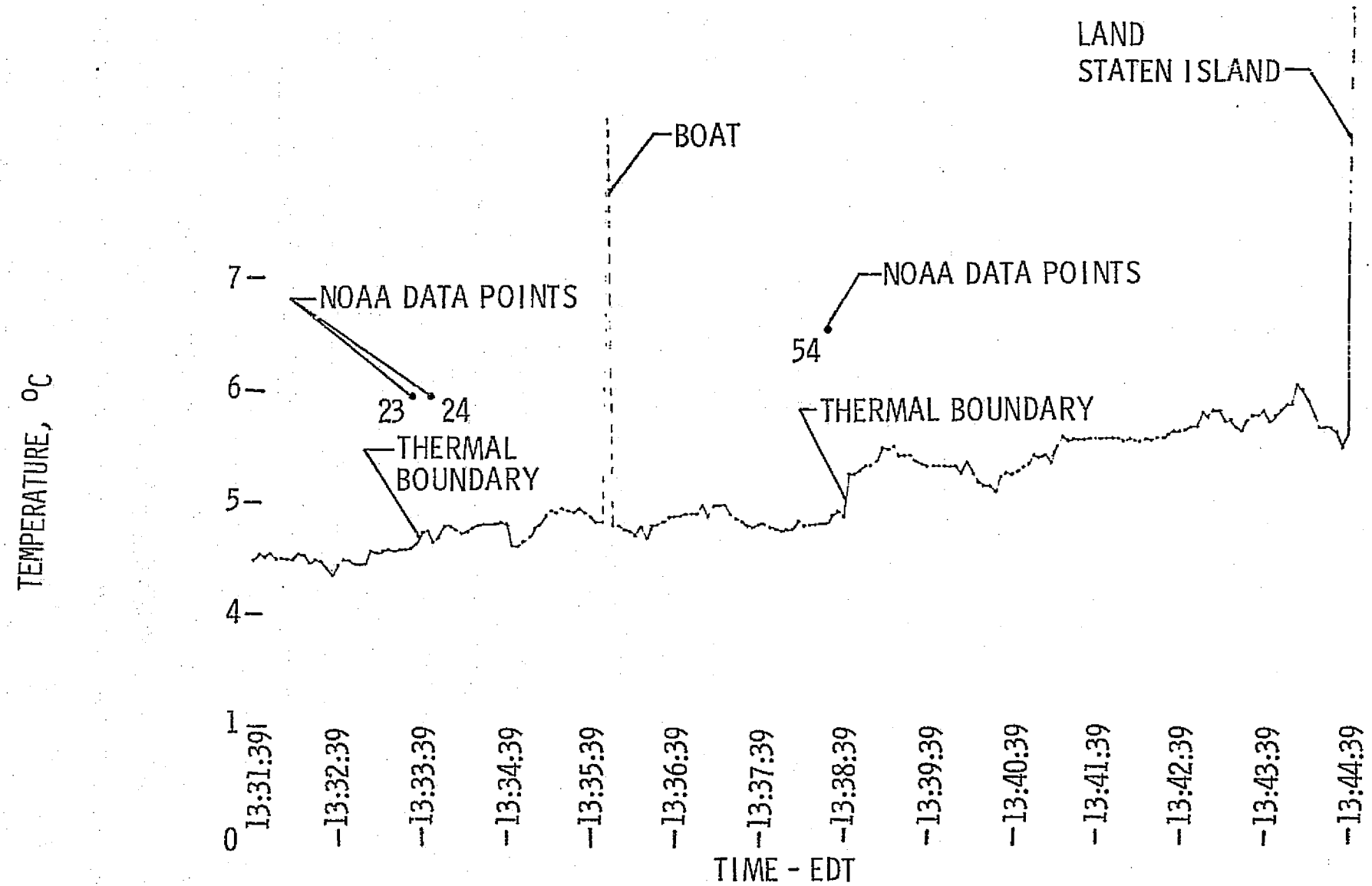

FIGURE 5 - PRT-5 RECORD - APRIL 13, 1975 - LOW LEVEL LINE C-1 FLOWN AT AN ALTITUDE OF 457 METERS.

5335 METER ALTITUDE

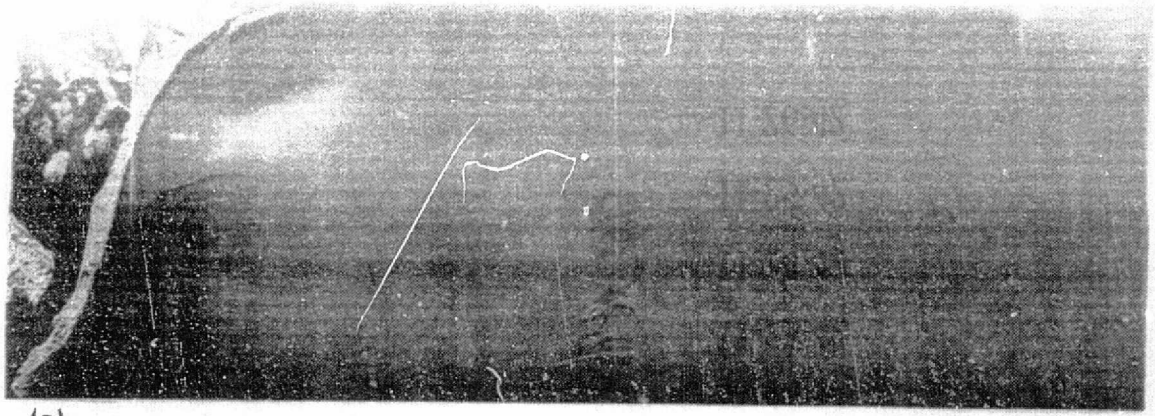

(a) LINE A-1

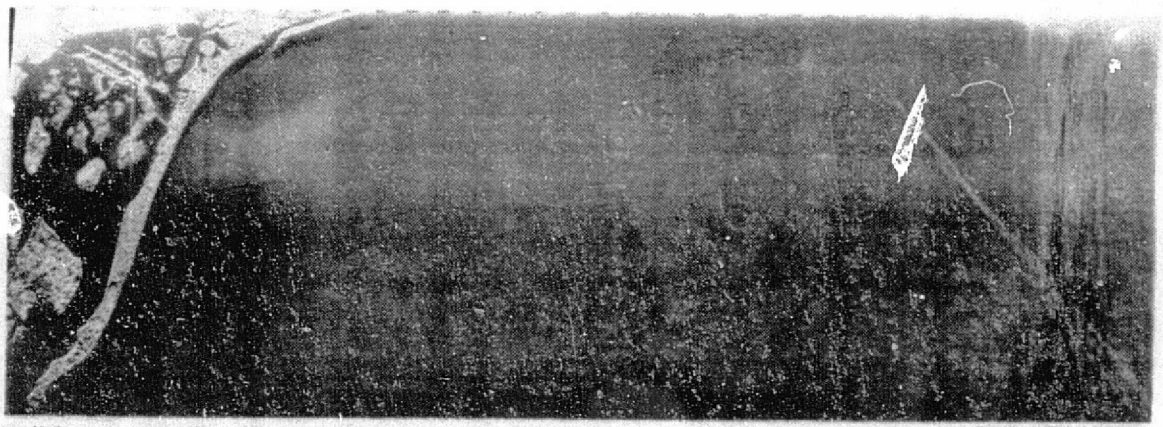

(b) LINE A-2

FIGURE 6 - Reconofax IV infrared scanner - April 10, 1975

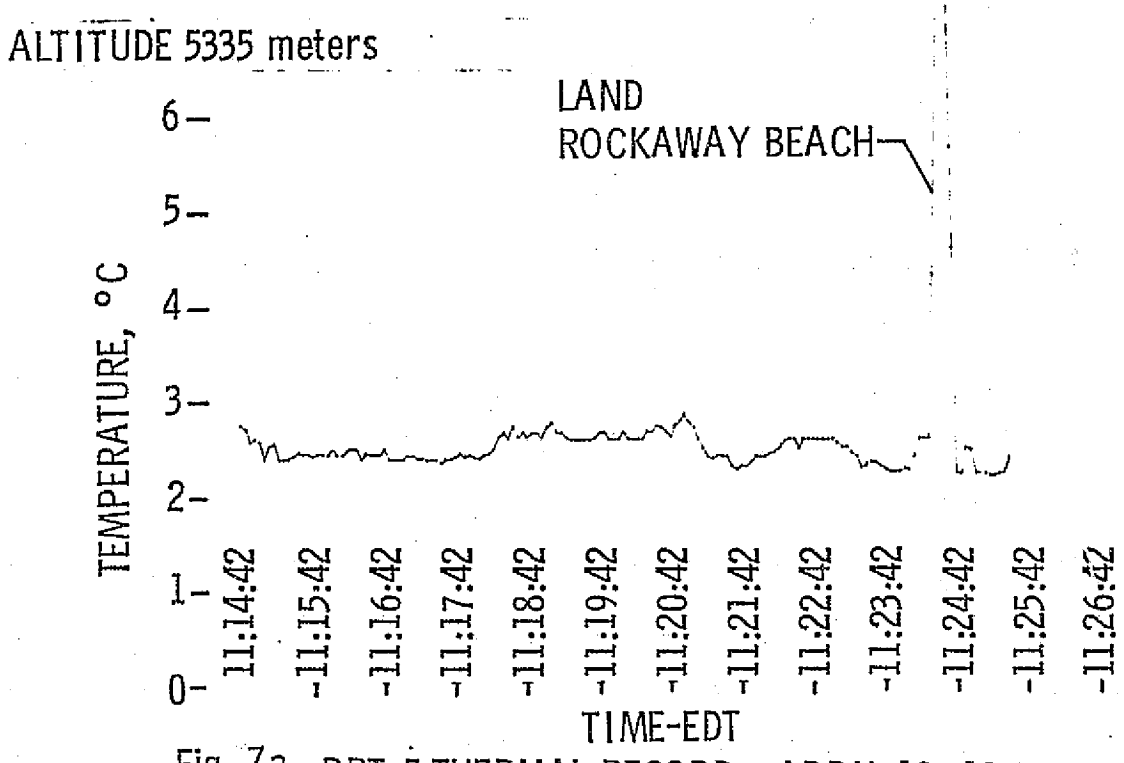

Fig. 7a - PRT-5 THERMAL RECORD - APRIL 10, 1975

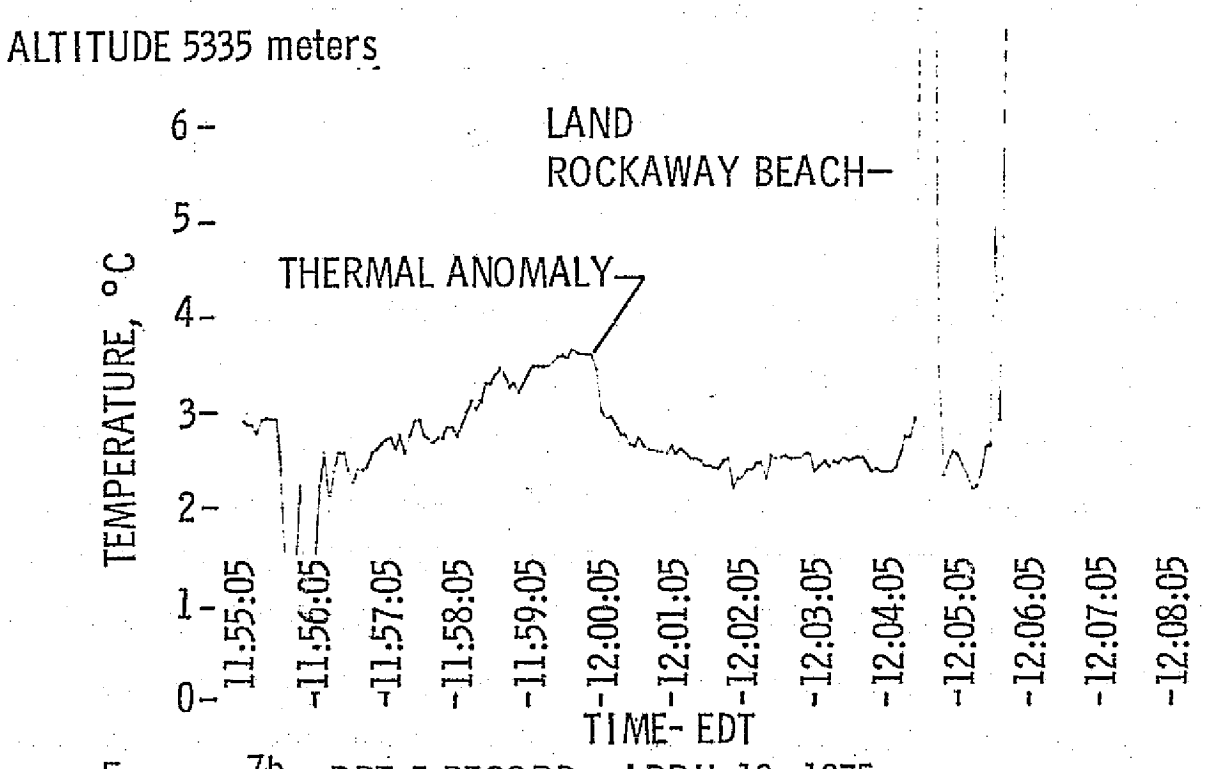

FIGURE 7b - PRT-5 RECORD - APRIL 10, 1975

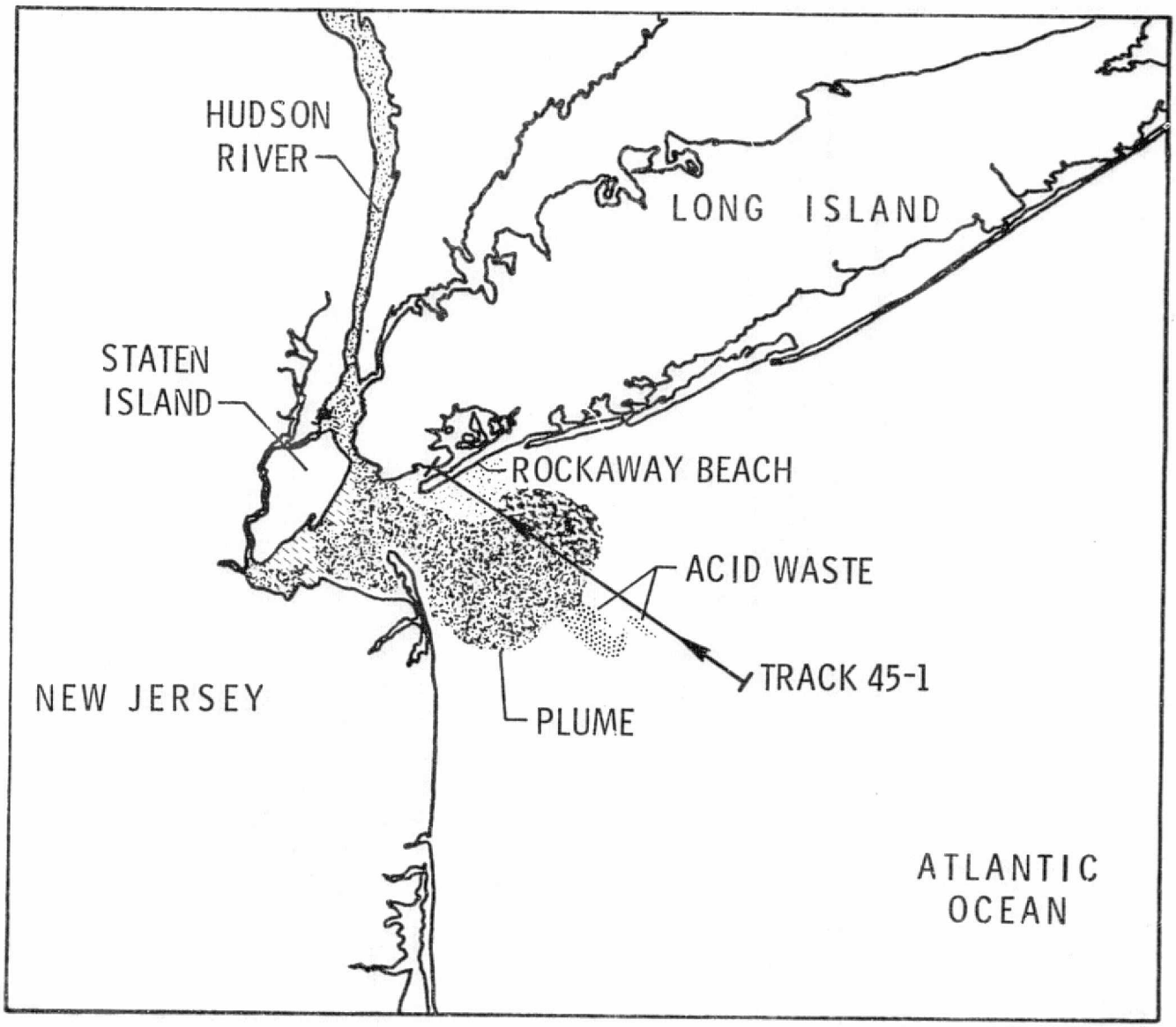

FIGURE 8 . - Sketch of the New York Bight

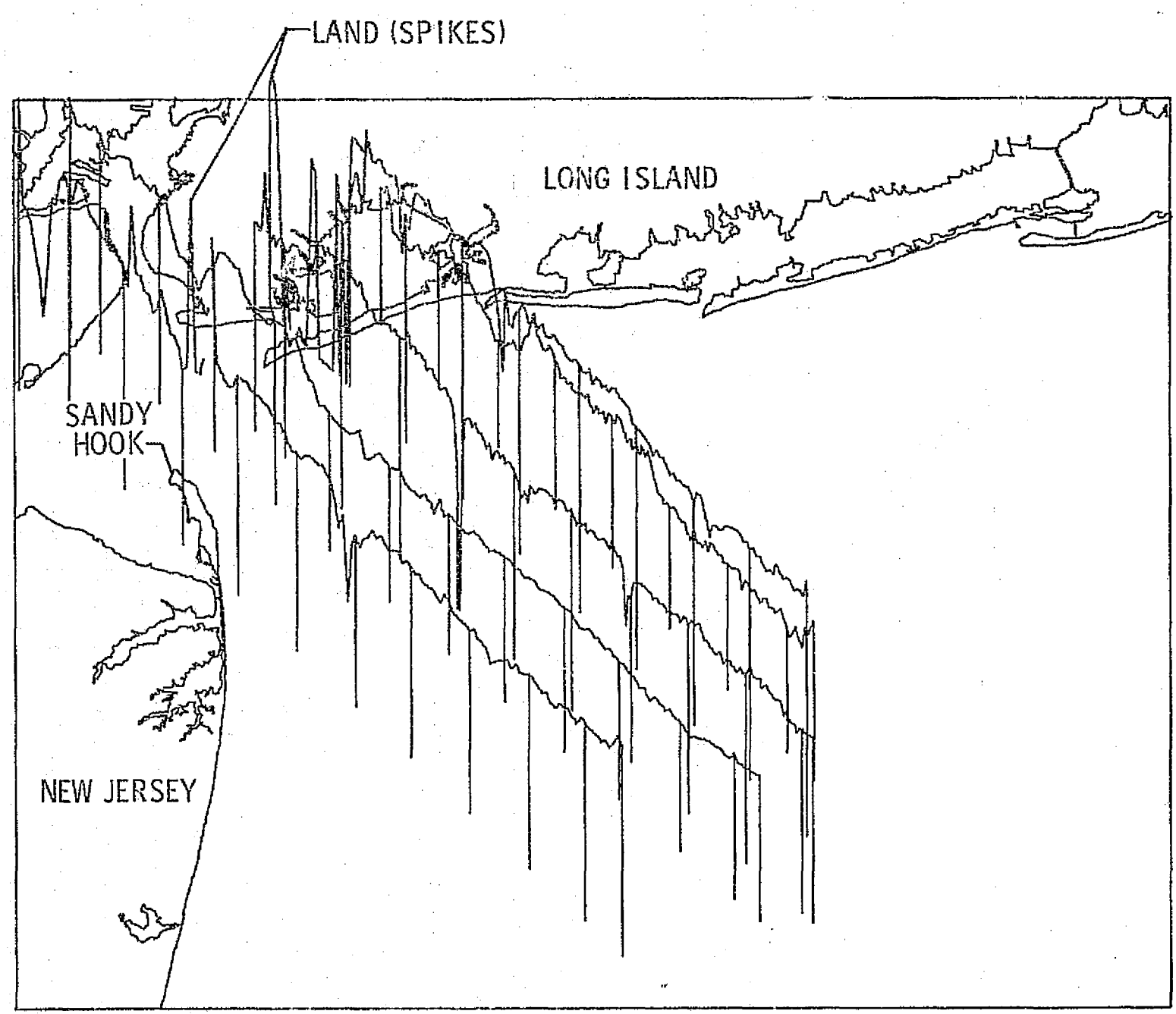

FIGURE 9 - PRT-5 thermal data for all five flight lines in the New York Bight on April 10, 1975

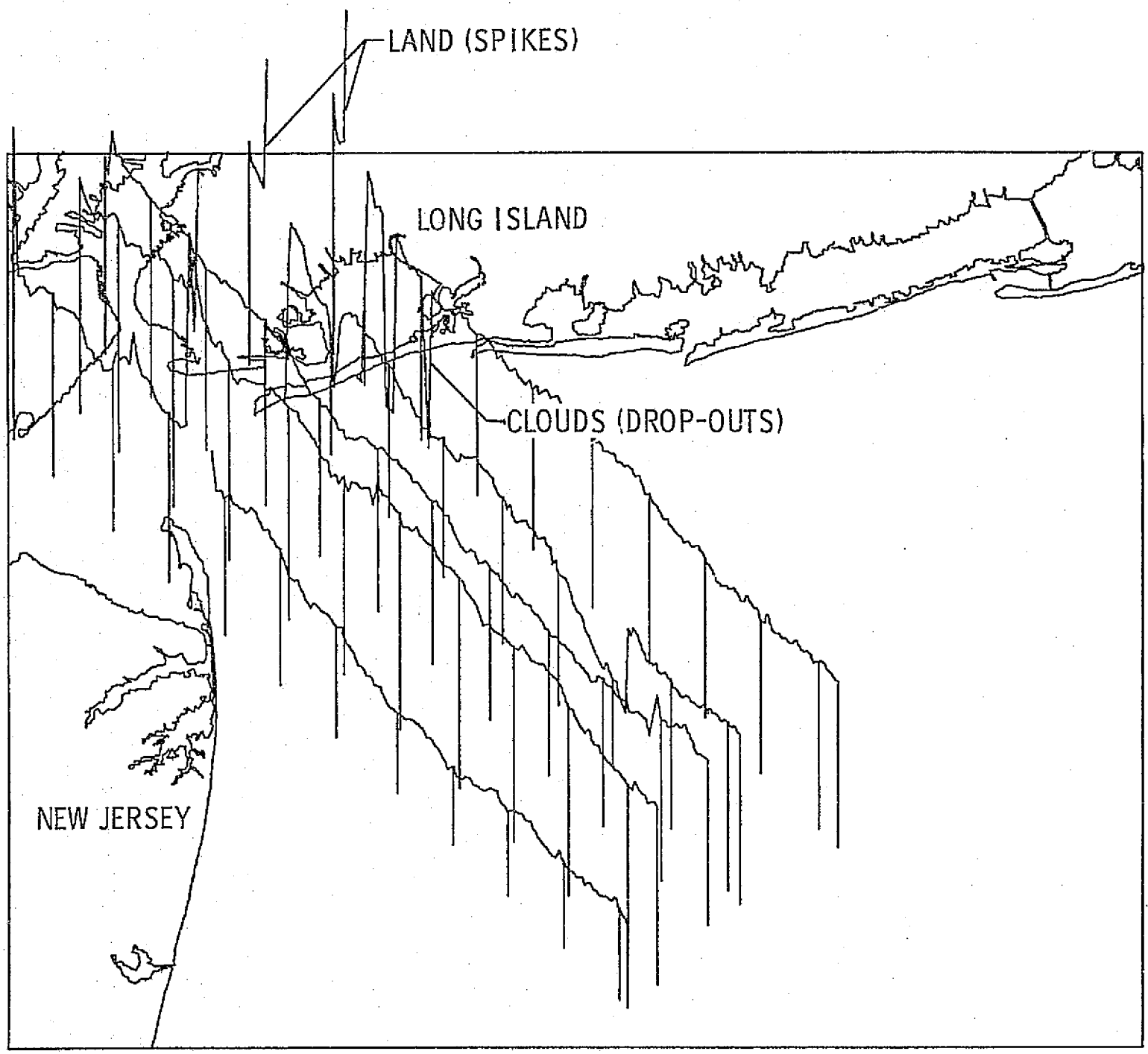

FIGURE 10 - PRT-5 thermal data for all five flight lines in the New York Bight on April 13, 1975

Mapping the Hudson River Plume and An Acid Waste Plume by Remote Sensing in the New York Bight Apex, April 1975.

by

Robert W. Johnson

MAPPING THE HUDSON RIVER PLUME AND AN ACID WASTE PLUME BY REMOTE SENSING IN THE NEW YORK BIGHT APEX, APRIL 1975

by

Robert W. Johnson

INTRODUCTION

Suspended sediment and chlorophyll-a concentrations and their distributions have been identified as important environmental parameters for monitoring water quality and pollution in coastal zones. Suspended sediment has been recognized as a natural tracer that may be used to measure flow and distributions in a water body, thereby providing information on pollutant concentrations and dispersions. Chlorophyll-a concentrations are a measure of the nutrient load and an indicator of current state of health of a water body. In addition, as yet unidentified materials in spectral anomalies such as plumes resulting from ocean dumping of acid wastes may be used to identify and map those features. Synoptic distributions of these environmental parameters may be determined from remotely sensed data, thereby providing information not readily available by any other means. Calibrated regression equations have been used by Johnson (ref. 1, 2) to quantitatively map distributions of water quality parameters such as suspended sediment and chlorophyll-a from remotely sensed multispectral scanner data.

It is the objective of this investigation to apply the methodology of reference 1 to a coastal zone environment and to develop calibrated regression equations to quantitatively map distributions of water quality parameters (e.g., suspended sediment and chlorophyll-a) measured in the sea truth

program.* In addition, other spectral anomalies in the scene, such as acid waste plumes, will be qualitatively mapped.

EXPERIMENTAL METHOD

Remotely sensed data were analyzed and interpreted using concurrently collected sea truth information. Data collections were made on April 9, 13, and 14, 1975, with the most complete set collected on April 13. Results presented here will be limited to analysis of remotely sensed data collected on April 13, 1975 (ref. 3).

Remotely sensed data were collected by the Ocean Color Scanner (OCS) and Mitchell-Vinten cameras from a U-2 aircraft platform at a flight altitude of 19.7 kilometers (km) (65,000 ft.). The OCS is a 10-band multispectral scanner with 10 bands in the visible and near IR spectral range. Band center wavelengths are from 433 nanometers (nm) to 772 nm for the nominally 20 nm wide bands, table I. Ground spatial resolution was about 75 meters (248 ft.). Data were recorded onboard the aircraft on magnetic tapes with four bands (2, 4, 5 and 8) digitized during flight and the others recorded in an analog format. Initial data reduction and formatting were performed by the NASA Goddard Space Flight Center (GSFC) with calibrated digitized data in Bands 1 through 8 supplied to the Langley Research Center on computer compatible tapes (CCT).

Sea truth measurements for this experiment were collected by helicopter over the 25 station matrix in the New York Bight apex. In addition, six

*I would like to acknowledge the contributions of Mr. Terry A. Nelsen of the AOML/NOAA for the collection and analysis of sea truth data during the experiment, and also, those of Messrs. Gilbert S. Bahn and Robert M. Glasgow of the Vought Corporation who contributed to the computerized data analysis and mapping products.

samples were collected at "sites of opportunity." Sample locations are shown in figure 1. Stations 4, 5, 10, 15, and 21 were outside of the OCS scan and X4 and X5 could not be located due to missing LORAN data. Suspended sediment and chlorophyll-a determinations were made at most of the sample locations. Table II is a listing of suspended sediment and chlorophyll-a concentrations analyzed in this report. In addition, particle size distributions were obtained within 24 hours by Coulter Counter from water samples taken at these stations (fig. 2). Station locations for the sea truth sampling were determined by LORAN A with an estimated absolute accuracy of 70 meters (220 ft).

DATA ANALYSIS AND RESULTS

Data Preprocessing

Representative radiance values corresponding to the sea truth measurements were determined by locating the sampling station as nearly as possible, and then by taking the average of an 11 by 11 field centered at that location to obtain the representative value. This field size was empirically determined as the area required to compensate for uncontrollable spectral and spatial "noise" or uncertainty. Radiance values (mw/cm^2-ster-μm) associated with the sea truth sampling stations are listed in table III.

Quantitative Data Analysis

Stepwise Regression Analysis (SWRA) was used to determine calibrated regression equations for quantitatively relating the sea truth measurements to remotely sensed data, as in references 1 and 2. In an SWRA, the independent variable (radiance in one OCS band) is selected that has the highest correlation with the dependent variable (water quality parameter; e.g.,

suspended sediment or chlorophyll-a). A number of variables are then selected consecutively until all of the independent variables (bands of OCS data) that make a significant contribution to determining the dependent variable are included in the regression equation and the others are "outside" the regression. Limiting the regression equation to significant variables reduces the analysis time and improves the accuracy of the results. The criterion for inclusion of variables is a 90-percent confidence level as determined by the statistical "F" test (see p. 171, ref. 4 for a discussion of the SWRA).

Quantitative Analysis Results

All values obtained in the sea truth program (that could be located in the scene) were included in the quantitative analyses of suspended sediment and chlorophyll-a except those in the spectral anomaly associated with the acid waste dump plume (e.g., all stations except 18, 23, X4 and X5 for suspended sediment and 18, 23, X1, X2, X3, X4, X5 and X6 for chlorophyll-a). There were a total of 22 observations for suspended sediment and 18 for chlorophyll-a. The plume from the acid waste dumps will be discussed under qualitative mapping in a later section.

Results of the SWRA applied to suspended sediment and subsequently to chlorophyll-a were as follows:

Water Quality Parameter	OCS Band, RN in Regression Equation	Standard Error of Estimate	Correlation Coefficient	Correlation to Suspended Sediment	Range of Sea Truth Measurements
Suspended Sediment	R6	1.39	0.79	-	0.46 - 8.38 mg/ℓ
Chlorophyll-a	R3, R6	3.87	0.83	0.90	2.20 - 24.30 mg/m^3

where RN is the radiance in OCS band N (i.e., R6 is radiance in band 6); standard error of estimate is a measure of the scatter about the fitted regression line; correlation coefficient is a measure of the relative change among variables; correlation coefficient to suspended sediment is the linear correlation of that variable to suspended sediment; and range of sea truth measurements are for the water quality parameter being analyzed.

Comparison of the remotely sensed (calculated from the regression equation) and measured sea truth values for suspended sediment and chlorophyll-a concentrations are shown in figures 3 and 4, respectively. Deviations from the fitted regression line occur approximately randomly, thus the linear model appears adequate. Johnson (ref. 1, 2) previously indicated linear responses in this range for suspended sediment and chlorophyll-a.

Interpretations of the remotely sensed data should consider the high correlation between changes in suspended sediment concentrations and changes in chlorophyll-a concentrations. In this case, where the correlation coefficient (0.90) of sea truth (suspended sediment to chlorophyll-a) is higher than for sea truth to remotely sensed data for either parameter, it should be interpreted as a combined response where neither parameter can be unambigiously separated by the analysis. The high correlation between suspended sediment and chlorophyll-a is shown in their comparison in figure 5.

Quantitative Mapping of Suspended Sediment and Chlorophyll-a

Quantitative mapping of water quality parameter concentration distributions may be determined from the regression equations. For each water quality parameter, concentrations are determined at each pixel (or equal spacings of lines or columns), this field of data is typically smoothed to remove

local spectral and spatial noise features and then a contour map is developed by a computerized plotting routine. The smoothing routine used in this analysis is an averaging on a line-by-line and column-by-column basis in the data field where the middle value is replaced by the mean of it and the two adjacent values. Edge values remain the same. In this analysis each pixel in every third line of data was used to generate the field of data for mapping. Two smoothing passes were made for suspended sediment concentrations and two were used for chlorophyll-a concentrations.

Maps of suspended sediment and chlorophyll-a distributions, figures 6 and 7, also indicate the high correlation (0.90, see fig. 5) between these parameters. The Hudson River plume extension into the Eight Apex, then a drift southward along the New Jersey shore, is clearly indicated in both figures. The previously located acid waste plume is shown in both the suspended sediment and chlorophyll-a distribution maps. Data interpretation of this feature is discussed in the following section. The more concentrated portion of the acid waste plume is at station 18 which is in or near the legal dump area. Less concentrated areas of the acid waste plume are probably due to dispersion and to earlier dumps. Acid waste dump plumes have been observed to persist for greater than 24 hours (ref. 5).

Qualitative Analysis of the Acid Waste Plume

There are not sufficient sea truth points in the acid waste plume to apply quantitative analysis techniques. However, investigation of spectral changes associated with plume dispersions indicates that the spectral range most indicative of plume changes are in the OCS band 3 to 6 spectral range. This is the same spectral range that indicates differences in suspended

sediment and chlorophyll-a. Thus, apparent changes in suspended sediment and chlorophyll-a concentrations in the acid waste plume area should be interpreted as qualitative mapping of the acid plume (qualitative since materials in the acid plume are known to be different from those in the other locations of the experimental area).

Spectral responses in the acid waste plume at locations of apparently different concentrations are shown in figure 8. For comparative purposes, spectral responses for the Hudson River Plume and background (Bight Apex) water are shown in figure 9. Radiance values in the acid plume are not as high or as spectrally wide as in the combined suspended sediment-chlorophyll-a in the Hudson River plume. This is shown in the ratios of plume to ocean water radiances in figure 10.

Particle Size Distributions

Particle size distributions for the basic areas in the sea truth and remotely sensed data are shown in figure 2 for the Hudson River plume, acid waste plume and background water. In the Hudson River plume, the dominant size particles are small (6 phi(ϕ) or 15 micrometers (μm)); those in the acid plume are relatively large particles (3.5ϕ or 80 μm); and those in the background water are essentially bimodal (both large and small) in character. It should be emphasized that these are relative counts of particles and only relative distributions may be compared since little is known about the shape or specific gravity of the constituents.

Identification of Pollutant Plumes

Identification of the two major spectral features (e.g., the Hudson River and acid waste plumes) would be possible in future experiments by

spectral responses in the remotely sensed data. Figures 8 and 9 are radiances (mw/cm^2-ster-μm) in the OCS bands for ranges of concentrations of the Hudson River and acid waste plumes, respectively. Note the general spectral similarity. However, when the highest concentration responses of the plumes are ratioed to an in-scene calibration (ocean water) the differences are quite apparent above wavelengths of 580 nm (fig. 10). It appears that both radiance values and ratios to an in-scene source will be useful for pollutant identification and monitoring by remote sensing.

Identification of plumes by sea truth measurements will be aided by the particle size characterization, figure 2. As indicated previously the Hudson River plume has predominantly small particles, the acid waste plume has predominately large particles and the ocean water is bimodal in character.

CONCLUDING REMARKS

Remote sensing may be effectively applied to locate, identify and map major water features in the New York Bight Apex. A multispectral scanner from an aircraft platform was used to map the synoptic dispersion patterns of plumes from the Hudson River and ocean dumping. The ocean dumping plume was from acid waste dumps in the Apex on April 13, 1975. Results indicate that the types of plumes may be identified from remotely sensed spectral responses without concurrent sea truth. In addition, particle size distributions from the sea truth measurements provided information to further characterize the river and acid waste dump plumes.

Digital data analysis techniques were used to develop quantitative relationships between remotely sensed data and the two water quality parameters of interest, suspended sediment and chlorophyll-*a*. Due to the

high correlation in the measured values of these two parameters in the sea truth program, it was not possible to determine unambiguous distributions of these parameters; however, their mutual changes have been used to map the dispersion of the Hudson River plume.

Qualitative and quantitative mapping of pollution related features were made for the New York Bight Apex. Additional sets of data with expanded sea truth measurements will be required to further evaluate the analysis techniques applied to this set of remotely sensed data.

REFERENCES

1. Johnson, Robert W. Quantitative Suspended Sediment Mapping Using Aircraft Remotely Sensed Data. Proceedings of the NASA Earth Resources Survey Symposium, Houston, Texas, June, 1975. pp. 2087-2098, NASA TM X-58168.

2. Johnson, Robert W. Application of Aircraft Multispectral Scanners to Quantitative Analysis and Mapping of Water Quality Parameters in the James River, Virginia. Presented at the XIXth Meeting of COSPAR, Philadelphia, PA June 14-19, 1976.

3. Usry, J. W. and J. B. Hall, Jr., National Aeronautics and Space Administration Operations - Remote Sensing Experiments in the New York Bight, April 7-17, 1975. NASA TM X-72802, November, 1975.

4. Draper, N. R. and H. Smith. Applied Regression Analysis, John Wiley & Sons, Inc. New York, N.Y., 1966.

5. Klemas, V., D. Bartlett, W. Philpott, R. Rogers and L. Reed. Skylab/ EREP Applications to Ecological, Geological, and Oceanographic Investigations of Delaware Bay. Final Report Contract NAS1-12304. NASA CR 144910.

TABLE I SPECTRAL CHARACTERISTICS OF THE OCEAN COLOR SCANNER

TEN CHANNEL SCANNER WITH 75-METER RESOLUTION,

SPECTRAL BAND:

433 NANOMETERS ± 10 nm,

* 471 NANOMETERS ± 10 nm,

509 NANOMETERS ± 10 nm,

* 547 NANOMETERS ± 10 nm,

* 583 NANOMETERS ± 10 nm,

620 NANOMETERS ± 10 nm,

* 662 NANOMETERS ± 10 nm,

698 NANOMETERS ± 10 nm,

733 NANOMETERS ± 10 nm,

772 NANOMETERS ± 10 nm,

* DIGITIZED ONBOARD U2,

INTERNAL CALIBRATION ONCE PER SCAN LINE.

TABLE II SEA TRUTH MEASUREMENTS*

STATION	SUSPENDED SEDIMENT CONCENTRATION mg/l	CHLOROPHYLL A CONCENTRATION mg/m^3
1	6.140	15.000
2	3.210	4.600
3	1.700	5.300
6	8.380	24.300
7	2.710	6.400
8	2.310	6.600
9	1.100	5.000
11	6.290	15.300
12	2.550	14.000
13	1.930	4.600
14	1.060	3.800
16	3.600	17.800
17	0.460	2.700
18**	9.030	-
19	0.680	2.400
20	0.560	2.200
22	0.710	4.200
23**	1.690	2.100
24	1.360	3.300
25	0.690	2.700
X1	1.730	-
X2	0.790	-
X3	0.580	-
X6	5.100	-

*Only data in the OCS scan are shown.

**In acid waste plume.

TABLE III REPRESENTATIVE RADIANCE VALUES AT THE SEA TRUTH STATIONS

Station	OCS BAND RADIANCE mw/cm^2-ster-μm Band							
	1	2	3	4	5	6	7	8
1	23.94	19.68	14.52	11.72	9.16	6.66	5.00	3.00
2	24.57	20.35	14.89	12.09	9.36	7.01	5.26	3.37
3	23.74	19.93	14.68	12.07	9.61	7.04	5.08	3.09
6	23.77	19.66	14.51	12.04	10.49	7.98	5.90	4.00
7	23.54	19.62	14.41	11.98	9.82	7.00	5.00	3.00
8	23.08	18.67	13.45	11.00	8.88	6.00	4.17	3.00
9	23.54	19.70	14.53	11.08	9.00	6.19	5.00	3.00
11	23.14	18.89	13.58	11.46	10.00	7.00	5.00	3.10
12	23.46	19.36	13.94	11.28	9.01	6.60	5.00	3.00
13	23.42	19.45	14.00	11.12	9.00	6.12	5.00	3.00
14	22.90	18.37	13.40	10.38	8.00	6.00	4.00	2.94
16	22.96	19.34	14.25	11.45	9.88	7.07	5.07	3.30
17	22.44	18.08	13.32	10.72	8.17	5.98	4.00	2.98
19	22.83	18.49	13.47	10.93	8.12	6.00	4.17	3.00
20	22.75	18.92	13.45	10.08	8.00	6.00	4.00	3.00
22	22.31	18.05	13.51	10.41	8.12	6.00	4.06	3.00
24	23.05	18.66	13.45	10.47	8.02	6.01	5.01	3.00
25	22.71	17.93	12.46	9.50	7.03	5.41	4.00	2.81
X1	23.05	18.79	13.59	11.15	8.58	6.02	4.84	3.00
X2	22.12	18.15	13.93	11.81	9.23	6.00	4.61	3.00
X3	22.19	18.12	13.86	11.51	8.89	6.00	4.47	3.00
X6	23.73	19.68	14.47	11.41	9.04	6.38	5.00	3.00

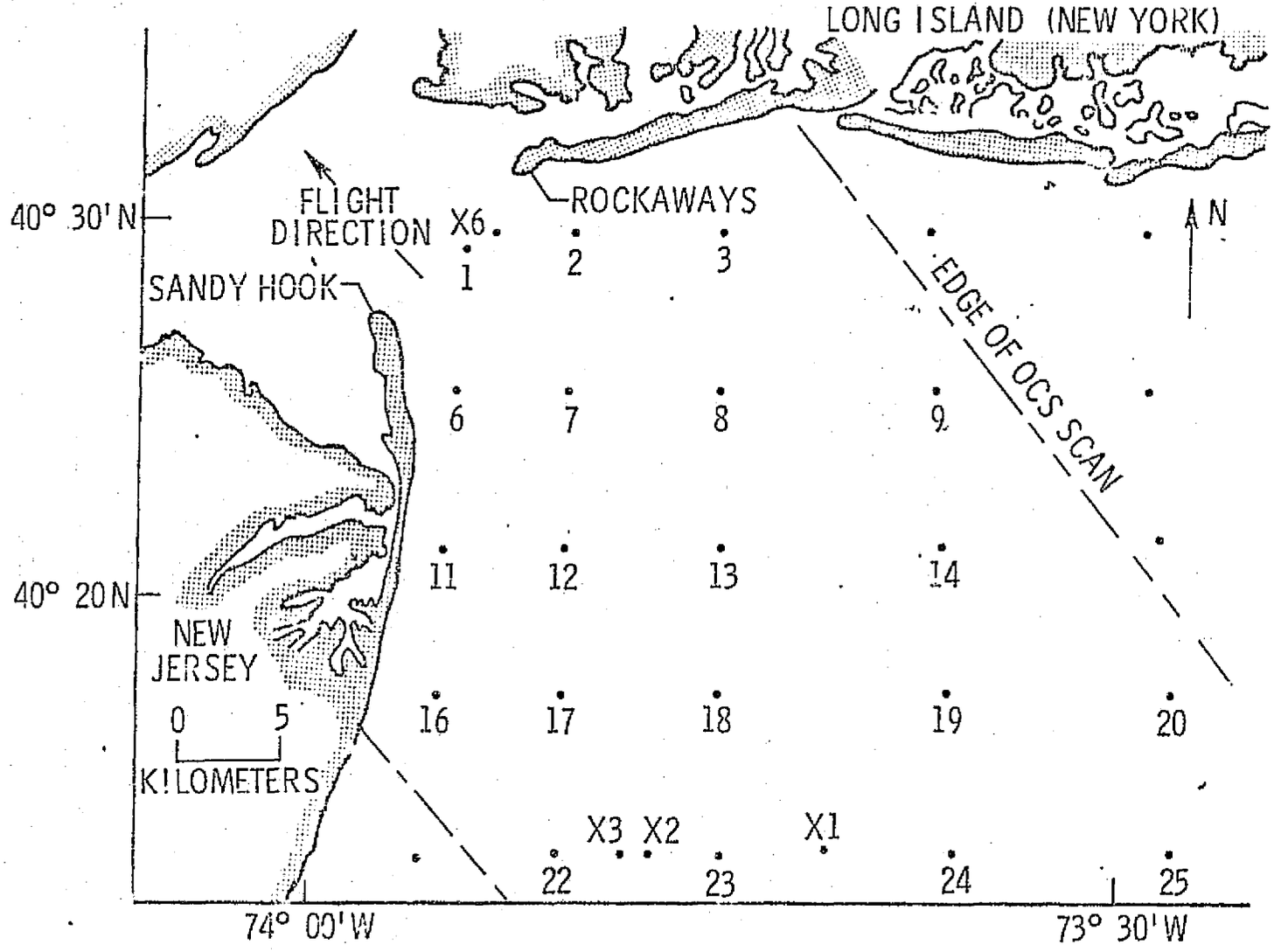

Figure 1. - Location of sea truth stations in the New York Bight Apex on April 13, 1975.

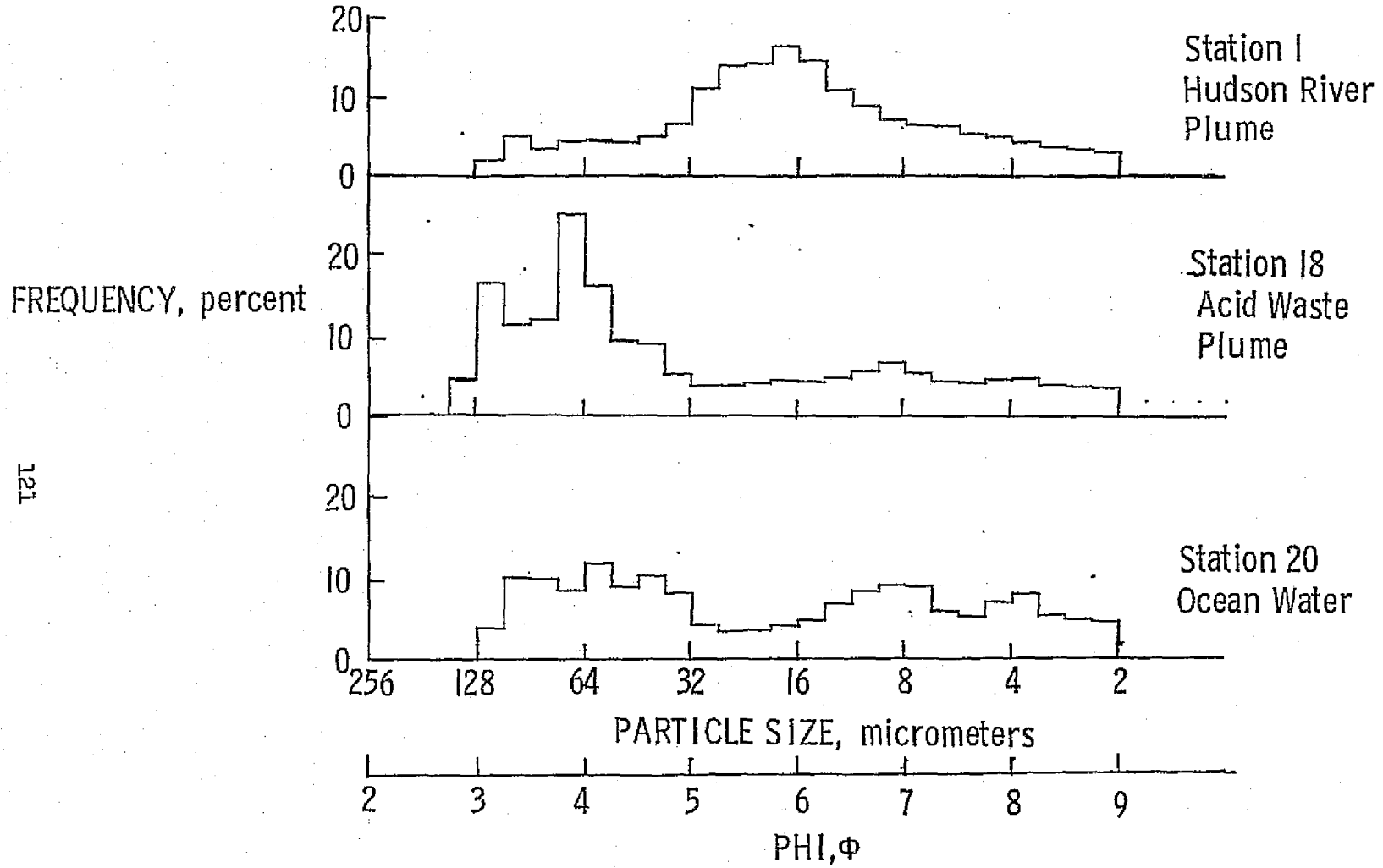

Figure 2. - Particle size distributions for the Hudson River and acid waste plumes, and N. Y. Bight Apex ocean water on April 13, 1975.

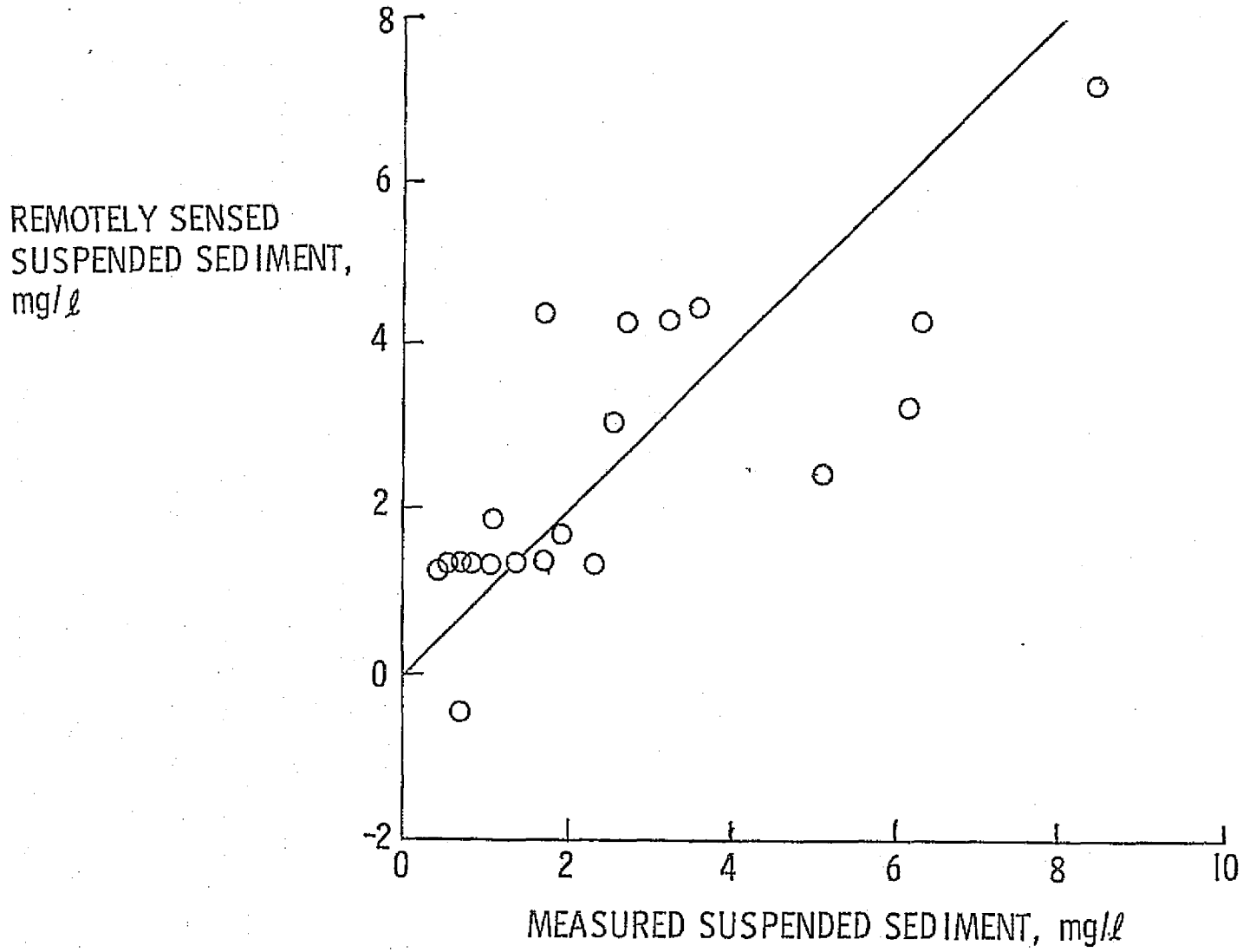

Figure 3. - Comparison of measured and remotely sensed values of suspended sediment.

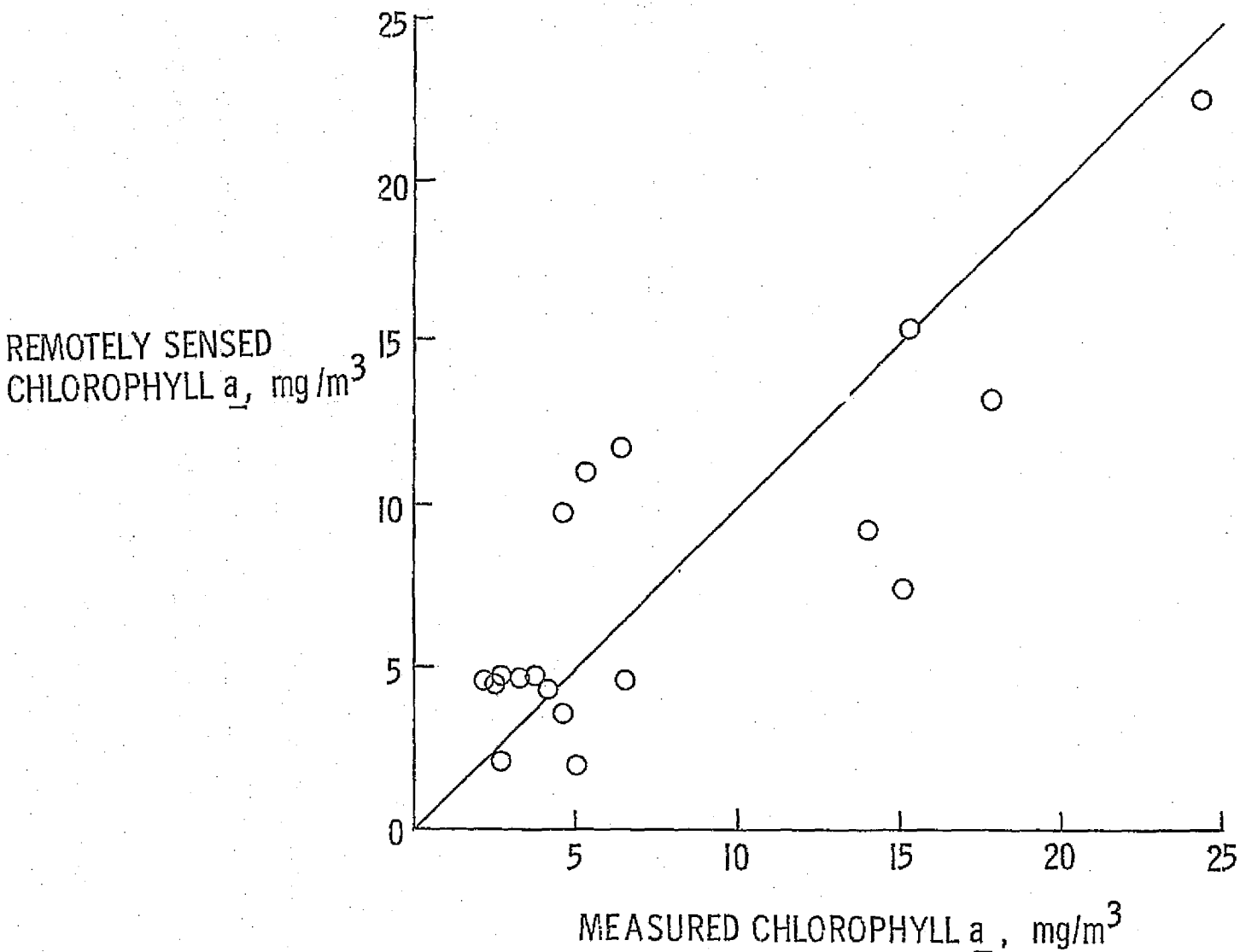

Figure 4. - Comparison of remotely sensed and measured values of chlorophyll a.

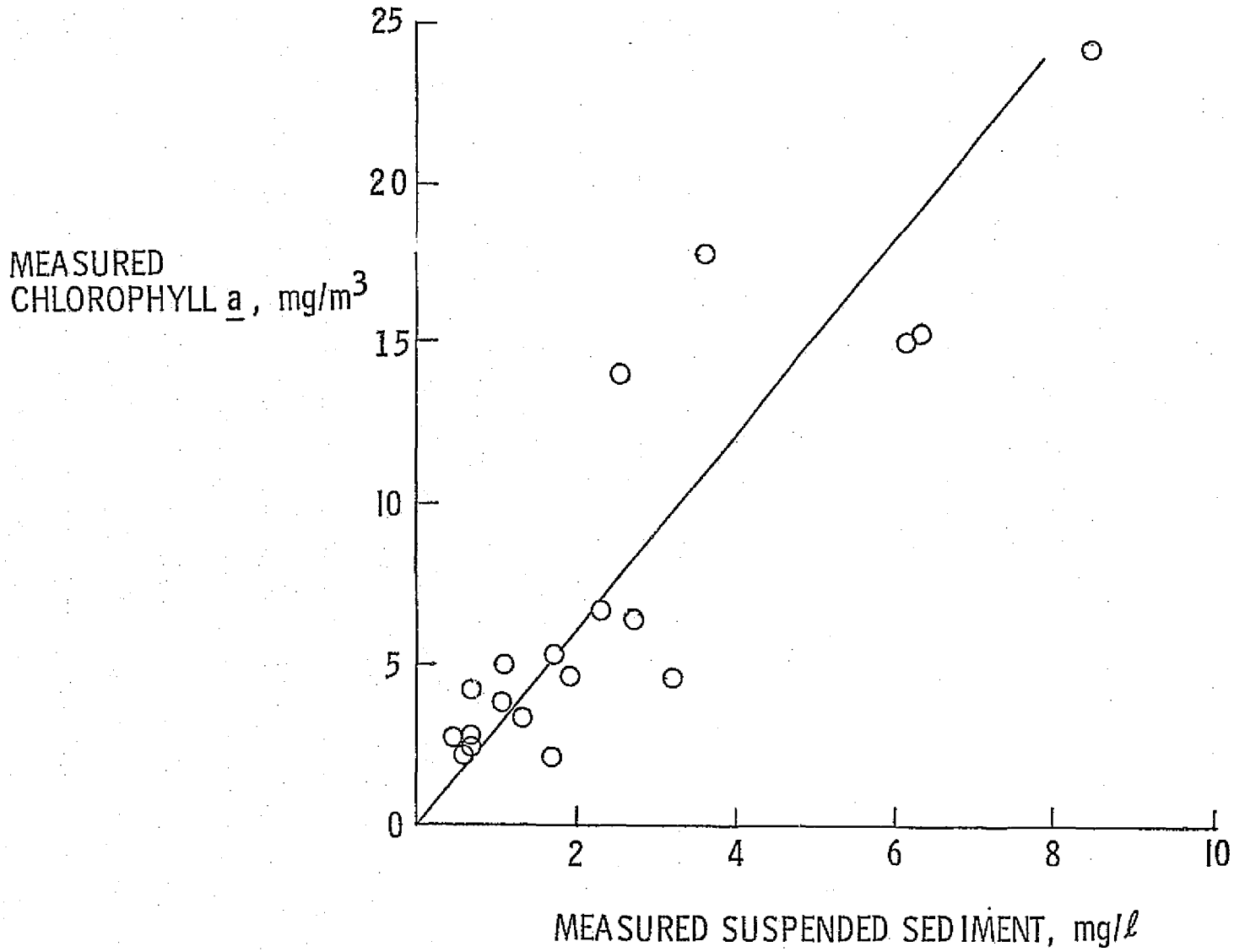

Figure 5. - Comparison of measured values of Chlorophlyy a and suspended sediment at sea truth stations.

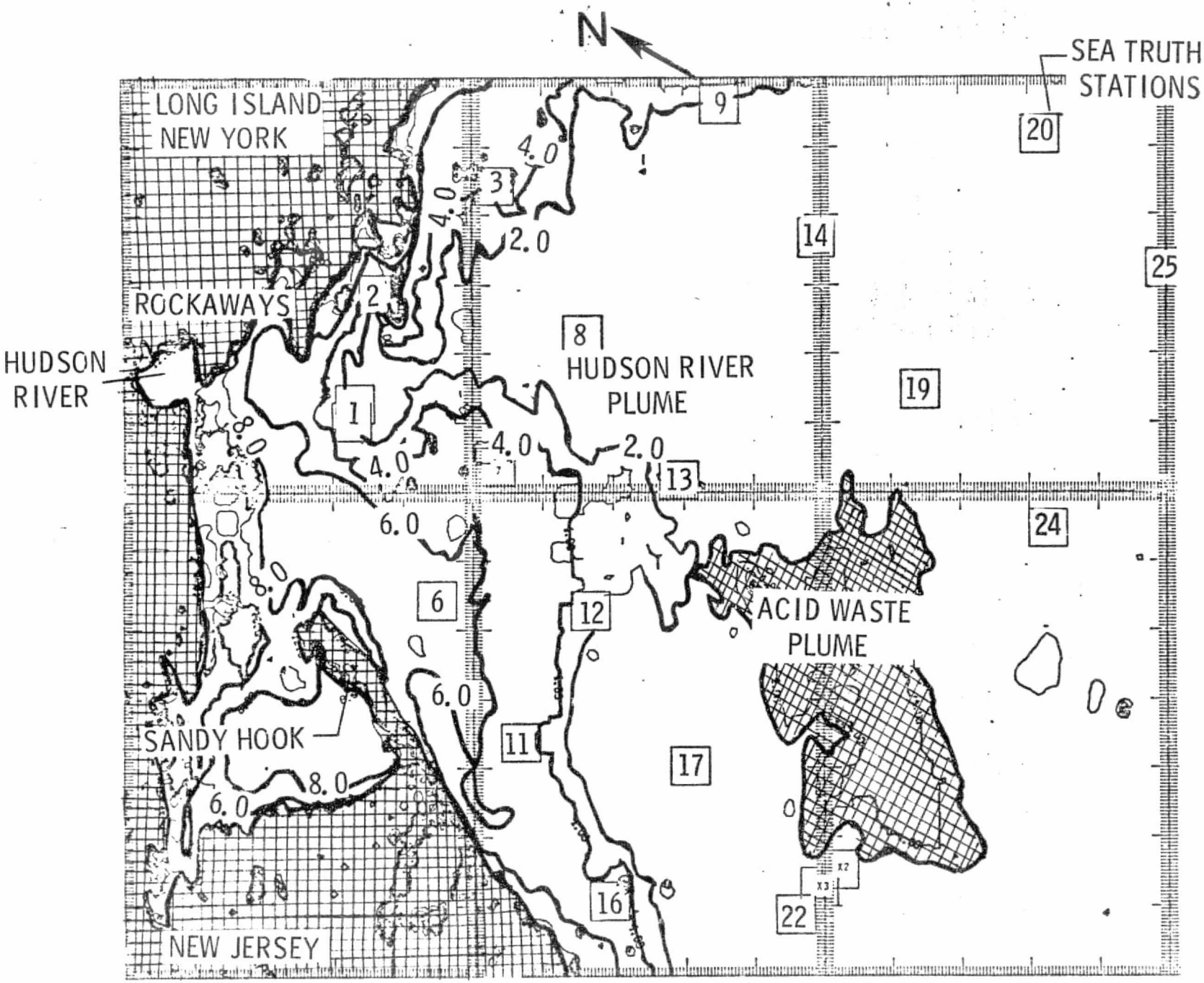

Figure 6. - Quantitative distribution of suspended sediment (mg/ℓ) in N. Y. Bight Apex. April 13, 1975.

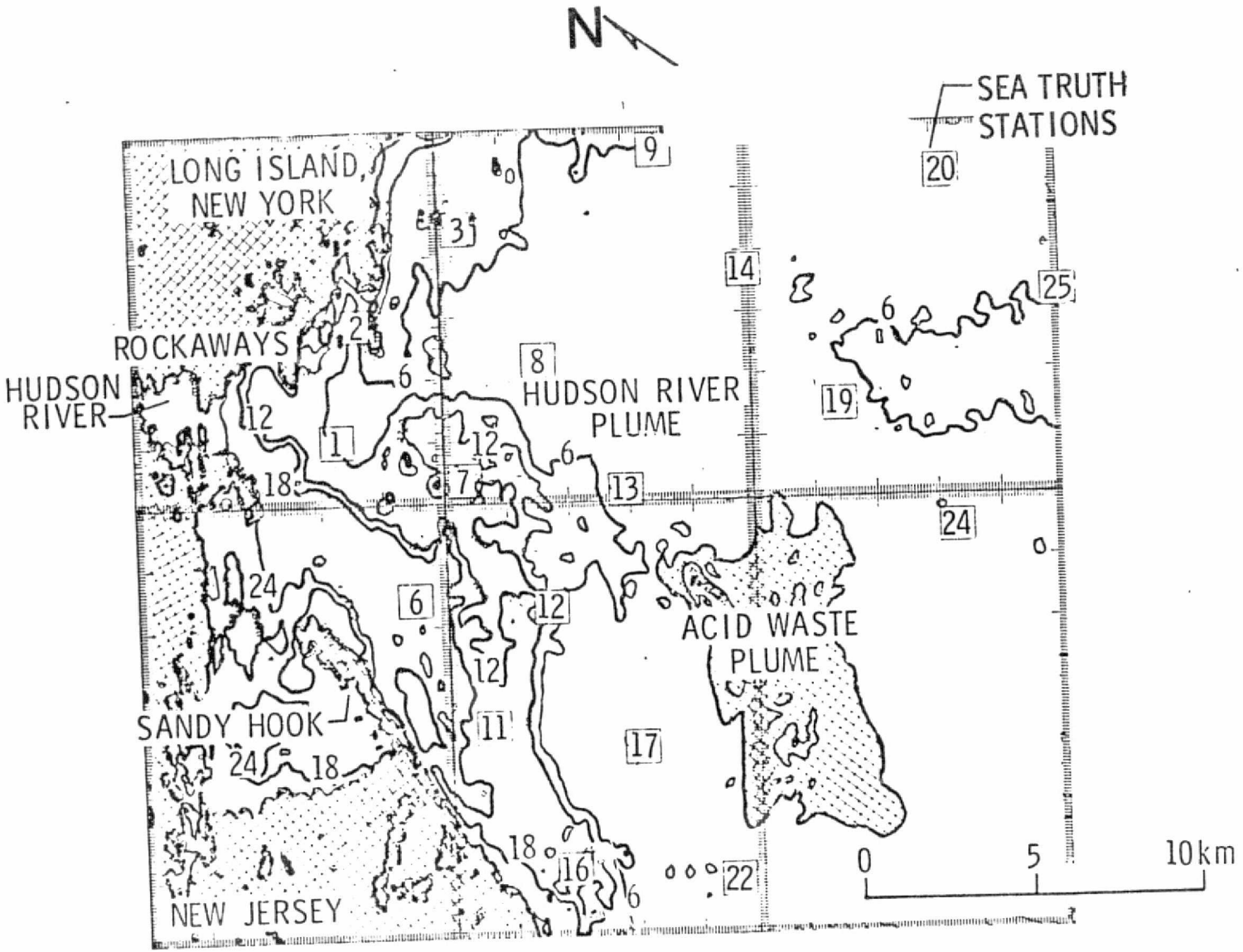

Figure 7. - Quantitative distribution of chlorophyll a (mg/m^3) in N. Y. Bight Apex April 13, 1975.

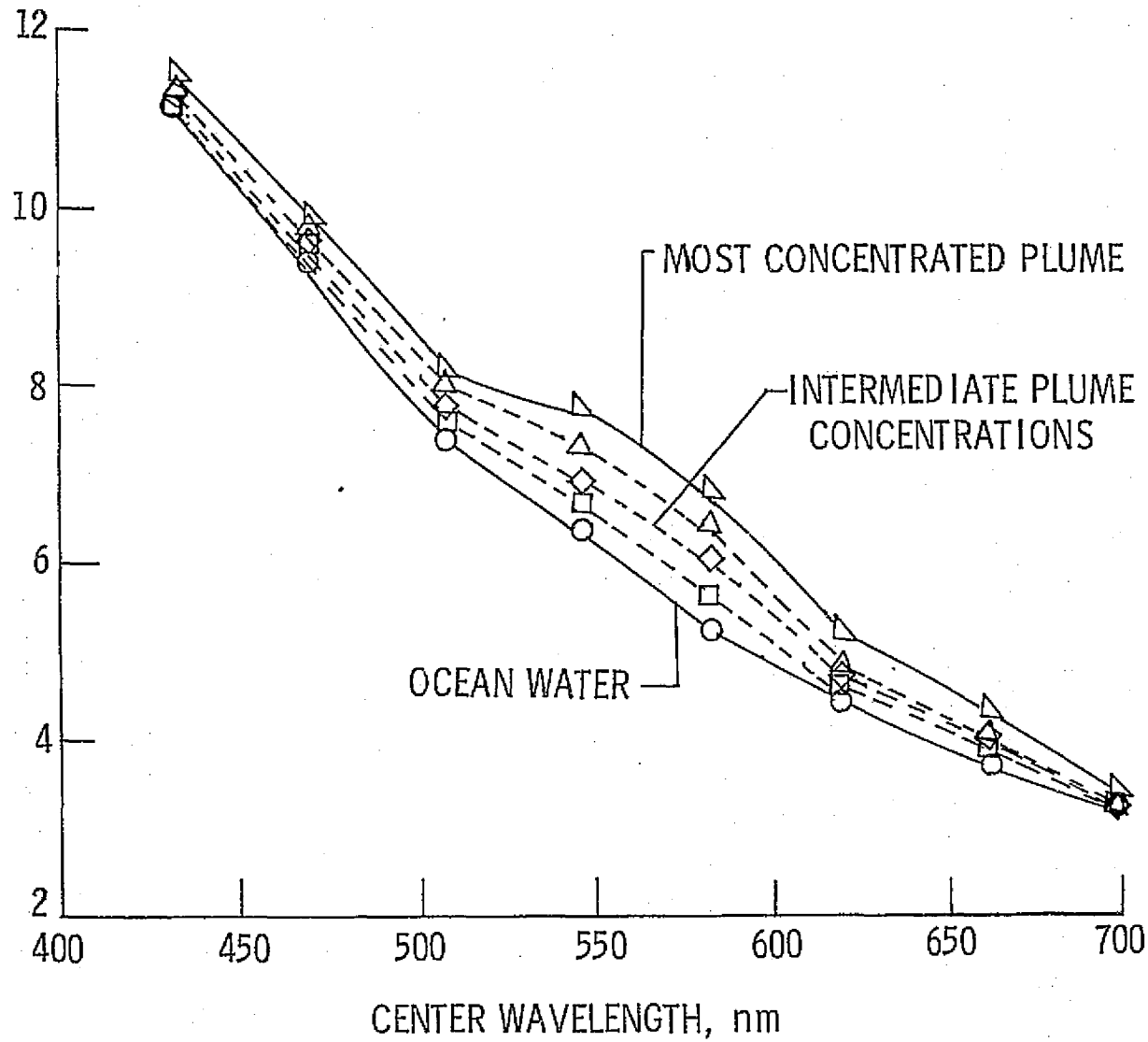

Figure 8. - Spectral responses in the plume resulting from acid waste dumps in the New York Bight.

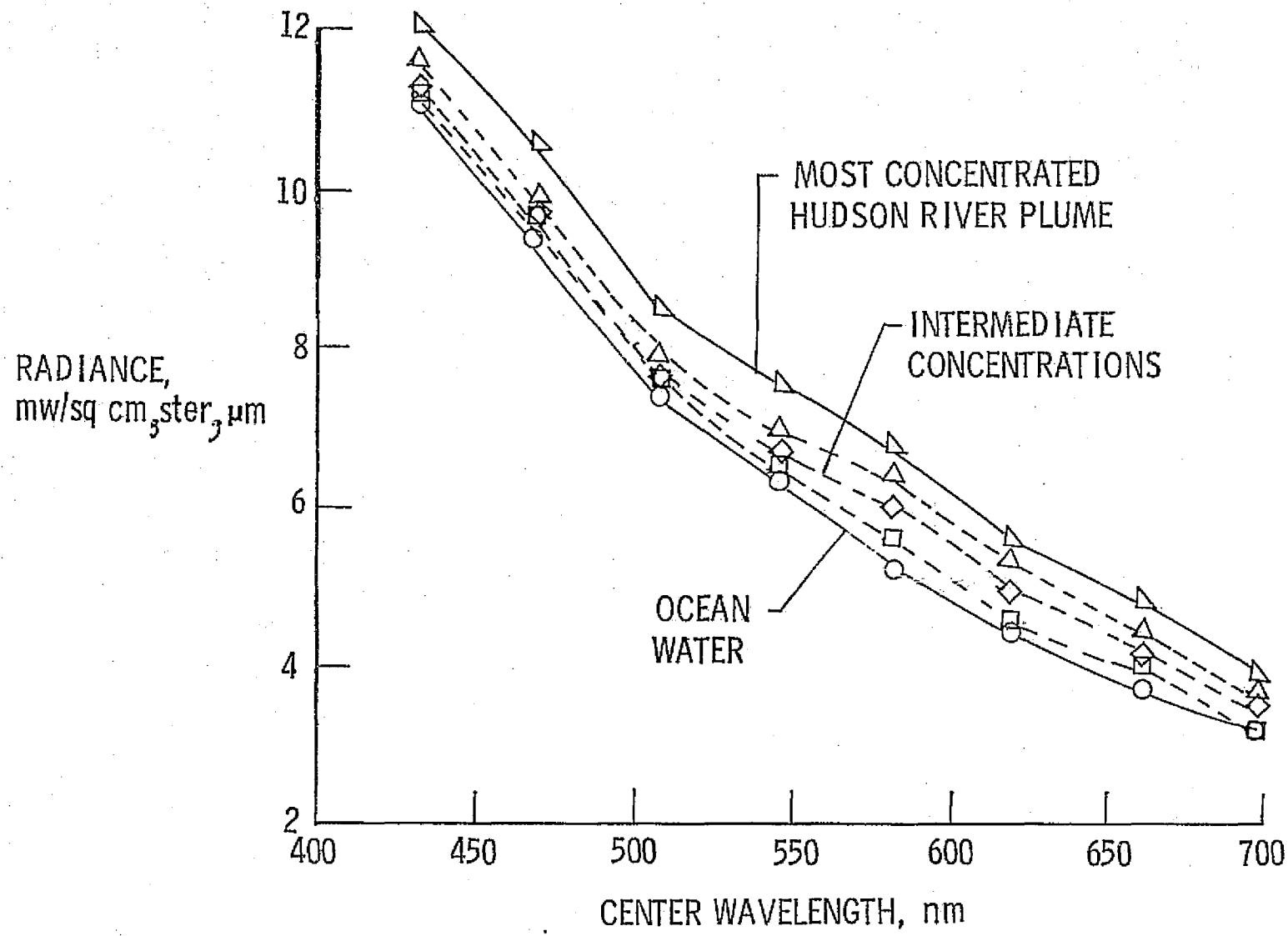

Figure 9. - Spectral responses of Hudson River plume at different concentrations and Ocean water on April 13, 1975.

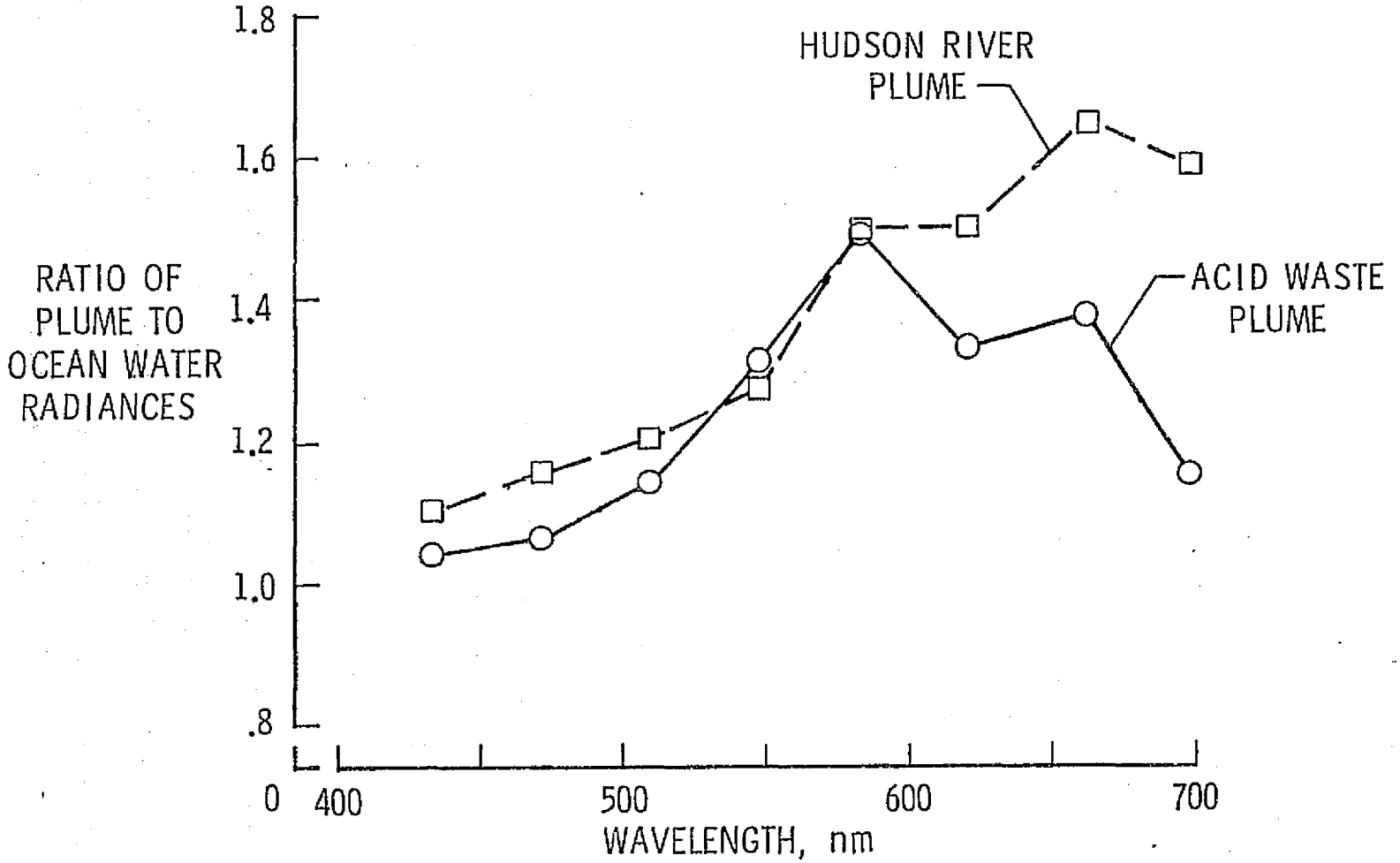

Figure 10. - Ratios of pollutant plume to ocean water radiances in the New York Bight on April 13, 1975.

BROADBAND SPECTRAL PHOTOGRAPHY

Walter E. Bressette

BROADBAND SPECTRAL PHOTOGRAPHY

Walter E. Bressette

SUMMARY

Comparison of broadband black and white photography at near-infrared wavelengths with green-yellow wavelengths shows that a substance being dumped in the New York Bight sludge dump area has a different spectral signature relative to the water background than does a substance from the acid dump area. Relative to the background water, the substance being dumped in the sludge dump area has greater reflectance at near-infrared wavelengths than at green-yellow wavelengths. The substance in the acid dump area has greater reflectance than the background water through both optical filters. In addition, the reflectance from the substance in the acid dump area is much greater in the green-yellow spectral region than it is in the near-infrared region.

Film density data, obtained from the green-yellow photography, show that waste dumping in the New York Bight increases the backscattered sunlight from the water over a much greater area than the designated dump site areas. It is clear from the photography that acid waste is the primary substance responsible for the increased backscattered sunlight, but the green-yellow wavelength data suggests that sludge dumping is also contributing.

Film density data indicate that upwelling radiance is greater from locations in the dump site area which contained less than 2 milligrams per liter total suspended material than from non-dump site areas which contained up to 9 milligrams per liter.

ACKNOWLEDGEMENTS

This remote sensing mission was performed on a National Aeronautics and Space Administration (NASA), Wallops Flight Center, C-54 aircraft and the photographic negatives from the mission are retained at the Chesapeake Bay Ecological Program Data Center, NASA, Wallops Flight Center. The ground truth measurement of total suspended material weight used in the data analysis was supplied by Terry A. Nelsen of the Atlantic Oceanographic Meteorology Laboratory, National Oceanographic and Atmospheric Administration (NOAA).

INTRODUCTION

An objective in the NASA Langley Research Center remote sensing program is to demonstrate that information derived from remote sensing of chlorophyll-a and suspended sediment can be used to control biodegradable water pollution. In reference 1 it is shown that chlorophyll-a produced by blue-green phytoplankton can be remotely mapped with a near-infrared detector when the concentration of chlorophyll-a is greater than 34 µg/l - a condition commonly referred to as a phytoplankton "bloom." However, as pointed out in reference 2, a "bloom" is a critical biodegradable condition where additional energy input above the "bloom" level becomes a stress, and the system becomes poisoned. Therefore, it is desirable to detect and monitor phytoplankton growth below "bloom" concentrations in order to provide biodegradable pollution control information. In reference 3 it is shown that below "bloom" concentrations the backscattered radiance through the optical filters flown was not proportional to chlorophyll-a concentrations,

and an optical filtering system for identifying the chlorophyll-a back-scattering from the total backscattered radiance is proposed. The major objective of the present reported photographic mission was to determine the effectiveness of the optical filtering system proposed in reference 3 for separating chlorophyll-a-containing phytoplankton radiance from total radiance when the concentration of phytoplankton is below "bloom" conditions.

EXPERIMENTAL METHOD

Two photographic missions were flown at an altitude of 5.3 kilometers (km) by an NASA, Wallops Flight Center, C-54 aircraft. One on April 10, 1975, between the hours of 10 a.m. and 11:25 a.m. eastern daylight time and the other on April 13, 1975, between the hours of 9:53 a.m. and 11:03 a.m. eastern daylight time. Four Hasselblad cameras were used in the missions. A description of the camera system and the C-54 aircraft is included in reference 4 along with pertinent documentation of the overall remote sensing missions. The camera settings and film type used for the mission are shown in table 1.

The time frame of both missions was over the later portion of the calculated sunglint free photographic window for a morning flight, 9 a.m. to 11 a.m. eastern daylight time. The calculated photographic window is dependent upon the location of the remote sensing site, the day of the year, the field of view of the camera system, and the condition of water surface roughness. Since water surface roughness is not predictable in advance, calculations to determine the sunglint free window were based upon a smooth water surface. Any increase in sunglint effects from surface waves was expected to be overcome by overlapping the photographs 50 percent. In figure 1 are shown the photographic flight lines over the New York Bight test site,

and the approximate location of the photographs taken during the April 10, 1975, mission. It can be seen in figure 1 that 50 percent overlap of the photographs occurred on three of the five flight lines, evidently, when the aircraft was heading into the wind. For the other two flight lines the overlap was on the order of 20 percent.

The Hasselblad cameras were equipped with different optical filters. The spectral transmittance (T) of each and the type used is shown in figure 2. Additional information concerning the filters can be found in references 5 and 6.

The bandwidth and location of the optical filters were selected based on the following:

The narrow-band filter centered at 525 nanometers in figure 2 integrates the radiance around the central wavelength where, as shown in reference 7, the ratio of the diffused backscattering to diffused absorption coefficient of chlorophyll-a is equal to that for water. It is also shown (ref. 7) that for wavelengths less than this central wavelength the ratio of diffused backscattering to absorption coefficients of chlorophyll-a is less than the ratio for water, and at wavelengths greater than this central wavelength the ratio is greater. Thus, since the diffused backscattering to absorption coefficient ratio is proportional to reflectance (ref. 7), it is expected that the radiance integrating narrowband filter centered at 525 nanometers will not detect radiance variations from chlorophyll-a in water. Therefore, it is assumed that it will be useful for detecting variations in radiance from suspended matter, including other substances in the phytoplankton that contain the chlorophyll-a. In reference 7 the wavelength at which the ratio of diffused backscattering to diffused absorption coefficients of a particulate is equal to that for water is called the hinge point wavelength.

In figure 3 transmission spectrums of two concentrations of blue-green phytoplankton Anacystis Marinus, relative to its suspension solution, illustrate the concept of hinge point wavelengths. The transmission spectrums were obtained from a Cary 14 spectrophotometer (ref. 8). The transmission spectrum of Anacystis Marinus for the heavier concentration is represented by the solid curve. It can be seen in figure 3 that the transmission spectrum of the heavier concentration of Anacystis Marinus phytoplankton crosses the transmission spectrum for the lesser concentration at three wavelengths. These hinge point wavelengths, illustrated in figure 3, are at approximately 520, 570, and 700 nanometers. At wavelengths less than 520 nanometers the relative transmission decreases, between the wavelengths of 520 and 570 nanometers increases, again decreases between 570 and 700 nanometers, and, finally, increases again beyond 700 nanometers with increasing concentration of chlorophyll a in Anacystis Marinus phytoplankton. The hinge points illustrated by the transmission spectrums in figure 3 are not necessarily located at the same wavelengths as hinge points from reflectance spectrums, because transmission spectrums can consist of both diffused and direct light while reflectance spectrums consist of only diffused light. Thus, the central wavelength for the narrowband filter that must normalize chlorophyll a reflectance with varying concentration was selected at 520 nanometers from results of the study in reference 7 and not from the transmission spectra shown in figure 3. This optical filter is labeled 525 B-3 filter and called the suspended sediment filter in figure 3.

It is further shown in reference 7 that the backscattering radiance at 560 nanometers from chlorophyll a concentrations between 1 and 30 μg/l is always greater than the radiance from water. This is also indicated by the

transmission spectra in figure 3, because between the wavelengths of 520 and 570 nanometers transmission relative to water increases when chlorophyll a increases. The narrow-band filter with the central wavelength located at 554 nanometers should be able to detect the change in upwelled radiance from varying concentrations of chlorophyll a below the chlorophyll a concentration of 30 μg/l. However, as shown in reference 3, the upwelled radiance from the chlorophyll a would be combined with the upwelled radiance from all other substances in the water, and must be separated from these substances in order to be useful for mapping chlorophyll a in a body of water. Therefore, it is surmised that the upwelled radiance from chlorophyll a concentrations below 34 μg/l can be obtained by a differencing or a ratio technique utilizing the radiance values from the two narrow-band filteres shown in figures 2 and 3.

The 89B near-infrared filter in figure 2 must be flown simultaneously with the two narrow-band filters to determine if the water area under surveillance is phytoplankton "bloomed," because as shown in reference 3, the two narrow-band filter systems would be required for "unbloomed" phytoplankton water. In the "bloomed" water areas the concentrations of chlorophyll a could be determined from the near-infrared system alone (ref. 1).

The 12 yellow filter in figure 2 has two purposes. It has potential for identifying phytoplankton color groups in phytoplankton "bloomed" water, as it did in reference 3 for blue-green phytoplankton, and the 12 yellow filter, along with the other filter systems, has a potential for detecting radiance in "nonbloomed" phytoplankton water from large particulates, because it fills the radiance spectral gap, between 580 and 700 nanometers, not covered by the other filters.

Increasing concentrations of large particulates are expected to increase reflected radiance from "nonbloomed" phytoplankton water in the yellow and red regions of the spectrum. This increased reflected radiance from large particulates is shown theoretically in reference 9 and is believed to be seen through the 12 yellow filter in photography over the Potomac River (ref. 3).

RESULTS AND DISCUSSION

Presented in figures 4 and 5 are 276 positive prints of photographs that were taken with the Hasselblad cameras over the New York Bight from 5.3 kilometer altitude on April 10 and 13, 1975. The negatives of these prints are retained at the Chesapeake Bay Ecological Program Data Center, Wallops Island, Virginia, 23377. The photographs taken on April 10 are shown in figure 4 and those taken on April 13 in figure 5. The positive prints, because they are reproduced from the negatives, do not show as much detail as can be seen in the negatives. Positive transparencies, which show more detail than the positive prints, but less than the negatives, were used to obtain the photographic film density data used in this report. On both days only two of the cameras functioned. On both days the 89B (near-infrared) Wratten optical filter system operated in addition to the 554 (green-yellow) B-3 Baird-Atomic optical filter system on April 10, 1975, and the 525 (blue-green) B-3 Baird-Atomic optical filter system on April 13, 1975. It is believed that the very cold temperature (-16 degrees C), existing in the camera compartment of the aircraft at the time of the mission, is responsible for the poor performance of the camera system. The cameras which operated, operated intermittently. This can be seen in pictures 6, 7, 8 from the 554 (green-yellow) B-3 Baird-

Atomic optical filter system in figure 4 and the lack of pictures 44 through 50 for the 525 (blue-green) B-3 Baird-Atomic optical filter system in figure 5. Because of the poor operating performance of the camera system any reference to location of features seen in the pictures relative to land is questionable, except in photographs which include land features or known buoy systems. In some cases, features seen in the pictures of one flight line were also seen in the pictures from the adjacent flight lines due to overlap of the photography, see figure 1 and pictures 6, 7, 8, 35, 36 of figure 4. When this happened the location of the pictures between the two flight lines became more exact.

The bright hemispherical spot originating on the border of nearly every picture in figures 4 and 5 is the image of the Sun reflected off the water surface. The Sun image is generally largest in area in near-infrared photographs, because the upwelling light (radiance from the water body) is very weak at near-infrared wavelengths. The weak upwelling light produces better contrast with the surface reflected Sun image in the near-infrared photographs than it does at other wavelengths, because at the other wavelengths the upwelling light is much greater. See pictures 2, 3, 4, and 5 of figure 4a and b. Whenever the image of the Sun appears in a photograph, the remotely sensed data obtained from that area of the photograph are not useful, because the direct reflection of the Sun off the water surface produces drastic effects upon the variation in off-nadir radiance that is not detected at other azimuth angles.

Many of the near-infrared photographs, figures 4a and 5a, contain white fuzzy lines. These lines are caused by light flashes in the camera, from the discharge of static electricity that builds up on 2424 near-infrared film.

A bright area, which appears to be symmetrical about the center of each picture, can be seen in all the scenes of figures 4b and 5b. The intensity of this bright area increases, in general, in photographs taken along the flight line as the aircraft heads toward land, and, decreases when the aircraft heads toward the open sea. See pictures 1 through 20, 33 through 47, and 61 through 74 with the aircraft heading towards land, and 21 through 32 and 48 through 60 with the aircraft heading out to sea in figure 4b. The intensity of the bright area, in general, is strongest near the center of each photograph and diminishes with increasing distance from the center of each photograph. It is shown in reference 10, from densitometer traces over photographs exposed from 3 kilometers altitude through two of the Hasselblad cameras used in this photographic mission, that the center of photographs are exposed to a higher degree than the edge. This effect is normal in photography, and is caused by camera-lens, off-axis, falloff, which in some camera systems must be corrected by as much as $1/(\cos \theta)^{12}$, where θ is the angle off the principal axis of the lens (ref. 11). However, for wide angle remote sensing the camera-lens, off-axis, falloff is not the only off-axis variable, because atmospheric backscattering also varies from the center of the picture to the edge of the border. The atmospheric backscattering increases from the center of the photograph to the edge of the film, and the increase is dependent upon increasing distance from the camera to the point of concern in the water. Since the increase in distance, similar to camera falloff, is dependent upon θ, the increased off-axis backscattering of sunlight compensates somewhat for the camera-lens, i.e., off-axis, falloff. Thus, the calibration of off-axis falloff must be performed during the photographic mission to account for atmospheric effects for a particular day. Whenever

off-axis radiance data are presented in this report it will have been normalized to nadir by multiplying it by a correction factor that is dependent upon the off-nadir viewing angle. The correction factors were obtained for each filter-film-camera system from densitometer traces through the center of photographs 61 (a and b) on April 10, 1975, and 14 (a and b) on April 13, 1975. For the reason previously explained, these correction factors cannot be applied in areas of the photographs containing the Sun's image.

In addition to camera-lens falloff and atmospheric backscattering, a third element affects the radiance values that expose the photographic film in combination with upwelling radiance from the water body. The third element is reflectance off the water surface of diffused sunlight. In reference 9 it is shown that reflectance of diffused sunlight from a water surface is essentially constant with a variation in Sun altitude when the altitude of the Sun is above 34 degrees. Since the altitude of the Sun was above 34 degrees for both photographic missions discussed in this report, it is assumed that the reflectance of diffused sunlight from the water surface is essentially constant in all photographs.

Because the altitude and camera system is the same for each flight line, the camera-lens falloff, the atmospheric backscattering, and the diffused reflectance off the water surface were assumed constant in consecutive photographs along the same flight line. It then follows from these assumptions that the general increase in brightness at the center of each photograph (nadir) along the same flight line with the aircraft heading toward land, and the decrease when the aircraft is heading towards the open sea, must result from increasing or decreasing upwelling radiance. It is further assumed that the general decrease in upwelling radiance along each

flight line as the aircraft heads out to sea results from the settling of reflecting substances being discharged from the rivers that flow into the New York Bight water.

In some photographs additional light scattering features can be seen in the water. This is most evident in pictures 6, 7, 8, 35, 36, 39, 40, 57 and 58 of figure 4b, and pictures 9, 10, 34 and 35 of figure 5b. These features and their approximate locations are more easily seen in figures 6, 7 and 8. Figures 6, 7 and 8, along with figure 9, are composite figures made from their corresponding photographs shown in figure 4 and 5. Figure 6, which is a composite made from the photographs in figure 4b, shows the features best. However, the features seen within the circle labeled sludge dump area in figure 6 are seen, because their reflectance is less than, while the features in the area labeled acid dump area are seen, because their reflectance is greater than the background water. In figure 7, a composite made from the near infrared photography of figure 4a, the same features can also be seen. However, the features within the circle in figure 7 are now seen, because their reflectance is greater than the background water, while in figure 6 the same features were seen, because their reflectance was less than the background water. In figure 7 the features in the acid dump area are seen, because their reflectance is slightly greater than, while in figure 6 these same features have a much greater reflectance than the background water. Therefore, the substance being dumped within the circle in figures 6 and 7 must be a different substance than that in the acid dump area, because it has different reflecting properties relative to the background water through the two broadband optical filters. Since the location of the circled area in figures 6 and 7 relative to the area labeled acid dump area is consistent

with the designated dump areas for waste sludge and waste acid, shown in reference 4, it is assumed that the substance being dumped within the circle in figures 6 and 7 is waste sludge and the substance in the acid dump area must be acid residue. If this assumption is correct, it should be possible to distinguish waste sludge from waste acid by a remote sensing technique. It is also apparent that the substance being dumped within the circled area of figures 6 and 7 has a hinge point wavelength, because at some wavelength, between the broadband optical filters used in this photography, the substance must have the same reflectance properties as the background water. The significance of a hinge point wavelength for the separation of one substance in water relative to another using a remote sensing technique is discussed in reference 7.

In figure 8 brightly reflecting features are visible from the water through the 525 (blue-green) B-3 Baird-Atomic optical filter. These bright features are labeled as drifting acid residue in lieu of sludge residue, because their location coincides more with the acid dump area than it does with the sludge dump area, and their reflectance is, as it was in figure 6 through the 554 (green) B-3 Baird-Atomic optical filter, much greater than the background water. The fact that its reflectance is greater than the background water through the 525 (blue-green) B-3 Baird-Atomic filter is important, because it relates to the assumed signature of acid and sludge obtained from figures 6 and 7, and illustrates the significance of the spectral response of reflecting substance for specific identification of these substances.

The sludge dump area cannot be identified in the photographs taken on April 13, 1975, because there are no easily identified areas in figure 8 where

visual observation shows reflectance from substances to be less than, and in figure 9 greater than, the background water.

In figure 10 is presented the variation of nadir radiance through the 554 (green) and 89B (NIR) optical filters along Loran line 4640 on April 10, 1975, versus miles from Staten Island. The radiance is in the form of relative film transmittance, R_n, obtained from densitometer traces over the center of positive transparencies of photographs 33 to 47, figures 1 and 4, from which has been subtracted relative film transmittance through the unexposed portion of the film. The nadir radiance values are unique in remote sensing, because they result from the perpendicular viewing distances through the atmosphere and into the water. As such, relative to each other, they require no off-nadir atmospheric or carera-lens corrections. In addition, since they are always in the plane of the sun, any effect upon radiance values from the variation in sun azimuth angle should be normalized.

In figure 10 the value of R_n at each location through the 554 (green) optical filter is always greater than the value of R_n through the 89B (NIR) optical filter. Through each optical filter the value of R_n is greatest over land, and least for the two data points beyond 33 nautical miles from Staten Island, labeled uniform water in figure 10. The two constant values of R_n through each optical filter beyond station 33 were obtained from photographs 33 and 34 in figure 4. The dashed lines, drawn through the minimum, constant values of R_n, in figure 4, represent the radiance values for uniform water. Thus, the dashed lines in figure 4 are base reference values for increased upwelling radiance resulting from suspended materials during this remote sensing mission.

In figure 10 there is a general decay in R_n through both optical filters as distance from land increases. The general decay in R_n is distributed over two areas; one area where the photographs showed that heavy clouds existed, and the other is over the waste dump area. The increase in R_n over the waste dump area, between 22 and 34 nautical miles from Staten Island, is much more prominent through the green filter system than through the near-infrared filter system, but the increase in R_n over the cloudy area, between 12 and 15 nautical miles from Staten Island, is more prominent at near-infrared wavelengths. Thus, there is a spectral difference in reflectance between clouds and the substances being dumped in the waste dump areas.

The increase in R_n over the waste dump area indicates, from the standpoint of biodegradable pollution, that a substance being dumped in the waste dump area is reflecting sunlight out of the water that, otherwise, might be available for photosynthetic activity. The extent of the effect of the waste dump area upon reflected sunlight can be seen better in figure 11.

In figure 11 R_n from each over-water photograph obtained through the 554 (green) optical filter on April 10, 1975, is plotted, for each loran line, against distance from Staten Island. Also drawn on the figure are two dashed circles. The smaller of the two circles encloses the area where visitle dumping is taking place during the photographic mission, and the larger circle is the area where the radiance from features in the water is very prominent in figure 6. The location of the smaller circle is also consistent with the location of the designated waste sludge dump area, and the larger circle with the designated acid waste dump area.

In figure 11 there is a high value of R_n along each loran line that increases in value from loran line 4550 to loran line 4610. At loran line 4610

R_n peaks, and then decreases again toward loran line 4670. This ridged value of R_n is shown by the solid line across the data. The peak value of R_n on loran line 4610 appears to be inside the designated acid waste dump area.

In front of the high value of R_n on each loran line there is a depressed value of R_n. The depressed value of R_n decreases in value from loran line 4550 to loran line 4640 and then increases again to loran line 4670. The depressed value of R_n is shown by the dashed line across the data. It appears from figure 11 that the minimum depressed value of R_n, along loran line 4640, is in the designated waste sludge dump area. It also appears, since the depressed value of R_n precedes the increased value of R_n along each loran line, that at optical wavelengths transmitted by the 554 (green) filter the upwelled radiance from the sludge waste area is less than from the acid waste area. This is the same conclusion arrived at from analysis of figures 6 and 7, but, in figure 11, it appears the influence of the dumping of sludge and acid waste upon R_n is much more extensive in area than the designated dump sites. It is also seen in figure 11 that the photographic mission did not overfly the complete area influenced by waste dumping, since the two outer flight lines still experience increased values of R_n at distances out to sea consistent with the location of the waste dump areas.

The effect of waste dumping upon the variation of R_n did not change appreciably from April 10, 1975, to April 13, 1975, because, as shown in figure 12, the variation in R_n along each loran line obtained from the 525 (blue-green) optical filter system shows the depressed value of R_n preceding an increasing value of R_n when the waste dump areas are overflown. R_n from each over-water photograph through the 525 (blue-green) optical filter on April 13, 1975, is shown in figure 12 by the square symbols, and

R_n from each over-water photograph through the 554 (green) optical filter on April 10, 1975, is represented by the circles. R_n is plotted against miles from Staten Island in a staggered formation to isolate R_n along each loran line from both days. The dashed lines in figure 12, shown and discussed for figure 10, are the minimum values of R_n for each filter-film camera system. The minimum value of R_n was different for each filter-film camera system, and on April 13, 1975, was obtained on only loran flight lines 4640 and 4670, perhaps, because the flight lines did not extend as far out to sea on that day as they did on April 10, 1975. Nevertheless, it is clear in figure 12 that the influence of waste dumping upon R_n was as extensive on April 13 as it was on April 10.

Since not a single in situ data area visited by the boat or the helicopter occurred in the center of a photograph, it was impossible to relate R_n to in situ data in this experiment. This was expected prior to the photographic mission, because in an area as extensive as the New York Bight, a photographic mission from 5.3 km altitude cannot be preplanned to pinpoint the center of a photograph to a specific location. In future experiments, the calibration of the optical filter system with in situ water data might better be accomplished from a helicopter. From a helicopter the remote sensing data could be taken over a location at the same time as the in situ water data.

Even off-nadir radiance data, R, was not obtained in this experiment from many of the in situ data point locations, because the lack of 50 percent overlap in the photography placed the boat, and some of the helicopter in situ data point locations in the sunglint areas of the photographs. In all, only eight in situ data points were considered useful for analysis of the

photographic radiance data. These were from the helicopter, and were restricted to April 13, because the helicopter did not fly on April 10. On April 13 two types of in situ data were obtained from helicopter dip samples; the concentration of chlorophyll-a and the total suspended material weight. Since two of the photographic systems did not operate on April 13, the calibration of the optical filtering system could not be accomplished with the chlorophyll-a data.

Presented in figure 13 is the variation of R through the 525 (blue-green) optical filter obtained from the in situ data point locations on April 13, 1975. R is plotted versus measured total suspended material weight in surface samples obtained from these same locations. Data points from the waste disposal areas are represented by the circles, and those considered to be outside of the waste disposal areas by the squares.

It is seen in figure 13 that the variation of R in this experiment is not very sensitive to total suspended material weight measured in surface samples, because with a factor of 10 variation in total suspended material weight R did not vary appreciably. It is also apparent that the remote sensing data shown here is affected more by other parameters in the water, since R is greatest in the waste disposal areas where the total suspended material weight in surface samples was the least.

CONCLUDING REMARKS

The major objective of this photographic experiment, the remote quantification of chlorophyll-a in chlorophyll-a containing phytoplankton when phytoplankton "bloom" conditions do not exist, was not accomplished, because of camera system malfunctions. However, some important results,

concerning the New York Bight waste dump area, were obtained from analysis of radiance data through the camera systems that did operate.

Comparison of broadband black and white photography, exposed through an optical filter that transmits only near-infrared wavelengths (700 to 900 nm) with photography exposed through an optical filter that transmits only green-yellow wavelengths (530 to 580 nm), shows that a substance being dumped in the sludge dump area, assumed to be sanitation sludge, has a different spectral signature relative to the background water than does a reflecting substance from the acid dump area, assumed to be acid waste residue.

The substance being dumped in the sludge dump area has a greater reflectance at near-infrared wavelengths and a lesser reflectance at green-yellow wavelengths than the background water.

The substance in the acid dump area has a greater reflectance than the background water through both optical filters. In addition, the reflectance from the substance in the acid dump area is much greater in the green-yellow spectral region than it is in the near-infrared region.

Film density data, obtained from the green-yellow wavelength photography, show that waste dumping in the New York Bight increases the backscattered sunlight from the water over a much greater area than the designated dump site areas. It is clear from the photography that acid waste is the primary substance responsible for the increased backscattered sunlight, but the green-yellow wavelength data suggests that sludge dumping is also contributing.

Film density data, from locations on photographs where in situ measurements of total suspended material weight in surface samples were obtained, indicate that upwelling radiance from areas in the dump site area containing

less than 2 milligrams per liter total suspended material weight is greater than radiance from non-dump site areas that contained values of total suspended material weight up to 9 milligrams per liter.

REFERENCES

1. Bressette, W. E.; and Lear, D. E., Jr.: "The Use of Near-Infrared Reflected Sunlight for Biodegradable Pollution Monitoring." Presented at the Second Conference on Environmental Quality Sensors, National Environmental Research Center, Las Vegas, Nevada. October 10-11, 1973.

2. Odum, E. P.: "Fundamentals of Ecology." Third Edition, W. B. Saunders Company.

3. Bressette, W. E.: "An Optical Filtering System for Remote Sensing of Phytoplankton and Suspended Sediment." Published in the 1974 Earth Environment and Resources Conference Digest of Technical Papers, September 1974, Publisher Lewis Winner, New York, NY.

4. Usry, J. W.; and Hall, J. B., Jr.: "National Aeronautics and Space Administration Operations - Remote Sensing Experiments in the New York Bight, April 7-17, 1974." NASA TM X-72802.

5. Baird-Atomic Company, Optical System Components. Catalog C-9, June 1973.

6. Eastman Kodak Company: "Kodak Wratten Filters for Scientific and Technical Use." Twenty-second Edition, First 1966 Printing.

7. Duntley, S. Q.: "Detection of Ocean Chlorophyll from Earth Orbit." Section 102, 4th Annual Earth Resources Program Review, Volume IV, Presented at the Manned Spacecraft Center, Houston, Texas, January 17-21, 1972.

8. Grew, Gary W.: "Signature Analysis of Reflectance Spectra of Phytoplankton and Sediment in Inland Waters." Presented at the Second Annual Remote Sensing of Earth Resources Conference, Tullahoma, Tennessee, March 26-28, 1973.

9. Williams, Jerome: "Optical Properties of the Sea." United States Naval Institute, Annapolis, Maryland, 1970.

10. Bressette, W. E.: "The Use of Near Infrared Photography for Aerial Observations of Phytoplankton Bloom." Volume II, Remote Sensing of Earth Resources, edited by F. Shahroki, The University of Tennessee, Tullahoma, Tennessee Space Institute. Copyright 1973.

11. Dybdahl, A. W.: "Detection of Dissolved Oxygen in Water Through Remote Sensing Techniques." Presented at the Second Conference on Environmental Quality Sensors, National Environmental Research Center, Las Vegas, Nevada, October 10-11, 1973.

TABLE 1.- PHOTOGRAPH SENSOR COMPLEMENT AND CAMERA SETTINGS

	Camera	Focal length mm (in)	Filter	Film format mm (in)	Film type[c]	Speed (sec)	f Number
1.	Hasselblad	40 (1.57)	554 (green-yellow)[a]	70 (2.76)	2402 Black & White	1/250	5.6
2.	Hasselblad	40 (1.57)	525 (blue-green)[a]	70 (2.76)	2402 Black & White	1/250	5.6
3.	Hasselblad	40 (1.57)	12 (blue-red)[b]	70 (2.76)	2402 Black & White	1/250	11
4.	Hasselblad	40 (1.57)	89B (near-infrared)[b]	70 (2.76)	2424 Black & White	1/250	5.6

[a]Baird-Atomic B-3 optical filter with central wavelength of 554 and 525 nanometers

[b]Kodak Wratten optical filter number

[c]Kodak Film number

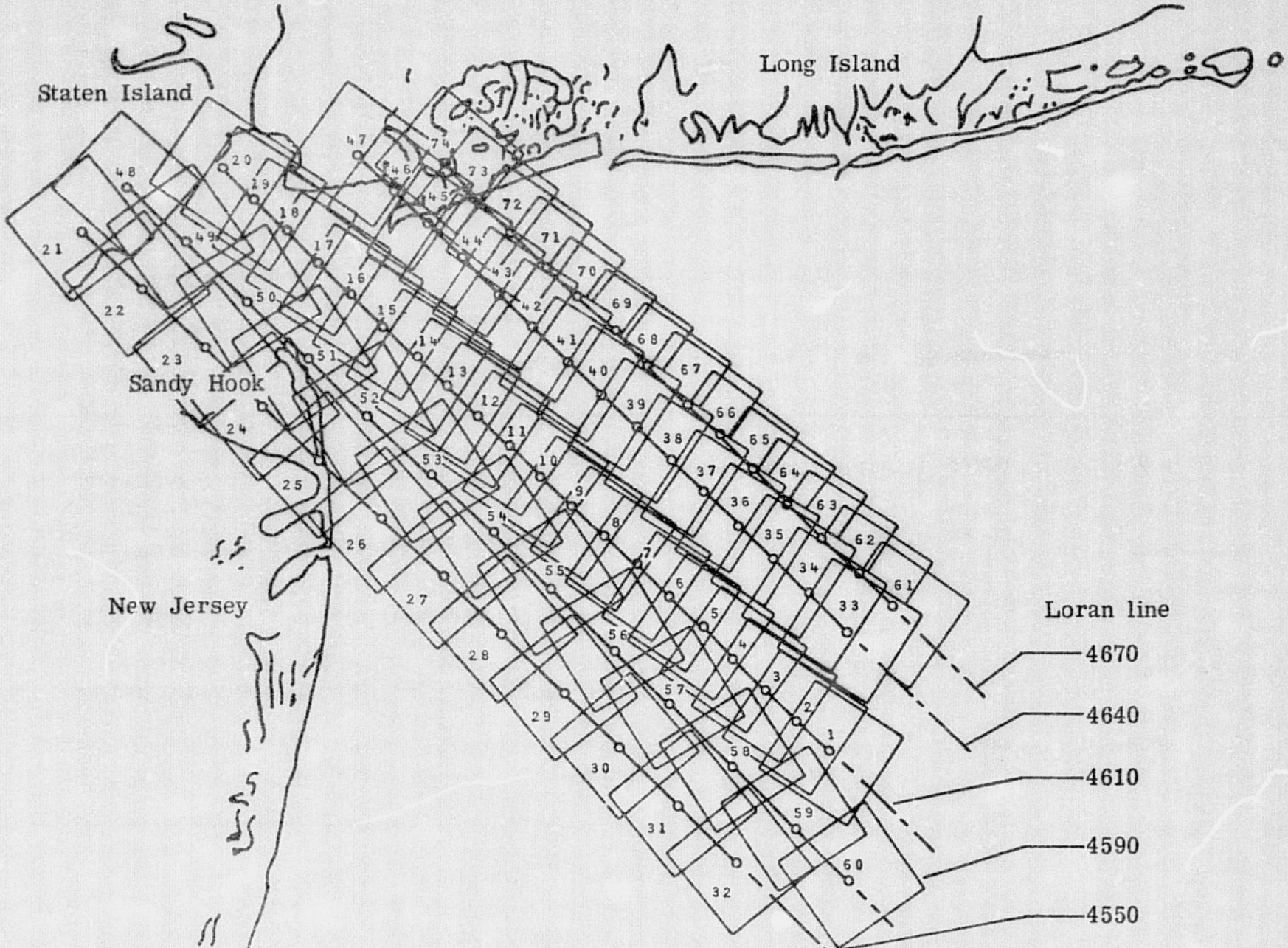

Figure 1.- Photographic flight lines over the New York Bight test site for April 10, 1975, showing the approximate location of each photograph.

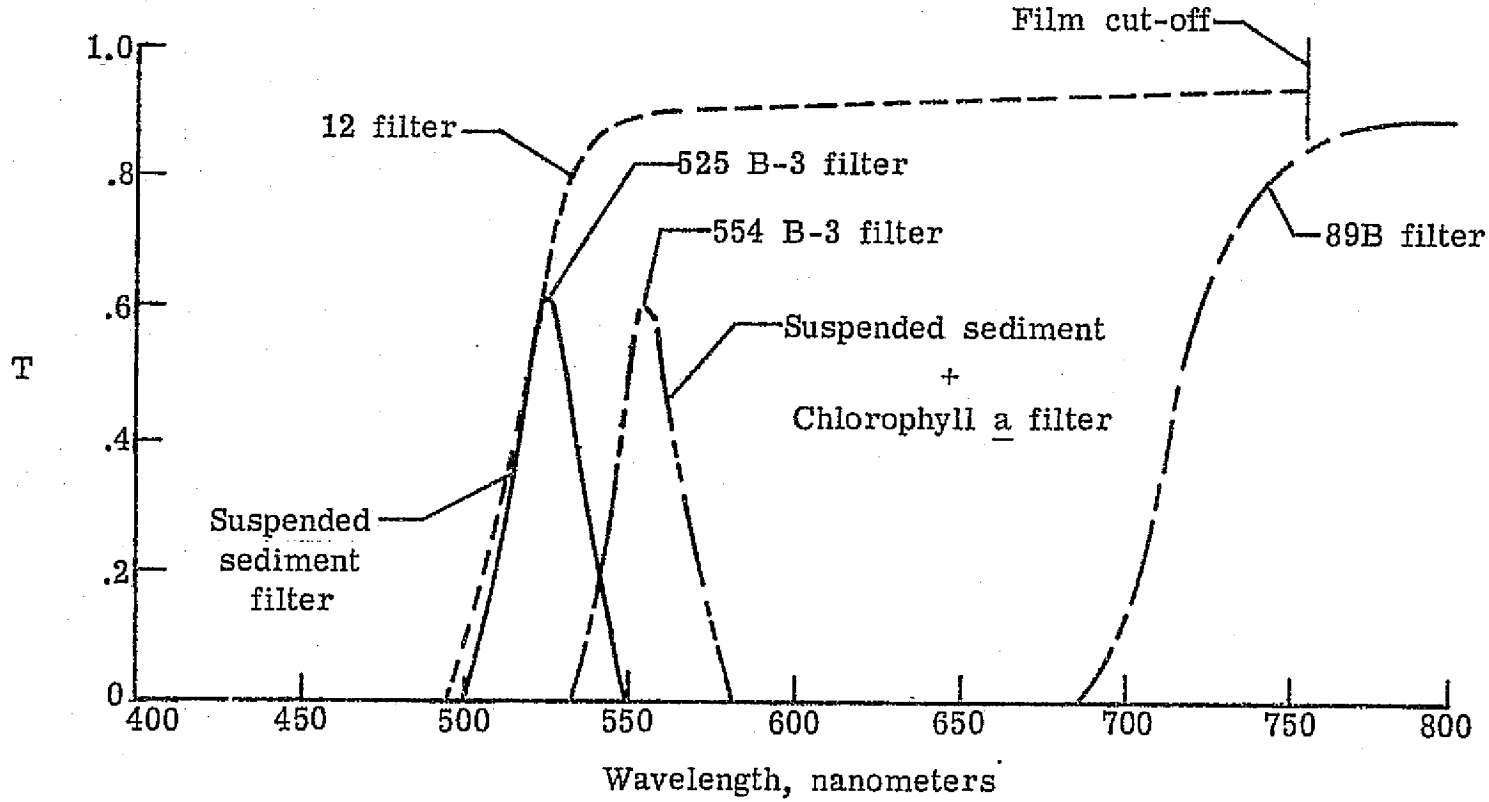

Figure 2.- The spectral variation of transmission, T, for the 525 central wavelength, B-3 Baird-Atomic, the 554 central wavelength, B-3 Baird-Atomic, the 12 Wratten, and the 89B Wratten optical filters.

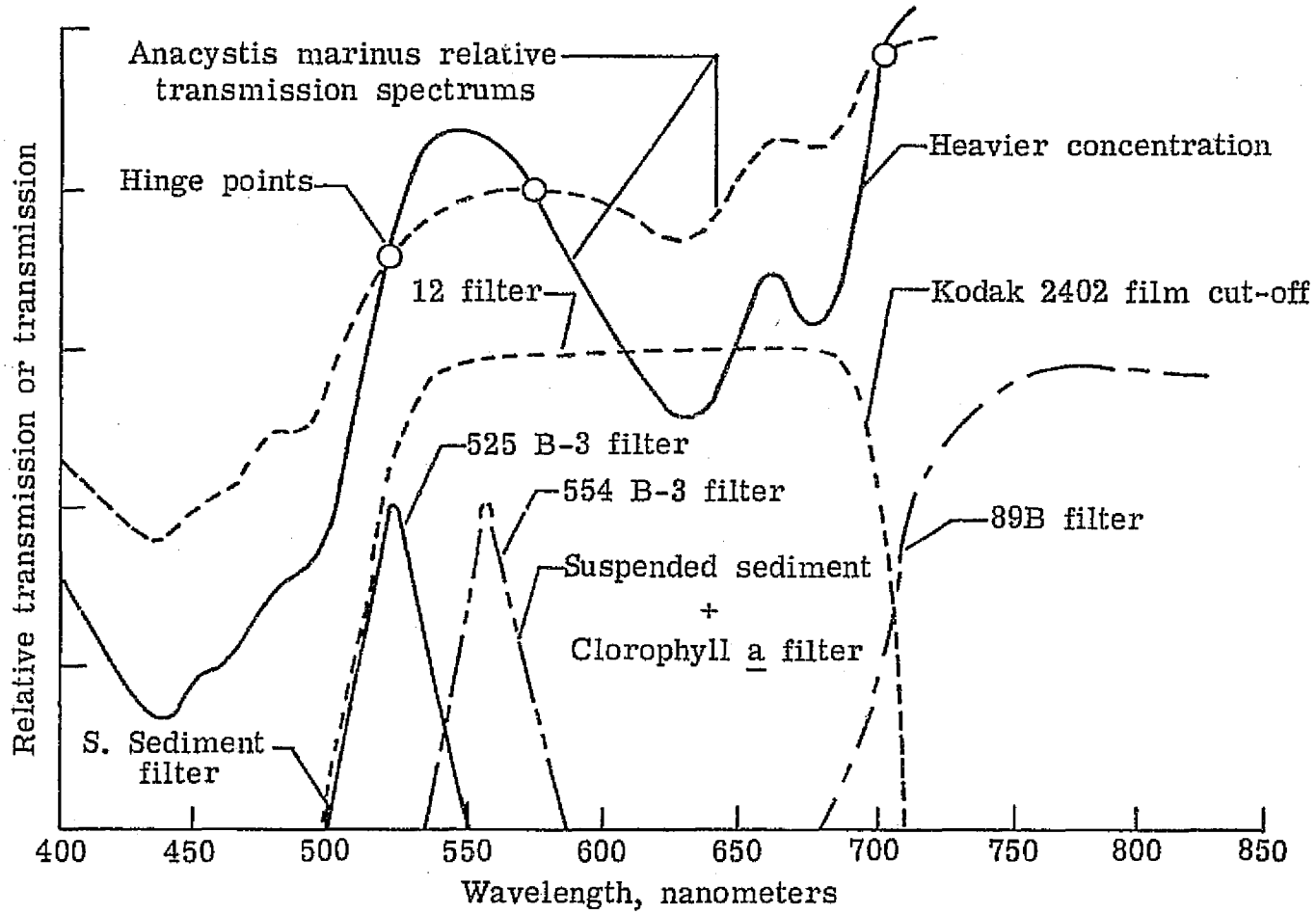

Figure 3.- Transmission spectrums of two concentrations of blue-green phytoplankton, Anacystis Marinus, relative to its suspension solution, the transmission of the 525 and 554 B-3 Baird-Atomic optical filter, and the transmission of the 12 and 89B Wratten optical filter.

(a) 89B (near-infrared) Wratten optical filter

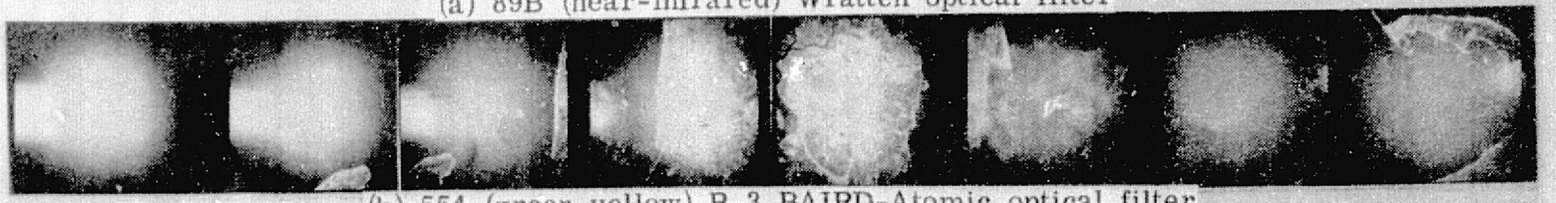

(b) 554 (green-yellow) B-3 BAIRD-Atomic optical filter

17 18 19 20 21 22 23 24

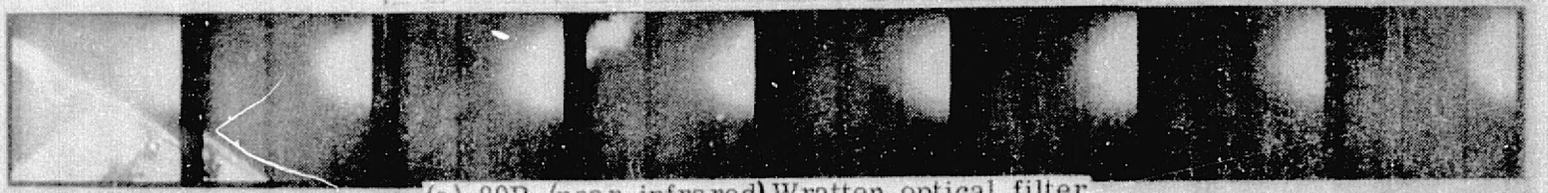

(a) 89B (near-infrared) Wratten optical filter

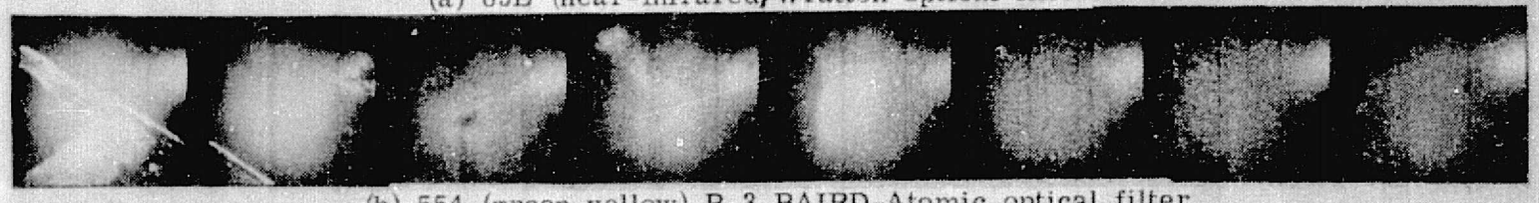

(b) 554 (green-yellow) B-3 BAIRD-Atomic optical filter

25 26 27 28 29 30 31 32

Figure 4 continued.- Photographs over the Hudson Canyon to Ambrose traffic approach to New York City from 5.3 kilometers altitude on April 10, 1975. Photographs 17 through 20 were taken between 10:14 and 10:17 eastern daylight time along the same loran line as photographs 1 through 16 ending over Staten Island. Photographs 21 through 32 were taken between 10:24 and 10:33 eastern daylight time beginning over Staten Island while heading out to sea on the loran line 3H4-4550 (coast and geodetic map 12326).

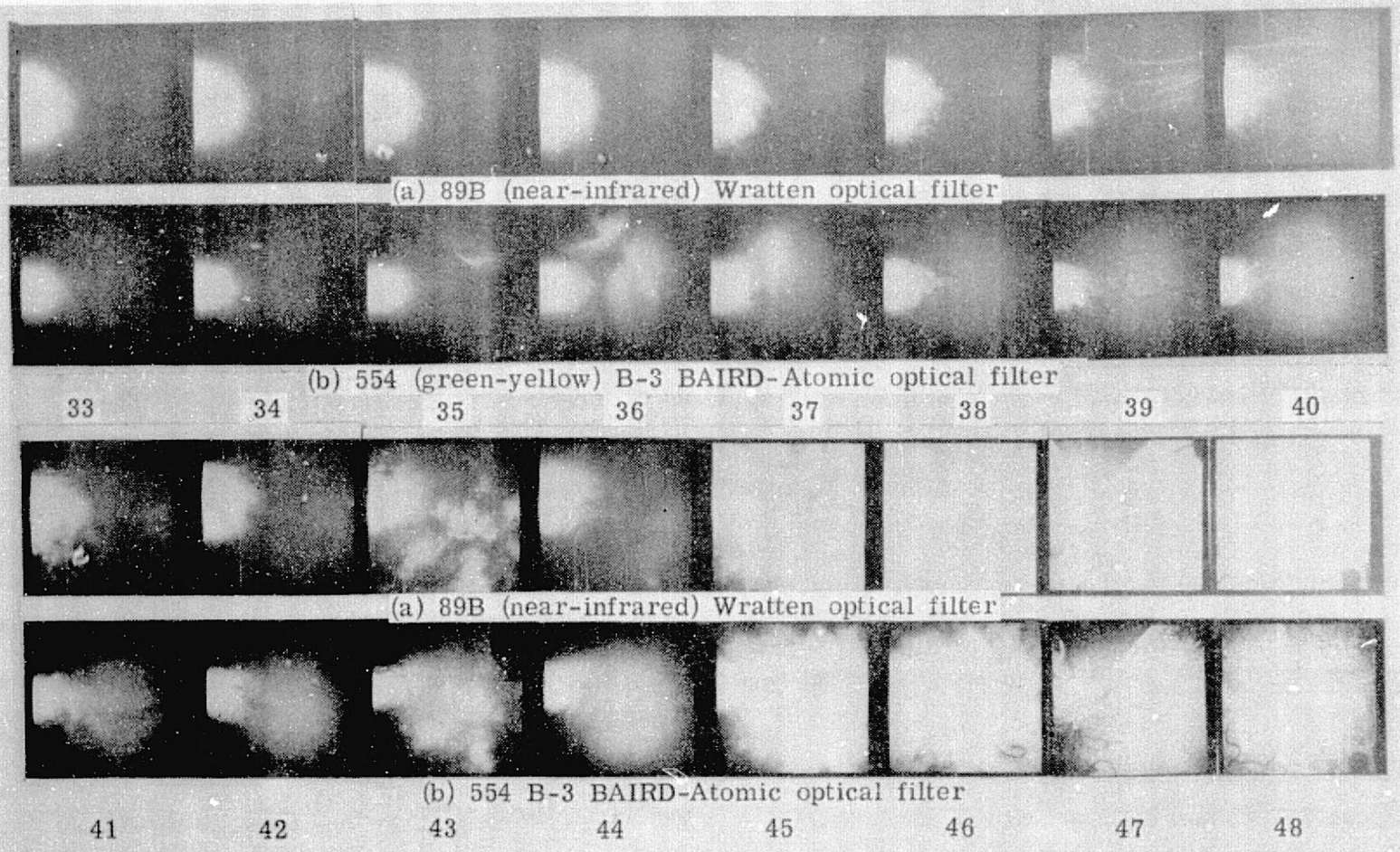

Figure 4 continued.- Photographs over the Hudson Canyon to Ambrose traffic approach to New York City from 5.3 kilometers altitude on April 10, 1975. Photographs 33 through 47 were taken between 10:42 and 10:54 eastern daylight time heading toward land over the loran heading of 4640 (coast and geodetic map 12326), ending over Coney Island. Photograph number 48 was taken over Staten Island at 10:59 heading out to sea on the same loran line as pictures 49 through 60.

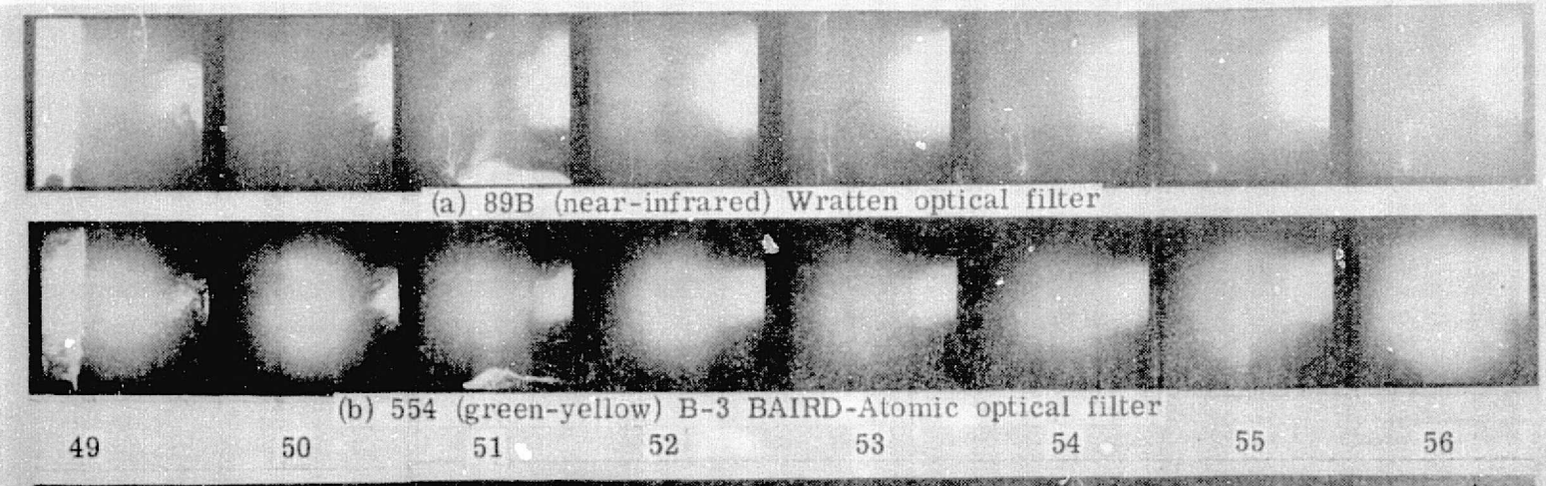

(a) 89B (near-infrared) Wratten optical filter

(b) 554 (green-yellow) B-3 BAIRD-Atomic optical filter

49 50 51 52 53 54 55 56

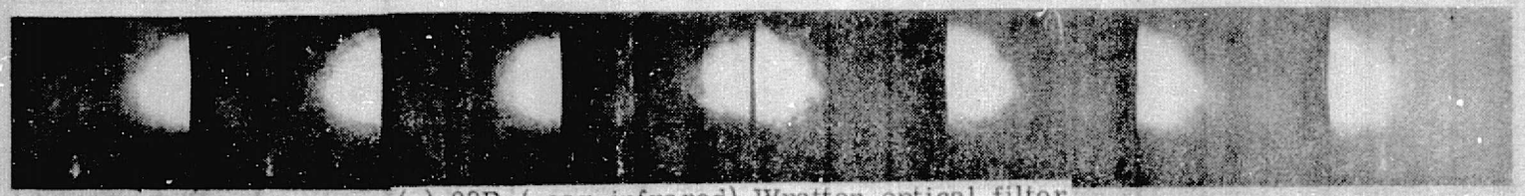

(a) 89B (near-infrared) Wratten optical filter

(b) 554 (green-yellow) B-3 BAIRD-Atomic optical filter

57 58 59 60 61 62 63 64

Figure 4 continued.- Photographs over the Hudson Canyon to Ambrose traffic approach to New York City from 5.3 kilometers altitude on April 10, 1975. Photographs 49 through 60 were taken between 11:00 and 11:09 eastern daylight time heading toward sea on the loran line of 4590 (coast and geodetic map 12326) beginning at Staten Island. Photographs 61 through 64 were taken between 11:14 and 11:17 eastern daylight time heading toward land on the loran line of 4670.

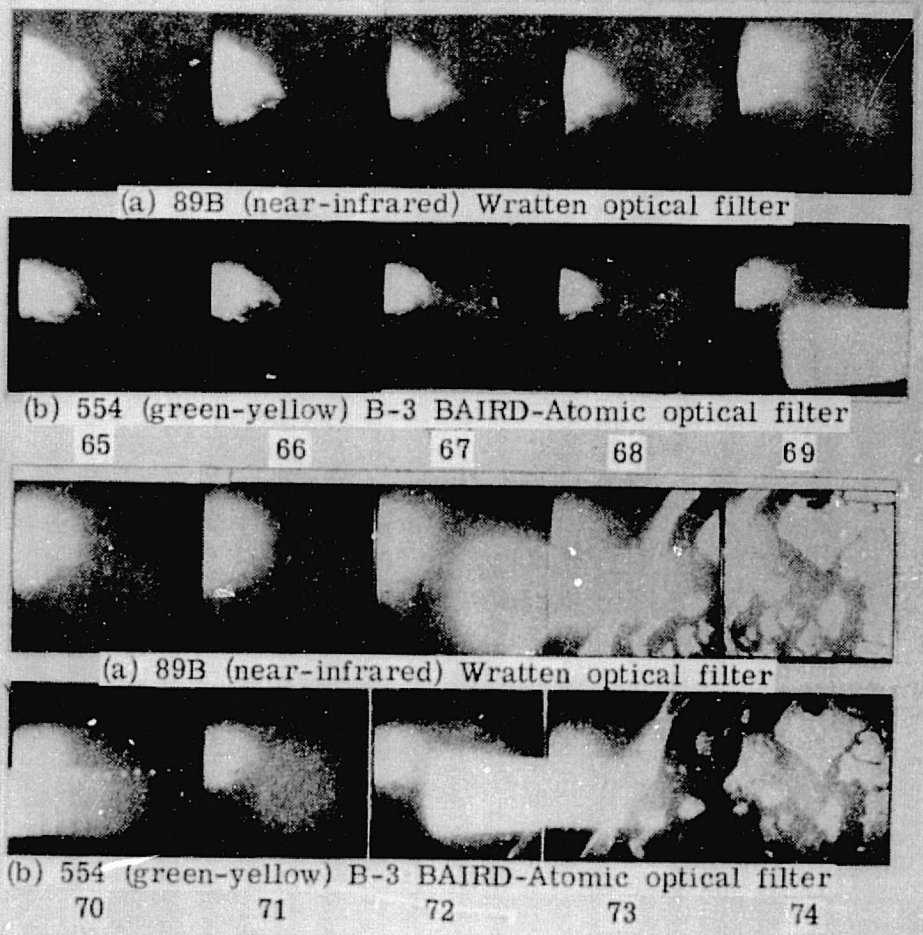

Figure 4 concluded.- Photographs over the Hudson Canyon traffic approach to New York City from 5.3 kilometers altitude on April 10, 1975. Photographs 65 through 74 were taken between 11:18 and 11:25 eastern daylight time heading toward land on the loran line of 4670 (coast and geodetic map 12326) and ending over Rockaway Beach.

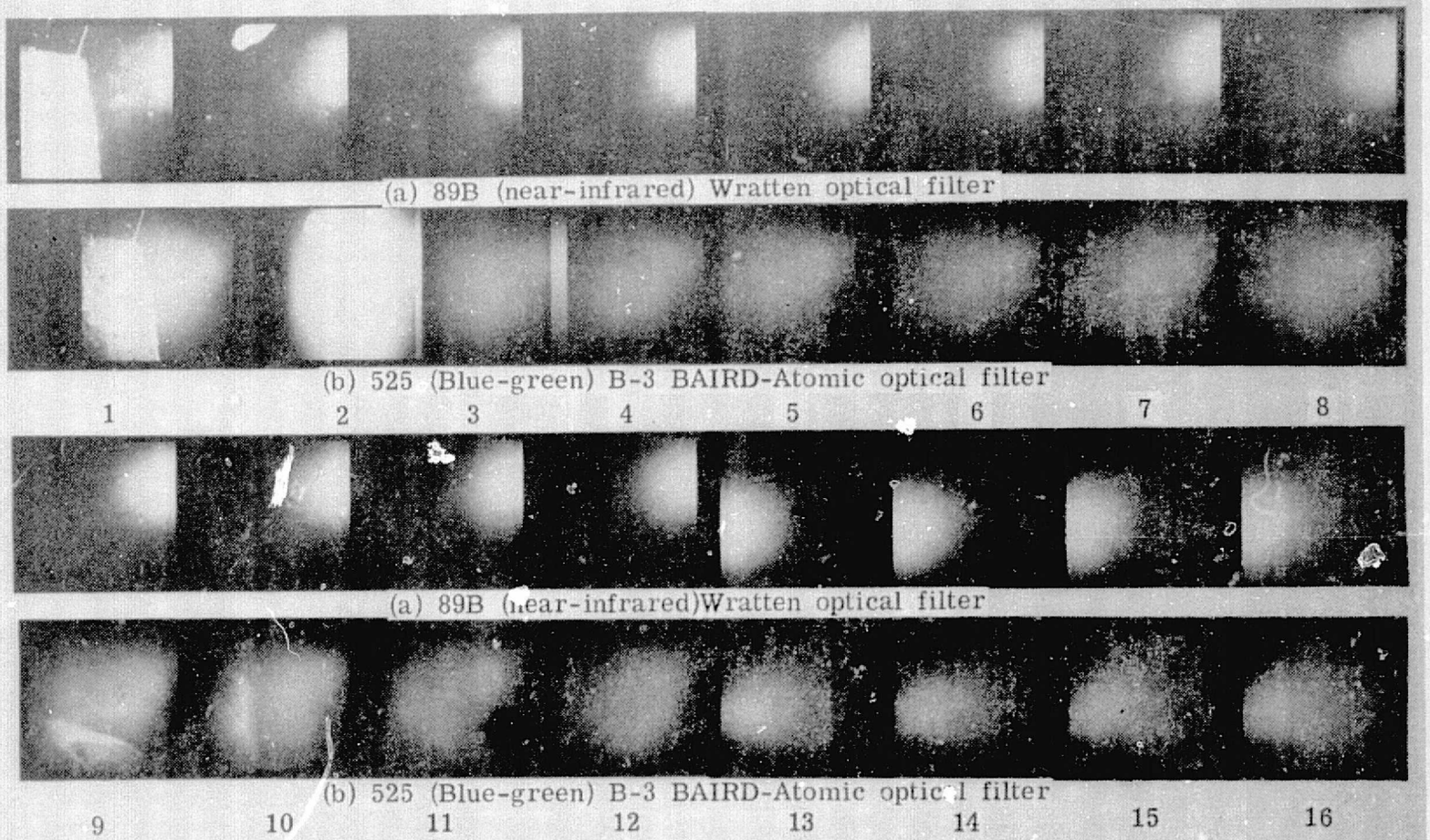

Figure 5.- Photographs over the Hudson Canyon to Ambrose traffic approach to New York City from 9.3 kilometers altitude on April 13, 1975. Photographs 1 through 12 were taken between 9:53 and 10:02 eastern daylight time heading out to sea on the loran line 3H4-4610 (coast and geodetic map 12326) beginning at Staten Island. Photographs 13 through 16 were taken between 10:06 and 10:08 eastern daylight time heading toward land on the same loran line as photographs 17 through 25.

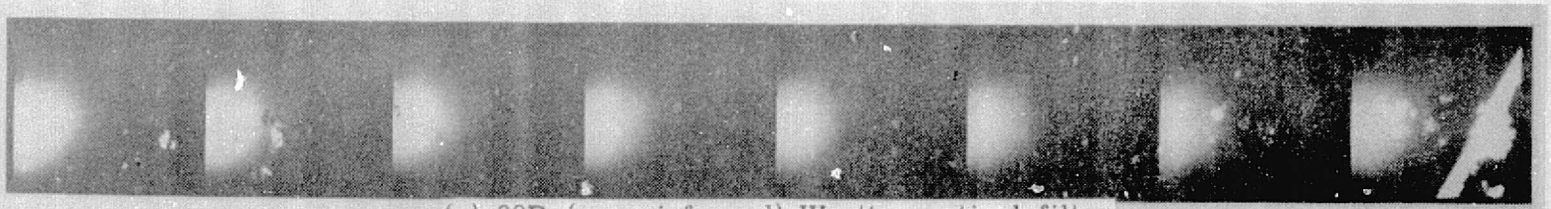

(a) 89B (near-infrared) Wratten optical filter

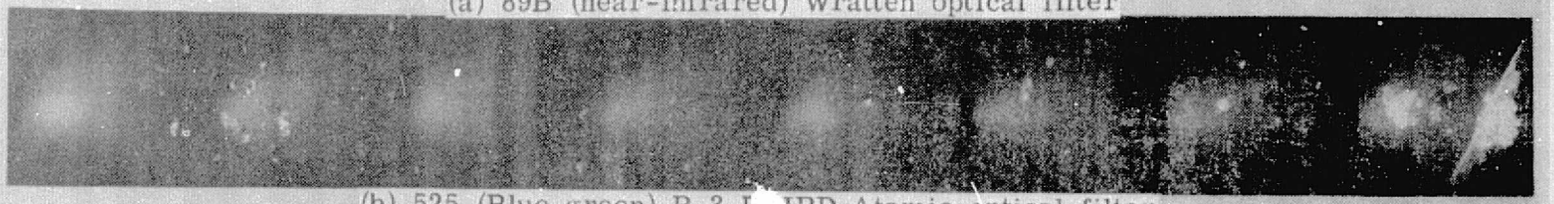

(b) 525 (Blue-green) B-3 BAIRD-Atomic optical filter

17 18 19 20 21 22 23 24

(a) 89B (near-infrared) Wratten optical filter

(b) 525 (Blue-green) B-3 BAIRD-Atomic optical filter

25 26 27 28 29 30 31 32

Figure 5 continued.- Photographs over the Hudson Canyon to Ambrose traffic approach to New York City from 5.3 kilometers altitude on April 13, 1975. Photographs 17 through 25 were taken between 10:09 and 10:15 eastern daylight time heading toward land on the loran line 4670 (coast and geodetic map 12326); ending over Rockaway Beach. Photographs 26 through 32 were taken between 10:22 and 10:27 eastern daylight time heading out to sea on the loran line of 4590 beginning over Staten Island.

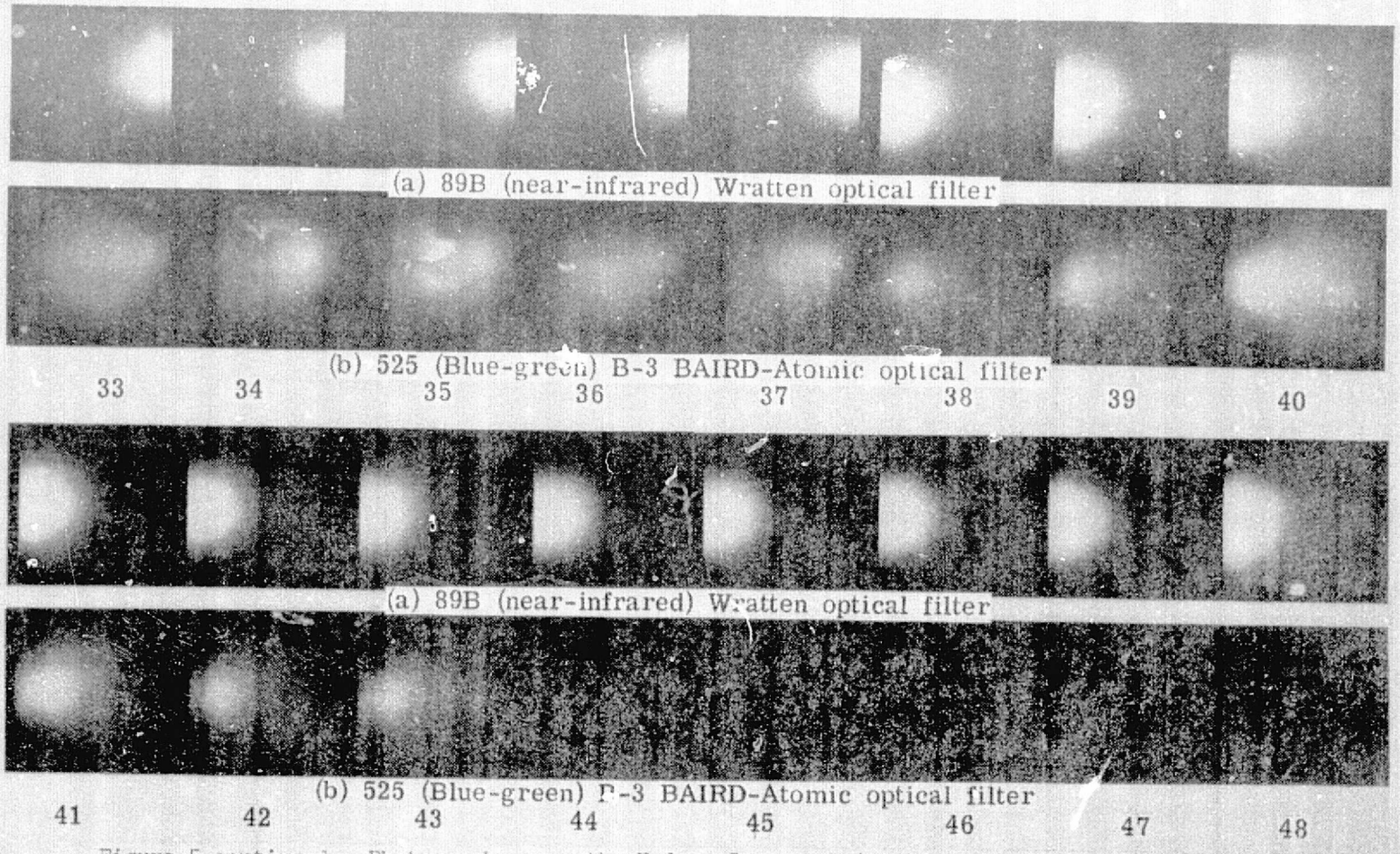

Figure 5 continued.- Photographs over the Hudson Canyon to Ambrose traffic approach to New York City from 5.3 kilometers altitude on April 13, 1975. Photographs 33 through 37 were taken between 10:27 and 10:31 eastern daylight time heading out to sea on the same loran line as photographs 26 through 32. Photographs 38 through 48 were taken between 10:36 and 10:44 eastern daylight time heading towards land on the loran line of 4640 (coast and geodetic map 12326).

(a) 89B (near-infrared) Wratten optical filter

(b) 525 (Blue-green) B-3 BAIRD-Atomic optical filter

49 50 51 52 53 54 55 56

(a) 89B (near-infrared) Wratten optical filter

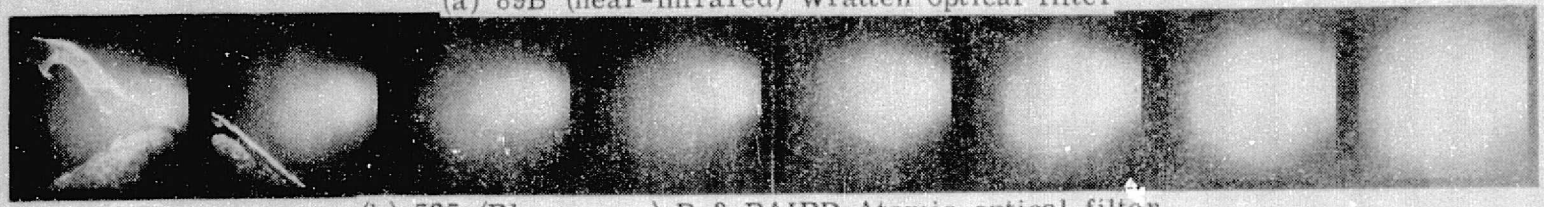

(b) 525 (Blue-green) B-3 BAIRD-Atomic optical filter

57 58 59 60 61 62 63 64

Figure 5 concluded.- Photographs over the Hudson Canyon to Ambrose traffic approach to New York City from 5.3 kilometers altitude on April 13, 1975. Photographs 49 through 52 were taken between 10:45 and 10:48 eastern daylight time heading toward land on the same loran line as photographs 38 through 48 ending over Coney Island. Photographs 53 through 64 were taken between 10:54 and 11:03 eastern daylight time heading out to sea on the loran line of 3H4-4550 (coast and geodetic map 12326) beginning over Staten Island.

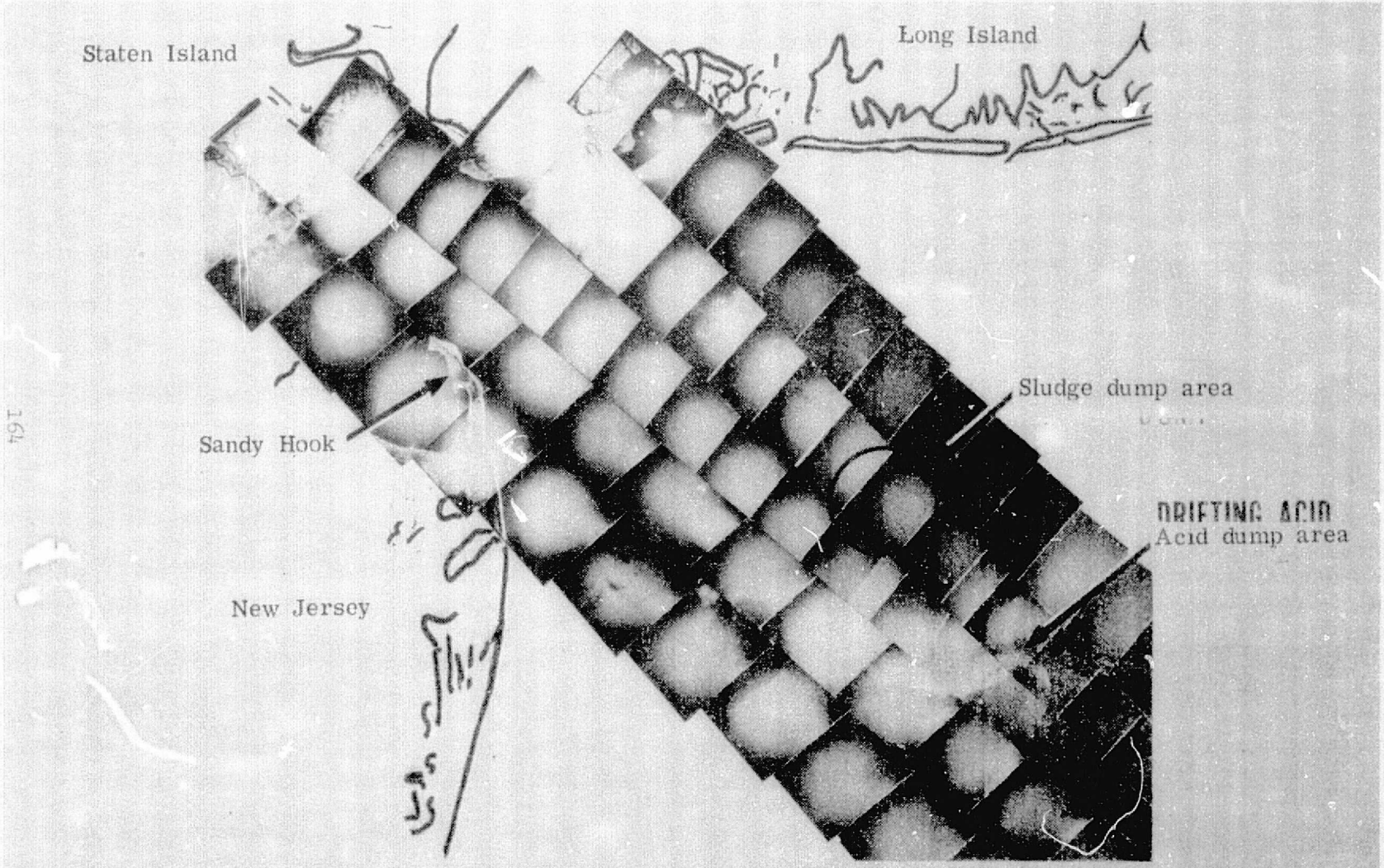

Figure 6.- Composite of photographs taken on April 10, 1975, over the New York Bight, through a 554 (green-yellow) R-3 Baird-Atomic filter from 5.3 kilometers altitude.

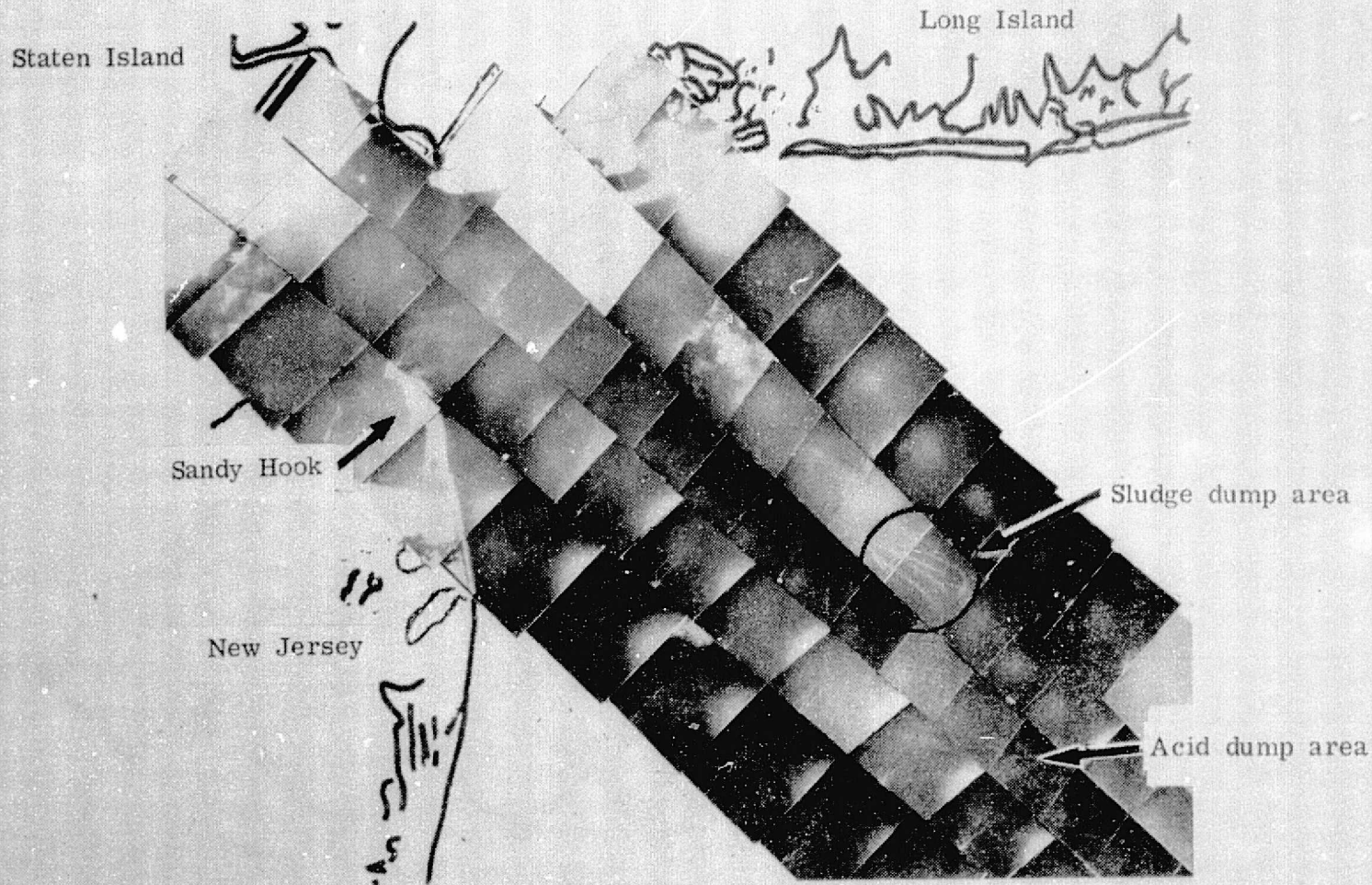

Figure 7.- Composite of photographs taken on April 10, 1975, over the New York Bight, through a 89B near-infrared Wratten optical filter, from 5.3 kilometers altitude.

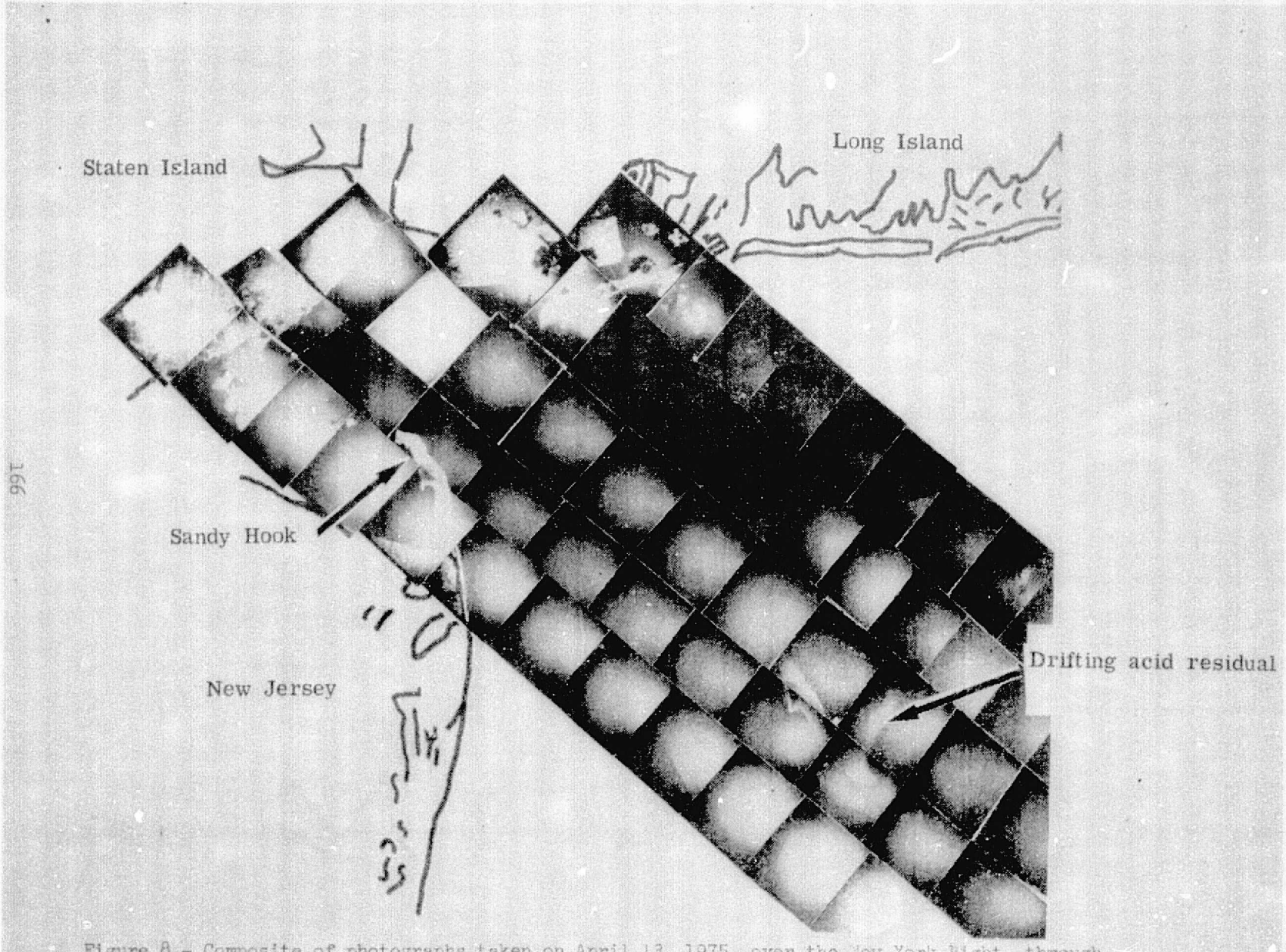

Figure 8.- Composite of photographs taken on April 13, 1975, over the New York Bight, through a 525 (blue-green) B-3 Baird-Atomic optical filter, from 5.3 kilometers altitude.

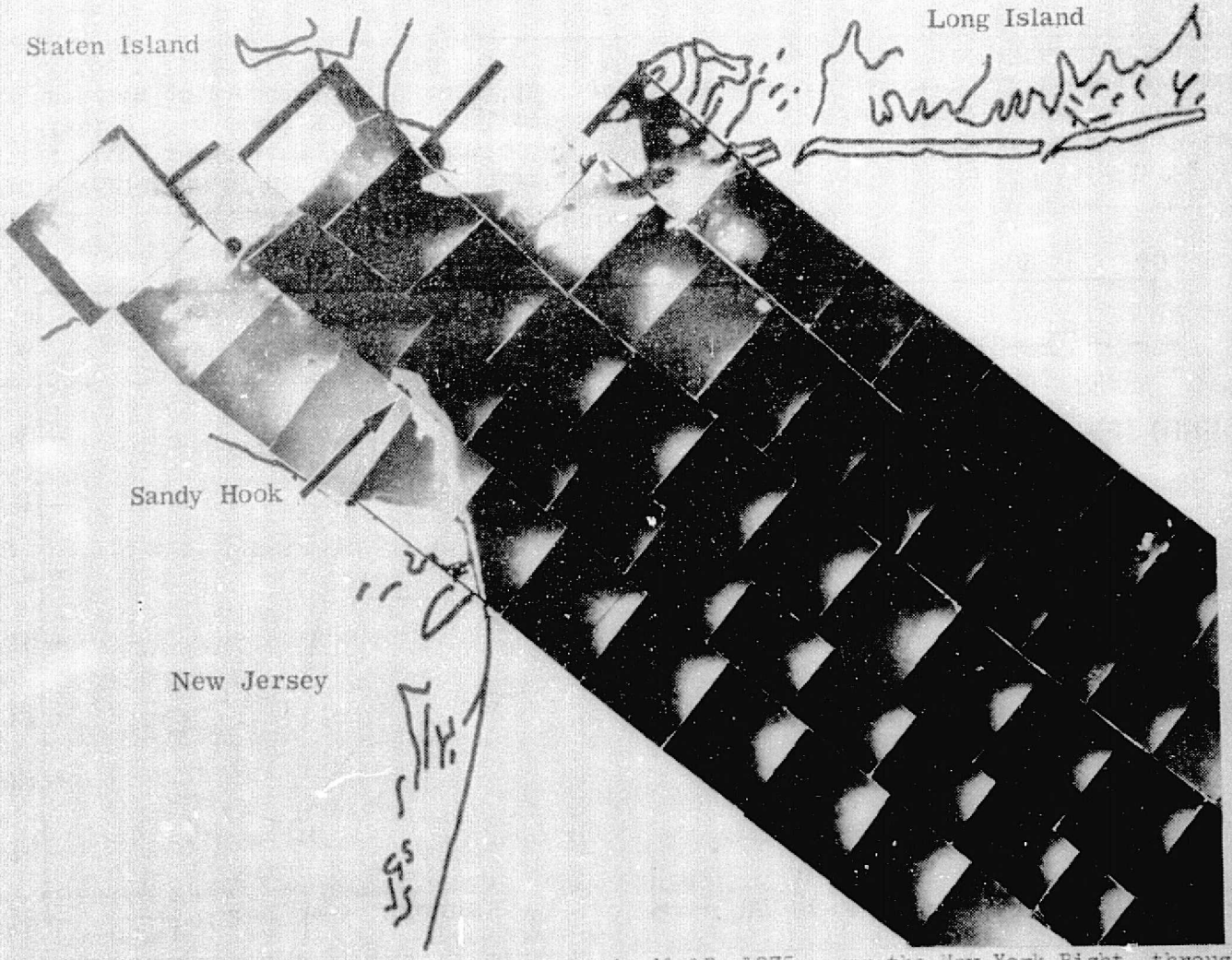

Figure 9.- Composite of photographs taken on April 13, 1975, over the New York Bight, through a 89B near-infrared Wratten optical filter, from 5.3 kilometers altitude.

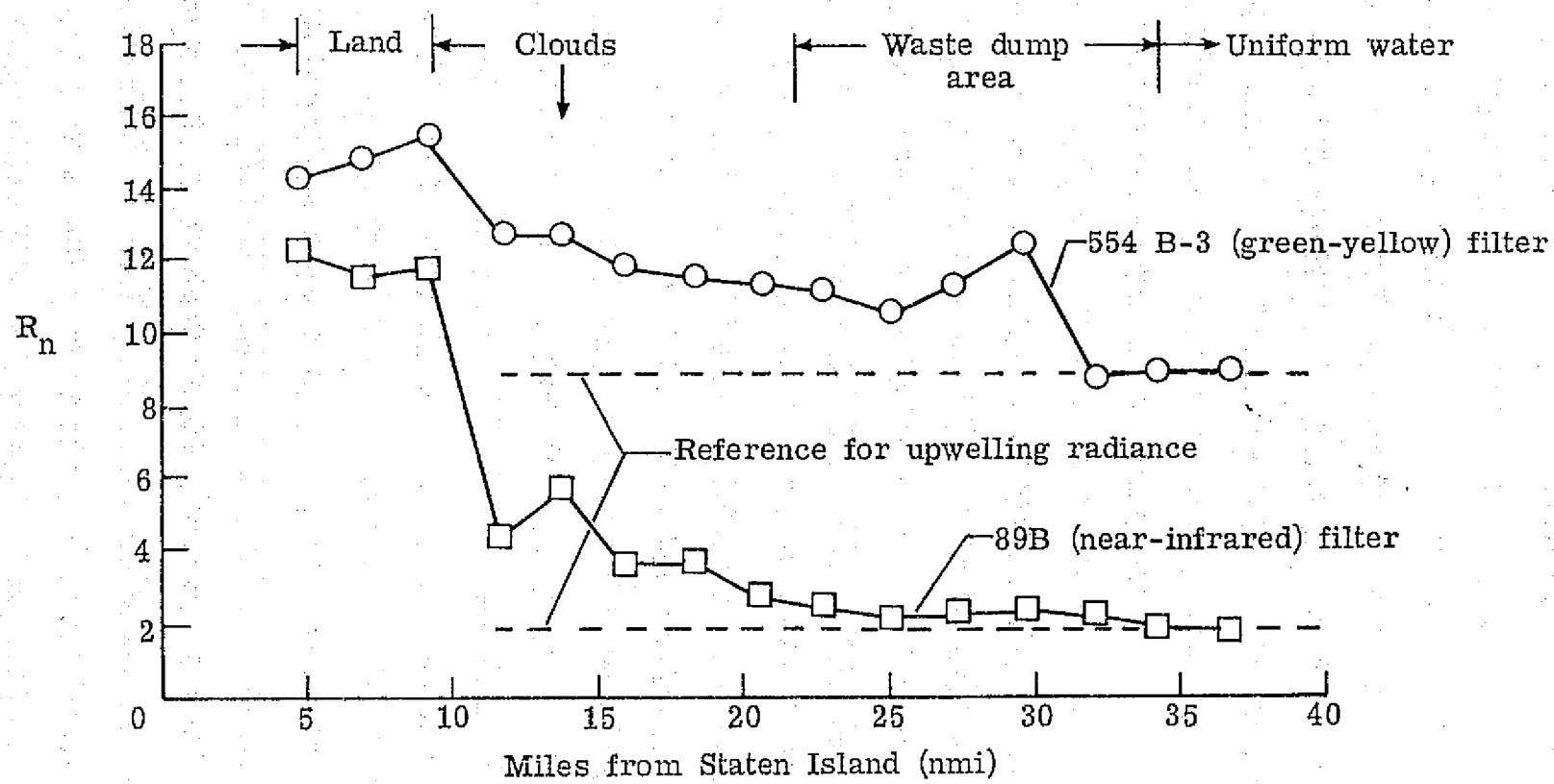

Figure 10.- Variation of nadir radiance through the 554 (green-yellow) and 89B (non-infrared) optical filters, along loran line 4640 on April 10, 1975, in the form of transmission through the photographic film relative to a density wedge, R_n, obtained from densitometer traces over the center of positive transparencies of photographs 33 to 47 in figure 4 from which has been subtracted relative film transmission through the unexposed border of the film, versus miles from Staten Island.

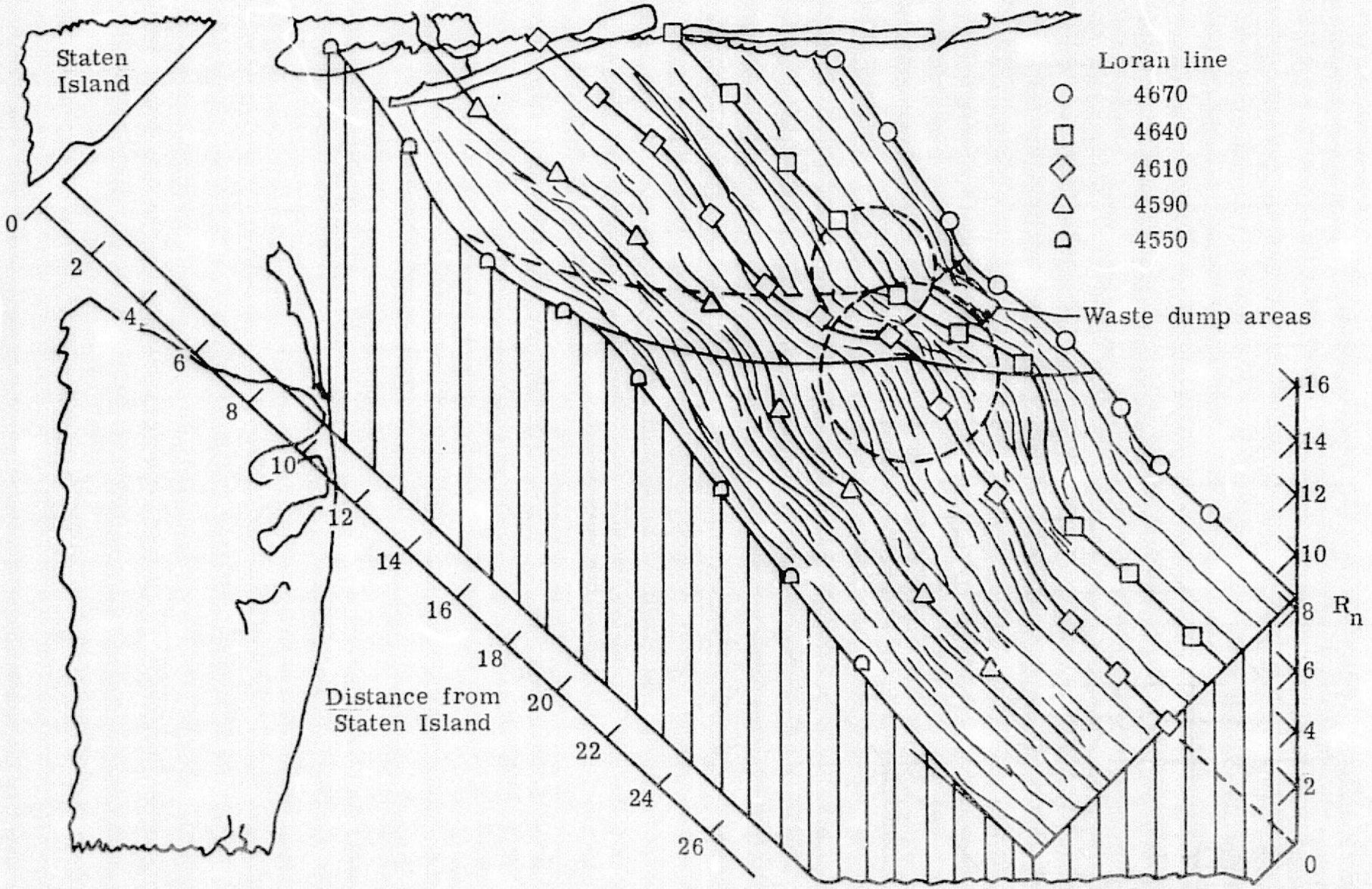

Figure 11.- Variation of nadir radiance from all photographs taken over water through the 554 (green-yellow) optical filter on April 10, 1975.

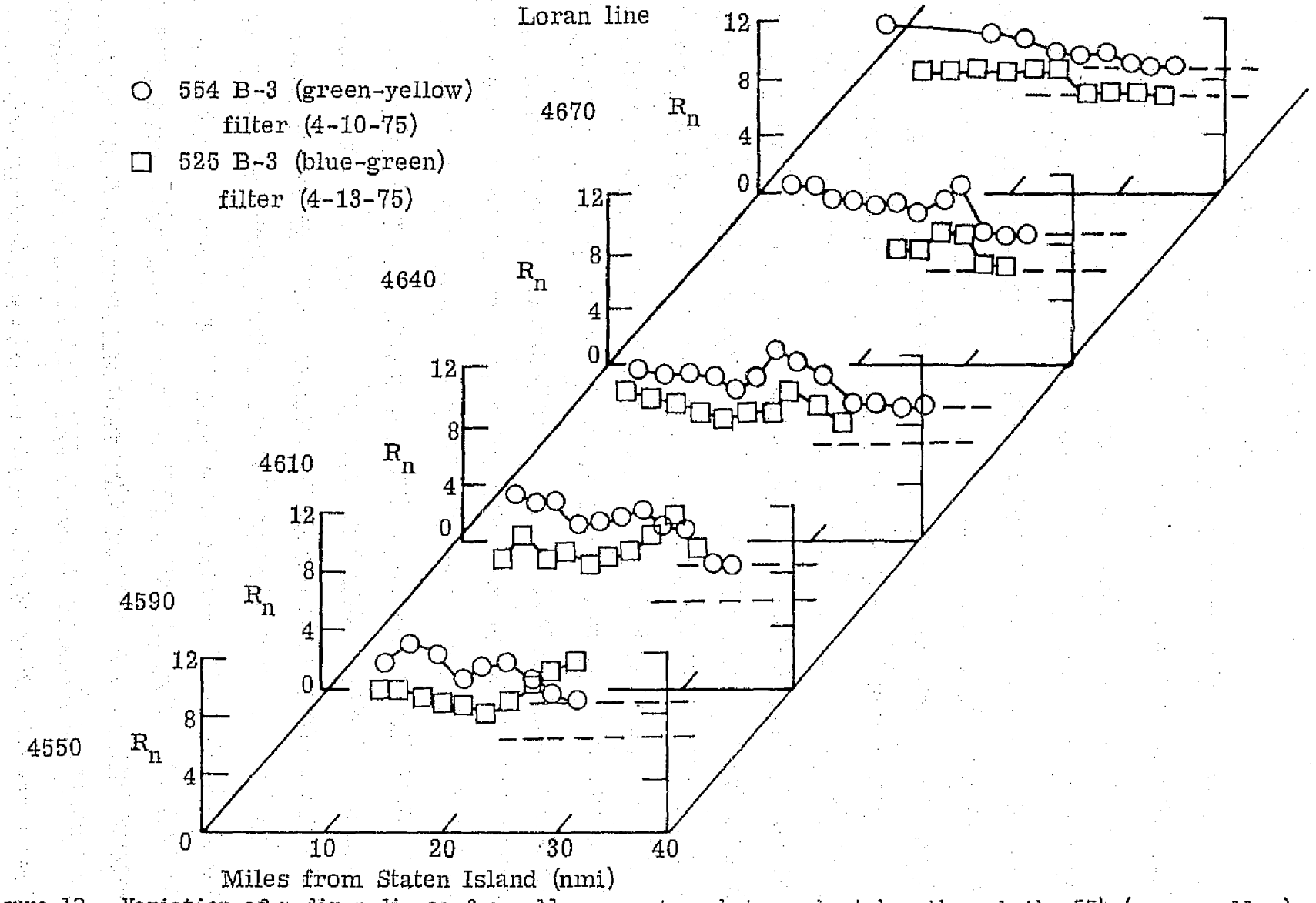

Figure 12.- Variation of nadir radiance from all over-water photographs taken through the 554 (green-yellow) optical filter on April 10, 1975, and those taken through the 525 (blue-green) optical filter on April 13, 1975.

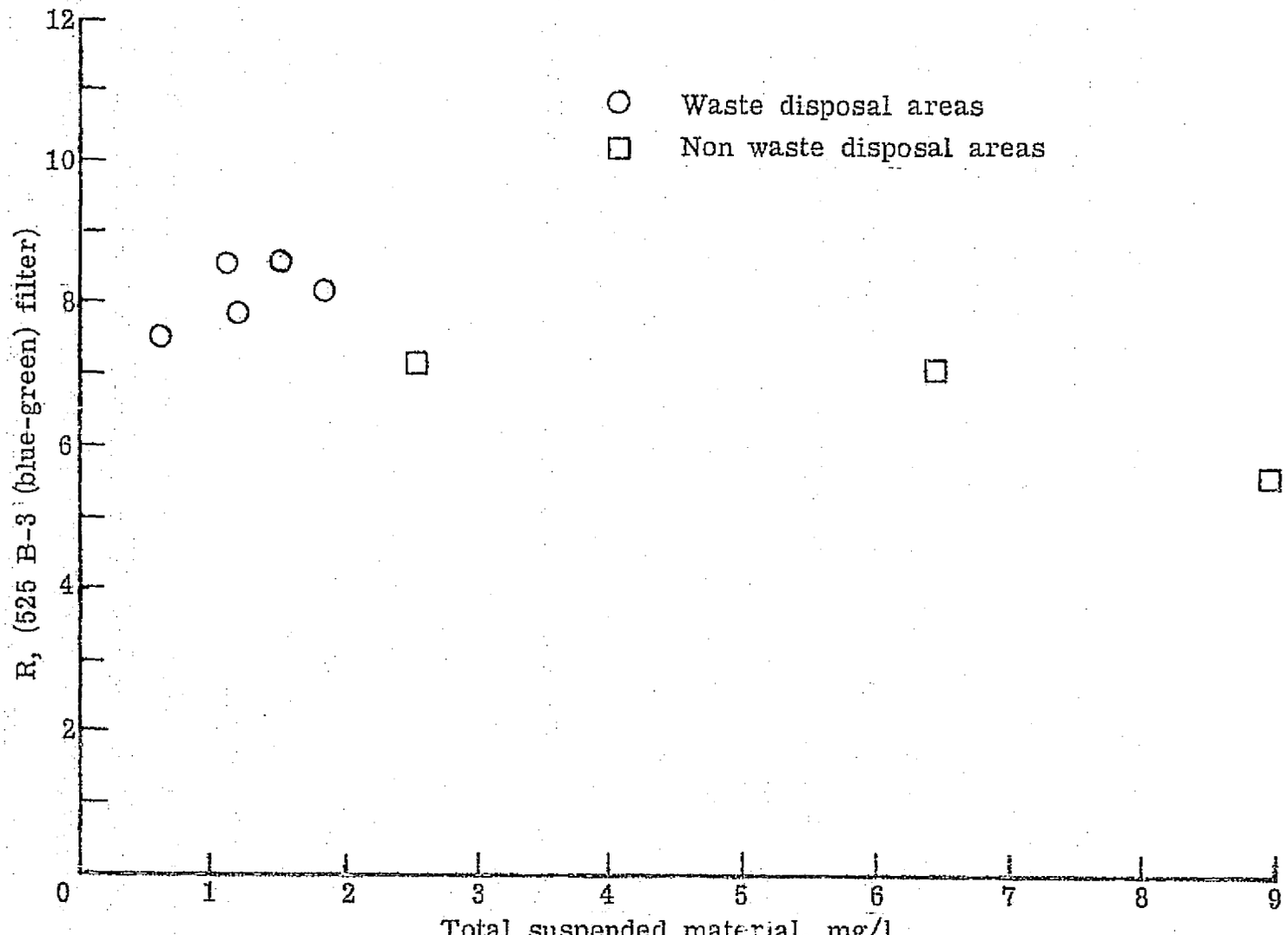

Figure 13.- Variation of off-nadir radiance through the 525 (blue-green) optical filter taken on April 13, 1975, which have been normalized to nadir.

RADSCAT Wind Measurements Over The New York Bight

By

L. C. Schroeder, W. L. Jones, Jr., and J. L. Mitchell

RADSCAT WIND MEASUREMENTS OVER THE NEW YORK BIGHT

By

L. C. Schroeder, W. L. Jones, and J. L. Mitchell

INTRODUCTION

On April 17, 1975, the Advanced Applications Flight Experiment (AAFE) radiometer/scatterometer (RADSCAT) experiment was conducted in the New York Bight as a part of the NOAA/NASA MESA Program. The objective of this experiment was to demonstrate the viability of the radar remote sensing technique for measurement of ocean surface wind vectors and to provide these measurements at selected sites for the investigation of wind-induced ocean currents in the bight. This report describes the RADSCAT measurement technique, presents the inferred wind vectors, and compares the radar derived wind vector with "surface truth" (tower wind vector measurements). The wind-induced ocean currents portion of this investigation is a NOAA responsibility and is not discussedin this report.

EXPERIMENTAL TECHNIQUE

Aircraft radar scattering measurements were obtained using the AAFE RADSCAT 13.9 GH_Z scatterometer* operating on the NASA Johnson Space Center's C-130 aircraft (NASA-929). RADSCAT was mounted to the ramp (lower cargo door) and was configured so that the antenna scanned across the aircraft

*The reader is referred to reference 1 for an in-depth discussion of the AAFE RADSCAT instrument.

ground track (fig. 1). During the ocean measurements, the aircraft performed a series of counter-clockwise 360 degree (360°) turns (20° bank angle), while the antenna was pointed to the left (inward) side of the aircraft at an angle of 50° from the aircraft vertical axis. This maneuver permitted the antenna to illuminate approximately the same surface areas while undergoing continuous azimuth rotation as illustrated in figure 2. The polarization was transmitted horizontal, received horizontal and the incidence angle was 30°.

In making the scatterometer measurements, the quantity of interest is the scattering coefficient σ^{o} which is a measure of the ocean reflectivity. For incidence angles greater than 25 degrees off the nadir, the mechanism for backscatter is a resonant (Bragg) scattering from ocean waves whose lengths are of the order of the microwave wavelength. At 13.9 GH_z the ocean σ^{o} is directly proportional to the amplitude of centimeter or capillary ocean waves. Since the generating force for capillary wave growth is the wind stress at the air/sea interface and since the time constant for this wave generation is a few seconds, these radar scatterers are in equilibrium with the local surface winds. Thus the radar remote sensing technique is to infer windspped from a measurement of σ^{o}.

In this experiment, radar data taken during four circle flight patterns at each preselected site were processed to produce the average scattering coefficient as a function of flight direction (azimuth), as shown in figure 3. Previous research (refs. 2 and 3) has shown that both windspeed and direction can be inferred from these anisotropic scattering signatures. As previously stated, the σ^{o} is proportional to the surface frictional

windspeed; however, this is a difficult quantity to measure. Historically the neutral stability* windspeed at 19.5 meters (m) altitude has been used by researchers as a geophysical parameter to be correlated with radar scattering measurements. An example of these radar scattering signatures for three different ocean 19.5 m windspeeds is shown in figure 4, where the abscissa is the radar azimuth relative to the crosswind direction. Note that the σ^{o} monotonically increases with windspeed and each plot is a quasi-sine-wave of twice the frequency of the azimuth angle. The peaks occur in the upwind and downwind directions and the minima in the crosswind direction; additionally, the upwind peak is slightly greater than the downwind peak. For the New York Bight RADSCAT measurements, wind vectors were inferred using "calibration" curves similar to those of figure 4. During the experiment, windspeed, wind direction, air temperature, and sea temperature were recorded every half hour at the United States Coast Guard Ambrose Tower located in the New York Bight. These measurements were used to provide surface truth for verifying the RADSCAT inferred wind vectors. The mission was flown so that the first and last RADSCAT circles would occur at Ambrose Tower to provide a direct comparison of RADSCAT measurements with truth data. In addition, NOAA investigators also obtained simultaneous current measurements from buoys at four sites within the test area.

MISSION RESULTS

The mission was flown on April 17, 1975. Figure 5 shows the location of sites where RADSCAT circle patterns were flown, along with a key which

*The 19.5 meter neutral stability windspeed is the surface frictional windspeed extrapolated to 19.5 meters using a logarithmic profile with an air-sea temperature differential of zero (ref. 4).

correlates these sites with those of the mission plan. Time would not allow taking data at every site originally planned.

Table I shows the wind vectors determined from analysis of the RADSCAT circle data. Windspeed was determined using both σ^{o} mean and σ^{o} downwind. The results obtained were consistent. The σ^{o} mean values were obtained by averaging the windspeeds over all azimuth angles. These wind vector data have also been plotted in figure 6. On this figure, the sequence of data taking is indicated by dashed lines, and vectors indicate the magnitude and direction of winds. From these results, it can be seen that the wind is nearly constant until 12:12 p.m. e.d.t. From that time and site on, the wind diminishes in speed and the direction becomes variable.

The wind and temperature measurements from Ambrose Tower are presented in figures 7 and 8. Also shown are the RADSCAT inferred wind vectors. The first and last RADSCAT measurements were taken at the Ambrose site. Accordingly, all other RADSCAT results should be considered in a qualitative sense. Concurrent with the first RADSCAT measurement, the Ambrose windspeed (measured at 40 meters altitude) dropped abruptly from 16 knots to approximately 10 knots while the air/sea temperature difference increased from + 2°C to + 6°C (fig. 7) Thereafter the Ambrose windspeed was constant while the air/sea temperature difference steadily increased to + 7°C by the completion of the flight. The large air/sea temperature difference will result in a neutral stability windspeed at Ambrose Tower which is significantly reduced from measured windspeeds. From reference 4, the Ambrose 10-knot windspeed and approximately + 7°C air/sea temperature difference measured at 1300 hours would produce a 19.5 m neutral stability windspeed of about 4.5 knots. Thus both RADSCAT windspeed measurements at Ambrose Tower are in good agreement

with the "surface truth". Furthermore, the comparison of wind direction shown in figure 8 is also in good agreement.

CONCLUDING REMARKS

RADSCAT scattering data have been used to infer windspeed and direction at preselected sites in the New York Bight with the intent of:

1. Demonstrating the RADSCAT's capability as a wind sensor.
2. Providing ground truth for current measurements made contemporarily with these measurements.

Through the use of "surface truth" wind measurements at Ambrose Tower, the demonstration of the RADSCAT instrument was in good agreement for both comparisons.

The analysis of ocean current effects is a NOAA responsibility and is not available at this time.

REFERENCES

1. Schroeder, L. C.; Jones, W. L.; and Mitchell, J. L.: Laboratory Calibration of AAFE Radiometer/Scatterometer (RADSCAT). NASA TM X-73900, April 1976.

2. Grantham, W. L.; Bracalente, E. M.; Jones, W. L.; Schrader, J. H.; Schroeder, L. C.; and Mitchell, J. L.: An Operational Satellite Scatterometer for Wind Vector Measurements Over the Ocean. NASA TM X-72672, March 1975.

3. Jones, W. L.; Schroeder, L. C.; and Mitchell, J. L.: Aircraft Measurements of the Microwave Scattering Signature of the Ocean. Trans. on Ant. and Prop./IEEE Journal of Oceanic Engineering, January 1977.

4. Cardme, V. J.: Specification of the Wind Distribution in the Marine Boundary Layer for Wave Forecasting. Report TR 69-1, New York University School of Engring. and Sc., March 1970. (Available as DDS No. AD 702 490.)

TABLE I. MESA WINDSPEED DATA FROM RADSCAT MEASUREMENTS (4-17-75)

SITE	START TIME (EDT)	LATITUDE	LONGITUDE	WIND DIRECTION (OUT OF)	WINDSPEED (KNOTS) FROM MEAN σ^0	FROM DOWNWIND σ^0
1	10 08	40.45	-73.88	310°	10.8	10.5
7	10 35	40.38	-73.50	330°	10.7	
6	10 48	40.20	-73.46	320°	9.9	
5	11 05	40.10	-73.56	310°	11.9	12.0
13	11 20	39.84	-73.58	320°	9.3	
12	11 38	40.01	-73.48	320°	11.1	11.1
11	11 54	40.04	-73.20	305°	8.5	
10	12 12	40.22	-73.24	290°	6.8	
9	12 29	40.40	-73.10	245°	5.5	5.4
8	12 47	40.52	-73.39	300°	6.3	
1	13 06	40.44	-73.90	285°	5.0	

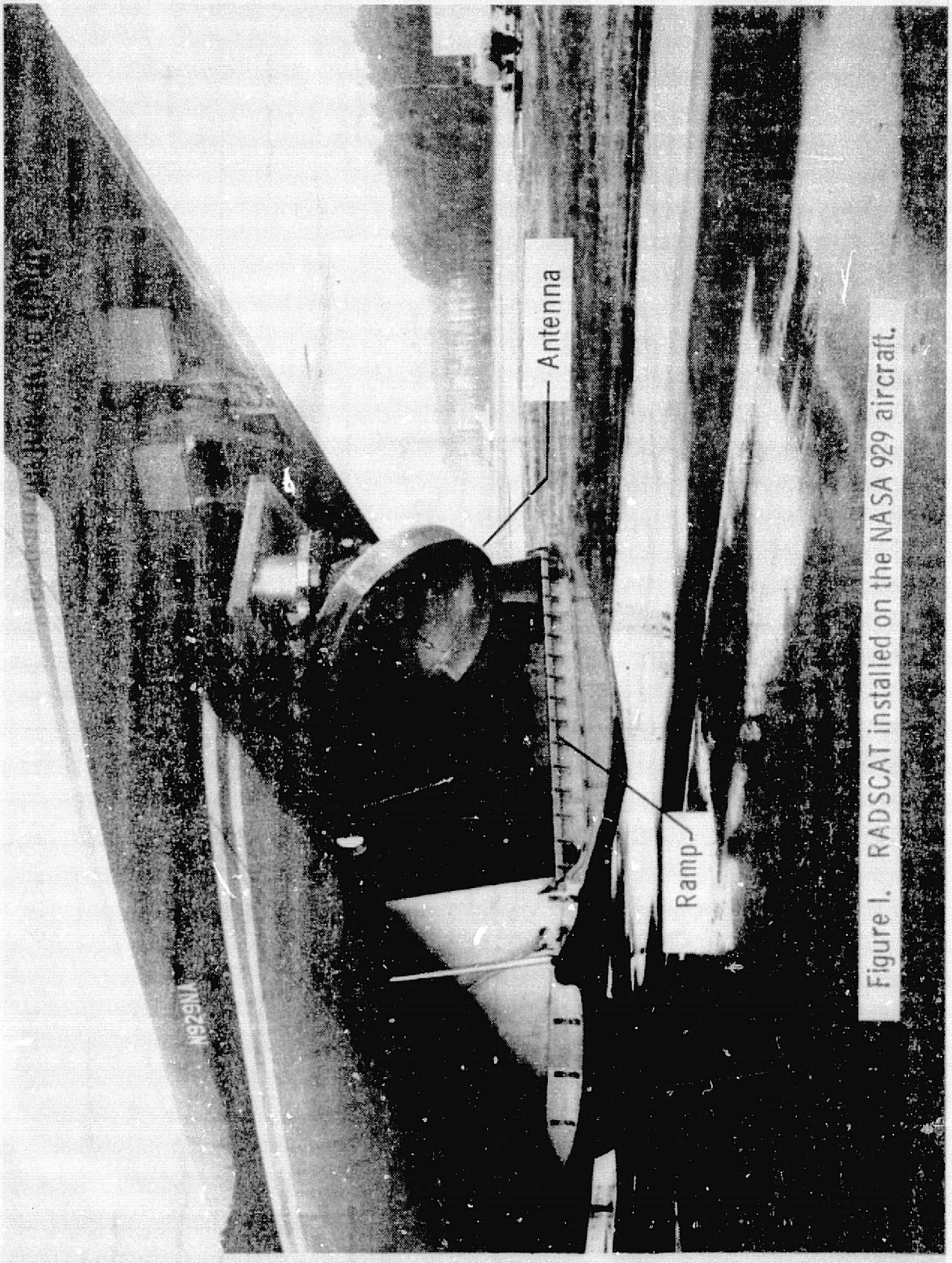

Figure I. RADSCAT installed on the NASA 929 aircraft.

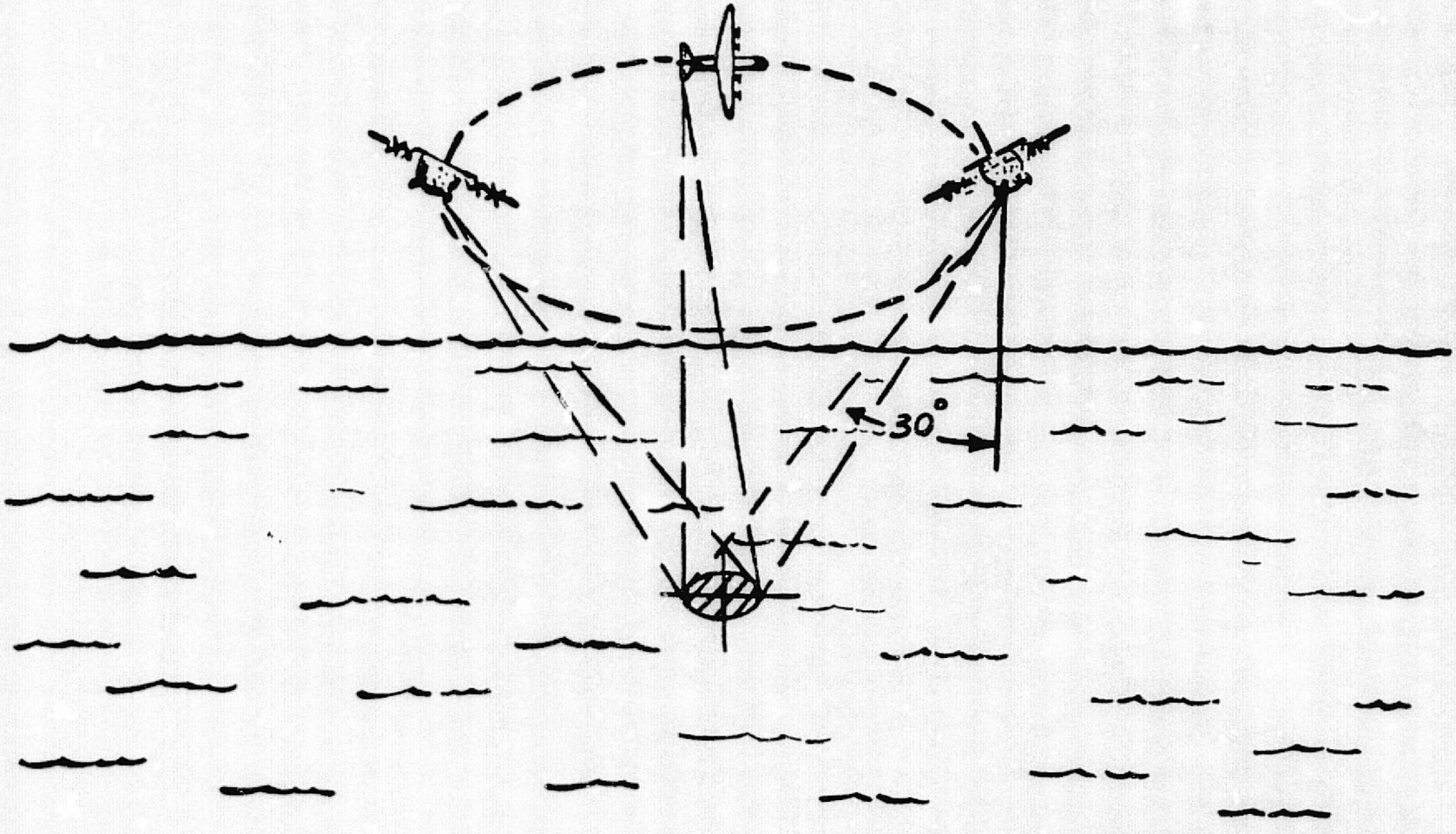

Figure ? - RADSCAT instrument taking data during circle flights.

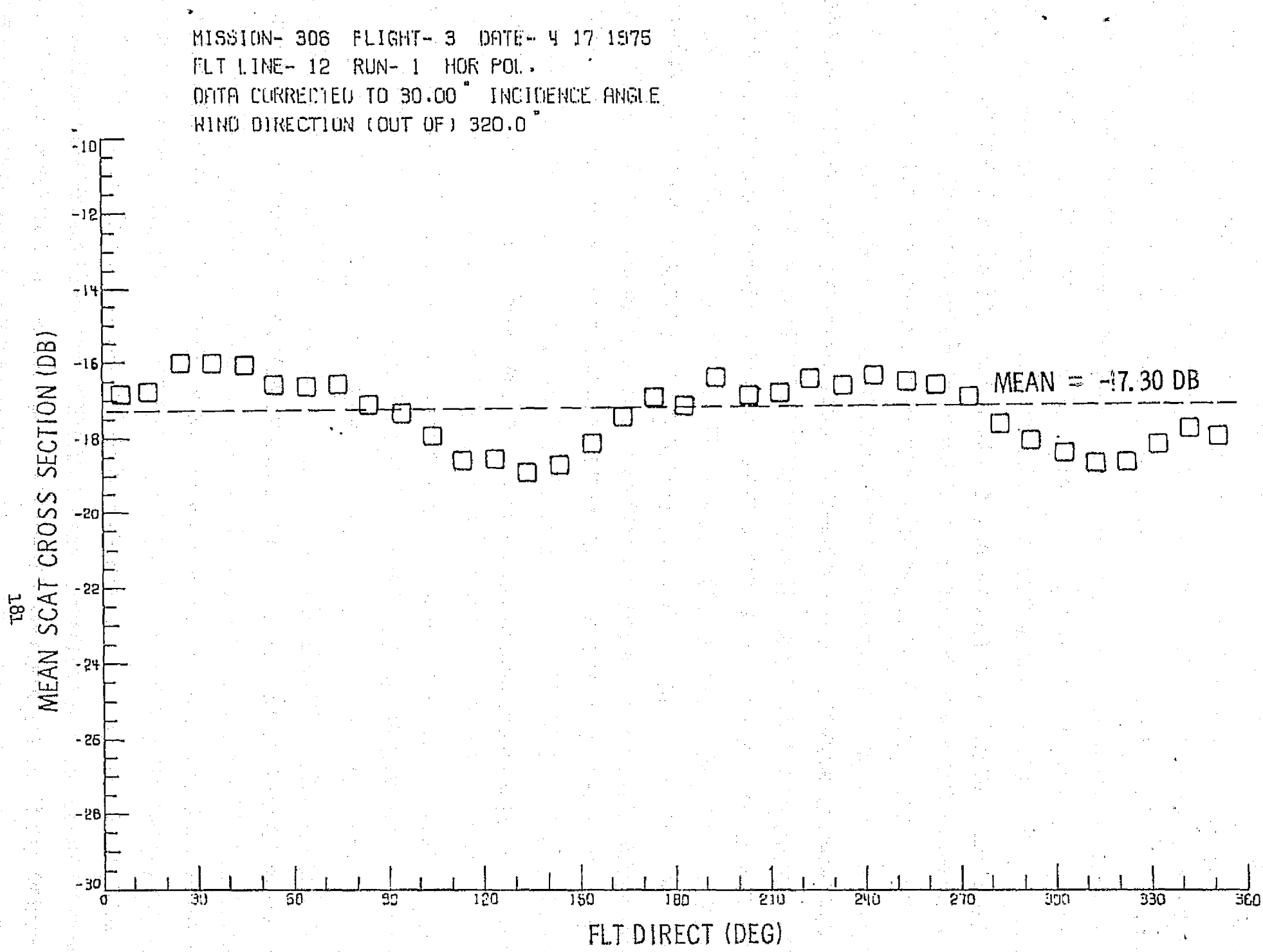

Figure 3. - Typical RADSCAT scattering data from a MESA circle flight.

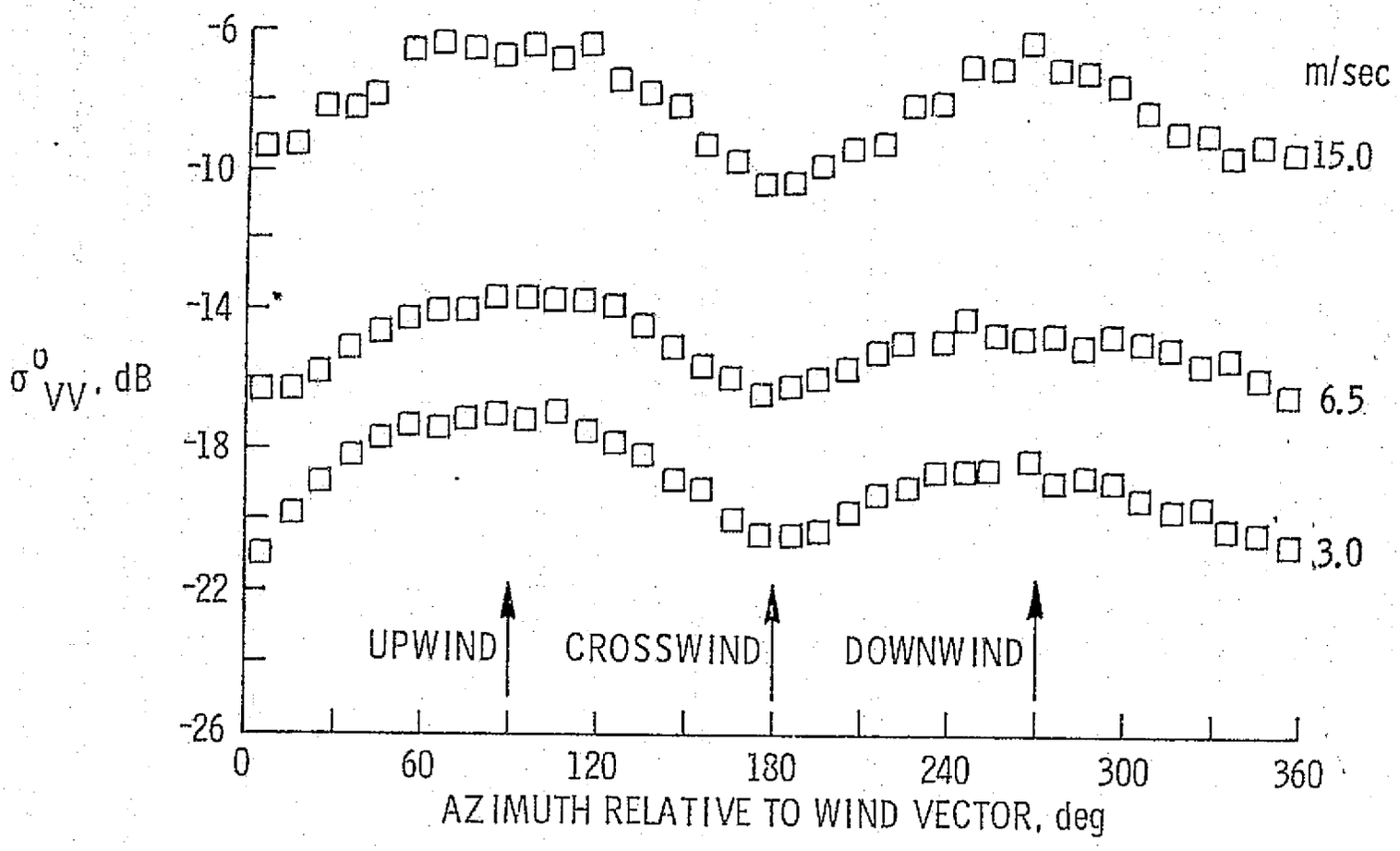

Figure 4. Typical scattering data from RADSCAT circle flights.

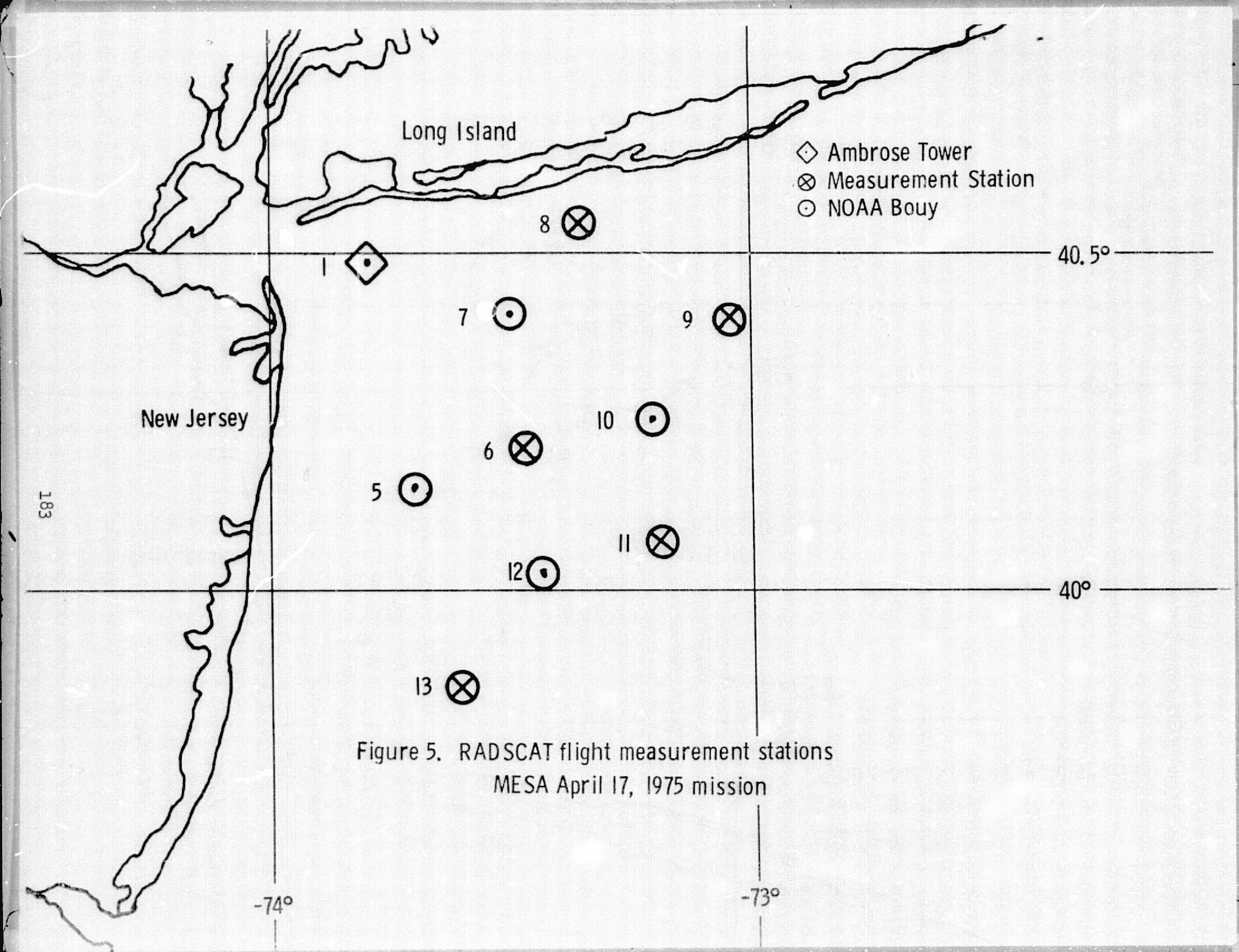

Figure 5. RADSCAT flight measurement stations
MESA April 17, 1975 mission

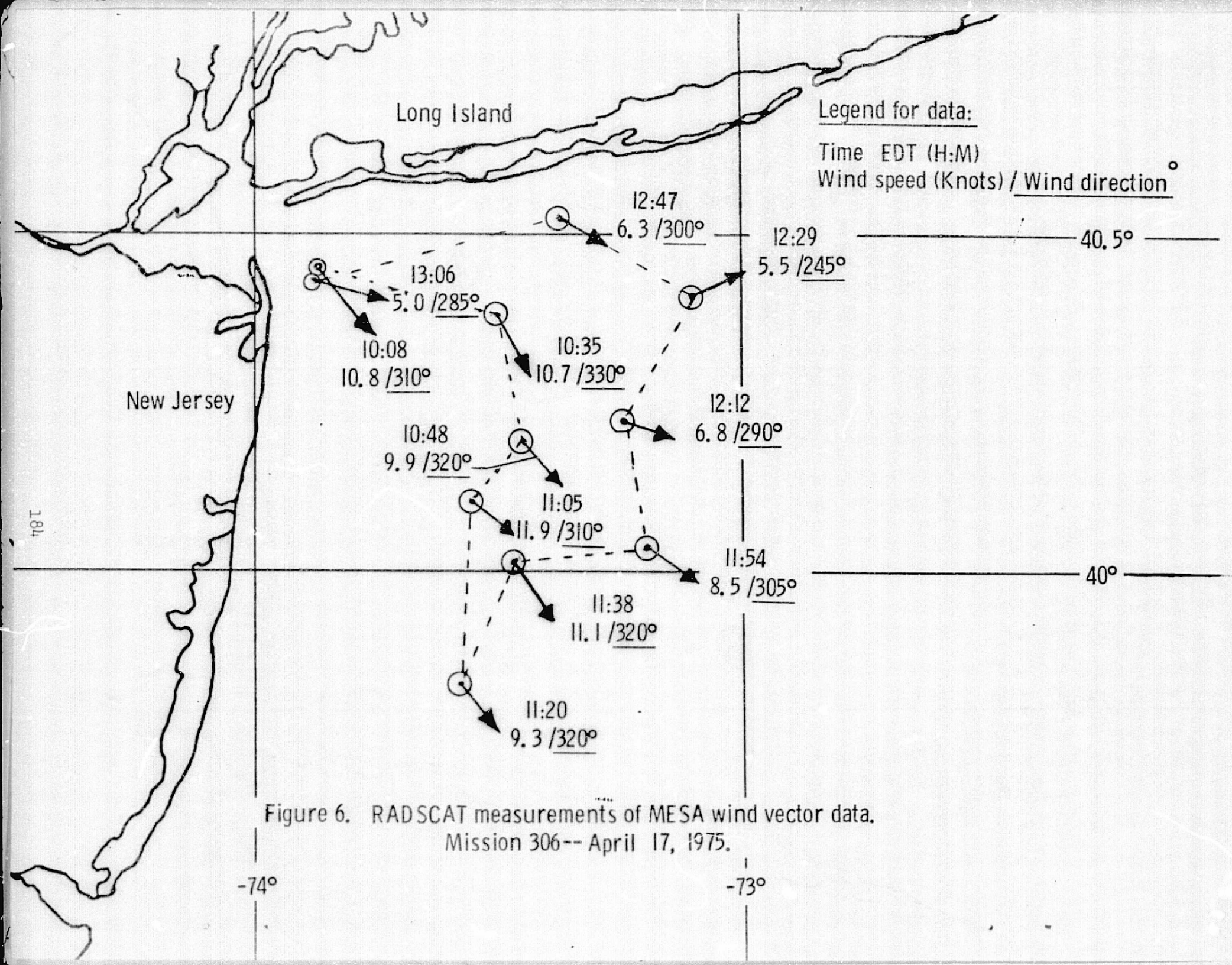

Figure 6. RADSCAT measurements of MESA wind vector data.
Mission 306-- April 17, 1975.

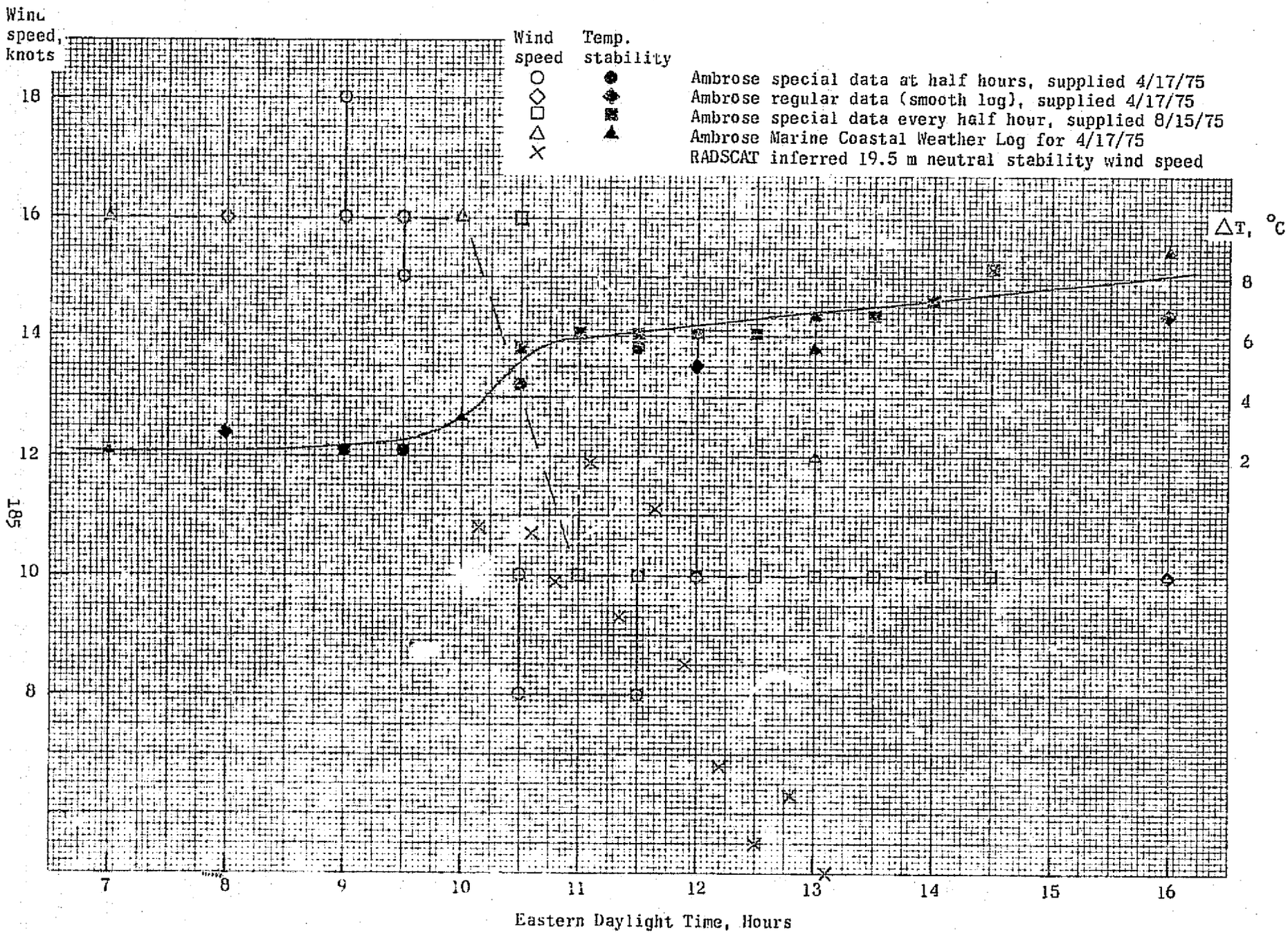

Figure 7. Time history of wind speed measurements for the 4/17/75 MESA mission.

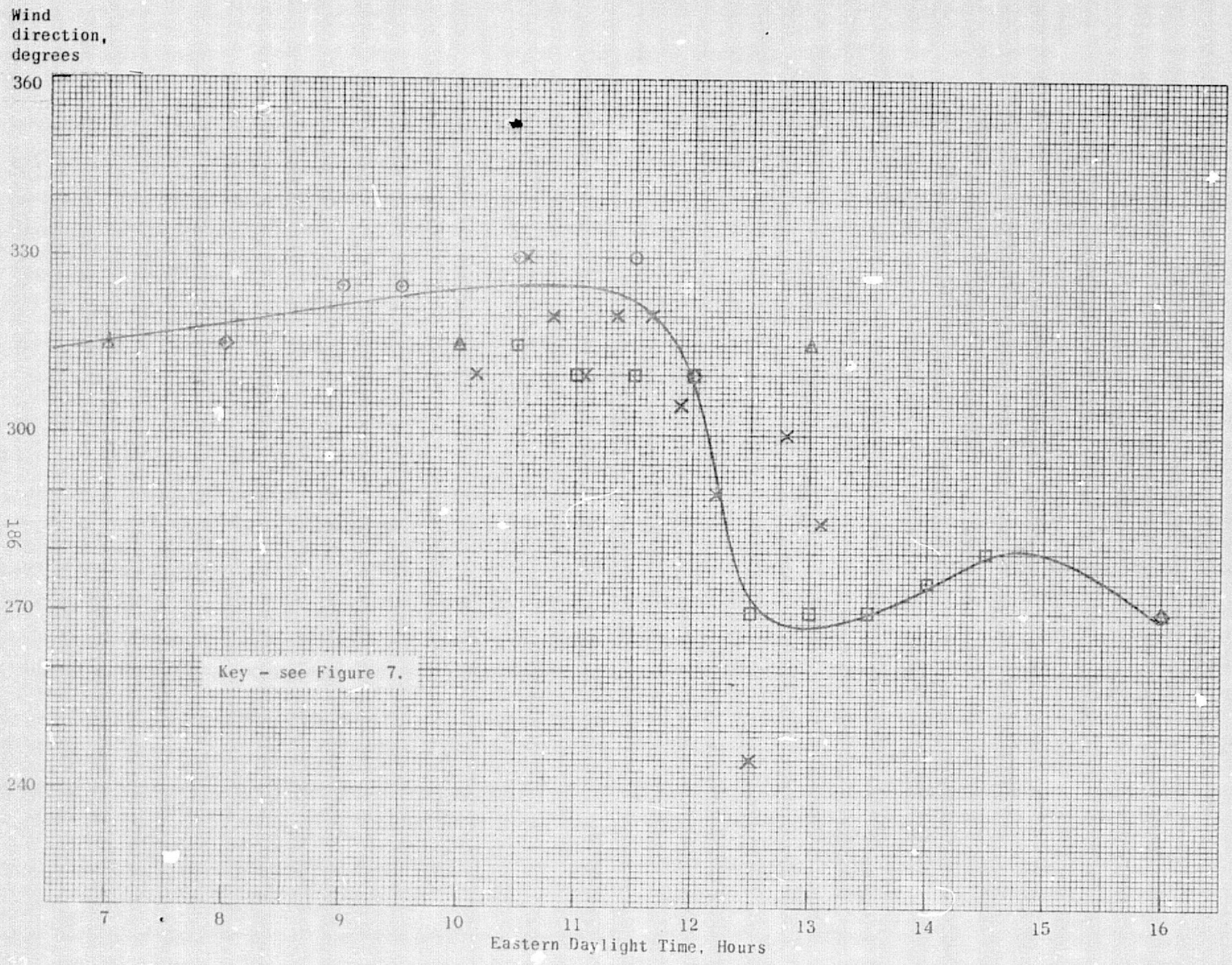

Figure 8. Time history of wind direction measurements for the 4/17/75 MESA mission.